STATE OF CALIFORNIA • DEPARTMENT OF TRANSPORTATION

TECHNICAL REPORT DOCUMENTATION PAGE

TR0003 (REV 10/98)

ADA Notice
For individuals with sensory disabilities, this document is available in alternate formats. For information call (916) 654-6410 or TDD (916) 654-3880 or write Records and Forms Management, 1120 N Street, MS-89, Sacramento, CA 95814.

1. REPORT NUMBER	2. GOVERNMENT ASSOCIATION NUMBER	3. RECIPIENT'S CATALOG NUMBER
CA15-2336		

4. TITLE AND SUBTITLE
Evaluation of the TowPlow for Caltrans Operations

5. REPORT DATE
09/30/2015

6. PERFORMING ORGANIZATION CODE

7. AUTHOR
Duane Bennett, George Burkett, Jaeyoung Kang, Steven A. Velinsky

8. PERFORMING ORGANIZATION REPORT NO.
UCD-ARR-15-09-30-01

9. PERFORMING ORGANIZATION NAME AND ADDRESS
Advanced Highway Maintenance and Construction Technology (AHMCT) Research Center
Department of Mechanical & Aerospace Engineering
University of California, Davis
Davis, California 95616-5294

10. WORK UNIT NUMBER

11. CONTRACT OR GRANT NUMBER
EA 65-680198, Task ID: 2336

12. SPONSORING AGENCY AND ADDRESS
California Department of Transportation
PO Box 942873, MS #83
Sacramento, CA 94273-0001

13. TYPE OF REPORT AND PERIOD COVERED
Final Report
April 2012 - September 2015

14. SPONSORING AGENCY CODE
Caltrans

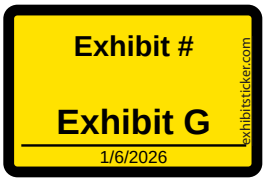
15. SUPPLEMENTARY NOTES

16. ABSTRACT

Caltrans is responsible for the safe operation of many mountainous highways and must ensure that they remain open and passable throughout the winter. Certain critical highways carry heavy seasonal recreational traffic as well as high volumes of truck traffic. Caltrans spends approximately $25 million annually on snow-fighting operations, which involve a fleet of over 800 snowplows, an array of additional equipment, and approximately 2,600 employees. Caltrans has been actively searching for safer and more efficient methods for winter snow-fighting operations. As such, Caltrans requested that the Advanced Highway Maintenance and Construction Technology (AHMCT) Research Center configure, procure, and deploy two Viking-Cives TowPlow systems and conduct an extensive evaluation to determine the most beneficial configuration and application of TowPlow technology for Caltrans. This report covers procurement of an initial TowPlow trailer system, development and testing through two winter seasons, the procurement and development of a second TowPlow trailer system, and discussion of particular modifications needed to allow for safe and legal operation on California highways. Due to three consecutive exceptionally light snow seasons in California that coincided with the project's testing period, an evaluation of TowPlow performance in conventional Caltrans snowplowing operations has not been possible. As an alternative, a detailed structure of data collection capabilities and analysis tools has been developed to evaluate plowing performance for future snow seasons. This document covers research through June 30, 2015.

17. KEY WORDS	18. DISTRIBUTION STATEMENT	
Roadway snow removal, TowPlow, Snowplowing trailer, Traction enhancing surface treatment, 2-lane snowplowing.	No restrictions. This document is available to the public through the National Technical Information Service, Springfield, Virginia 22161.	
19. SECURITY CLASSIFICATION *(of this report)*	**20. NUMBER OF PAGES**	**21. COST OF REPORT CHARGED**
Unclassified	182	

Reproduction of completed page authorized.



Copyright 2018. the authors

DISCLAIMER/DISCLOSURE STATEMENT

The research reported herein was performed as part of the Advanced Highway Maintenance and Construction Technology (AHMCT) Research Center, within the Department of Mechanical and Aerospace Engineering at the University of California – Davis, and the Division of Research, Innovation and System Information at the California Department of Transportation. It is evolutionary and voluntary. It is a cooperative venture of local, State and Federal governments and universities.

This document is disseminated in the interest of information exchange. The contents of this report reflect the views of the authors who are responsible for the facts and accuracy of the data presented herein. The contents do not necessarily reflect the official views or policies of the State of California, the Federal Highway Administration, or the University of California. This publication does not constitute a standard, specification or regulation. This report does not constitute an endorsement of any product described herein.

For individuals with sensory disabilities, this document is available in Braille, large print, audiocassette, or compact disk. To obtain a copy of this document in one of these alternate formats, please contact: the Division of Research, Innovation and System Information, MS-83, California Department of Transportation, P.O. Box 942873, Sacramento, CA 94273-0001.

Copyright 2018. the authors

Advanced Highway Maintenance and Construction Technology Research Center

Department of Mechanical and Aerospace Engineering
University of California at Davis

Evaluation of the TowPlow for Caltrans Operations

Duane Bennett: Senior Development Engineer
George Burkett: Development Engineer
Jaeyoung Kang: Graduate Student Researcher
Steven A. Velinsky: Principal Investigator

Report Number: CA15-2336
AHMCT Research Report: UCD-ARR-15-09-30-01
Final Report of Contract: EA 65-680198,
Task ID: 2336

September 30, 2015

California Department of Transportation

Division of Research, Innovation and System Information

Copyright 2018. the authors

ABSTRACT

Caltrans is responsible for the safe operation of many mountainous highways and must ensure that they remain open and passable throughout the winter. Certain critical highways carry heavy seasonal recreational traffic as well as high volumes of truck traffic. Caltrans spends approximately $25 million annually on snow-fighting operations, which involve a fleet of over 800 snowplows, an array of additional equipment, and approximately 2,600 employees. Caltrans has been actively searching for safer and more efficient methods for winter snow-fighting operations. As such, Caltrans requested that the Advanced Highway Maintenance and Construction Technology (AHMCT) Research Center configure, procure and deploy two Viking-Cives TowPlow systems and conduct an extensive evaluation to determine the most beneficial configuration and application of TowPlow technology for Caltrans. This report covers procurement of an initial TowPlow trailer system, development and testing through two winter seasons, the procurement and development of a second TowPlow trailer system, and discussion of particular modifications needed to allow for safe and legal operation on California highways. Due to three consecutive exceptionally light snow seasons in California that coincided with the project's testing period, an evaluation of TowPlow performance in conventional Caltrans snowplowing operations has not been possible. As an alternative, a detailed structure of data collection capabilities and analysis tools has been developed to evaluate plowing performance for future snow seasons. This document covers research through June 30, 2015.

Copyright 2018. the authors

Vermeer Manufacturing Company – Ex. 2045
Kubota v. Vermeer
IPR2025-00168
Page 4 of 182

EXECUTIVE SUMMARY

Caltrans is responsible for the safe operation of many mountainous highways and must ensure that they remain open and passable throughout the winter. Certain critical highways carry heavy seasonal recreational traffic as well as high volumes of truck traffic. Caltrans spends approximately $25 million annually on snow-fighting operations, which involve a fleet of over 800 snowplows, an array of additional equipment, and approximately 2,600 employees. [24]. In order to investigate methods for improving the efficiency of seasonal snow-fighting operations, Caltrans Division of Maintenance requested a research project through the Advanced Highway Maintenance and Construction Technology (AHMCT) Research Center. Specifically, AHMCT was directed to configure, procure, and deploy two Viking-Cives TowPlow systems for Caltrans winter operations. Viking-Cives advertises that operating TowPlow systems reduces the number of vehicles and drivers needed in multiple lane highway plowing operations. Testimonials from other state departments of transportation support this claim. AHMCT was tasked to perform an extensive study of the equipment, conduct an in-service evaluation, and determine the most beneficial configuration and application of TowPlow technology for Caltrans operations. This report documents the results of the research. The intent is that at the end of the evaluation process, the TowPlows and snowplow (also known as prime mover truck) can be transferred into the Caltrans fleet.

The research started with the procurement of a TowPlow brine trailer system, referred to as TowPlow1. The TowPlow1 system employed a 354.8 kw (475 horsepower) Caltrans standard fleet snowplow and was tested on Interstate 80 (I80) in Caltrans District 3 during winter 2013-14. Caltrans subsequently transferred TowPlow1 into their fleet and modified the snowplow's hydraulic system to be more compatible with the TowPlow trailer's hydraulics. Modifications done by the Caltrans Division of Equipment (DOE) improved the operability of the TowPlow1 system. The modified system is referred to as TowPlow1C in this report. TowPlow1C was first deployed and tested in Caltrans District 3 on I80 during winter 2014-15.

A second TowPlow system, hereto referred to as TowPlow2, was procured in a standard configuration similar to TowPlow systems used in other states. The purpose was to acquire a "turn-key" system that would require minimal modifications to meet Caltrans requirements. TowPlow2 was procured and delivered to AHMCT in December 2014. Despite the intent of the system to be turn-key, the as delivered TowPlow2 did not fully meet Caltrans requirements, the most important of which was excessive weight on the system's axles. As such, several modification options were proposed. The modifications, referred to as Option 3 modifications, were completed on the TowPlow2 system in June 2015. The primary goal of these modifications was to keep a fully loaded TowPlow2 system within legal weight limits. While the analysis results indicate that the TowPlow2.3 can carry a full load of sand without overloading the axles, the trailer is assumed to be level and the sand density equal to 16,870 N/m^3 (2,900 lb/yd^3). As

Copyright 2018. the authors

Vermeer Manufacturing Company – Ex. 2045
Kubota v. Vermeer
IPR2025-00168
Page 5 of 182

such, it is recommended that the fully loaded system be weighed to ensure that axle legal limits are not exceeded.

Due to three consecutive exceptionally light snow seasons that coincided with the research project's testing period, a TowPlow system performance evaluation in Caltrans snowplowing operations has not been completed. As an alternative, a detailed means of data collection and analysis capabilities have been developed to assist with evaluating TowPlow performance in future snow seasons. In addition, analysis of various TowPlow configurations and utilization strategies are presented based on Caltrans winter snow removal operational techniques and system capabilities. This document covers work through June 30, 2015.

Copyright 2018. the authors

Vermeer Manufacturing Company – Ex. 2045
Kubota v. Vermeer
IPR2025-00168
Page 6 of 182

TABLE OF CONTENTS

Abstract ii
Executive Summary iii
Table of Contents v
List of Figures x
List of Tables xiv
List of Acronyms and Abbreviations xv
Chapter 1: Background 1
TowPlow Description and Requirements 3
Prime Mover Truck: 3
Control System: 3
Direct Brine Application Configuration: 4
Sander/Brine Application Configuration: 4
Literature Search/Survey of States 5
Report Outline 7
Chapter 2: Dynamics and Control of the TowPlow 8
Chapter 3: Caltrans TowPlow Considerations 10
Chain Controls: 10
Steep Grades: 11
Dedicated Operators: 11
Off Season Uses: 12
Chapter 4: TowPlow1 Procurement and Testing in the 2012-13 Winter Season 13
TowPlow1 Configuration: 13
TowPlow1 Operational Controls: 13
Telemetry Unit 14
System Hydraulics: 14
Adaptation for the Use of Chains 15
Operator Training 15
TowPlow1 Testing and Results: 15

Copyright 2018. the authors

Vermeer Manufacturing Company – Ex. 2045
Kubota v. Vermeer
IPR2025-00168
Page 7 of 182

Chapter 5: TowPlow1 Development and Testing in the 2013-14 Winter Season 17
TowPlow1 Hydraulic Modification 17
TowPlow1 Controls Development 17
TowPlow1 Operation Testing and Results 18
TowPlow1 - Caltrans Operator Survey 18
TowPlow1C - Caltrans Modified System for the 2014-15 Winter Season 19
TowPlow1 and 1C Performance Evaluations 19
Data Acquisition System 19
Performance Summary 19
Chapter 6: TowPlow2 Procurement 20
TowPlow2 Configuration 20
Sanding TowPlow 21
Circulated Specifications 22
Chapter 7: Preliminary Evaluation of TowPlow2 23
Arrival of the TowPlow2 23
Evaluation of the Static Axle Loads as Delivered 24
Background of Legal Axle Limits 24
Static Weight Evaluation 24
Chapter 8: Adapting TowPlow2 to DOE Requirements 26
DOE Proposed System Modifications 26
Load Analysis 27
Implementation of DOE Option 3 Modification 27
TowPlow2 Prime Mover Truck Modifications: 27
TowPlow2 Trailer Modifications: 28
Implementation of the Modifications 28
Chapter 9: TowPlow2 with Option 3 Modification (TowPlow2.3) 29
TowPlow2.3 Axle Weight Verification: 29
Comparing the Static Empty Weights 29
Additional Desired Testing 30
Chapter 10: Data Visualization - Storm Reports 31
The Data Postprocessing Approach 31

Copyright 2018. the authors

Vermeer Manufacturing Company – Ex. 2045
Kubota v. Vermeer
IPR2025-00168
Page 8 of 182

Chapter 11: Summary and Conclusions 34
Appendix A: TowPlow Dynamic Analysis 36
Literature Survey 36
Kinematics of the Articulated Vehicle 36
Dynamics of the Articulated Vehicle 39
Snow Resistance Model 42
Stability Control of the Articulated Vehicle 44
Kinematics of the TowPlow 45
Kinematic Model – Instantaneous Centers of Velocity 45
Derivation of Kinematic Equations 46
Defining Steering Inputs 47
Simulation of Constant Radius Turning 49
Summary 51
Linear Vehicle Dynamics and Stability of the TowPlow 52
Linear Planar Model of the TowPlow 52
Stability and Controllability of the TowPlow 58
Dynamics and Open-loop Control of the TowPlow 63
Summary 65
Nonlinear Vehicle Dynamics of the TowPlow 69
Equations of Motion for the TowPlow 69
Modified Dugoff's Tire Friction Model 72
Tire Rotation Dynamics 78
Load Transfer Effect 79
Experimental Validation 80
Experimental Configuration 81
Steady-State Circular Test – Constant Speed 82
Transient Maneuver Test 85
Summary 87
Snow Resistance Model and Dynamic Simulation of the TowPlow 89
Snow Resistance Model 89
Application of the Snow Resistance Model 93

Copyright 2018. the authors

Vermeer Manufacturing Company – Ex. 2045
Kubota v. Vermeer
IPR2025-00168
Page 9 of 182

Dynamic Simulation of the TowPlow Without Control of the Trailer Axle 96
Driver Model 97
Deploying trailer plow and cornering 98
Slalom, Up, and Down Hill 99
Split Friction Coefficient Braking 102
Summary 106
Control of the TowPlow for the Snow Removal Operation 107
Optimal Controller Design - LQR 107
PI Controller Design 111
Dynamic Simulation of the TowPlow With PI Control of the Trailer Axle 111
Slalom, Up, and Down Hill 112
Split Friction Coefficient Braking 112
Summary 116
Appendix B: TowPlow Operator Survey - Questionnaire with Results 117
Appendix C: Power vs. Performance Analysis 122
Appendix D: Preliminary Axle Load Analysis 130
Establishing a Baseline from the TowPlow2 Static Weights 130
Fully Loaded Weight of the TowPlow2 132
Group Axle Weights 133
Appendix E: Predictive Load Analysis for Moving the TowPlow2 Trailer's Sander 136
Analyzing the Axles on the TowPlow2 Trailer 142
Principle of stationary potential energy approach 142
Newton-Euler approach 147
Comparing the two approaches 149
Evaluation of spring constants 153
Prime Mover Truck's Spring Stiffness 154
Tire Spring Stiffness 154
Analytical Results 155
Evaluating the Indeterminate Forces 156
Appendix F: Analytical Estimate of Loaded Axle Weights of the Option 3 Modified TowPlow2 (TowPlow2.3) 159

Copyright 2018. the authors

Vermeer Manufacturing Company – Ex. 2045
Kubota v. Vermeer
IPR2025-00168
Page 10 of 182

References 162

Copyright 2018. the authors

Vermeer Manufacturing Company – Ex. 2045
Kubota v. Vermeer
IPR2025-00168
Page 11 of 182

LIST OF FIGURES

Figure 1. A TowPlow system in its deployed configuration 2
Figure 2. Ohio DOT identified considerations TowPlow implementation [52] 6
Figure 3. Onspot chain system [www.onspot.com] 11
Figure 4. Nevada DOT sander body TowPlow 20
Figure 5. The as-delivered TowPlow2 23
Figure 6. Return of the DOE TowPlow for DOE Option 3 implementation 28
Figure 7. TowPlow1 operation pie chart (seasonal total) 32
Figure 8. Final TowPlow usage 33
Figure 9. Jindra's tractrix integrator [30] 37
Figure 10. Pretty's tractrix from steering in circle [47] 37
Figure 11. Instantaneous centers of logging trucks by Erkert et al [21] 38
Figure 12. Cornering of tractor-trailer combination: (a) without trailer steering, (b) with trailer steering by Chen and Velinsky [9] 39
Figure 13. Manesis' sliding kingpin mechanism [43] 39
Figure 14. Typical unstable states of articulate vehicles by Vlk [59] 40
Figure 15. Coordinate system for the articulated vehicle by Chieh and Tomizuka [10] 41
Figure 16. Concept of friction between bristles for the LuGre model [7] 41
Figure 17. Friction circle concept for the Dugoff's tire friction model by Guntur and Sankar [26] 42
Figure 18. Mellor's wedge plow model [44] 43
Figure 19: Kaku's snow flow assumption in snow resistance model [34] 43
Figure 20. Control volume in front of the plow by Ravani et al. [49] 43
Figure 21. Control scheme of active braking control in [33] 44
Figure 22. Control scheme of active all wheel steering control in [17] 45
Figure 23. Schematic of the TowPlow system and associated notations 46
Figure 24. Radius of curvature of the road vs. trailer wheel steering angle for constant total articulation angle $\theta_t = 30^o$ 49
Figure 25. Tractor steering angle vs. Trailer wheel steering angle for constant total articulation angle $\theta_t = 30^o$ 49
Figure 26. Simulation results of the constant radius turning: (a) angles without trailer corrective steering, (b) angles with trailer corrective steering, (c) intruding distance without trailer corrective steering, (d) intruding distance with trailer corrective steering 51
Figure 27. Linear planar TowPlow model and parameters 52
Figure 28. Forces at the hitch points and the tongue assembly 55
Figure 29. Locus of the eigenvalues of the matrix $M^{-1}A$ with varying longitudinal velocity 60

Copyright 2018. the authors

Vermeer Manufacturing Company – Ex. 2045
Kubota v. Vermeer
IPR2025-00168
Page 12 of 182

Figure 30. Locus of the eigenvalues of the matrix $M^{-1}A$ with varying inertias 61
Figure 31. Locus of the eigenvalues of the matrix $M^{-1}A$ with varying inertias: (a) Minimum tractor inertia with varying trailer inertia, (b) Maximum trailer inertia with varying tractor inertia 62
Figure 32. Scheme of the uncontrolled system simulation 64
Figure 33. Scheme of the open-loop controlled system simulation using the lookup table show in in Error! Reference source not found. 64
Figure 34. Simulation results of the TowPlow comparing uncontrolled and controlled system for the step input: (a) Tractor steering angle, (b) Trailer steering angle, (c) Tractor yaw rate, (d) Trailer yaw rate, (e) Total articulation angle 66
Figure 35. Simulation results of the TowPlow comparing uncontrolled and controlled system for the pulse input: (a) Tractor steering angle, (b) Trailer steering angle, (c) Tractor yaw rate, (d) Trailer yaw rate, (e) Total articulation angle 67
Figure 36. Simulation results of the TowPlow comparing uncontrolled and controlled system for the sine input: (a) Tractor steering angle, (b) Trailer steering angle, (c) Tractor yaw rate, (d) Trailer yaw rate, (e) Total articulation angle 68
Figure 37. Scheme of the tractor unit and forces 70
Figure 38. Scheme of the trailer unit and forces 71
Figure 39. Scheme of the tongue assembly and forces 72
Figure 40. Flow chart of the tire force calculation [26] 74
Figure 41. Computed longitudinal and lateral tire forces 75
Figure 42. Carpet plots: (a) Longitudinal tire force and (b) lateral tire force varying normal load 76
Figure 43. Load factors in relation with (a) friction coefficient and (b) lateral stiffness 77
Figure 44. Carpet plots considering load change effect: (a) Longitudinal tire force and (b) lateral tire force 78
Figure 45. Free body diagram for a driving wheel 79
Figure 46. (a) Side and (b) rear views of the tractor unit and applied forces 79
Figure 47. Layout of sensors and microcontrollers 82
Figure 48. Test procedure of the steady-state test for a speed and direction 83
Figure 49. Steady-state test results compared with simulation results 85
Figure 50. Test procedure of the transient maneuver test 86
Figure 51. Transient test inputs for the experiment and simulation 87
Figure 52. Transient test results compared with simulation results 88
Figure 53. Components of the snow resistance 89
Figure 54. Scheme of the snow resistance 90
Figure 55. Comparison of resistance ratios for longitudinal snow resistance 93
Figure 56. Comparison of resistance ratios for lateral snow resistance 93
Figure 57. Schemes of the snowplows: (a) front plow and (b) trailer plows 94
Figure 58. Longitudinal snow resistant forces of the plows 95

Copyright 2018. the authors

Vermeer Manufacturing Company – Ex. 2045
Kubota v. Vermeer
IPR2025-00168
Page 13 of 182

Figure 59. Lateral snow resistant forces of the plows 96
Figure 60. Driver model – control scheme of the driving/braking torque 98
Figure 61. Driver model – control scheme of the tractor steering angle 98
Figure 62. Simulation results of the TowPlow running straight with and without driver model 100
Figure 63. Simulation results of deploying trailer plow and cornering 101
Figure 64. Simulation results of slalom, up and down hill 102
Figure 65. Simulation results of braking on a snow packed road ($\mu_0 = 0.4$) 104
Figure 66. Simulation results of split friction coefficient braking – tractor on a wet road ($\mu_0 = 0.6$) and trailer on a snow packed road ($\mu_0 = 0.4$) 105
Figure 67. Simulation results of split friction coefficient braking – tractor on a snow packed road ($\mu_0 = 0.4$) and trailer on a yet road ($\mu_0 = 0.6$) 106
Figure 68. Locus of the eigenvalues of the controlled system with varying longitudinal velocity 108
Figure 69. LQR control scheme for the active steering of the trailer axle 109
Figure 70. Cornering simulation results of the active trailer steering control 110
Figure 71. PI control scheme for the active steering of the trailer axle 111
Figure 72. PI control scheme for the active steering of the trailer axle 112
Figure 73. Slalom, up and down hill simulation results of the active trailer steering control 113
Figure 74. Split friction coefficient simulation results of the active trailer steering control - tractor on a wet road ($\mu_0 = 0.6$) and trailer on a snow packed road ($\mu_0 = 0.4$) 114
Figure 75. Split friction coefficient simulation results of the active trailer steering control - tractor on a snow packed road ($\mu_0 = 0.4$) and trailer on a wet road ($\mu_0 = 0.6$) 115
Figure 76. Basic diagram for power analysis 122
Figure 77. Power demand curves for the TowPlow 125
Figure 78. Power demand on for an empty TowPlow on 3% grade 126
Figure 79. Power demand on for a loaded TowPlow on 3% grade 127
Figure 80. Power demand on for an empty TowPlow on 6% grade 127
Figure 81. Power demand on for a loaded TowPlow on 6% grade 128
Figure 82. Legend for power demand curves 128
Figure 83. Free body diagram of TowPlow2 131
Figure 84. Free body diagram of TowPlow2 134
Figure 85. TowPlow2 trailer free body diagrams 136
Figure 86. Free body diagram for computing new weights after moving the sander. 137
Figure 87. Free body diagram for the prime mover truck 139
Figure 88. Prime mover truck free body diagram 140
Figure 89. Free body diagram for the indeterminate analysis of the TowPlow trailer 143
Figure 90. Force vs. displacement of the trailer tires 155
Figure 91. Resultant forces vs. stiffness ratio 158

Copyright 2018. the authors

Vermeer Manufacturing Company – Ex. 2045
Kubota v. Vermeer
IPR2025-00168
Page 14 of 182

Figure 92. FBD of DOE Option 3 system 159
Figure 93. DOE Option 3 prime mover truck FBD 160

Copyright 2018. the authors

Vermeer Manufacturing Company – Ex. 2045
Kubota v. Vermeer
IPR2025-00168
Page 15 of 182

LIST OF TABLES

Table 1. Certified Scale Axle weights of the empty as-delivered Towplow2 25
Table 2. Predicted Static Weights of TowPlow2 25
Table 3. Summary of DOE TowPlow capabilities (including TowPlow1 and the TowPlow2) 27
Table 4. TowPlow2.3 empty weights 29
Table 5. Vehicle parameters for kinematic analysis 48
Table 6. Vehicle parameters for stability analysis 59
Table 7. Parameters for tire friction calculation [26] 75
Table 8. Vehicle parameters for model validation 84
Table 9. Plow parameters for the snow resistance calculation [34,49] 92
Table 10. Vehicle parameters for dynamic simulation 97
Table 11. Summary of estimated axle loads for determining rolling resistance 123
Table 12 Comparison on UC-Davis analysis and published Caterpillar data 125
Table 13. Prediced top speeds for the TowPlow in various conditions 129
Table 14. Excess power available to plow snow at 25mph 129
Table 15. TowPlow2 static weights 130
Table 16. Physical system measurements 131
Table 17. Summary of hopper/tank capacities and corresponding weights for the TowPlow2 132
Table 18. Additional distance parameters need to compute the overloaded axle load which were measured by AHMCT 133
Table 19. Parameter summary for analysis 156

Copyright 2018. the authors

Vermeer Manufacturing Company – Ex. 2045
Kubota v. Vermeer
IPR2025-00168
Page 16 of 182

LIST OF ACRONYMS AND ABBREVIATIONS

Acronym	**Definition**
AASHTO	American Association of State Highway and Transportation Officials
ABS	Anti-lock Braking System
AHMCT	Advanced Highway Maintenance & Construction Technology Research Center
ATIRC	Advanced Transportation Infrastructure Research Center
Caltrans	California Department of Transportation
CG	Center of Gravity
DLI	Donner Lake Interchange
DOE	Division of Equipment
DOT	Department of Transportation
DPF	Diesel Particulate Filter
DYM	Direct yaw moment
EPA	Environmental Protection Agency
FBD	Free Body Diagram
GCWR	Gross Combined Weight Rating
GPS	Global Positioning System
I80	Interstate 80
IMU	Inertia Measurement Unit
Inc.	Incorporated
IO	Input/Output
ISO	International Organization for Standardization
LQR	Linear-quadratic regulator
META	Maintenance Equipment Training Academy
PI	Proportional-Integral
PLC	Programmable Logic Controller
SSRE	Steady-State Riccati Equation
TAG	Technical Advisory Group
UC-Davis	University of California Davis

Copyright 2018. the authors

Vermeer Manufacturing Company – Ex. 2045
Kubota v. Vermeer
IPR2025-00168
Page 17 of 182

CHAPTER 1:
BACKGROUND

Caltrans is responsible for the safe operation of many mountainous highways and must ensure that they remain open and passable throughout the winter. Certain critical highways carry heavy seasonal recreational traffic as well as high volumes of truck traffic. Caltrans spends approximately $25 million annually on snow-fighting operations which involve a fleet of over 800 snowplows, an array of additional equipment and approximately 2,600 employees [24]. In order to investigate methods for improving the efficiency of seasonal snow-fighting operations, Caltrans Division of Maintenance requested a research project through the Advanced Highway Maintenance and Construction Technology (AHMCT) Research Center. The goal of the work was to develop an understanding of the efficacy of Viking-Cives TowPlow in Caltrans' winter snow-fighting operations. AHMCT was directed to configure, procure, and deploy two Viking-Cives TowPlow systems. Viking-Cives advertises that operating TowPlow systems reduces the number of vehicles and drivers needed in multiple lane highway plowing operations. Testimonials from other state deparments of transportation support this claim. AHMCT was tasked to perform an extensive study of the equipment, conduct an in-service evaluation, and determine the most beneficial configuration and application of TowPlow technology for Caltrans operations. The specific tasks of this research work are:

1. Literature search and survey, and TowPlow acquisition
2. Development of test methods and data acquisition approach
3. Observation of TowPlow use and test participation
4. TowPlow engineering evaluation
5. TowPlow performance evaluation
6. Documentation.

This report is the primary deliverable for task 6 and documents the results of the research. The intent is that at the end of the evaluation process, the TowPlows and snowplow (also known as prime mover truck) can be transferred into the Caltrans fleet and are the primary deliverables of this work.

The patented TowPlow is exclusively distributed by Viking-Cives Midwest, Incorporated (Inc.) [40]. The TowPlow is a trailer with steerable axles that allow the trailer to attain an articulation angle relative to the towing snowplow. This allows the trailer to occupy a lane adjacent to the snowplow. As such, the TowPlow operates as a side wing plow and can plow snow from two adjacent lanes. The TowPlow operates with two in-cab controls; one control lifts and lowers the blade, while the other steers the rear axles and swivel tongue. When not in use, the TowPlow trailer remains in line behind the snowplow and is towed similar to any other towable trailer. Figure 1 depicts a TowPlow system in the deployed configuration. The TowPlow manufacturer claims the following features of the TowPlow:

Copyright 2018. the authors

Vermeer Manufacturing Company – Ex. 2045
Kubota v. Vermeer
IPR2025-00168
Page 18 of 182

- Operates at any angle up to 30 degrees
- Clears a path of 7.3 m (24 ft) or more with a 3.7 m (12 ft) front plow
- Capable of plowing at normal speeds; operated to 88 km/h (55 mph)
- Truck requirements: 400,300 N (90,000 lb) pintle hook, one double and one single acting hydraulic remote, 7-wire trailer plug with Anti-lock braking system (ABS) and standard trailer air package
- Units purchased by DOT's in the U.S. include: Missouri, Minnesota, Utah, Maine, Indiana, Pennsylvania, Tennessee, North Dakota, Iowa, Nebraska, and Wisconsin. Kansas Turnpike has also procured a TowPlow(s).
- Operating Cost—fuel may increase by 10-18%
- Maintenance Cost—standard shoes and cutting edges



Figure 1. A TowPlow system in its deployed configuration

Copyright 2018. the authors

Vermeer Manufacturing Company – Ex. 2045
Kubota v. Vermeer
IPR2025-00168
Page 19 of 182

TowPlow Description and Requirements

The TowPlow system consists of a TowPlow trailer matched with a dedicated snowplow. The prime mover truck provides hydraulic power and all the necessary electrical controls to operate the TowPlow trailer. The driver controls the TowPlow steering, moldboard and surface treatment applications from in the cab. An additional operator is not required. As such, a single driver in one TowPlow system could potentially clear two lanes of snow. Moreover, he could simultaneously apply roadway surface treatment as well. Standard surface treatment options available for the TowPlow include abrasives, pre-wet and direct brine.

Prime Mover Truck:

The effectiveness of the TowPlow trailer is largely determined by the configuration and capabilities of the prime mover truck to which it is mated. Typically, the prime mover truck is a standard 7.6 m^3 (10 yd^3) dump truck with a front mounted, multi-directional plow. There are two major differences between a standard Caltrans snowplow and the TowPlow prime mover truck being developed for Caltrans operations. First, Caltrans exclusively utilizes an open center hydraulic system on all of their standard fleet trucks. This is in contrast to the typical prime mover truck used with TowPlow systems in other states, which use a close centered system. AHMCT and Caltrans Division of Equipment engineers have been unsuccessful in modifying the TowPlow hydraulic system to work with full functionality and effectiveness when connected to the open center hydraulic system on Caltrans' trucks.

Also, a substantial increase in the prime mover truck engine power is necessary to adequately pull the approximately 88,960 kN (20,000 lb) empty weight of the TowPlow up the mountain grades where plowing operations are needed. Two major highways, Interstate 80 in northern California and Interstate 15 in southern California, both contain steep grades reaching six percent stretching for several miles. Snowplowing operations must be capable of plowing near the prevailing traffic speeds to avoid being a traffic hazzard. Typically, plowing operations travel at speeds in the range of 40 km/h (25 mph) when chain restrictions are in force, and they travel at a higher rate when restrictions are lifted. Because the TowPlow system clears two lanes, the prime mover truck engine's power and drive wheel traction must be able to compensate for the additional snow load and weight associated with the trailer. This is less of an issue on relatively flat highways, but for Caltrans, this is a critical issue due to the typical mountain grades. This could potentially be mitigated with higher-powered prime mover trucks and/or increasing traction through the use of tire chains and added load on the drive axles of the prime mover truck.

Control System:

The driver operates the TowPlow system from the prime mover truck's cab. The controls for the moldboard and steering axles consist of a simple 4-axis joystick. Caltrans additionally requires a return button, which when pressed immediately retracts the moldboard and steers the trailer back into the stowed position behind the prime mover truck. These hydraulic valve actions

Copyright 2018. the authors

Vermeer Manufacturing Company – Ex. 2045
Kubota v. Vermeer
IPR2025-00168
Page 20 of 182

can be controlled either by direct wiring to the solenoids or through computer controllers. The type of controller needed is usually determined by the optional pavement surface treatment function and capabilities. Both types of hydraulic valve controls were tested during the research.

Direct Brine Application Configuration:

Caltrans is expanding their use of brine in salt application operations statewide. Granular salt spread from moving trucks tends to bounce away from the intended location or be blown off of the highway. Brine, on the other hand, efficiently sticks were it is applied thus reducing the amount of salt that must be applied on the highway. Caltrans typically applies a thin layer of brine on the highway before the arrival of a cold snowstorm to reduce the formation of ice on the pavement. Furthermore, should an ice layer subsequently form on the pavement, the pre-application of brine acts as a barrier to reduce bonding and aids in its later removal with a snowplow. Following a storm event, Caltrans will often apply brine to the highway to help soften any residual ice layer as chain controls are being lifted. Caltrans continues to plow until the highway is clear of ice and snow. Since Caltrans does not store salt in their equipment between storm events, brine provides an additional benefit of being easier to load and unload than granular salt.

TowPlows can be purchased from the manufacturer with tanks of various capacities. The largest capacity brine capable TowPlow has two trailer mounted 3,780 liter (1,000 gallon) tanks. Additional capacity can be attained with a prime mover truck bed mounted brine tank. The application pump is mounted on the TowPlow trailer, but powered and controlled by the prime mover truck. The standard TowPlow direct brine system is configured for three-lane coverage utilizing vertical manifold spray bars to extend brine coverage to the adjacent lanes. Each of the three spray bars is controlled with separate motorized valves. For computer controlled applications, flow meter feedback and discrete proportional flow control are available.

Sander/Brine Application Configuration:

The bulk of Caltrans snowplows deployed to conduct snow-fighting operations are configured with granular material spreading capability with either tailgate spreader bodies or V-box sander bodies. During storms, Caltrans snowplows patrol the highways. As appropriate, they either plow or apply granular material and can also plow and apply material simultaneously. Popular granular materials utilized by Caltrans include sand and salt. Caltrans does not typically apply brine during a snow event, apparently because the brine causes the snow to become gummy and more difficult to plow.

A TowPlow with a granular spreading body is a common configuration. The granular spreading body is referred to as the sander. The sander is comprised of 1) a stainless steel hopper for carrying the load of sand and 2) motorized spinner disk for casting granular material. The hopper has a capacity of 6.0 m^3 (7.8 yd^3) and is mounted over the TowPlow trailer's tandem axles. The motorized spinner disk is forward facing on the TowPlow trailer and casts the granular material behind the steered out TowPlow trailer. This stainless steel hopper is designed specifically for the TowPlow trailer and is currently the only size available. An optional brine

Copyright 2018. the authors

Vermeer Manufacturing Company – Ex. 2045
Kubota v. Vermeer
IPR2025-00168
Page 21 of 182

pre-wet system can be added to the prime mover truck's sander body configuration to promote the adhesion of the granular material to the road surface. An alternative TowPlow configuration is also available that adds the function of direct brine application to the highway through three separately controllable spray banks on the TowPlow trailer. In such a configuration, one to three lanes can be covered and the trailer can have an onboard liquid carrying capability up to 2,740 liters (725 gallons) for the direct brining function.

Literature Search/Survey of States

The TowPlow is a relatively new piece of snow-fighting equipment first developed for commercial use in 2008 [40]. The system consists of a truck, frequently with a front plow, often referred to as the prime mover truck, and a steerable trailer with a moldboard for plowing snow. The concept is to allow a single truck to plow two lanes. The concept was patented in 2008 [40]. The claimed benefit of the TowPlow is that it reduces the number of vehicles required for plowing the road. Since the TowPlow's commercial release, several organizations have been integrating TowPlow systems into their snow-fighting fleet.

The Maine Department of Transportation (DOT) began a 2-year evaluation of the TowPlow starting in 2009 ([13] and [14]) using a truck rated at 274 kW (375 hp). Overall, the report presents a positive review of the TowPlow. The report notes that there were 4 instances where the TowPlow system could not climb a hill and the operator had to back down and retry to before successfully ascending the hill. This issue may be resolved by using a higher power prime mover truck or by increasing traction. To follow are the key recommendations to improve the TowPlow from the Maine reports:

1) Improve the salt application capability of the TowPlow trailer,
2) Improve the pre-wetting system,
3) Enable salt application from both the TowPlow and prime mover truck for Interstate applications,
4) Improve the hook-up and removal procedures,
5) Improve the hopper cover,
6) Consider Purchasing a laser alignment system,
7) Increase the maximum power of the prime mover truck.

Wisconsin DOT performed an evaluation of the TowPlow [51]. A noteworthy observation contained in the report is "The comparison was made for highways with two lanes per direction because the TowPlow does not provide any additional benefits compared to a single snowplow with wings for two lane undivided highways." This provides some insight as to what types of roadways the system should be used on. This report compares the TowPlow to regular snowplows (without wings) and shows that the TowPlow becomes cost effective after about 1,350 hours of plowing. The report shows that the operational cost of the TowPlow is 32%-43% lower than using two snowplows.

Ohio DOT also performed an evaluation of the TowPlow [52]. They compared a TowPlow and a wing snowplow. Their report shows that it takes 1.71 wing snowplows to equal a single TowPlow. Figure 2 (from the Ohio report) gives a list of suggested considerations to use when

Copyright 2018. the authors

Vermeer Manufacturing Company – Ex. 2045
Kubota v. Vermeer
IPR2025-00168
Page 22 of 182

deciding to implement a TowPlow. The most notable comment relevant to Caltrans implementation is that the power of the prime mover truck is an issue in areas that have hilly terrain.

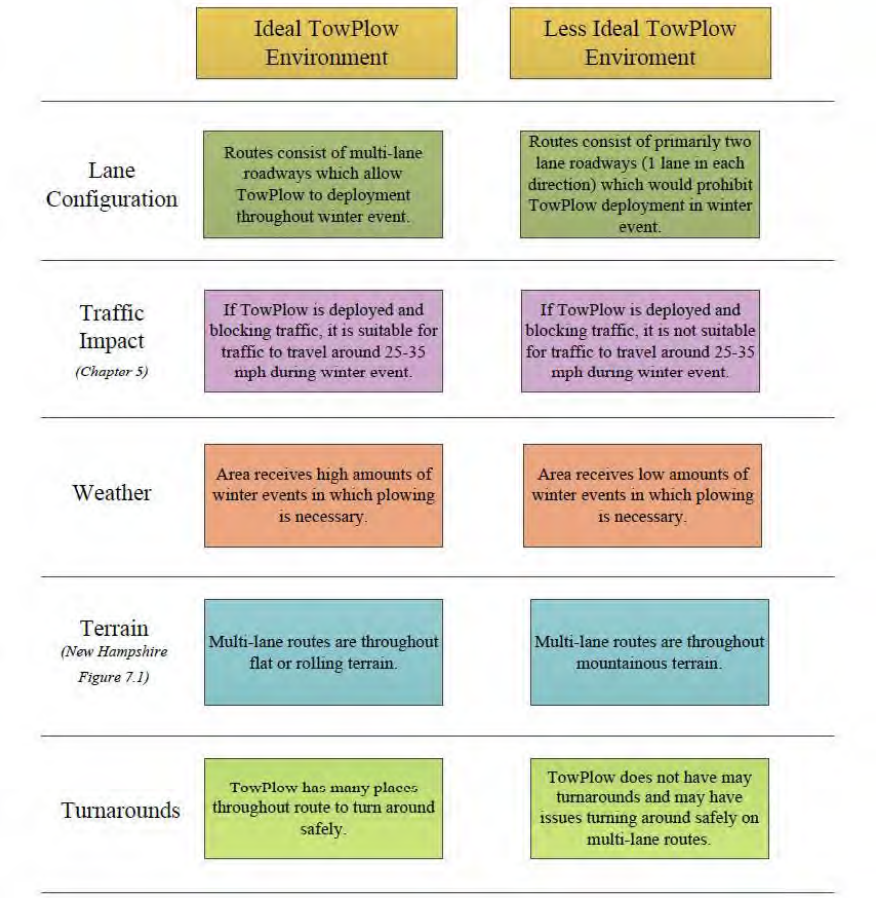


Figure 2. Ohio DOT identified considerations TowPlow implementation [52]

A TowPlow study was also performed by Brun-Way Highways Operations, Inc., a Canadian road construction company [15]. This report points out that the fuel savings is not as high as expected since a more powerful prime mover truck is needed to pull the trailer. This report mentions that the system requires more power in order to maintain an acceptable speed when going up hills.

The American Association of State Highway and Transportation Officials (AASHTO) also produced a report on the TowPlow [11]. This report identifies an operational safety benefit of the TowPlow over more traditional equipment. One safety benefit highlighted is that the TowPlow trailer is pushed to a position behind the prime mover truck when it hits a fixed object. This is different than a wing snowplow where the impact puts a torque on the truck's frame and may

Copyright 2018. the authors

Vermeer Manufacturing Company – Ex. 2045
Kubota v. Vermeer
IPR2025-00168
Page 23 of 182

result in a spin of the snowplow. The authors also comment that a TowPlow is more responsive than a wingplow making collision avoidance maneuvers easier.

Report Outline

The goal of this research work was to develop an understanding of the efficacy of Viking-Cives TowPlow in Caltrans' winter snow-fighting operations. This report documents the results of the research. Earlier in the chapter, the TowPlow system was introduced and literature review of the use of the TowPlow in other states reported. Chapter 2 discusses an analytical study of the dynamics and stability of the TowPlow system in general. Chapter 3 presents some of the considerations necessary for implementation in California. Chapters 4 and 5 discuss the purchase of an initial TowPlow trailer and report on early experiences that lead to the development of specifications for the purchase of a second system. Chapters 6, 7, and 8 discuss the purchase and experiences with the second TowPlow system, which lead to modifications necessary for operation on California's highways. Initial measurements on the final modified second TowPlow system are discussed in Chapter 9. While the lack of sufficient snow to test the TowPlow systems over the last 3 years has inhibited the collection of performance data, a data post-processing scheme has been developed that will allow quick and easy performance evaluation in future years. This post-processing approach is discussed in Chapter 10. Finally, Chapter 11 provides conclusions.

A few items are noted as follows. First, the various TowPlow systems are given specific nomenclature to avoid confusion as they are discussed in more detail later in this report. The lack of snow has prevented the complete evaluation of the TowPlow system for use in California and it is anticipated that a follow on project will allow continued data collection and support of the TowPlows in future years. Lastly, this document reports work through June 30, 2015. This cut off date was selected since there are still issues that need to be resolved at the time of this report's writing.

Copyright 2018. the authors

Vermeer Manufacturing Company – Ex. 2045
Kubota v. Vermeer
IPR2025-00168
Page 24 of 182

CHAPTER 2:
DYNAMICS AND CONTROL OF THE TOWPLOW

As noted in Chapter 1, the TowPlow is a unique type of snowplow system consisting of a conventional snowplow and a steerable trailer-mounted plow. With a 12-foot front plow and a 26-foot moldboard equipped at the trailer, the TowPlow is capable of clearing two typical highway lanes by steering the trailer up to 30 degrees relative to the prime mover truck. Although the TowPlow has seen increased use in North America, no engineering evaluation has been documented. A fundamental engineering analysis can provide significant understanding of the behavior of the TowPlow. Of primary concern is the path of the TowPlow through various maneuvers that are typically encountered in actual plowing operations. For example, the TowPlow system will need to traverse curves on a regular basis, yet no work has examined the TowPlow's path and whether it will intrude into adjacent lanes of traffic. More importantly, the stability of the TowPlow system is essential as it climbs and descends mountain roads in low friction winter conditions.

This portion of the research provides detailed dynamic modeling of the TowPlow, experimental validation of the model, control system design, and dynamic simulations for various maneuvers. The goal of this modeling is to understand the dynamic performance of the TowPlow and to suggest modifications to improve its safety and efficiency. Appendix A includes the details of this dynamics and control analysis of the TowPlow, which is summarized to follow.

A literature survey is provided on existing modeling and control methods for articulated vehicles, since the TowPlow is a kind of the articulated vehicle with trailer steering feature. The literature is reviewed in the following categories: kinematics, dynamics, snow resistance, and stability control.

Then, the kinematic characteristics of the TowPlow are evaluated with the use of an extended bicycle model of the TowPlow. Kinematic equations that relate velocity of each axle and the articulation points and rotation of the prime mover truck and trailer are derived using the 'instantaneous centers of velocity'. Kinematic simulations of the constant radius turning are performed, and the results clearly demonstrate that trailer's corrective steering is necessary for the TowPlow to maintain its total articulation angle.

A linear dynamic model of the TowPlow is then developed that considers lateral and yaw motion and the TowPlow's stability is evaluated. In addition to the typical linear dynamic model of the tractor-trailer combination, linearization of the trailer steering angle and total articulation angle around their operating angle is suggested. With the developed model, stability and controllability of the system are evaluated for various longitudinal velocities and inertia combinations. Also, dynamic responses of the TowPlow to the inputs like step, pulse and sine are demonstrated with and without the trailer's corrective steering. The responses clearly show that

Copyright 2018. the authors

Vermeer Manufacturing Company – Ex. 2045
Kubota v. Vermeer
IPR2025-00168
Page 25 of 182

the corrective steering, even though it is obtained from kinematics, helps the TowPlow reduce deviation of the total articulation from its initial angle.

Next, the nonlinear dynamic model of the TowPlow for longitudinal, lateral, and yaw motions is provided. The model considers nonlinearity through a modified Dugoff's tire friction model, tire rotation dynamics, and quasi-static load transfer. A set of vehicle experiments is conducted to validate the developed model in steady-state and transient conditions. The comparison between the experiment data and simulation results demonstrate that the model accurately predicts the dynamic performance of the TowPlow.

For the completion of the nonlinear dynamic model of the TowPlow, the snow resistance model, which makes the TowPlow different from ordinary tractor-trailer combinations, is proposed. Ideas of two existing models – control volume method and snow compressibility effect – are combined to develop the new model. Longitudinal and lateral snow forces calculated with the proposed model compare more favorably to experimental data than the existing models. Also, dynamic simulations of the nonlinear TowPlow model including the snow resistance model applied to each plow are conducted for cornering, slalom, up and down hill and split friction coefficient braking maneuvers, which the TowPlow is expected to encounter during its snow removal operation. In accordance with the kinematic and linear analyses, the simulation results show that the TowPlow's trailer intrudes into the adjacent lane or misses large portions of the road during the maneuvers.

Active steering control of the trailer axle to improve safety and efficiency of the TowPlow is then proposed. Active control of the trailers of articulated vehicles has not been implemented due to the relatively high expense of actuators, which are not normally present. However, in the case of the TowPlow, the trailer wheels are already steerable through on board actuators. As such, active trailer steering control can easily be implemented and the primary emphasis of this work is thus on algorithms to positively impact the vehicle's stability.

For the control algorithm, Linear-quadratic regulator (LQR) control, based on the linear TowPlow model developed and Proportional-Integral (PI) control are proposed and their performances are evaluated through dynamic simulations for various maneuvers. The comparison of the simulation results between the controlled system and the uncontrolled system clearly demonstrates that the implementation of active steering control for the trailer axle will improve safety and efficiency of the TowPlow. Such control keeps the TowPlow from either intruding into the adjacent lane or missing large portions of the lane by maintaining its total articulation angle in its snow removal operation.

Copyright 2018. the authors

Vermeer Manufacturing Company – Ex. 2045
Kubota v. Vermeer
IPR2025-00168
Page 26 of 182

CHAPTER 3:
CALTRANS TOWPLOW CONSIDERATIONS

This chapter summarizes issues concerning the implementation of the TowPlow in Caltrans' winter snow clearing operations. The issues are first discussed. Then, the corrections taken to ensure that the TowPlows of this research project meet California's needs are presented.

Chain Controls:

Interstate 80 over the Donner Pass is a location with high potential for implementation of the TowPlow. Chain control restrictions are regularly instituted on this route during snow season and these typically coincide with most snow removal operations. Other potential TowPlow deployment sites less likely to require chain controls include State Route 58 near Tehachapi between Bakersfield and Mojave, Interstate 15 over Cajon Pass between Victorville and San Bernardino, and Interstate 5 over Tejon Pass between Los Angeles and Bakersfield. When highway chain control restrictions are instituted, vehicles towing trailers with brakes are required to have chains on at least one trailer axle. On trailers with multiple axles and anti-lock braking systems (ABS), typically only one axle is fitted with the ABS. Chains are placed on the trailer's ABS equipped axle. Operating the TowPlow with tire chains is unique to Caltrans and the current TowPlow's fender design lacks sufficient tire chain clearance. The TowPlow manufacturer recommends against the use of tire chains. However, as California requires chains, efforts to allow for chain use on the TowPlow were made.

It is necessary to test how well the TowPlow will function with chains. A chain-equipped TowPlow will have a higher coefficient of friction between the tires and the road. In is anticipated that the additional friction due to the chains will help to keep the outer edge location of the TowPlow's moldboard at a more consistent location on the road.

The Onspot chain system shown in Figure 3 was also investigated. The system is deployed from the cab through a pneumatic actuator. When actuated from a switch in the cab, a wheel outfitted with chain segments is lowered in such a manner that a friction drive contacts the inside of the vehicle tire. This causes the chainwheel to rotate, which creates enough centrifugal force to flail the chains out in front of the tire. The system can be considered an "on-demand" chain system. One major challenge to implementing this system on the TowPlow is that the axles are steerable, which is atypical. It was decided that traditional tire chains provide the best solution for the TowPlow.

Copyright 2018. the authors

Vermeer Manufacturing Company – Ex. 2045
Kubota v. Vermeer
IPR2025-00168
Page 27 of 182



Figure 3. Onspot chain system [www.onspot.com]

Steep Grades:

In California, significant snowfall and icy conditions are generally limited to higher mountain passes. The major highways and routes over these passes contain grades up to 6 percent and can stretch for several miles. Caltrans Division of Maintenance has an interest in operating TowPlow systems in the following locations:

- District 8 Interstate 15 - Cajon pass has 6 percent grade for 4 miles
- District 7 Interstate 5 - The Grapevine has 6 percent grades over 5 miles
- District 3 Interstate 80 - Donner Pass has 3 to 6 percent grades stretched over 30 miles.

In contrast, TowPlow applictions in states other than California have fairly uniform statewide winter conditions and relatively flat terrain.

The TowPlow system is 40% heavier than just the prime mover truck alone, but has the same overall power and drive axle traction, critical factors for climbing grades. The extra weight reduces travel speed and snow pushing capability due to the much greater power demands. All the added weight increases the demand for drive traction, while only a portion of it contributes to traction availability. For the Caltrans application of plowing snow on steep mountain grades, the prime mover snowplow used with the TowPlow must have significantly more power than the standard snowplow in order to provide comparable snow clearing performance.

Dedicated Operators:

TowPlow system operational controls can range from basic to complex depending on system capabilities, configuration and the level of control desired. All TowPlow systems have in common a basic 4-position joystick that controls the moldboard and trailer steering. Surface treatment application capabilities increase the complexity of the TowPlow's controls. A TowPlow configured with a basic direct application brine system can be controlled with simple toggle switches and operated by a typical experienced Caltrans plow operator. However, TowPlow's are available with increased capabilities that require more complex controllers. For example, a TowPlow can be configured to allow granular, pre-wet and direct brine application treatments simultaneously from both the prime mover truck and the TowPlow trailer. Such a

Copyright 2018. the authors

Vermeer Manufacturing Company – Ex. 2045
Kubota v. Vermeer
IPR2025-00168
Page 28 of 182

multifunctional system requires a complex controller, or Programmable Logic Controller (PLC) and Viking-Cives offers a fully integrated Force America controller package specifically designed for such a system. The complete TowPlow Force America controller system has feedback sensing for accurate application control and a cellular telemetry unit to support web based system data collection. This type of controller requires much additional training and thus it may be appropriate to designate dedicated plow operators for such complex machines.

Off Season Uses:

The TowPlow was developed exclusively for winter snow-fighting operations. In order to improve the cost benefit value of the TowPlow system, additional non-winter uses for the TowPlow should be identified and developed. Some ideas for potential future TowPlow use are in the support of wildfire fighting operations or as a traffic barrier for improved worker highway safety.

Copyright 2018. the authors

Vermeer Manufacturing Company – Ex. 2045
Kubota v. Vermeer
IPR2025-00168
Page 29 of 182

CHAPTER 4:
TOWPLOW1 PROCUREMENT AND TESTING IN THE 2012-13 WINTER SEASON

The first step towards implementation in Caltrans winter operations was the purchase and use of a TowPlow in actual snowplowing operations. Such an approach would allow for the identification of an optimum TowPlow system configuration for use in California, as well as best practices to maximize system performance and efficiency. As such, a single TowPlow trailer was purchased with intent of implementation during Fall 2012. Then, a second system could be best configured and purchased for the following winter season. This chapter reports on the experiences and challenges associated with this initial TowPlow unit and its use in winter operations.

TowPlow1 Configuration:

The TowPlow research project was started in April 2012. Since the TowPlow can only be tested during the snow season, any delay in deployment would delay testing a full year. Therefore AHMCT needed to purchase a TowPlow trailer immediately in order to meet the 4-month development window and have the TowPlow in service by the beginning of the Caltrans snow season in early November. The Caltrans technical advisory group (TAG) selected the direct brine application version TowPlow over the granular application configuration, and Viking-Cives developed a standard purchase specification. The TAG subsequently reviewed and approved the specification, and the purchase order was expedited at the University of California at Davis (UC-Davis). The TowPlow was registered and assigned to the UC-Davis fleet. Caltrans designated a District 3 fleet snowplow without a wing plow (C537266) as the prime mover truck to be adapted to support the operation of the TowPlow. This first TowPlow and snowplow is collectively referred to as TowPlow1.

TowPlow1 Operational Controls:

Viking-Cives TowPlows have the appearance of a self-contained system, but in actuality they function like an attachment or implement. The prime mover truck provides all power and control to the TowPlow trailer through a series of quick-connect hoses and electrical cables mounted on the hitch plate. The hydraulic valves that control the moldboard and steering cylinders of the TowPlow system are typically on the prime mover truck, which additionally houses the application motors and pumps. The electronics, which control these valves, are also typically integrated onto the prime mover truck's platform. It was desirable to use a standard Caltrans fleet snowplow as the prime mover truck, but these do not have the needed components. As such, the additional hydraulic control valves that are needed to operate the TowPlow were installed on the TowPlow trailer. Also, an electrical enclosure was added to contain the additional electrical control connections. A basic in-cab control box was developed and connected to the TowPlow electrical enclosure with a multiple conductor cord. In doing so, the driver then had access to a 4-

Copyright 2018. the authors

Vermeer Manufacturing Company – Ex. 2045
Kubota v. Vermeer
IPR2025-00168
Page 30 of 182

position electrical joystick to control the TowPlow's moldboard and steering, along with toggle switches to individually power the brine spray nozzle banks. The Caltrans' standard Muncie controller powered the brine pump using the spinner circuit, which is proportionally linked to ground speed. Other toggle switches for various beacon and work lights for trailer lighting were also included on the control box.

One new feature required by Caltrans was an "Auto Return" feature, which retracts both the steering and moldboard on the TowPlow with a single push of a button. This provides for both improved safety and operator convenience. The first Auto Return feature developed for the TowPlow1 system was a combination of latching relays in the control box that retracted the moldboard and steering for a set time interval. A flashing light and beeper gave the driver positive affirmation that the TowPlow was in the process of being retracted.

Telemetry Unit

AHMCT installed a Precise IX-101 data telemetry unit in the electrical enclosure on TowPlow1. The Precise IX-101 is a basic data collection unit with built-in Global Positioning System (GPS) tracking. This unit relays the collected information to Force America (the manufacturer of the Precise unit) through a wireless network. Force America stores the collected data on their server and provides their customers with remote access. This allows for web-based remote monitoring of the equipment. The GPS system provides the TowPlow's location and speed information. In addition to the GPS data, the IX-101 has 2 input/ouput (IO) channels. One indicates whether the moldboard is in the retracted position and the other input registers when the trailer axle is in its stowed position (i.e., unsteered). The collected data can be sorted and filtered to develop a good representation of the TowPlow activities on the highway.

System Hydraulics:

The standard Caltrans snowplow utilizes an open center hydraulic system driven by a gear pump and utilizes air over hydraulic valves. Viking-Cives TowPlows operate on a closed center hydraulic system driven by pressure compensated pumps and utilize electrical over hydraulic valves. Based on the incompatibility of the two hydraulic control approaches, it was necessary to develop a method to adapt the TowPlow to standard Caltrans snowplow vehicles. The first TowPlow hydraulic adaptation developed by AHMCT provided full TowPlow control, but tended to cause hydraulic oil overheating when the system ran for a prolonged period with the moldboard retracted. This was due to a buildup in hydraulic pressure, which can only be relieved by passing the fluid through a pressure relief valve in the system. The short snow season ended and the TowPlow was returned to UC-Davis before the overheating problem could be mitigated.

Conventional TowPlows' moldboards do not float when deployed, but instead use rubber bumpers to hold a fixed moldboard height when plowing. In contrast, Caltrans front and wing plow designs provide for float and therefore it was determined that the TowPlow's moldboard should also float thus allowing for accommodation to the pitch of the roadway. Moldboard float was added to the TowPlow1 system by simply driving the lift cylinder valve spool to relief while the moldboard is deployed.

Copyright 2018. the authors

Vermeer Manufacturing Company – Ex. 2045
Kubota v. Vermeer
IPR2025-00168
Page 31 of 182

Adaptation for the Use of Chains

As stated above, it was necessary to incorporate chains on the TowPlow trailer. The gap between the air pod and the tire presented a clearance issue. In order to increase this distance, two changes were made. First, narrower tires with similar load ratings as the stock TowPlow tire were installed. Then, the new tires were mounted on rims with a higher offset.During year one testing, AHMCT modified the factory fender brackets to relocate the fender. The modified fender brackets provided increased radial clearance for chains and also added the capability of easily removing the fenders.

Operator Training

Prior to the 2012-13 winter season, operator training occurred at the Caltrans' Maintenance Equipment Training Academy (META). This involved general TowPlow training provided by Viking-Cives, which also allowed Viking-Cives to disseminate some of their user experiences to Caltrans maintenance personnel. Also, additional training was provided on the customized features that AHMCT implemented.

TowPlow1 Testing and Results:

Due to the unusually short and light snow season, the TowPlow1 system saw minimal use plowing snow during the winter of 2012-13. The TowPlow's ability to clear even average snow accumulation was never tested. Caltrans plow operators drove the TowPlow1 system over the Interstate 80 grades in the absence of snow to develop experience operating the system. Additionally, this allowed them to develop an understanding of the TowPlow1's capability to overcome typically encountered grades. Caltrans plow operators driving the TowPlow1 system climbing the steepest Donner summit grades on dry pavements were only able to attain speeds of 27-37 km/h (17-23 mph) with a loaded system. Also, plow operators were doubtful that the prime mover truck (Caltrans C537266 snowplow) possessed sufficient power to clear a moderate snow accumulation on such slopes.

In an effort to quantify the necessary power for the prime mover, Caltrans had the C537266 prime mover truck tested on a dynamometer, which measured the actual power output at the drive wheels. The measured power output was 252 kW (338 hp). The dynamometer technician estimated that approximately 20% of power is lost through the drivetrain. Accordingly, the power rating for the engine was estimated at 317.5 kW (425 hp). During the test, it was discovered that the diesel particulate filter (DPF) had failed. It is noted that an operational DPF would result in reduced power output.

The TAG decided that a more powerful Caltrans prime mover truck would have to be identified to replace the snowplow currently paired with the TowPlow trailer. Without a sufficiently powered TowPlow prime mover truck, the TowPlow trailer would not be usable. Additionally, the oil overheating issue would need to be addressed. The TowPlow1 trailer was returned to UC-Davis to begin the rebuilding process for the 2013-14 snow season testing.

Based on the experience gained during year one, the Division of Equipment (DOE) further improved the fender system design to better allow for chain usage. DOE replaced the factory

Copyright 2018. the authors

Vermeer Manufacturing Company – Ex. 2045
Kubota v. Vermeer
IPR2025-00168
Page 32 of 182

provided plastic fenders with metal fenders and also modified the fender brackets to further increase the clearance.

Copyright 2018. the authors

Vermeer Manufacturing Company – Ex. 2045
Kubota v. Vermeer
IPR2025-00168
Page 33 of 182

CHAPTER 5:
TOWPLOW1 DEVELOPMENT AND TESTING IN THE 2013-14 WINTER SEASON

The TowPlow1 system was returned to UC-Davis for rebuilding in summer 2013. Caltrans assigned a new snowplow with a 355 kW (475 hp) motor as the prime mover truck. AHMCT rebuilt the TowPlow trailer's hydraulic and control systems to accommodate the prime mover truck change and to mitigate other issues. Also, AHMCT rebuilt the TowPlow's controller at the UC-Davis Advanced Transportation Infrastructure Research Center (ATIRC) and the updated TowPlow1 system was deployed to Caltrans District 3's Truckee maintenance facility in November 2013 for winter operational testing. This chapter reports on specifics of the system updates, issues encountered during use of the updated system, and other issues associated with the use of the TowPlow in future years.

TowPlow1 Hydraulic Modification

In order to simplify the hydraulic system, the individual hydraulic valves utilized on the TowPlow1 system were replaced with a single valve block. The previous hydraulic system had a backpressure issue that caused the TowPlow's moldboard to rise when any of the prime mover truck hydraulic cylinders were dead-headed. The solution was to install a pressure sensor in the TowPlow's hydraulic return line and pause the float mode until the backpressure state ceases. This mitigates the TowPlow backpressure issue without making any changes to the Caltrans prime mover truck.

Also, the brine pump was not generating sufficient pressure to operate the brine nozzle banks on the TowPlow1 system. This was diagnosed as originating from the prime mover truck's hydraulic system. This issue was not was not addressed in TowPlow1 as it would be resolved in the later modifications performed by DOE.

TowPlow1 Controls Development

The TowPlow1 controls were upgraded with a basic programmable logic controller (PLC) with a small in-cab operator interface that utilized a graphical display. The PLC was necessary to support expanded system functionality and more sophisticated control logic in order to improve the performance of the TowPlow1. The PLC also reduced the wiring requirements from the TowPlow trailer into the prime mover truck's cab. The additional functionality included operator configurable Auto Return function controls, active hydraulic system backpressure mitigation and enhanced operator system status indicators. The increased controller automation simplified system operation while reducing the operators' training requirements. The TowPlow1 retained the Precise IX-101 data telemetry unit, and the TowPlow IO input sensors were upgraded.

Copyright 2018. the authors

Vermeer Manufacturing Company – Ex. 2045
Kubota v. Vermeer
IPR2025-00168
Page 34 of 182

TowPlow1 Operation Testing and Results

AHMCT provided basic TowPlow1 operator training to a Caltrans District 3 permanent equipment operator. This operator subsequently trained 2 other equipment operators in the Truckee maintenance station who were assigned to operate the TowPlow1 system in the 2013-14 snow season. Once again, the snow season was unusually light and the TowPlow1 plowing performance could not be evaluated. However, operators did gain experience operating the TwoPlow1 on Interstate 80 in winter conditions and were able to assess system performance issues. The TowPlow usage caused the hydraulic backpressure sensor to fall out of adjustment thus inerfering with moldboard lifting commands. The TAG recommended removing the TowPlow from service based on this failure.

TowPlow1 - Caltrans Operator Survey

AHMCT conducted a detailed survey of operators on their experience with TowPlow1 at the end of the 2013-14 snow season. The 475 hp snowplow with Caltrans standard hydraulic system was employed as the prime mover truck during that snow season. This survey's purpose was twofold - operator feedback would allow for evaluation of the effectiveness of TowPlow1 and would also drive the development of specifications for the purchase of the second TwoPlow system. Due to the lack of snow, there was a minimal amount of experience with the TowPlow1 and only 5 operators completed the survey. Appendix B includes all details associated with the survey.

The survey first addressed the material application functionality of the TowPlow. Results indicated that operators prefered a machine that is capable of applying sand behind both the truck and trailer and also indicated that application rate should be logged as part of a data collection system.

The next group of questions focused on operational safety. Generally speaking, the operators showed a desire to improve visibility for both the operator and the travelling public. In general, the operators did not support the use of a rear view camera system unless the system is robust and can be proven to work in snow conditions. The operators were interested in including the Laserline system, which provides feedback on the location of the TowPlow's moldboard when it is deployed. Lastly, the operators were not interested in the use of the Onspot system for the TowPlow.

The operators generally felt that the TowPlow system has the potential to improve winter snow clearing operations. Concerning TowPlow's operator controls, most of the operators felt that the controls were simple to understand, and all respondents indicated preference for additional training. Operators felt that Auto Return functionality would be critical for efficient operation.

AHMCT was interested in the overall snow-fighting process. Survey results indicated that surface treatments were typically only applied on the ramps and high-speed travel lanes. Brine was applied both before and after the storm, while granular abrasives were applied during and after the storm.

Copyright 2018. the authors

Vermeer Manufacturing Company – Ex. 2045
Kubota v. Vermeer
IPR2025-00168
Page 35 of 182

The survey results proved valuable in several ways. First, the results helped in the development of purchase specifications for TowPlow2. As a result, camera and laser guidance systems were included in order to help improve operator visibility. Second, it was made clear that a prime mover truck with maximum possible power is highly desirable. Lastly, it would be beneficial for the next system to be able to apply both sand and brine, but if only one were possible, then a sanding system would have priority.

TowPlow1C - Caltrans Modified System for the 2014-15 Winter Season

In preparation for the 2014-15 winter season, the TAG decided that TowPlow1 should be transferred into the Caltrans fleet. After the transfer, DOE switched the prime mover truck's hydraulic system from the typical Caltrans open center system to a closed center system. This modification allowed for the TowPlow trailer to be operational in its "as delivered" state and was done because testing had revealed such would result in the best TowPlow system performance. AHMCT staff did not participate in these modifications. Accordingly, the interested reader should contact Caltrans DOE for details. TowPlow1 as modified by Caltrans DOE is referred to as TowPlow1C.

TowPlow1 and 1C Performance Evaluations

TowPlow system performance has been very difficult to assess during the course of this project due to insufficient snow. However, AHMCT has developed post-processing methods to present the on-board acquisition's system data in an intuitive and easy way with the goal of maximum understanding of the TowPlow's use in future operations. This data post-processing approach is provided in detail in Chapter 10.

Data Acquisition System

AHMCT outfitted the TowPlow1 and TowPlow1C systems with a Precise IX-101 data collection unit. The IX-101 is a basic data collection unit that has built in GPS. This unit relays the collected information to Force America through a wireless network, which allows the data to be remotely monitored while the equipment is in the field. The GPS system provides system location information and helps to give a sense of vehicle speed.

In addition to the GPS, the IX-101 has 2 IO channels that are connected to two sensors. One sensor changes state when the trailer deviates from the stowed position. The other sensor indicates whether the system is spraying brine. The data will be employed in the storm reporting data post-processing developed in Chapter 10.

Performance Summary

The ability of the TowPlow system to navigate the expected grades during plowing is of critical concern. This is primarily based on the power of the prime mover truck. Based on the lack of snow, insufficient data has been acquired to discuss system performance in great detail. Operator feedback through the noted survey results has indicated that the highest powered prime mover truck available is desireable.

Copyright 2018. the authors

Vermeer Manufacturing Company – Ex. 2045
Kubota v. Vermeer
IPR2025-00168
Page 36 of 182

CHAPTER 6:
TOWPLOW2 PROCUREMENT

The TAG desired that the second TowPlow be a Viking-Cives standard turn-key configuration. The turn-key reference is meant to indicate that the TowPlow could be purchased from the vendor in a configuration that requires no significant modifications to be integrated into the Caltrans fleet. The TAG desired that AHMCT have Viking-Cives submit a specification and quote for their standard configuration, identical to the units built and operated in other state DOT's such as Nevada (see Figure 4). Since Caltrans may potentially add several TowPlow units to their fleet, it would be advantageous if future units could be purchased without any necessary modifications from a standard, commercially available configuration. The perception was that since other states are successfully operating standard TowPlow systems, that Caltrans could also deploy a standard system in California. Standard TowPlow systems are purchased with a prime mover truck. The mated prime mover truck provides the power and control systems to operate the TowPlow system. As such, AHMCT was directed to purchase a prime mover truck with maximum available power in combination with the TowPlow trailer. This chapter discusses some aspects of the TowPlow configuration selected and the procurement process.



Figure 4. Nevada DOT sander body TowPlow

TowPlow2 Configuration

AHMCT developed a specification and quote for the turn-key TowPlow system, which will be referred to as TowPlow2 hereafter. This involved developing specifications for both the truck and the trailer. TowPlow1 has a brining trailer. For TowPlow2, Caltrans desired a trailer that could accomplish both brining and sanding operations. Based on the experience gained from using the first unit in the Donner Pass area, it was also determined that buying a truck from the

Copyright 2018. the authors

Vermeer Manufacturing Company – Ex. 2045
Kubota v. Vermeer
IPR2025-00168
Page 37 of 182

vendor would be the best approach for obtaining a turn-key unit. During the procurement process of TowPlow2, the vendor was required to allow for chain use on the TowPlow. The vendor redesigned the fender brackets so that they are removable and to provide adequate chain clearance.

Sanding TowPlow

The typical operation involves sanding behind the snowplows during chain control events. Thus, TowPlow2 was primarily designed for use as a sanding unit. The TowPlow trailer can be purchased with a 6.0 m^3 (7.8 yd^3) sander body in place. This version of the TowPlow trailer typically comes with an 852 liter (225 gal.) pre-wet tank. Viking-Cives has an additional configuration that replaces that tank with a larger 2,840 liter (750 gal.) tank. The larger tank can feed a Vari-tech spray system for direct liquid application. This configuration was selected based on feedback from the Division of Maintenance, which expressed an interest in being able to brine with the system. This goal was to maximize the methods of operation of the system.

Based on previous experience, it was determined that the single most important factor for the success or failure of the TowPlow system is the prime mover truck. As noted, all operators reported a desire for additional power delivered by the prime mover truck. Additionally, functionality and safety are critically important.

The prime mover truck's power rating was the single most important truck specification. A simple analysis was performed which illustrates the power demands of the system and this analysis is presented in "Appendix C: Power vs. Performance Analysis". Caltrans standard fleet vehicles have a power rating of 325 kW (435 hp). During the project, Caltrans had a truck available that was rated at 355 kW (475 hp), which is currently being used as the prime mover truck for TowPlow1C. Experience showed that this truck faced some challenges pulling the fully loaded system, particularly up steep grades. Through discussion with the TAG, it was determined that a prime mover truck with the maximum power available be acquired. Initially, AHMCT was informed that 374 kW (500 hp) was the maximum power available for a snowplow obtained through the vendor. The limitation on engine size was due to interference issues with the radiator and the front mounted hydraulic pump. Through an iterative process, Viking-Cives was able to convince Western Star Engineering to ultimately assemble a TowPlow compatible truck with a 411 kW (550 hp) rating.

A camera system was added to the prime mover truck in order to facilitate operation. The system installed on the prime mover truck has 2 wireless cameras and an in-cab display. One camera is mounted below the dump bed. The point of this camera is to aid in connecting the TowPlow trailer to the prime mover truck. Another camera is mounted on the passenger side mirror to give the operator an additional view of the operational area of the trailer. This system is easily expandable and a third camera may be added. This third camera would be mounted on the rear of the prime mover truck with the intent of providing a view of the area the trailer occupies when stowed. There were some instances in which vehicles drove so close to the prime mover truck that the trailer could not be retracted. The third camera would help the operator monitor such situations.

Copyright 2018. the authors

Vermeer Manufacturing Company – Ex. 2045
Kubota v. Vermeer
IPR2025-00168
Page 38 of 182

A GL3000PMC laser line was also added to the prime mover truck to provide the operator with a forward projected reference point of the TowPlow trailer's position when fully deployed. As an added level of safety, the system was wired such that when the TowPlow trailer deviates from the stowed position, the laser automatically turns on. This is not controlled programmatically, but is directly connected to the switch that indicates a stowed TowPlow trailer. As such, if the trailer deviates from the stowed position for any reason, the operator will have a visual cue.

Sanding capability was also added to the prime mover truck. The sanding system on the TowPlow trailer is typically limited to providing single lane coverage. In order to eliminate a truck from the overall snow clearing pack, the lane behind the prime mover truck needs to have sand coverage. By placing a sander in the back of the prime mover truck, both lanes can be covered. Alternatively, an additional truck will need to follow behind the prime mover truck for sand placement. If a separate sanding vehicle is required, the ability to reduce the number of vehicles in a snow clearing operation though use of the TowPlow is diminished. The Viking-Cives standard sanding package consists of a 7.3 m^3 (9.5 yd^3) slip-in sander in the prime mover truck's bed.

Circulated Specifications

The specifications for TowPlow2 were circulated through the various functions in Caltrans for review and approval. Throughout the process, there were some minor changes to the specifications. Most notably, the front moldboard was changed to be consistent with the Caltrans standards. The TAG agreed upon the modified specifications.

Copyright 2018. the authors

Vermeer Manufacturing Company – Ex. 2045
Kubota v. Vermeer
IPR2025-00168
Page 39 of 182

CHAPTER 7:
PRELIMINARY EVALUATION OF TOWPLOW2

The TowPlow2 system was procured and delivery to AHMCT occurred on December 27, 2014. On January 8, 2015, Caltrans DOE personnel conducted a pre-delivery inspection of the TowPlow2 system in the ATIRC facility at UC-Davis. This chapter reports on the delivered unit.

Arrival of the TowPlow2

TowPlow2 is shown in Figure 5. The vendor came to ATIRC on January 8, 2015 in order to review the equipment with the AHMCT team and provide initial operational training. Caltrans was invited to inspect the equipment on the same day. This was done in an effort to expedite acceptance of the purchase and ultimate field deployment for the 2014-2015 snow season.



Figure 5. The as-delivered TowPlow2

The vendor was on hand with two goals in mind. First, the vendor wanted to familiarize AHMCT staff with the physical hardware. Another key goal was to work with AHMCT in order to understand the Force America programmable logic controller. This controller, which was not included on TowPlow1, is very different than the Muncie controller, which is employed in standard Caltrans snowplows. Ultimately through the deployment of TowPlow2, software updates may be required and will be provided by the vendor. The AHMCT team's initial

Copyright 2018. the authors

Vermeer Manufacturing Company – Ex. 2045
Kubota v. Vermeer
IPR2025-00168
Page 40 of 182

impression was that the Force America controller appears to be very robust and user-friendly system.

Caltrans Division of Equipment performed a detailed inspection of the equipment[1] at the ATIRC facility. The inspection's purpose was to identify major issues that needed to be addressed prior to field deployment. During the inspection of the equipment, DOE felt that the system could be overloaded. This issue was also brought to the attention of the vendor, who was present. The vendor stated that many states, including Nevada DOT, routinely operate their TowPlow sanding systems in an overloaded state on the highway. They reason that the load diminishes as the sand is dispensed and that the machine is being operated in a workzone. This issue was later presented to the TAG group for consideration. The group decided that TowPlow2 must conform to legal weight limits when fully loaded, as it may need to travel outside of a workzone before being used. Therefore, Caltrans DOE engineers requested that AHMCT perform a detailed analysis of the static axle loads of the complete TowPlow2 system.

Evaluation of the Static Axle Loads as Delivered

Background of Legal Axle Limits

Typically, tractor semi-trailers are provided operational permits based on static axle weights. The maximum allowable weight on a front steering axle is 89,000 N (20,000 lb). When multiple axles are close together, the maximum allowed weight is determined based on a group value, which has a maximum value of 151,200 N (34,000 lb). Also, the gross combined vehicle weight (GCWR) has a maximum value of 355,900 N (80,000 lb).

Static Weight Evaluation

Following the inspection at ATIRC, AHMCT analyzed the static axle weights of the mover truck and TowPlow trailer. A detailed presentation of this analysis is given in "Appendix D: Preliminary Axle Load Analysis". This analysis was done using static weight measurements from a certified scale and these are presented in

[1] The detailed report is available from Caltrans Division of Equipment.

Copyright 2018. the authors

Vermeer Manufacturing Company – Ex. 2045
Kubota v. Vermeer
IPR2025-00168
Page 41 of 182

Table 1. With use of the measured weights and assumed material densities of brine and sand, the axle loads can be predicted. According to Caltrans DOE, the density of the materials is 11.8 N/liter (10 lb/gal.) for brine and 17.5 kN/m^3 (3,000 lb/yd^3) for sand. Table 2 presents the results of this analysis and shows that the TowPlow2 axles can be significantly overloaded. Independently, DOE arrived at the same conclusion[2].

[2] The interested reader is referred to Caltrans Division of Equipment for their analysis and results.

Copyright 2018. the authors

Vermeer Manufacturing Company – Ex. 2045
Kubota v. Vermeer
IPR2025-00168
Page 42 of 182

Table 1. Certified Scale Axle weights of the empty as-delivered Towplow2

TowPlow2 Trailer Configuration	Prime mover truck front axle	Prime mover truck tandem axle set	TowPlow2 trailer tandem axle set	Total
Connected	56,670 N (12,740 lb)	100,710 N (22,640 lb)	66,280 N (14,900lb)	223,660 N (50,280 lb)
Disconnected	60,050 N (13,500 lb)	79,890 N (17,960lb)	83,720 N (18,820 lb)	223,660 N (50,280 lb)

Table 2. Predicted Static Weights of Fully Loaded TowPlow2

Prime mover truck front axle	49,800 N	11,200 lb
Prime mover truck rear tandem axle set	288,500 N	64,900lb
TowPlow2 trailer tandem axle set	170,000 N	38,200 lb
Total	508,300 N	114,00 lb

Copyright 2018. the authors

Vermeer Manufacturing Company – Ex. 2045
Kubota v. Vermeer
IPR2025-00168
Page 43 of 182

CHAPTER 8:
ADAPTING TOWPLOW2 TO DOE REQUIREMENTS

Once it was determined that the system was overloaded, DOE developed three modification options[3] in order to bring the system within legal limits; i.e., DOE described possible system modifications to reduce axle weights. A brief explanation of the possible modifications will be presented here. Each option required changes to both the prime mover truck and the TowPlow trailer.

DOE Proposed System Modifications

The proposed system modifications were as follows. Option 1 maintained the dual functionality (sanding and brining) of the TowPlow trailer while eliminating the ability of the prime mover truck to dispense sand. This change required eliminating the slip-in sander from the prime mover truck. This means that only enough sand will be placed in the dump bed for sufficient traction. The second change would de-rate the capacities of the trailer to 1,890 liters (500 gals.) of brine and 3.8 m^3 (5 yd^3) of sand.

Option 2 converted the TowPlow2 to a brining system. The prime mover truck's slip-in sander would be removed as in option 1. The TowPlow2 trailer's sander would also be removed and replaced by a brine tank.

Option 3 was presented as a way to maximize the ability to sand with the TowPlow2 by retaining the trailer's sander. Similar to the previous options, the prime mover truck slip-in sander would be removed. This process involved moving the sander on the TowPlow2 trailer forward in order to take weight off of the trailer tandem axles and shift it to the prime mover truck tandem axles through the tongue.

The options were presented to the TAG. A brief summary of the operational functions of the various systems, as delivered and with the proposed modifications, is presented in Table 3. Through various meetings, it was determined that DOE Option 3 was the most desirable option. It became necessary to ascertain the distance to move the sander forward to achieve maximum benefit for Option 3.

[3] The interested reader is referred to Caltrans Division of Equipment for their analysis and results.

Copyright 2018. the authors

Vermeer Manufacturing Company – Ex. 2045
Kubota v. Vermeer
IPR2025-00168
Page 44 of 182

Table 3. Summary of DOE TowPlow capabilities (including TowPlow1 and the TowPlow2)

	Prime Mover Truck				TowPlow Trailer			
	Plow	Sand	Prewet	Spray	Plow	Sand	Spray	Prewet
TowPlow1	X				X		X	
TowPlow2	X	X	X		X	X	X	X
DOE Option1	X				X	X	X	X
DOE Option2	X				X		X	
DOE Option3	X				X	X		

Load Analysis

In order to move the sander forward, a detailed analysis of the axle loads was performed and this is included as Appendix E. The analysis first focuses on shifting the sander forward on the trailer as presented by DOE Option 3. Based on physical limitations of the TowPlow trailer, the sander could be moved forward a maximum of 1.16 m (45 3/8 in.) without a complete trailer redesign. This yielded a maximum trailer payload of 100,600 N (22,600 lb) based on maximizing the axle loads on the trailer to meet legal requirements. Furthermore, this analysis shows that based on the 355,800 N (80,000 lb) legal maximum, the prime mover truck can carry an additional 37,200 N (8,400 lb) of weight for ballast. The purpose of the ballast is to increase the weight on the snowplow's rear axle for the purposes of traction. Increasing the tongue weight has the same effect.

In addition to the traditional static analysis, where the tandem axles are lumped into a single support force, an indeterminate analysis was preformed to illustrate that the axle loads on the TowPlow trailer's tandem axle will be equal when the trailer is parallel to the ground. In order to perform this analysis, both a Newton-Euler approach and an energy-based approach were used. These two methods resulted in the same analytical solution - the axle loads are equal when the trailer is sitting parallel to the ground.

Implementation of DOE Option 3 Modification

AHMCT calculated and presented to the TAG the maximum axle weight of the suggested TowPlow Option 3 modification. The TAG endorsed the Option 3 plan, which modifies the second TowPlow system to be within legal highway weight restrictions when fully loaded, subject to a granular maximum weight of 16,900 N/m^3 (2,900 lb/yd^3). The TAG directed AHMCT to return the TowPlow2 trailer to the manufacturer for modification in accordance with the DOE Option 3 plan guidelines. Specific details and redesign information was not supplied to Viking-Cives. Viking-Cives needed to engineer the necessary modifications to the TowPlow trailer to accommodate the desired move of the sander. The original UC-Davis purchase specification was not changed to include the Option 3 modifications.

TowPlow2 Prime Mover Truck Modifications:

The Option 3 TowPlow2 system modifications involved completely removing the slip-in sander from the prime mover truck's bed. AHMCT removed the sander and returned it to Viking-Cives. This will signficantly reduce the weight on the prime mover truck's rear axles as

Copyright 2018. the authors

Vermeer Manufacturing Company – Ex. 2045
Kubota v. Vermeer
IPR2025-00168
Page 45 of 182

mentioned above. Based on the Option 3 modification, the Force America control software needed to be updated for the modified hardware. This modification could be handled locally. Additionally, by updating the controller firmware locally, AHMCT staff members will be able to better support the system during field testing due to the additional knowledge of the controller.

TowPlow2 Trailer Modifications:

As discussed above, moving the sander was the biggest change to the trailer in order to implement DOE Option 3. Through dialog with Viking-Cives, it was determined that the trailer design could accommodate a sander shift forward of 1.15 m (45.38 in). Also, in order to further reduce weight, the brine tank on the TowPlow2 trailer was removed. Efforts were made to keep the hydraulic system associated with the liquid application system in place in order to facilitate any future research and development of the system. It is noted that by moving the sander forward on the trailer, some additional testing will needed in order to adjust the spinner to provide ample sander lane coverage.

Implementation of the Modifications

Once approval was given to modify the system to the DOE Option 3 configuration, efforts were made to return the system to Viking-Cives in Utah. During this process, it was determined that only the trailer could be returned. This was due to issues associated with the prime mover trucks's insurance. At the time, UC-Davis owned the prime mover truck, and therefore the vendor was unable to insure the system for transport. The TowPlow2 trailer was sent to Utah on May 3, 2015 as shown in Figure 6 for modifications. Since the prime mover truck could not be transported to Utah, Viking-Cives and Force America representatives would modify its controller at UC-Davis.



Figure 6. Return of the DOE TowPlow for DOE Option 3 implementation

Copyright 2018. the authors

Vermeer Manufacturing Company – Ex. 2045
Kubota v. Vermeer
IPR2025-00168
Page 46 of 182

CHAPTER 9:
TOWPLOW2 WITH OPTION 3 MODIFICATION (TOWPLOW2.3)

The Caltrans Option 3 adapted TowPlow2 trailer was delivered to AHMCT on May 16, 2015. Viking-Cives and Force America representatives made a site visit in order to reprogram the prime mover truck's controller. This was primarily to disable controls for the components and functions that were removed in accordance with the Option 3 modifications. This chapter discusses the resulting axle weights following the Option 3 modifications. This version of the TowPlow system will be referred to as TowPlow2.3.

TowPlow2.3 Axle Weight Verification:

The biggest issue with the original TowPlow2 configuration was the static maximum axle weights. Once returned, the TowPlow2.3 system was transported to the scales and weighed. Similar to what was done on the original TowPlow2, the TowPlow2.3 system was weighed in both the connected and disconnected states. The measured weights are presented in Table 4. There are some notable differences when TowPlow2.3 was weighed compared to TowPlow2 as follows. For weighing TowPlow2.3

- The front moldboard was installed ($W_{moldboard}$=~8,450 N (1,900 lb))
- There was no slip-in sander in the prime mover truck (W_{sander}=~13,880 N (3,120 lb))
- There was a driver in the cab (W_{driver}=~890 N (200 lb)

where $W_{moldboard}$ denotes the moldboard weight, W_{sander} denotes the sander weight, and W_{driver} denotes the driver weight.

Table 4. TowPlow2.3 empty weights

TowPlow trailer configuration	Prime mover truck front axle (F_{front})	Prime mover truck tandem axle set (Ft_{tan})	TowPlow trailer tandem axle set (Ftp_{tan})	Row Total
Connected	68,860 N (15,480 lb)	83,630 N (18,800lb)	63,970 N (14,380lb)	216,450 N (48,660 lb)
Disconnected	72,510 N (16,300 lb)	61,830 N (13,900 lb)	82,030 N (18,440 lb)	216,450 N (48,660 lb)

Comparing the Static Empty Weights

A few observations are noted. The TowPlow2 weight measurements are given in

Copyright 2018. the authors

Vermeer Manufacturing Company – Ex. 2045
Kubota v. Vermeer
IPR2025-00168
Page 47 of 182

Table 1. These measurements gave a front prime mover truck axle weight of 60,050 N (13,500 lb) and a prime mover truck tandem axle set weight of 79,890 N (17,960 lb). This yielded a total prime mover truck weight of 139,940 N (31,460 lb). The measurements from Table 4 yield a total weight for TowPlow2.3 of 134,340 N (30,200lb). As such, the prime mover truck of TowPlow 2.3 weighs 5,600 N (1,260 lb) less. Analytically, the weight difference, Δ_W, can be predicted as

$$\Delta_W = W_{hopper} - W_{moldboard} - W_{Driver}. \quad \textbf{(1)}$$

Using the numbers given above, this yields a difference of 4,540 N (1,020 lb), which is reasonably close to the measured difference. The TowPlow2 trailer weighed 83,720 N (18,820 lb) on delivery vs. 82,020 N (18,440 lb) for the TowPlow2.3 trailer as delivered. This weight reduction is based on the hardware of the brine system that was removed.

An analysis of the predicted axle weights was performed based on the certified weight measurements and this is presented in "Appendix F: Analytical Estimate of Loaded Axle Weights of the Option 3 Modified TowPlow2." This analysis shows that the newly predicted axle weights were consistant with the values that were predicted prior to physically moving the sander.

Additional Desired Testing

The TowPlow2.3 trailer was weighed empty on a certified scale upon being returned to UC-Davis from the manufacturer. The measured axle weights verified the predicted distribution calculated from the AHMCT TowPlow system weight model. With use of the empty TowPlow system measured weights and the AHMCT analytical model, the TowPlow2.3 configuration was determined to be within highway legal axle weight limits when fully loaded with up to 16,870 N/m^3 (2,900 lb/yd^3) sand and the trailer being parallel to the ground. It would be highy useful to verify total operational weight by loading the system fully with actual Caltrans sand. In addition, driving the TowPlow2.3 system over the Donner Summit grades at maximum capacity (prior to utilization in a winter maintenance operation) would be useful in verfying whether the 411 kW (550 hp) system provides adequate grade climbing ability.

Copyright 2018. the authors

Vermeer Manufacturing Company – Ex. 2045
Kubota v. Vermeer
IPR2025-00168
Page 48 of 182

CHAPTER 10:
DATA VISUALIZATION - STORM REPORTS

The lack of snow through the last three winters has inhibited the collection of large amounts of data on the TowPlow systems' productivity. Still, a data post-processing approach has been developed that allows information from Force America's Precise IX-101 units to be converted to easily readable information. It is anticipated that the graphically presented data will allow much information to be easily attained on the TowPlow system's usage including such aspects as when the brine system was used in combination with plowing, locations at which the TowPlows were most often used, etc. Such information will help in evaluating TowPlow operational performance and will be useful to AHMCT and Caltrans. This chapter reports concisely on this system.

The Data Postprocessing Approach

A plotting routine has been developed to help visualize the TowPlow data that will be acquired in future storm events. The post-processed data will be presented graphically and these graphs will be referred to as storm reports. The material to follow discusses detail of the approach.

First, the data collected includes GPS information as well as information on whether the TowPlow trailer is deployed and the state of the brine system. There are some fundamental aspects associated with the area in which the system is being used. First, if the system is being used on a road that is generally in an East-West direction, then the latitude value in the data can be focused upon. For roads that travel generally in a North-South direction, than the longitude values are used. Second, highway exits are relatively distant from each other in the anticipated winter maintenance locations. It will be assumed that the TowPlow system is operated in a constant manner between ramps; i.e., trailer deployed or not and brine system on or not. Also, the Precise IX-101 unit reports data when there is a significant change in heading or change in state. As such, when the TowPlow system is turning around (e.g., exiting and re-entering in the opposite highway direction) a large number of data points result.

Using a histogram, the areas between exits can be identified and are defined as a route. The data for a route is then decomposed into individual trips. For TowPlow1C, the system's usage for each trip is established from the state of the two input channels of the data acquisition module at the midpoint for each trip. The data can then be compiled to present information in a concise manner and for the period of time desired. For example, Figure 7 presents information on the snow-fighting efforts of the TowPlow1C for the entire 2014-15 winter snow season. It is noted that the categories displayed in the pie chart can be tailored for each specific system. For example, TowPlow1C allows for plowing, spraying brine, and combined plowing and spraying. The distribution of use is clearly shown in the figure.

Copyright 2018. the authors

Vermeer Manufacturing Company – Ex. 2045
Kubota v. Vermeer
IPR2025-00168
Page 49 of 182

Figure 8 extends the representation of data to show the actual routes covered as well as the system operation over the route. The route endpoints are indicated by solid vertical lines and they are explicitly labeled to allow understanding of the exact locations of the operation (e.g., Unknown, Kingvale, Donner Lake Interchange (DLI), Truckee, and Stateline). Additionally, unlabeled vertical lines represent the midpoint of the specific route. The latitude values are overlaid on a map of the area in order to facilitate data visualization. The pie chart for each route is aligned with the midpoint of the respective route and concisely presents the compiled data. The time stamp for each data point is used to position the specific route on the plot. Incorporating the date information facilitates correlating the operational information with any snowfall information obtained from other sources. The overall goal of this process is to help understand TowPlow operational specifics in an easy, visual way.

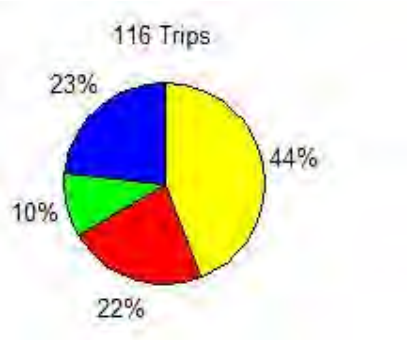


Figure 7. TowPlow1 operation pie chart (seasonal total). Note that trip type is defined in Figure 8.

Copyright 2018. the authors

Vermeer Manufacturing Company – Ex. 2045
Kubota v. Vermeer
IPR2025-00168
Page 50 of 182

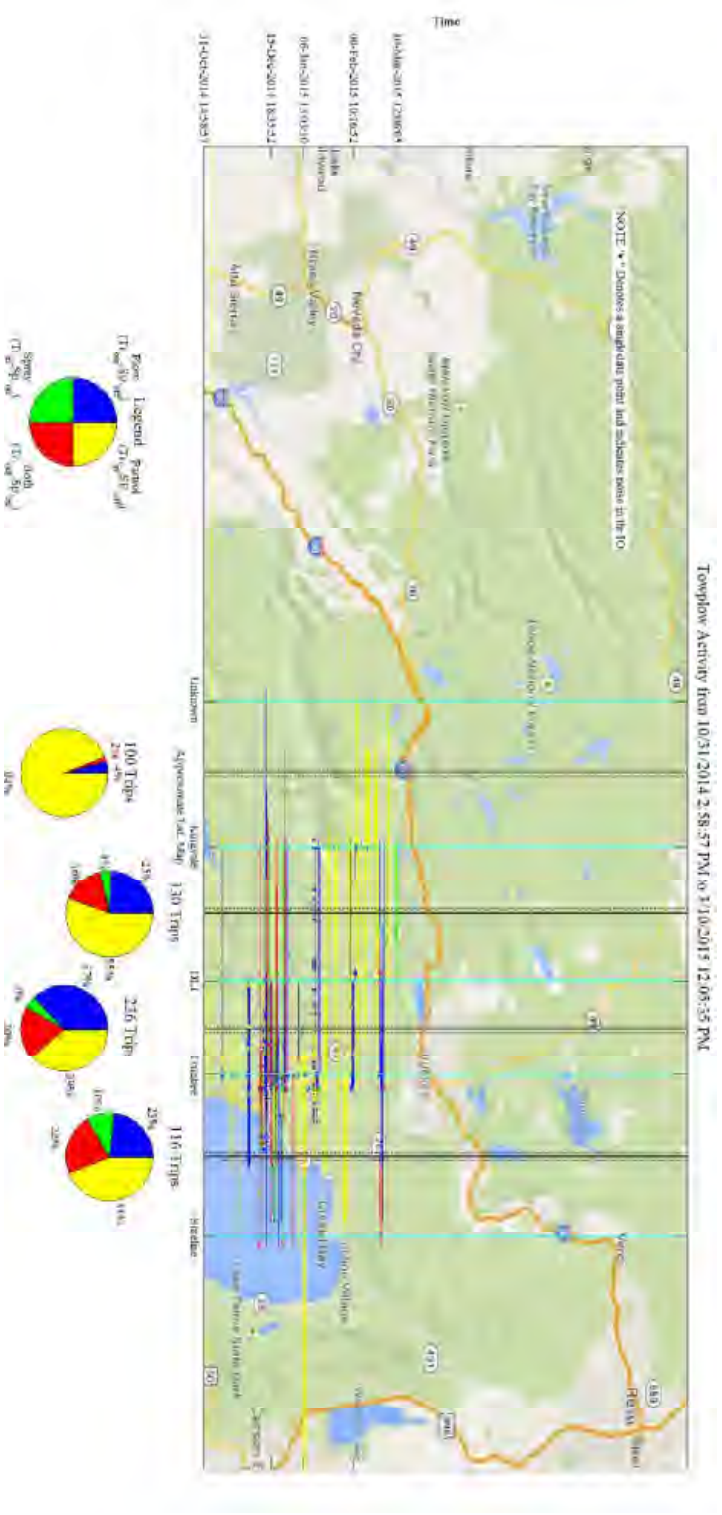


Figure 8. Final TowPlow usage

Copyright 2018. the authors

Vermeer Manufacturing Company – Ex. 2045
Kubota v. Vermeer
IPR2025-00168
Page 51 of 182

CHAPTER 11:
SUMMARY AND CONCLUSIONS

The Advanced Highway Maintenance and Construction Technology (AHMCT) Research Center was tasked by the California Department of Transportation (Caltrans) to develop an understanding of the efficacy of Viking-Cives TowPlow in Caltrans' winter snow-fighting operations. This document has reported on research performed for such purposes.

First, the prior research work on the TowPlow was reviewed to understand the experiences of TowPlow deployment in other departments of transportation. In parallel, an initial TowPlow trailer with a brine system was procured, and this TowPlow trailer in combination with a prime mover truck is referred to as TowPlow1. The TowPlow1 system employed a 354.8 kw (475 horsepower) Caltrans standard fleet snowplow and was tested on I80 in Caltrans District 3 during winter 2013-14. Caltrans subsequently transferred TowPlow1 into their fleet and modified the snowplow's hydraulic system to be more compatible with the TowPlow trailer's hydraulics. Modifications done by the Caltrans Division of Equipment (DOE) improved the operability of the TowPlow1 system. The modified system is referred to as TowPlow1C in this report. TowPlow1C was first deployed and tested in Caltrans District 3 on I80 during winter 2014-15.

While the TowPlow1 and TowPlow1C systems were not used extensively due to minimal snowfall, several Caltrans operators were trained and had experience driving the TowPlow1 and TowPlow1C systems over the mountainous portions of I80 in the Donner Pass vicinity. These operators were surveyed and provided valuable feedback, which led to the development of specifications for the purchase of a second TowPlow system. Operators desired camera and laser guidance systems in order to help improve operator visibility. Additionally, based on their experience travelling over the relatively steep grades, it was determined that the prime mover truck should have the highest engine power available.

A second TowPlow system, referred to as TowPlow2, was procured from the vendor in a standard configuration similar to TowPlow systems used in other states. This configuration included a TowPlow trailer and a snowplow truck. The purpose was to acquire a "turn-key" system that would require minimal modifications to meet Caltrans' requirements. TowPlow2 was procured and delivered to AHMCT in December 2014. Despite the intent of the system to be turn-key, the as delivered TowPlow2 did not fully meet Caltrans' requirements, the most important of which was excessive weight on the system's axles. As such, several modification options were proposed. The modifications, referred to as Option 3 modifications, were completed on the TowPlow2 system in June 2015. The primary goal of these modifications was to keep a fully loaded TowPlow2 system within legal weight limits.

AHMCT developed the analytical ability to predict axle loads of the TowPlow system based on weighing the unloaded TowPlow2 and adding predicted sand and/or brine weight. Additionally, the analysis allowed for calculation of the individual trailer axle loads. As such, the

Copyright 2018. the authors

Vermeer Manufacturing Company – Ex. 2045
Kubota v. Vermeer
IPR2025-00168
Page 52 of 182

analysis was used to predict the axle loads prior to implementation of the Option 3 modification. Also, following delivery of the Option 3 modified TowPlow2, referred to as TowPlow2.3, the unloaded system was weighed and loaded axle weights calculated analytically. While the analysis results indicate that the TowPlow2.3 can carry a full hopper of sand without overloading the axles, the trailer is assumed to be level and the sand density equal to 16,870 N/m^3 (2,900 lb/yd^3). As such, it is recommended that the fully loaded system be weighed to ensure that axle legal limits are not exceeded.

While the TowPlow system is used to clear roads in numerous states across the country, the dynamic properties and stability of the system had not been studied analytically. As such, several models were developed based on advanced engineeirng methods and included such aspects as a snowplow model. Moreover, the modeling was verified through actual dynamic handling experiments. This work has indicated that the TowPlow system's dynamics and stability can be improved by implementing active steering conrol on the trailer's axles and the best control approach presented.

Due to three consecutive exceptionally light snow seasons that coincided with the research project's testing period, a TowPlow system performance evaluation in Caltrans' snowplowing operations has not been completed. As an alternative, a detailed means of data collection and analysis capabilities have been developed to assist with evaluating TowPlow performance in future snow seasons.

Based on the research completed to date, the following are the significant issues identified that require consideration or resolution before the TowPlow system could be successfully implemented into Caltrans' operations:

- Investigation of the axle loading issues
- TowPlow trailer hydraulic systems are not compatible with Caltrans' standard hydraulic systems
- TowPlow systems do not provide any added value if used to clear 2 lane highways
- Sufficient prime mover truck power is critical to satisfactory operation on grades.

It is anticipated that a follow on project will allow continued data collection and support of the TowPlows in future years to offset the light snow seasons encountered during the course of research. Lastly, this document reports work through June 30, 2015. This cutoff date was selected to allow adequate time for research documentation. Research conducted after this date will be reported in the follow on project.

Copyright 2018. the authors

Vermeer Manufacturing Company – Ex. 2045
Kubota v. Vermeer
IPR2025-00168
Page 53 of 182

APPENDIX A: TOWPLOW DYNAMIC ANALYSIS

IntroductionThe TowPlow trailer is equipped with steerable axles so that the trailer can be steered up to 30 degrees with respect to the prime mover truck, or referred to as a tractor in this section of the report. A hydraulic ram connected to the tractor's hitch assists in controlling the trailer. The combination of the tractor's front plow and the trailer-equipped plow is able to clear a path up to approximately 7.3 m (24 ft) wide, which is nearly the width of two highway traffic lanes.

While the TowPlow may increase the efficiency and performance of the snow removal operation, the stability of the system under the harsh winter conditions may be compromised by implementation of the steerable trailer, and stability of the system must be ensured in terms of the lateral and yaw dynamics, load transfer, hill climbing, and low friction road conditions. This dissertation examines the stability of the TowPlow through both kinematic analysis and detailed dynamic modeling considering snow resistance, load transfer and gradability. The addition of control to the TowPlow to enhance its operational performance and stability, and broaden its applicability in the challenging winter operational conditions is also studied.

Literature Survey

For the study of dynamic modeling and control of the TowPlow, related literature is reviewed in the following categories: kinematics, dynamics, snow resistance, and stability control. To constrain the scope of the review, it is confined to work related to articulated vehicles since the TowPlow is a unique type of this vehicle.

Kinematics of the Articulated Vehicle

Kinematics of articulated vehicles has been studied mainly to investigate off-tracking, which describes the difference in path radii between the front axle of the towing unit and the rear axle of the trailer unit, and to generate trajectories of an autonomous vehicle or a mobile robot system. The design of articulated vehicles, highway exit ramps, and parking lots is affected by kinematics of the articulated vehicle due to its geometry [12,60]. Jindra (1963) published his work on the tracking of a tractor-trailer combination in a steady turn. He developed equations that determine the kinematic path of a single-unit vehicle using general tractrix, and applied the results to the tractor-trailer combination. He also developed the tractrix integrator instrument, shown in Figure 9, which can trace maneuvering patterns of any trailer combination with two-wheel steering [30].

Copyright 2018. the authors

Vermeer Manufacturing Company – Ex. 2045
Kubota v. Vermeer
IPR2025-00168
Page 54 of 182

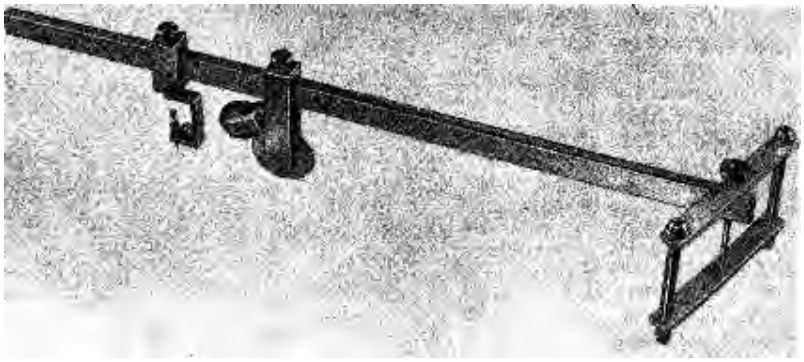


Figure 9. Jindra's tractrix integrator [30]

Pretty (1964) provided a full evaluation of off-tracking paths for large vehicle combinations considering the basic geometry of steering and tracking in a circular curve and a straight line. Figure 10 shows the tractrix generated from steering in a circle and by the rear of the trailer when the towing pintle follows the curve [47].

The Western Highway Institute (1970) performed a set of comprehensive analyses measuring off-tracking of vehicles and vehicle combinations using the following methods: (1) the use of models (i.e. the general tractrix), (2) the graphical method, and (3) the mathematical method. They concluded that there are no significant differences in measuring off-tracking for the same equipment whichever methods are applied, and that the amount of off-tracking is most likely dependent on the components of the wheelbases such as the distance between each axle and the articulation point [61].

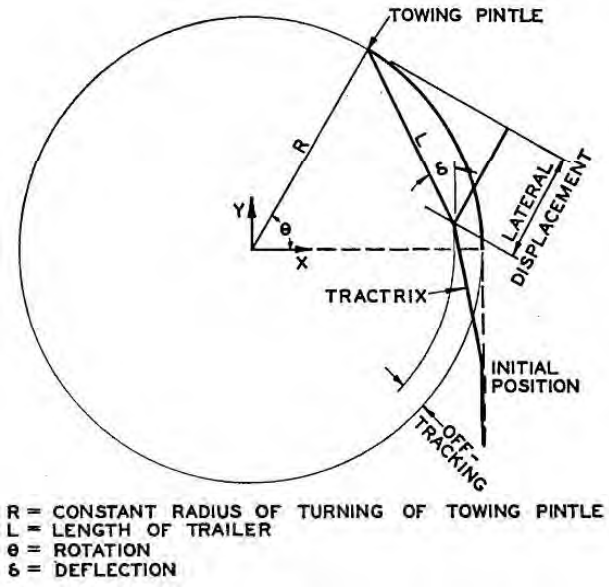


Figure 10. Pretty's tractrix from steering in circle [47]

Copyright 2018. the authors

Vermeer Manufacturing Company – Ex. 2045
Kubota v. Vermeer
IPR2025-00168
Page 55 of 182

Off-tracking has been a significant issue causing disruption to traffic flow by large trucks and tractor-trailer combinations intruding into adjacent lanes. Saito (1979) associated articulation angle and forward velocity of the semi-trailer with rear-wheel steering to reduce the off-tracking [50]. Alexander and Maddocks (1988) derived equations that relate the centers of curvature of the wheels to the center of rotation of the vehicle, and utilized the results for problems of off-tracking and optimal steering [1]. Erkert et al. (1989) investigated off-tracking of logging trucks for road design in forests utilizing the method of general tractrix and instantaneous centers of rotation (Figure 11), and the results compared favorably with experimental data [21].

Chen and Velinsky (1992) suggested a kinematic design methodology to optimize the geometry of the vehicles and the roadways for low-speed maneuverability. Also, they ascertained that the low-speed maneuverability of an articulated vehicle can be improved through steering of trailer axles as a linear function of the articulation angle and front-wheel-steer angle, as shown in Figure 12 [9].

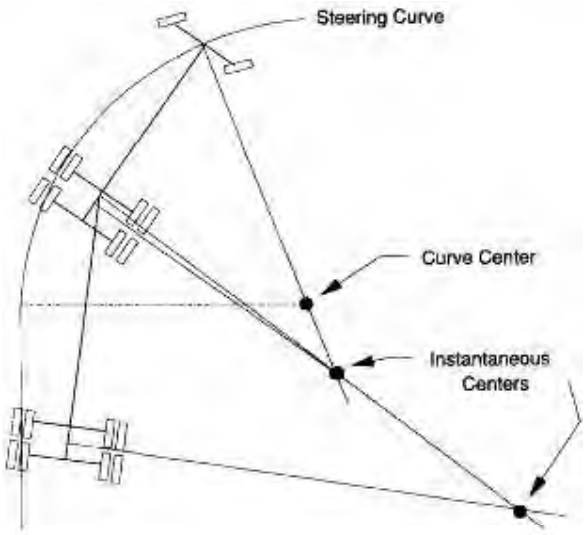


Figure 11. Instantaneous centers of logging trucks by Erkert et al [21]

Copyright 2018. the authors

Vermeer Manufacturing Company – Ex. 2045
Kubota v. Vermeer
IPR2025-00168
Page 56 of 182

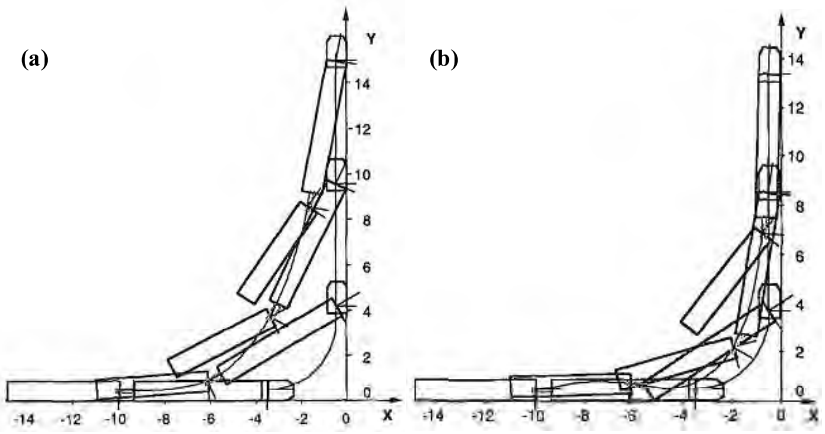


Figure 12. Cornering of tractor-trailer combination: (a) without trailer steering, (b) with trailer steering by Chen and Velinsky [9]

Manesis (1998) introduced a sliding kingpin mechanism, shown in Figure 13, to eliminate the off-tracking of heavy duty trucks with semi-trailers, and also designed various types of sliding control [16,42,43].

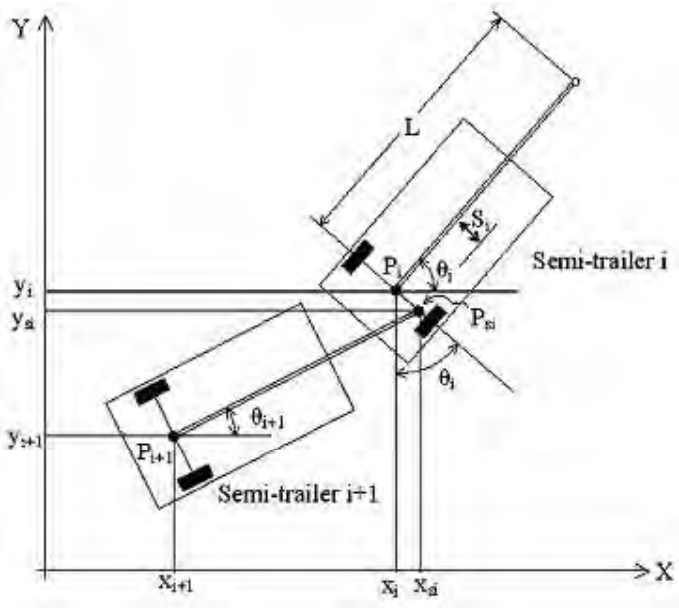


Figure 13. Manesis' sliding kingpin mechanism [43]

Dynamics of the Articulated Vehicle

From the 1930s, a substantial amount of work has been performed concerning the directional dynamics of articulated vehicles. Vlk (1985) comprehensively reviewed and summarized studies on handling performance of truck-trailer vehicles. According to his review, the early theoretical works of articulated vehicles are limited to only unstable states of the trailer until Schmid (1964)

Copyright 2018. the authors

Vermeer Manufacturing Company – Ex. 2045
Kubota v. Vermeer
IPR2025-00168
Page 57 of 182

and Jindra (1965) introducing the interdependence between truck and trailer motions [59]. In the 1960s, Jindra (1965) and Bundorf (1967) developed linear differential equations for the simplified mechanical model of a tractor double trailer combination and an automobile-trailer combination, respectively, and examined the directional instability and steady-state turning performance through steady-state and transient responses to steering inputs [5,31]. Ellis (1969) developed both linear and simplified nonlinear models for the planar motion of articulated vehicles neglecting the roll motion of the vehicles, and analyzed dynamic responses to show how instability of the trailer occurs [20]. Segal and Ervin (1981) classified handling instability of articulated vehicles into: (1) jack-knifing – occurring when the tractor oversteers and the trailer understeers or slightly oversteers above a critical speed; (2) trailer swing – occurring when the tractor oversteers and the trailer oversteers strongly above a critical speed [53]. Vlk (1985) also characterized three typical directional unstable states of articulated vehicles: (1) snaking – trailer yaw oscillation that occurs at high speed; (2) jack-knifing – instability of tractor yaw motion; and (3) trailer swing – instability of trailer yaw motion [59].

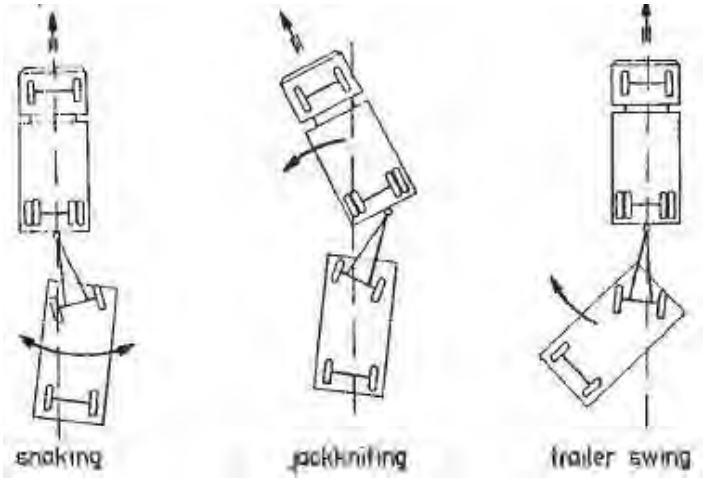


Figure 14. Typical unstable states of articulate vehicles by Vlk [59]

Later, a more complex nonlinear model of articulated vehicles considering the lateral, yaw and roll motions together was developed by Chen and Tomizuka (1995) [10].

Copyright 2018. the authors

Vermeer Manufacturing Company – Ex. 2045
Kubota v. Vermeer
IPR2025-00168
Page 58 of 182

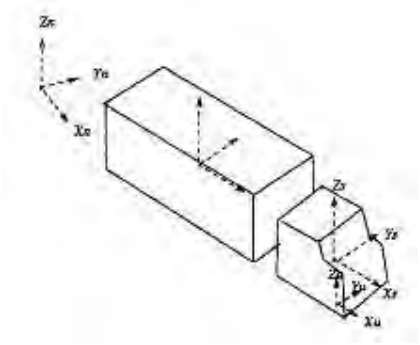


Figure 15. Coordinate system for the articulated vehicle by Chieh and Tomizuka [10]

Analysis on non-linear dynamics of the vehicle had been enhanced through development of non-linear tire friction models because forces and moments generated by the friction between tire and road surface influence vehicle dynamics significantly. The tire models that have been used commonly for vehicle dynamics are the LuGre model, Pacejka's model, and Dugoff's model. The LuGre friction model is originally suggested by Canudas de Wit et al. [7]. It describes the mechanism of friction as contact of two rigid bodies through elastic bristles. When one body travels on the other, the bristles randomly deflect like springs, and the bending of the bristles generates the friction force. Initially, the LuGre model was only used for the longitudinal friction force. However, it was extended to allow for a combination of longitudinal and lateral forces [57].

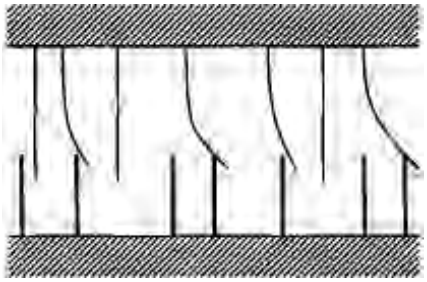


Figure 16. Concept of friction between bristles for the LuGre model [7]

Pacejka's model, also known as the Magic Formula tire model, are mathematical equations composed of several tunable coefficients to accurately describe the measured data of the longitudinal and lateral tire force [3]. The coefficients in the model may not have physical interpretation.

Dugoff's model is a derivative of the freely rolling tire by Fiala [23]. Dugoff extended the previous work to general tire-road interaction either for pure-slip or combined-slip condition [18]. A simplified Dugoff's model assuming that both longitudinal and lateral forces are linearly dependent on the normal force of the tire is developed by Krauter [38]. In addition to the simplified model, Guntur and Sankar implemented the friction circle concept to Dugoff's model; i.e., if the desired friction is less than or equal to half of the available friction, described by inside

Copyright 2018. the authors

Vermeer Manufacturing Company – Ex. 2045
Kubota v. Vermeer
IPR2025-00168
Page 59 of 182

of the circle in Figure 17, the longitudinal and lateral tire forces have linear relationship with the slip ratio and slip angle, respectively; however, if the desired friction outside of the circle, the tire forces attenuate nonlinearly. They also presented a procedure to calculate the tire forces for vehicle simulation [26].

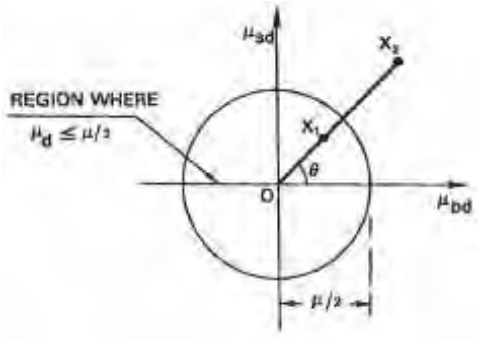


Figure 17. Friction circle concept for the Dugoff's tire friction model by Guntur and Sankar [26]

Snow Resistance Model

The snow resistance model is significant in modeling of the TowPlow because forces on the plows affect the system dynamics, and may cause instability. There has been an effort to estimate forces on the plow during the snow removal operation. Some of the models found in the literature are based on Croce's model, which is a simple Bernoulli fluid flow model under the assumption that the velocity of the snow is constant throughout the entire process. The model approximates the snow resistance force more closely at higher plowing speed [35]. Mellor (1965), for modeling of wedge shaped plow (Figure 18), modified Croce's model through introducing a coefficient that compensates the velocity change of the snow due to compression of the snow [44]. Zhou et al. (2000) modified Mellor's model to be used in vehicle dynamic modeling [62]. However, the model still fails to consider the compression of the snow accurately.

Kaku's model (1979, Figure 19), based on the theory of conservation of momentum, considers the velocity change of the snow due to its compressibility [34]. Kempainen et al. (1998) presented a complex snow resistance model that includes compressibility of the snow, shear and turbulent zones in front of the wing plow. He also conducted experiments on snowplowing with a wing plow and concluded that the plowing forces and velocity have a linear relationship at low plowing speeds [35].

Copyright 2018. the authors

Vermeer Manufacturing Company – Ex. 2045
Kubota v. Vermeer
IPR2025-00168
Page 60 of 182

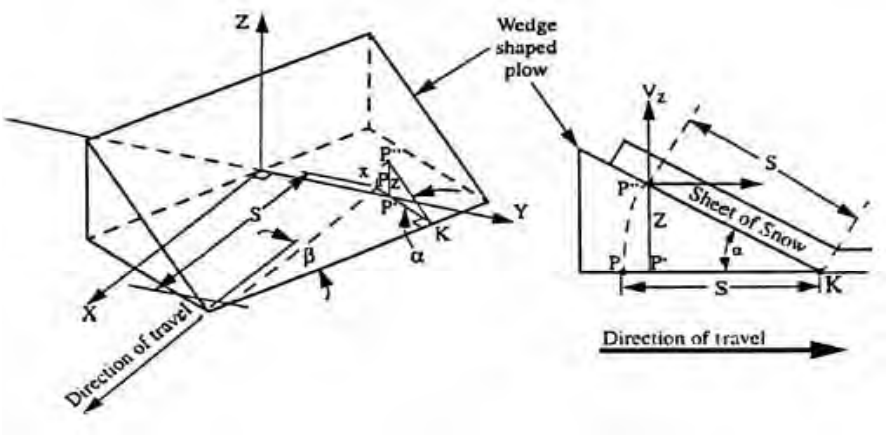


Figure 18. Mellor's wedge plow model [44]

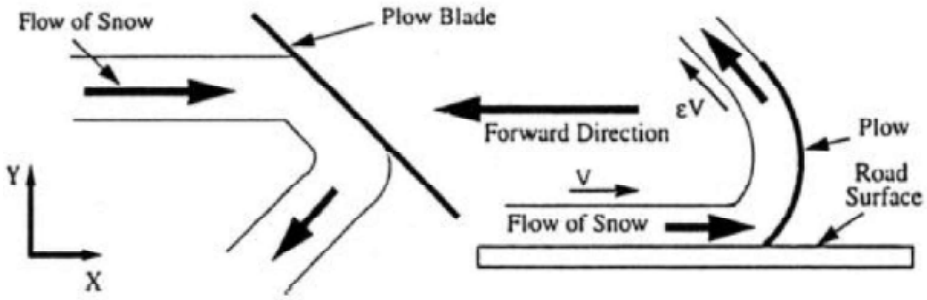


Figure 19: Kaku's snow flow assumption in snow resistance model [34]

Ravani et al. (2005) proposed the control volume approach for the snow resistance model (Figure 20). This model includes snow-removing resistance, sliding resistance on the road surface and air resistance of the plow as components of the snow resistance, and considers compression of the snow based on conservation of mass of the incoming and outgoing snow [49].

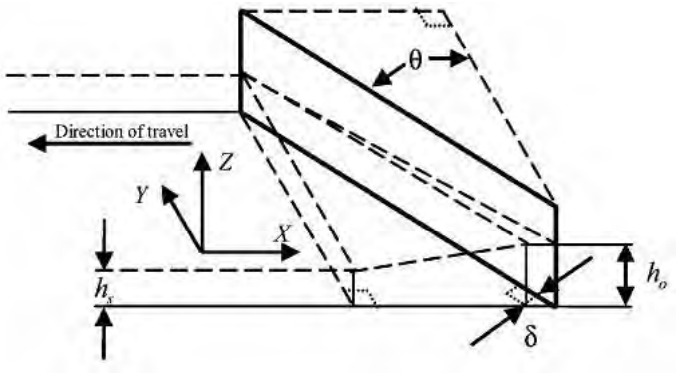


Figure 20. Control volume in front of the plow by Ravani et al. [49]

Copyright 2018. the authors

Vermeer Manufacturing Company – Ex. 2045
Kubota v. Vermeer
IPR2025-00168
Page 61 of 182

Stability Control of the Articulated Vehicle

Anti-lock Braking Systems (ABS) have been one of the common stability control technologies in a vehicle system, which adjusts the application of brake forces on the wheels to allow the driver to maintain handling of the vehicle, especially during emergency braking. Implementation of ABS to articulated vehicles has improved their stability to some extent [54]. However, Burton et al. (2004) claimed that ABS increases stopping distance of a vehicle on snow or gravel, and novel control technologies together with ABS are required for stability of vehicles [6].

Direct yaw moment (DYM) control that stabilizes yaw motion of a vehicle is a prevailing technology for non-articulated vehicles, but seldom available in production articulated vehicles. However, a great deal of literature about DYM control in articulated vehicles has been found for severe driving maneuvers such as split-coefficient of friction braking [33,63], cornering [54], and braking-in-turn [25]. DYM control typically utilizes either braking or steering to generate moment at the centers of gravity of the system for yaw stabilization [55]. Some of the examples for articulated vehicles using DYM control of braking are asymmetric braking (differential braking) of the tractor [27,33], active control of trailer braking [22,41], and active control of both tractor and trailer braking with optimized braking force distribution [25] in Figure 21

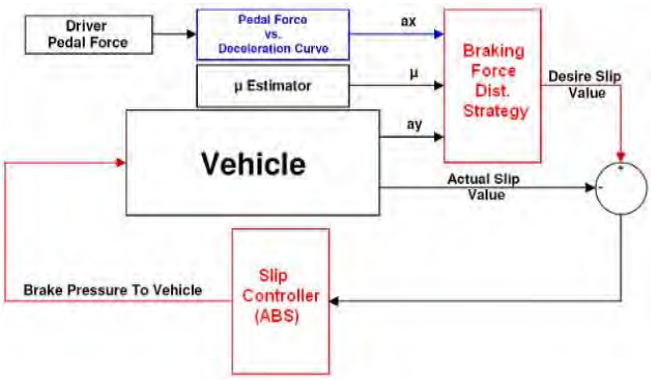


Figure 21. Control scheme of active braking control in [33]

Active steering control is another method to stabilize vehicle motions. Some example applications to articulated vehicles are active rear steering of the tractor [37], active trailer steering [45,48], and active all-wheel steering [17] in Figure 22.

Copyright 2018. the authors

Vermeer Manufacturing Company – Ex. 2045
Kubota v. Vermeer
IPR2025-00168
Page 62 of 182

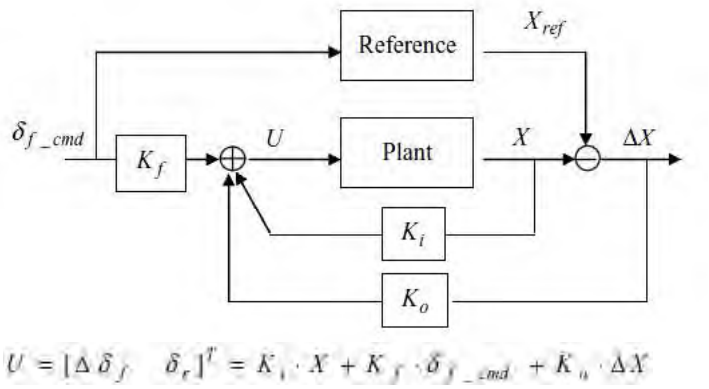


Figure 22. Control scheme of active all wheel steering control in [17]

Kinematics of the TowPlow

For the purposes of snow removal, the TowPlow, as a multi-articulated vehicle, operates with a specific articulation angle. To be most efficient, an angle of 30 degrees is required so that the TowPlow can cover two lanes of the typical U.S. Interstate Highway, which have lane widths of 3.66 *m* (12 *ft*). However, there is a potential problem that the articulation angle alters during cornering, and the TowPlow either misses large portions of the road or intrudes into the adjacent lane. Thus, the trailer of the TowPlow may need to be steered at varying angles to maintain the articulation angle through a corner. Through kinematic analysis of the TowPlow, the relation between radius of curvature of the road and the trailer wheel steering angle is determined in this.

Kinematic Model – Instantaneous Centers of Velocity

The kinematic model of the TowPlow – extended bicycle model – is derived under the following assumptions:

- The TowPlow is considered a vehicle combination of tractor and steerable trailer;
- The tractor and trailer with the tongue assembly are rigid bodies;
- Slip between the tires and the road surface is negligible;
- Internal or external forces on the vehicle units do not exist, including snow resistance;
- Mass and inertia of the vehicle units are neglected;
- Only planar motion is considered.

Figure 23 shows the top-view of the tractor-trailer and associated coordinate systems. The vehicle units move in the global coordinate frame, X-Y, and each unit has two local coordinate systems, one that expresses the rotation of each unit, subscripted as *1* (tractor) and *2* (trailer), and

Copyright 2018. the authors

Vermeer Manufacturing Company – Ex. 2045
Kubota v. Vermeer
IPR2025-00168
Page 63 of 182

the other that represents the angle of the steerable wheels, subscripted as F (front wheel of tractor) and T (wheel of trailer). One should note that the angle formed by the tongue assembly and the center line of the trailer is the same as the trailer steering angle, δ_T, because of hydraulic coupling, which is inherent to the TowPlow's design. Therefore, for a constant trailer steering angle, δ_T, the trailer unit and the tongue assembly can be considered as one rigid body. The kinematic relation of each wheel and the point P, the articulation point of the tractor and trailer, is derived using 'instantaneous centers of velocity'.

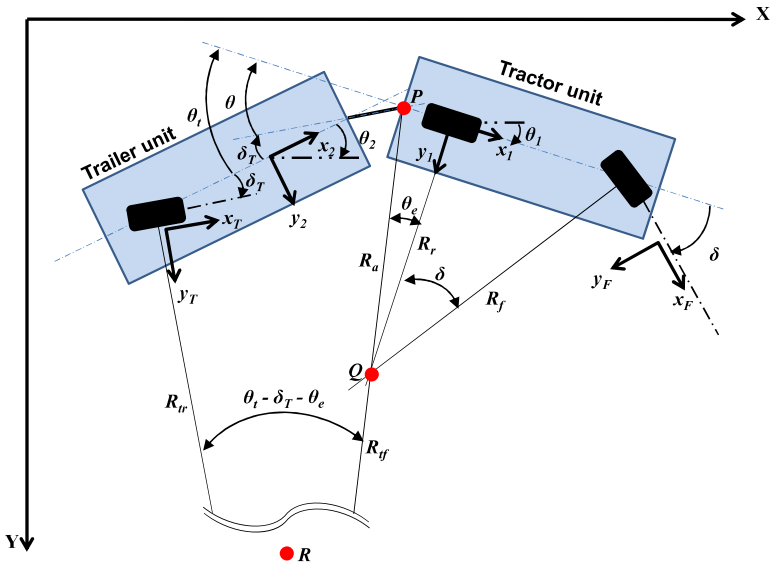


Figure 23. Schematic of the TowPlow system and associated notations

Derivation of Kinematic Equations

As shown in Figure 23, point P, the hitch point between the tractor and the tongue assembly as a part of the trailer unit is the instant center of velocity for relative motion between these 2 bodies. That is, point P has the same absolute velocity whether it is considered as a point on the tractor or a point on the trailer. Also, point Q represents the instant center of velocity for the tractor with respect to the ground and point R represents the instant center of velocity for the trailer with respect to the ground. Moreover, from the Aronhold-Kennedy theorem [56], points P, Q and R must lie on a straight line. As such, the motion of the bodies and the required steering angles are easily determined.

If the front wheel of the tractor moves by Δs_f in the tangential direction of the circle having radius R_f during the time period Δt with the steering angle δ and constant forward velocity v_f, the tractor will rotate by an angle $\Delta\theta_1$. As Δt becomes infinitesimal, the following equations describe motion of the tractor on the plane:

$$d\theta_1 = \frac{ds_r}{R_r} = \frac{ds_f}{R_f} = \frac{v_f}{R_f} \cdot dt \,, \tag{2}$$

Copyright 2018. the authors

Vermeer Manufacturing Company – Ex. 2045
Kubota v. Vermeer
IPR2025-00168
Page 64 of 182

$$v_r = \frac{R_r}{R_f} \cdot v_f = \frac{\sin \delta}{\tan \delta} \cdot v_f = \cos \delta \cdot v_f \quad , \tag{3}$$

$$v_a = \frac{R_a}{R_f} \cdot v_f = \frac{\sqrt{R_r^2 + l_a^2}}{l_1 / \sin \delta} \cdot v_f \quad , \tag{4}$$

where s denotes displacement, v denotes velocity, R is the radius of rotation, subscripts f, r, and a represent the front wheel, the rear wheel, and the articulation point, respectively, θ_1 is the rotation angle of the tractor, δ is the steering angle, l_1 is wheelbase of the tractor, and l_a is distance between the rear wheel of the tractor and the articulation point P.

The trailer's motion is represented in a similar manner for given constant steering angle of the trailer wheel, δ_T, as

$$d\theta_2 = \frac{ds_{tr}}{R_{tr}} = \frac{ds_a}{R_{tf}} = \frac{v_a}{R_{tf}} \cdot dt \quad , \tag{5}$$

$$v_{tr} = \frac{R_{tr}}{R_{tf}} \cdot v_a = \frac{\dfrac{l_s + l_2 \cdot \cos \delta_T}{\tan(\theta_t - \delta_T - \theta_e)} - l_2 \sin \delta_T}{\dfrac{l_s + l_2 \cdot \cos \delta_T}{\sin(\theta_t - \delta_T - \theta_e)}} \cdot v_a \quad , \tag{6}$$

where subscripts tr and a represent the trailer wheel and the articulation point, respectively, θ is the articulation angle between the tractor unit and the tongue assembly, θ_t is the total articulation angle between the tractor unit and the trailer unit, θ_e is the angle between R_r and R_a, and l_2 is the distance between the articulation point P and the trailer's axle. θ_t and θ_e can be obtained as

$$\theta_t = \theta + \delta_T = \theta_1 - \theta_2 \quad , \tag{7}$$

and

$$\theta_e = \arctan\left(\frac{l_a}{R_r}\right) \quad . \tag{8}$$

Defining Steering Inputs

Once the desired path of the tractor is determined, the tractor steering angle, δ, can be calculated from the wheelbase of the tractor and the radius of curvature of the path as

$$\delta = \arcsin\left(\frac{l_1}{R_f}\right) \quad . \tag{9}$$

To maintain the articulation angle of the tractor-trailer and to prevent the vehicle from intruding into the adjacent lane, the trailer steering angle, δ_T, should be adjusted in a proper way that the tractor-trailer units operate with the same yaw rate, which means that the instantaneous centers of velocity of the tractor with respect to the ground (point Q) and the trailer with respect

Copyright 2018. the authors

Vermeer Manufacturing Company – Ex. 2045
Kubota v. Vermeer
IPR2025-00168
Page 65 of 182

to the ground (point R) are coincident. As shown in Figure 23, when the trailer steering angle changes, the location of point R changes, and so does R_{tf}. From Eq. (6), R_{tf} can be expressed as

$$R_{tf} = \frac{l_s + l_2 \cos \delta_T}{\sin(\theta_t - \delta_T - \theta_e)}. \tag{10}$$

Using the coordinate system, x_1-y_1, the origin of which is the center of the tractor rear wheel, the coordinates of point Q are $(0, R_r)$, and those of point R are $(-l_a+R_{tf}\sin\theta_e, R_{tf}\cos\theta_e)$. If points Q and R coincide, then

$$R_{tf} = \frac{l_a}{\sin \theta_e}. \tag{11}$$

For the given radius of curvature of the road, R_f, the desired total articulation angle, θ_t, and the vehicle geometry, substituting Eq. (11) into Eq. (10) and solving the equation provides the trailer steering angle that yields a constant articulation angle. Figure 24 shows the necessary trailer steering angle for different turning radii. CW and CCW indicates clockwise and counter-clockwise turning, respectively. Vehicle parameters, which are representative of a typical snowplow and the TowPlow, used in the calculation are shown in Table 5. Since the initial total articulation angle is set to be 30 degrees, the trailer wheel steering angle saturates at 30 degrees as the radius of curvature increases. When the road has infinite radius of curvature, which means the road is straight, the trailer wheel steering angle should be 30 degrees for the tractor-trailer moving straight while maintaining the total articulation angle of 30 degrees. Figure 25 presents the trailer wheel steering angle, which allows the total articulation angle to be constant as the tractor steering angle changes.

Table 5. Vehicle parameters for kinematic analysis

Symbol	Value	Unit	Description
l_1	5.28	m	Wheel base of tractor
l_a	1.67	m	Distance from rear axle of tractor to hitch point P
l_s	2.19	m	Length of tongue assembly
l_2	5.49	m	Distance from tongue assembly to trailer axle
θ_t	30	deg	Initial value of the total articulation angle
w_{fp}	3.66	m	Width of front plow
w_{tp}	7.92	m	Width of towed plow
θ_{fp}	45	deg	Snowplowing angle of front plow

Copyright 2018. the authors

Vermeer Manufacturing Company – Ex. 2045
Kubota v. Vermeer
IPR2025-00168
Page 66 of 182

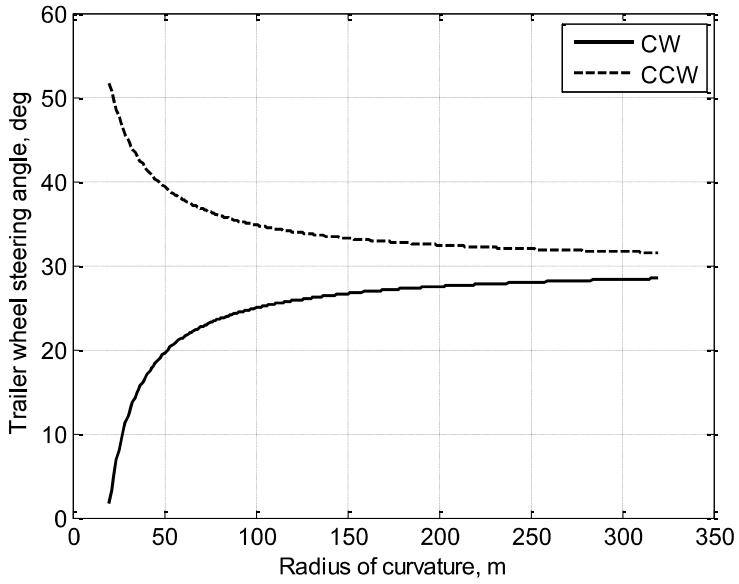


Figure 24. Radius of curvature of the road vs. trailer wheel steering angle for constant total articulation angle θ_t =30º

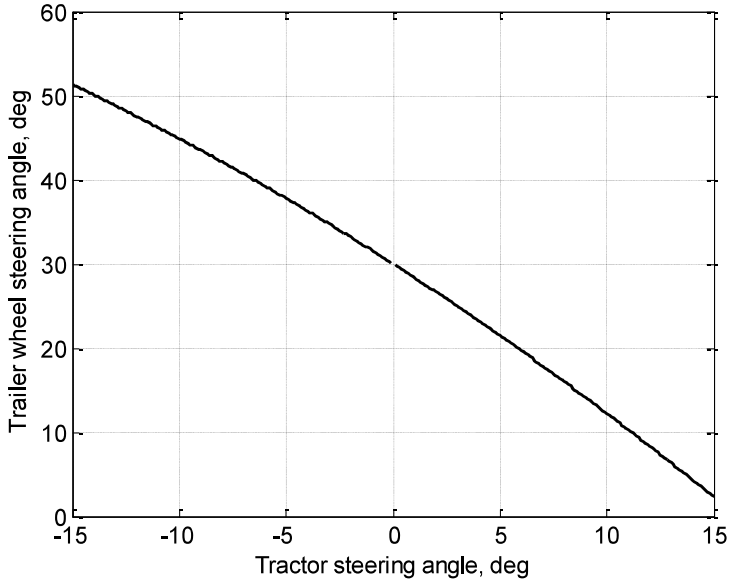


Figure 25. Tractor steering angle vs. Trailer wheel steering angle for constant total articulation angle θ_t =30º

Simulation of Constant Radius Turning

Using the equations derived in the preceding section, simulation is conducted for the following scenario:

1) The TowPlow moves forward on a straight road with zero articulation angle.

Copyright 2018. the authors

Vermeer Manufacturing Company – Ex. 2045
Kubota v. Vermeer
IPR2025-00168
Page 67 of 182

2) One second later, the trailer unit is deployed with trailer steering angle of 30 degrees.

3) The deployed TowPlow turns around a constant 50 *m* (164 ft) radius road in a clockwise direction. The trailer's corrective steering angle of 19.57 degrees is selected during the turning according to Figure 24.

Figure 26 presents the simulation results for constant radius turning. Angles of total articulation, tractor steering and trailer steering without and with trailer wheel's corrective steering during the cornering are shown in Figure 26a and Figure 26b, respectively. Also, intruding distance, which indicates how far the TowPlow intrudes into the adjacent lane, is shown in Figure 26c and Figure 26d for the cases without and with trailer wheel's corrective steering, respectively, during the cornering. Intruding distance (*ID*) is based on the plowing width of the snowplows and assumes that the TowPlow, with 30 degrees of the total articulation, completely covers the two-lane width of the road. *ID* is calculated by subtracting the plowing width of the TowPlow with the total articulation angle of 30 degrees ($W_{30\circ}$) from that with an arbitrarily angle due to the cornering (W_{θ_t}) as

$$ID = W_{\theta_t} - W_{30^\circ}, \tag{12}$$

where

$$W_{\theta_t} = w_{tp} \sin(\theta_t) + w_{fp} \cos \theta_{fp}, \tag{13}$$

w_{fp} is the width of the front plow, and w_{tp} is the width of the towed plow. The negative sign (-) of *ID* means that the TowPlow is within the two-lane width, and a positive sign (+) means intrusion of the TowPlow into the adjacent lane.

As shown in Figure 26, initially, the articulation angle of the TowPlow is zero in the straight road section for one second, *ID* is –3.96 *m* only with the front snowplowing since the first term of Eq. (13) is zero; i.e. there is no plowing of the adjacent lane. As the trailer wheel is steered to 30 degrees, the total articulation angle increases up to 30 degrees since the TowPlow is driving straight. After the trailer is completely deployed (after 7 *sec*), the tractor unit is steered to maneuver the constant radius turn (a, b). In the case of the simulation without corrective trailer steering, the total articulation angle is altered to 39.94 degrees (a) meaning that the trailer swings out and intrudes into the adjacent lane about 1.13 *m* (c). In the other case, however, the articulation angle is maintained at 30 degrees through steering of the trailer wheel (b), and the *ID* is zero, meaning the TowPlow system is kept within the two lanes being plowed (d).

Copyright 2018. the authors

Vermeer Manufacturing Company – Ex. 2045
Kubota v. Vermeer
IPR2025-00168
Page 68 of 182

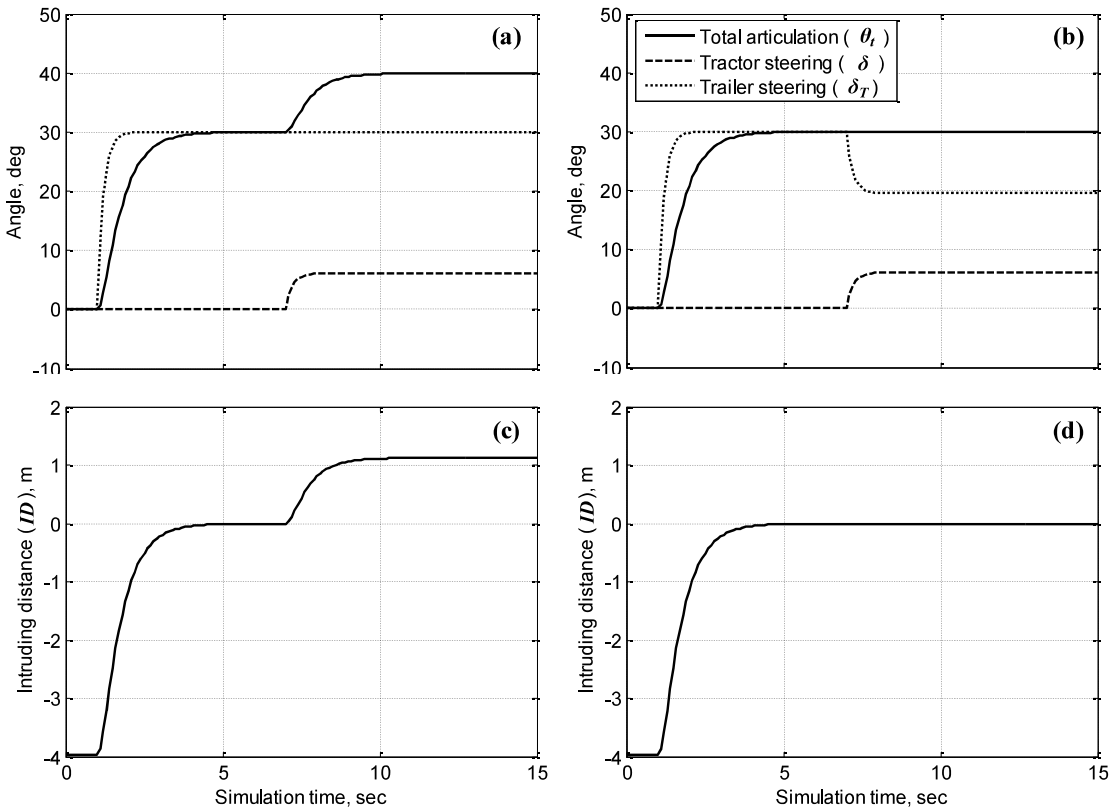


Figure 26. Simulation results of the constant radius turning: (a) angles without trailer corrective steering, (b) angles with trailer corrective steering, (c) intruding distance without trailer corrective steering, (d) intruding distance with trailer corrective steering

Summary

In this section, the kinematic characteristics of the TowPlow, which is represented as a tractor-trailer combination, are investigated. The kinematic equations are derived using instantaneous centers of velocity. Based on the derived equations, the relation between the radius of curvature and the trailer wheel steering angle that allows the tractor-trailer to maintain its initial total articulation angle is derived. Also, kinematic simulations of constant radius turning are performed with and without the trailer's corrective steering, and results are compared. Even though the kinematic analysis does not take forces and inertias into account, it is clearly demonstrated in the simulation results that appropriate steering of the trailer wheel is necessary to maintain the articulation angle of the TowPlow and to prevent the device from intruding into the adjacent lane or missing large segments within its lane. In the following section, the trailer's corrective steering, defined in this section (Figure 25, is implemented as a control input to the linear TowPlow model to investigate its dynamic performance.

Copyright 2018. the authors

Vermeer Manufacturing Company – Ex. 2045
Kubota v. Vermeer
IPR2025-00168
Page 69 of 182

Linear Vehicle Dynamics and Stability of the TowPlow

Even though the TowPlow may improve efficiency of the snow removal operation, implementation of the steerable trailer with a plow will affect overall system dynamics and could adversely affect stability of the system. In this section, lateral and yaw stability of the TowPlow is examined with a linear model, and a simple open-loop controller, utilizing the results from the kinematic analysis, is applied to the TowPlow.

Linear Planar Model of the TowPlow

Linear modeling of a vehicle has been widely used to investigate stability of the vehicle system and to develop a controller to enhance the stability. In this section, a linear model of the TowPlow is developed that only considers lateral and yaw motion of the TowPlow combination. Typical linear modeling of the truck-trailer combinations includes a small angle approximation of the articulation angle because the angle is small for the typical situations examined (e.g. highway travel). However, unlike the ordinary truck-trailer combinations, the trailer unit of the TowPlow has to be steered at a certain angle, which is not small enough to apply the small angle approximation when the TowPlow is in a snow removal operation. Thus, the linear TowPlow model requires the approximation of the trailer steering angle and the total articulation angle around their typical operating angles.

Figure 27 illustrates the linear planar model of the TowPlow in consideration of the lateral forces on each tire. Each unit has its own body-fixed coordinates, x-y-z coordinate system for the tractor unit and x_T-y_T-z_T for the trailer unit. Selected state variables for the model are lateral velocity (v_y) and yaw rate (ω) of the tractor unit, yaw rate of the trailer unit (ω_T) and total articulation angle (θ_t), which is the sum of articulation angle (θ) and trailer steering angle (δ_T) as defined in the section that started on page 45.

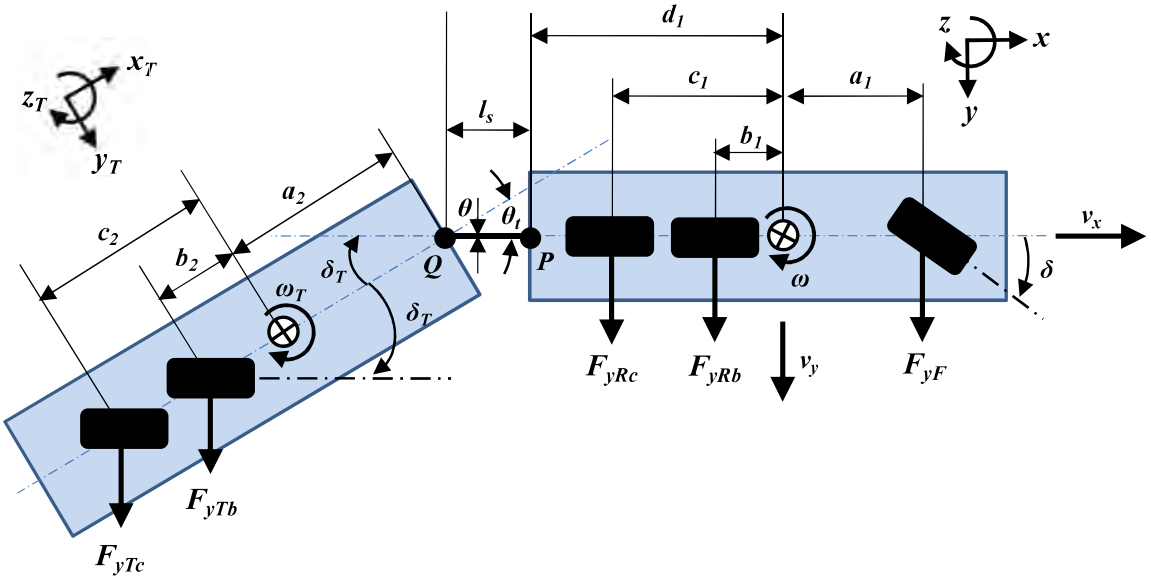


Figure 27. Linear planar TowPlow model and parameters

Copyright 2018. the authors

Vermeer Manufacturing Company – Ex. 2045
Kubota v. Vermeer
IPR2025-00168
Page 70 of 182

Since the model is an extended bicycle model, the following assumptions are employed:

- The wheels on each axle are represented by a single wheel at the center of each axle;
- Only lateral and yaw motions of the TowPlow are considered;
- Forward velocity of the TowPlow is constant in the longitudinal direction of the tractor unit;
- Longitudinal slip between the tire and the road surface is negligible;
- Forces on the plows are negligible;
- The tractor and trailer are rigid bodies;
- The tractor steering angle (δ) and articulation angle (θ) are infinitesimal. Thus, the small angle approximation can be applied to their trigonometric functions.
- The trailer steering angle (δ_T) and the total articulation angle (θ_t) can be expressed with the sum of an initial angle (δ_{Ti} and θ_{ti}) and the deviation angle ($\Delta\delta_T$ and $\Delta\theta_t$) as

$$\delta_T = \delta_{Ti} + \Delta\delta_T ; \theta_t = \theta_{ti} + \Delta\theta_t \quad , \tag{14}$$

  and trigonometric functions of the angles can be approximated around the initial angles using Taylor's series with truncation of the higher order terms as

$$\sin(\delta_T) \approx \sin(\delta_{Ti}) + \cos(\delta_{Ti})\Delta\delta_T ; \ \cos(\delta_T) \approx \cos(\delta_{Ti}) - \sin(\delta_{Ti})\Delta\delta_T \quad , \tag{15}$$

$$\sin(\theta_t) \approx \sin(\theta_{ti}) + \cos(\theta_{ti})\Delta\theta_t ; \ \cos(\theta_t) \approx \cos(\theta_{ti}) - \sin(\theta_{ti})\Delta\theta_t \quad . \tag{16}$$

- For the linear model, the initial angles of the trailer steering angle and the total articulation angle are identical.

Based on these assumptions, equations of lateral and yaw motions for the tractor unit are derived in its local coordinate system as

$$ma_y = m(\dot{v}_y + \omega v_x) = F_{yF} + F_{yRb} + F_{yRc} + F_{yTow} \quad , \tag{17}$$

$$I_{zz}\alpha = I_{zz}\dot{\omega} = a_1 F_{yFR} - b_1 F_{yRb} - c_1 F_{yRc} - d_1 F_{yTow} \quad , \tag{18}$$

where m denotes mass, I_{zz} denotes the moment of the inertia around z-axis, a_y signifies lateral acceleration, F_y is the lateral force of each tire, subscripts F and R indicate front and rear wheel of the tractor unit, subscripts b and c indicate the first and the second axle of the tandem rear axle, respectively, F_{yTow} denotes the lateral component of the towing force at the hitch point (point P), a_1, b_1, c_1, and d_1 signify the distance from the center of gravity (CG) to the front axle, to the first rear axle, to the second rear axle, and to the hitch point, respectively.

Copyright 2018. the authors

Vermeer Manufacturing Company – Ex. 2045
Kubota v. Vermeer
IPR2025-00168
Page 71 of 182

For the trailer unit, its dynamics are considered in the longitudinal, lateral and yaw directions, unlike the tractor unit having only two directions, because the tractor unit is steered at an arbitrary angle when the TowPlow is operating. Equations of motion for the trailer unit are derived in its local coordinate system as

$$m_T a_{xT} = m_T(\dot{v}_{xT} - \omega_T v_{yT}) = -F_{yTb}\sin(\delta_T) - F_{yTc}\sin(\delta_T) + F_{xTowed} \quad , \tag{19}$$

$$m_T a_{yT} = m_T(\dot{v}_{yT} + \omega_T v_{xT}) = F_{yTb}\cos(\delta_T) + F_{yTc}\cos(\delta_T) + F_{yTowed} \quad , \tag{20}$$

$$I_{zzT}\alpha_T = I_{zzT}\dot{\omega}_T = a_2 F_{yTowed} - b_2 F_{yTb}\cos(\delta_T) - c_1 F_{yTc}\cos(\delta_T) \quad , \tag{21}$$

where subscript T indicates the variables represent the trailer unit, F_{xTowed} and F_{yTowed} are longitudinal and lateral components of the towed force at hitch point of the trailer unit (point Q), and a_2, b_2 and c_2 are distance from the CG to the hitch point, to the first axle and to the second axle of the trailer unit, respectively.

When the tractor unit and the trailer unit are connected to each other through the tongue assembly, kinematic constraints at the hitch point should be considered. The velocity vector of Q in the tractor unit and that in the trailer unit are expressed using each coordinate system as

$$\underline{v}^{Q}_{tractor} = \underline{v}^{P}_{tractor} + \underline{\omega}^{Q}_{tractor} \times \underline{r}^{PQ} = (v_x + l_s\dot{\theta}\sin\theta)\hat{i} + (v_y - d_1\omega + l_s\dot{\theta}\cos\theta)\hat{j} \quad , \tag{22}$$

$$\underline{v}^{Q}_{trailer} = (v_{xT})\hat{i}_T + (v_{yT} + a_2\omega_T)\hat{j}_T \quad , \tag{23}$$

where $\hat{i}$ and $\hat{j}$ are unit vectors of the tractor's local coordinate system, $\hat{i}_T$ and $\hat{j}_T$ are those of the trailer's local coordinate system. The hitch point Q has the same velocity whichever coordinate system is used. Considering transformation of the coordinate system, Eq. (22) can be rewritten as

$$\begin{aligned} \underline{v}^{Q}_{tractor} = {} & \{v_x\cos(\theta_t) - (v_y - d_1\omega)\sin(\theta_t) - l_s\dot{\theta}\sin(\delta_T)\}\hat{i}_T \\ & + \{v_x\sin(\theta_t) + (v_y - d_1\omega)\cos(\theta_t) + l_s\dot{\theta}\cos(\delta_T)\}\hat{j}_T \end{aligned} \quad , \tag{24}$$

where

$$\begin{bmatrix} \hat{i} \\ \hat{j} \end{bmatrix} = \begin{bmatrix} \cos(\theta_t) & \sin(\theta_t) \\ -\sin(\theta_t) & \cos(\theta_t) \end{bmatrix} \begin{bmatrix} \hat{i}_T \\ \hat{j}_T \end{bmatrix} . \tag{25}$$

Eq. (25) shows the transformation between the two coordinate systems. The velocity components of the trailer unit can be expressed with the state variables based on the kinematic constraint from Eq. (23) and Eq. (24) as

$$v_{xT} = v_x\cos(\theta_t) - (v_y - d_1\omega)\sin(\theta_t) - l_s\dot{\theta}\sin(\delta_T) \quad , \tag{26}$$

$$v_{yT} = v_x\sin(\theta_t) + (v_y - d_1\omega)\cos(\theta_t) + l_s\dot{\theta}\cos(\delta_T) - a_2\omega_T \quad , \tag{27}$$

Copyright 2018. the authors

Vermeer Manufacturing Company – Ex. 2045
Kubota v. Vermeer
IPR2025-00168
Page 72 of 182

$$\begin{aligned}\dot{v}_{xT} &= -v_x \sin(\theta_t)\dot{\theta}_t - (\dot{v}_y - d_1\dot{\omega})\sin(\theta_t) - (v_y - d_1\omega)\cos(\theta_t)\dot{\theta}_t \\ &\quad - l_s\ddot{\theta}\sin(\delta_T) - l_s\dot{\theta}\cos(\delta_T)\dot{\delta}_T\end{aligned} \quad , \tag{28}$$

and

$$\begin{aligned}\dot{v}_{xT} &= v_x \cos(\theta_t)\dot{\theta}_t + (\dot{v}_y - d_1\dot{\omega})\cos(\theta_t) - (v_y - d_1\omega)\sin(\theta_t)\dot{\theta}_t \\ &\quad + l_s\ddot{\theta}\cos(\delta_T) - l_s\dot{\theta}\sin(\delta_T)\dot{\delta}_T - a_2\dot{\omega}_T\end{aligned} \quad . \tag{29}$$

An additional constraint which relates the total articulation angle, tractor yaw rate, and trailer yaw rate is considered as

$$\dot{\theta}_t = \omega - \omega_T \quad . \tag{30}$$

Also, when both units are connected through the tongue assembly, adequate force relationship should be defined. Figure 28 highlights forces on the hitch points (P and Q) and on the tongue assembly, where the sum of the forces should be equal to zero. Assuming that the articulation angle is small, the force relation can be defined as

$$F_{yTow} = F_{xTowed}\sin(\delta_T) - F_{yTowed}\cos(\delta_T) \quad . \tag{31}$$

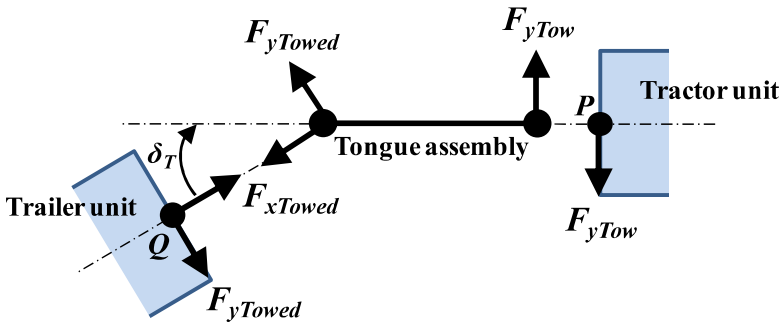


Figure 28. Forces at the hitch points and the tongue assembly

Eq. (14) ~ Eq. (31) are reduced to four differential equations by combining the equations of the tractor unit and the trailer unit together and truncating higher order terms. The differential equations are formulated as

$$\begin{aligned}Y: \quad &(m + m_T)\dot{v}_y - m_T(d_1 - l_s)\dot{\omega} - m_T\{l_s + a_2 c(\theta_{ti})\}\dot{\omega}_T \\ &= F_{yF} + F_{yRb} + F_{yRc} + F_{yTb} + F_{yTc} - (m + m_T)v_x\omega\end{aligned} \quad , \tag{32}$$

$$\begin{aligned}Z: \quad &- m_T d_1\dot{v}_y + \{I_{zz} + m_T d_1(d_1 - l_s)\}\dot{\omega} + m_T d_1\{l_s + a_2 c(\theta_{ti})\}\dot{\omega}_T \\ &= a_1 F_{yF} - b_1 F_{yRb} - c_1 F_{yRc} - d_1(F_{yTb} + F_{yTc}) + m_T d_1 v_x\omega_T\end{aligned} \quad , \tag{33}$$

Copyright 2018. the authors

Vermeer Manufacturing Company – Ex. 2045
Kubota v. Vermeer
IPR2025-00168
Page 73 of 182

$$Z_T: \quad -m_T a_2 c(\theta_{ti})\dot{v}_y + m_T a_2 c(\theta_{ti})(d_1 - l_s)\dot{\omega} + \{I_{zzT} + m_T a_2 c(\theta_{ti})(l_s + a_2 c(\theta_{ti})\}\dot{\omega}_T$$
$$= -a_2 c(\theta_{ti})(F_{yTb} + F_{yTc}) + m_T a_2 c(\theta_{ti}) v_x \omega - b_2 F_{yTRb} c(\delta_{Ti}) - c_2 F_{yTRc} c(\delta_{Ti}) \quad , \tag{34}$$

and Eq. (30), where *s*() and *c*() indicate sine and cosine of the angles, respectively.

In addition to the equations, forces on each tire need to be defined to demonstrate the motion of the TowPlow. The linear relationship of the lateral tire force with the slip angle is applied to each tire force of the linear model as

$$F_y = C_y \alpha \quad , \tag{35}$$

where α is the slip angle for tires on each axle approximated as

$$\alpha_F \approx \delta - \frac{v_y + a_1\omega}{v_x}; \quad \alpha_{Rb} \approx -\frac{v_y - b_1\omega}{v_x}; \quad \alpha_{Rc} \approx -\frac{v_y - c_1\omega}{v_x} \quad , \tag{36}$$

$$\alpha_{Tb} \approx \delta_{Ti} + \Delta\delta_T - \frac{v_x\{s(\theta_{ti}) + c(\theta_{ti})\Delta\theta_t\} + c(\theta_{ti})(v_y - d_1\omega) + l_s\dot{\theta}c(\delta_{Ti}) - a_2\omega_T - b_2\omega_T}{c(\theta_{ti})v_x};$$

$$\alpha_{Tc} \approx \delta_{Ti} + \Delta\delta_T - \frac{v_x\{s(\theta_{ti}) + c(\theta_{ti})\Delta\theta_t\} + c(\theta_{ti})(v_y - d_1\omega) + l_s\dot{\theta}c(\delta_{Ti}) - a_2\omega_T - c_2\omega_T}{c(\theta_{ti})v_x}. \tag{37}$$

Substituting Eq. (35) ~ Eq. (37) into Eq. (32) ~ Eq. (34) yields the linear differential equations of the TowPlow in the state-space representation as

$$\dot{\bar{x}} = M^{-1}A\bar{x} + M^{-1}B\bar{u} \quad , \tag{38}$$

where $\bar{x}$ is a vector of the state variables, $\bar{u}$ is a vector of the inputs, *M* is inertia matrix, and *A* and *B* are matrices defining the system. Vectors and matrices in Eq. (38) are specified as

$$M = \begin{bmatrix} m_{11} & m_{12} & m_{13} & m_{14} \\ m_{21} & m_{22} & m_{23} & m_{24} \\ m_{31} & m_{32} & m_{33} & m_{34} \\ m_{41} & m_{42} & m_{43} & m_{44} \end{bmatrix}, \quad A = \begin{bmatrix} a_{11} & a_{12} & a_{13} & a_{14} \\ a_{21} & a_{22} & a_{23} & a_{24} \\ a_{31} & a_{32} & a_{33} & a_{34} \\ a_{41} & a_{42} & a_{43} & a_{44} \end{bmatrix}, \quad B = \begin{bmatrix} b_{11} & b_{12} & b_{13} & b_{14} \\ b_{21} & b_{22} & b_{23} & b_{24} \\ b_{31} & b_{32} & b_{33} & b_{34} \\ b_{41} & b_{42} & b_{43} & b_{44} \end{bmatrix}, \quad \bar{x} = \begin{bmatrix} v_y \\ \omega \\ \omega_t \\ \Delta\theta_t \end{bmatrix},$$

$$\bar{u} = \begin{bmatrix} \delta \\ \Delta\delta_T \end{bmatrix}$$

where

Copyright 2018. the authors

Vermeer Manufacturing Company – Ex. 2045
Kubota v. Vermeer
IPR2025-00168
Page 74 of 182

$$m_{11} = m + m_T \text{ , } m_{12} = -m_T (d_1 - l_s) \text{ , } m_{13} = -m_T \{l_s + a_2 c(\theta_{ti})\} \text{ , } m_{14} = 0 \text{ ,}$$

$$m_{21} = -m_T d_1 \text{ , } m_{22} = I_{zz} + m_T d_1 (d_1 - l_s) \text{ , } m_{23} = m_T d_1 \{l_s + a_2 c(\theta_{ti})\} \text{ , } m_{24} = 0 \text{ ,}$$

$$m_{31} = -m_T a_2 c(\theta_{ti}) \text{ , } m_{32} = m_T a_2 c(\theta_{ti})(d_1 - l_s) \text{ , } m_{33} = I_{zzT} + m_T a_2 c(\theta_{ti})\{l_s + a_2 c(\theta_{ti})\} \text{ , } m_{34} = 0 \text{ ,}$$

$$m_{41} = 0 \text{ , } m_{42} = 0 \text{ , } m_{43} = 0 \text{ , } m_{44} = 1 \text{ ,}$$

$$a_{11} = -2 \times \left(\frac{C_{yF} + 2C_{yR} + 2C_{yT}}{v_x} \right),$$

$$a_{12} = 2 \times \left(\frac{-a_1 C_{yF} + b_1 C_{yR} + c_1 C_{yR} + 2d_1 C_{yT}}{v_x} - \frac{2l_s c(\delta_{Ti}) C_{yT}}{c(\theta_{ti}) v_x} \right) - (m + m_T) v_x \text{ ,}$$

$$a_{13} = 2 \times \left(\frac{\{l_s c(\delta_{Ti}) + a_2 + b_2\} C_{yT} + \{l_s c(\delta_{Ti}) + a_2 + c_2\} C_{yT}}{c(\theta_{ti}) v_x} \right),$$

$$a_{14} = -2 \times \left(2C_{yT} \right),$$

$$a_{21} = 2 \times \left(\frac{-a_1 C_{yF} + b_1 C_{yR} + c_1 C_{yR} + 2d_1 C_{yT}}{v_x} \right),$$

Copyright 2018. the authors

Vermeer Manufacturing Company – Ex. 2045
Kubota v. Vermeer
IPR2025-00168
Page 75 of 182

$$a_{22} = 2 \times \left(\frac{-a_1^2 C_{yF} - b_1^2 C_{yR} - c_1^2 C_{yR} - 2d_1(d_1 - l_s)C_{yT}}{v_x} \right) + m_T d_1 v_x ,$$

$$a_{23} = -2 \times d_1 \left(\frac{\{l_s c(\delta_{Ti}) + a_2 + b_2\}C_{yT} + \{l_s c(\delta_{Ti}) + a_2 + c_2\}C_{yT}}{c(\theta_{ti})v_x} \right),$$

$$a_{24} = 2 \times d_1 \left(2C_{yT}\right),$$

$$a_{31} = 2 \times c(\delta_{Ti}) \left(\frac{a_2 C_{yT} + a_2 C_{yT} + b_2 C_{yT} + c_2 C_{yT}}{v_x} \right),$$

$$a_{32} = -2 \times c(\delta_{Ti})(d_1 - l_s) \left(\frac{a_2 C_{yT} + a_2 C_{yT} + b_2 C_{yT} + c_2 C_{yT}}{v_x} \right) + m_T a_2 c(\delta_{Ti}) v_x ,$$

$$a_{33} = -2 \times c(\delta_{Ti}) \left(\frac{a_2\{l_s c(\delta_{Ti}) + a_2 + b_2\}C_{yT} + a_2\{l_s c(\delta_{Ti}) + a_2 + c_2\}C_{yT}}{c(\theta_{ti})v_x} + \ldots \right.$$
$$\left. \ldots \frac{b_2\{l_s c(\delta_{Ti}) + a_2 + b_2\}C_{yT} + c_2\{l_s c(\delta_{Ti}) + a_2 + c_2\}C_{yT}}{c(\theta_{ti})v_x} \right),$$

$$a_{34} = 2 \times c(\delta_{Ti}) \left(a_2 C_{yT} + a_2 C_{yT} + b_2 C_{yT} + c_2 C_{yT}\right),$$

$$a_{41} = 0 , a_{42} = 1 , a_{43} = -1 , a_{44} = 0.$$

Stability and Controllability of the TowPlow

Once the linear differential equations of a system are established in the state-space representation, stability and controllability of the system can be examined using the system matrix and the input matrix. The system matrix of the linear TowPlow model is $M^{-1}A$ in Eq. (38), and the input matrix is $M^{-1}B$ in Eq. (38). They are highly dependent on the longitudinal velocity of the tractor unit. Since the total articulation angle of 30-degree is required to clear the width of two typical highway lanes, the linearized model of the TowPlow is approximated around 30 degrees of the total articulation angle and trailer steering angle in the evaluation.

Stability of the system is evaluated by the eigenvalues of the system matrix which can be easily obtained using MATLAB® for different values of the parameters. Table 6shows vehicle parameters used in the calculation.

Copyright 2018. the authors

Vermeer Manufacturing Company – Ex. 2045
Kubota v. Vermeer
IPR2025-00168
Page 76 of 182

Table 6. Vehicle parameters for stability analysis

Symbol	Value	Unit	Description
m	13,925 ~ 29,031	kg	Mass of tractor unit
m_T	4,654 ~ 17,040	kg	Mass of trailer unit
I_{zz}	40,018 ~ 78,210	kg·m^2	Moment of inertia for tractor unit
I_{zzT}	13,374 ~ 48,968	kg·m^2	Moment of inertia for trailer unit
C_{yF}	168,000	N/rad	Lateral tire stiffness for tractor front axle
C_{yR}	168,000	N/rad	Lateral tire stiffness for tractor rear axles
C_{yT}	168,000	N/rad	Lateral tire stiffness for trailer axles
a_1	3.30	m	Distance from CG to front axle (tractor)
b_1	1.27	m	Distance from CG to first rear axle (tractor)
c_1	2.69	m	Distance from CG to second rear axle (tractor)
d_1	3.65	m	Distance from CG to articulation point (tractor)
l_s	2.19	m	Length of tongue assembly
a_2	4.34	m	Distance from CG to articulation point (trailer)
b_2	0.44	m	Distance from CG to first trailer axle
c_2	1.86	m	Distance from CG to second trailer axle
θ_{ti}	30	deg	Initial total articulation angle
δ_{Ti}	30	deg	Initial trailer steering angle

One should note that the inertia of the TowPlow, for both units, can be varied when the TowPlow is in the snow removal operation because the tractor unit has a dump body, which may contain salt, sand or gravel, and the trailer unit also has one or more storage containers equipped with spraying or discharging systems to distribute salt, sand, gravel or deicing compositions during the operation. The minimum combination of the TowPlow only has the tractor and trailer, with their dump body and container emptied and without moldboards for the snowplows. The maximum combination includes the dump body and container fully loaded up to the rated weight as well as moldboards for the snowplows. Figure 29 depicts the locus of the eigenvalues with varying longitudinal velocity of the tractor from 1 *km/h* (0.6 *mph*) to 130 *km/h* (80 *mph*) with the maximum weight combination of the TowPlow. Arrows in the figure indicate the direction of increasing velocity. Even though the recommended velocity is about 90 *km/h* (55 *mph*) with the trailer deployed, velocity is increased up to 130 *km/h* (80 *mph*) to verify the stability limitation. When the longitudinal velocity is lower than the characteristic velocity, 120 *km/h* (75 *mph*), the TowPlow is stable in terms of lateral and yaw motion. However, as the velocity becomes higher than the characteristic velocity, one of the eigenvalues becomes greater than zero and moves to the right-hand plane. Thus, the TowPlow becomes unstable causing trailer-swing or jack-knifing.

Copyright 2018. the authors

Vermeer Manufacturing Company – Ex. 2045
Kubota v. Vermeer
IPR2025-00168
Page 77 of 182

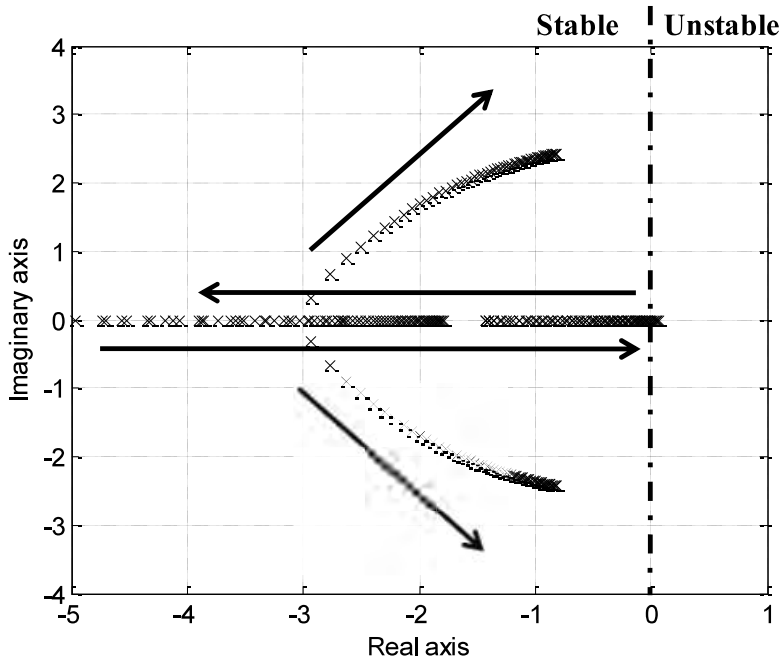


Figure 29. Locus of the eigenvalues of the matrix $M^{-1}A$ with varying longitudinal velocity

Stability of the TowPlow varying the inertias is also considered. Figure 30**Error! Reference source not found.** shows locus of the eigenvalues of the system matrix. The tractor mass and moment of inertia are increased stepwise from its minimum up to its maximum, and at each step the trailer mass and moment of inertia are also increased stepwise from the minimum to the maximum. The longitudinal velocity of the TowPlow is constant at 105 *km/h* (65*mph*), slightly higher than the velocity recommended by the manufacturer of the TowPlow because it is possible that, in real operation, driver may exceed the speed limit particularly when traveling downhill. As shown in the figure, the TowPlow is stable for most inertia combinations, but there exist some combinations that the TowPlow loses its stability; i.e., the TowPlow's spraying or discharging systems to distribute salt, sand, gravel or deicing compositions during the operation have potential problem that the TowPlow system becomes unstable. Figure 31 presents examples of such cases to examine stability trend with varying inertias. In figures, arrows indicate the direction of increasing inertia. Figure 31a depicts locus of the eigenvalues for the system that has the minimum tractor inertia with varying trailer inertia. From the results, it is found that the TowPlow is unstable when the trailer inertia is greater than 106.3% of the tractor inertia. Figure 31b is for the system that has the maximum trailer inertia with varying tractor inertia. In this case, the TowPlow is unstable when the tractor inertia is smaller than 124.4% of the trailer inertia.

Copyright 2018. the authors

Vermeer Manufacturing Company – Ex. 2045
Kubota v. Vermeer
IPR2025-00168
Page 78 of 182

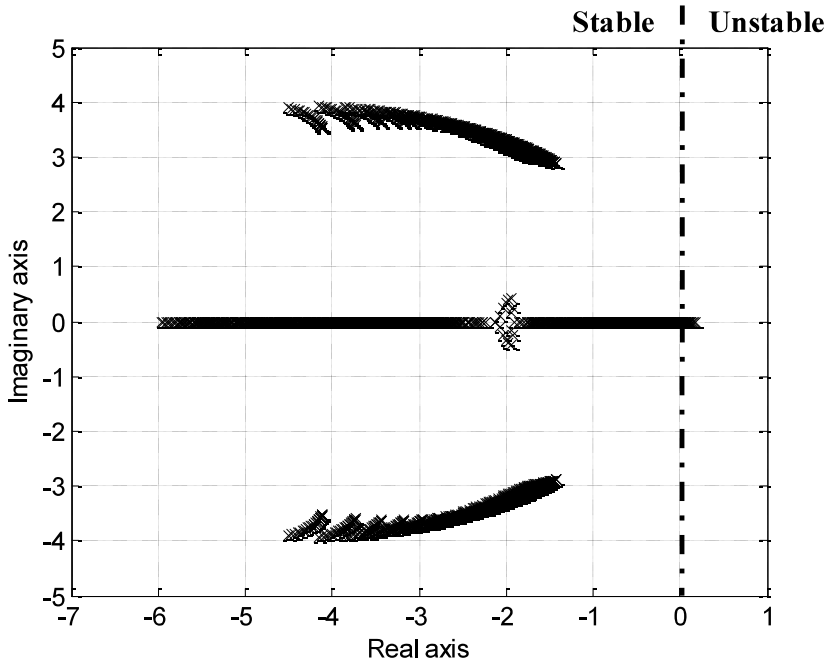


Figure 30. Locus of the eigenvalues of the matrix $M^{-1}A$ with varying inertias

Copyright 2018. the authors

Vermeer Manufacturing Company – Ex. 2045
Kubota v. Vermeer
IPR2025-00168
Page 79 of 182

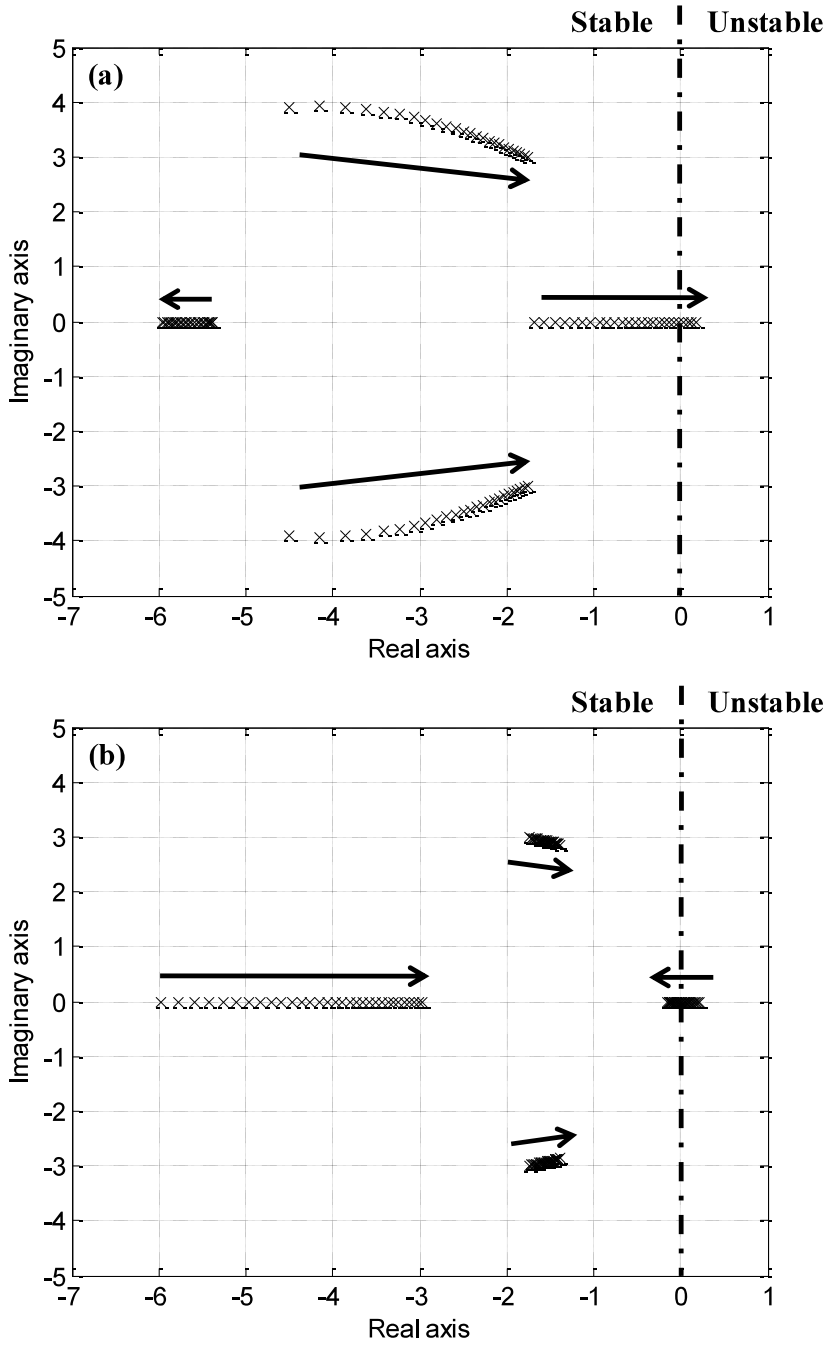


Figure 31. Locus of the eigenvalues of the matrix $M^{-1}A$ with varying inertias: (a) Minimum tractor inertia with varying trailer inertia, (b) Maximum trailer inertia with varying tractor inertia

Furthermore, even though the TowPlow is generally stable with the recommended longitudinal velocity, it does not necessarily mean the TowPlow is safe. As addressed in the section starting on page 45, the TowPlow has a potential problem of either missing large portions

Copyright 2018. the authors

Vermeer Manufacturing Company – Ex. 2045
Kubota v. Vermeer
IPR2025-00168
Page 80 of 182

of the road or intruding into the adjacent lane during cornering, and with proper control input such as steering of the trailer axles, safety and efficiency of the TowPlow can be enhanced.

Controllability of the TowPlow is also investigated using the matrices of the state-space representation of the linear TowPlow model. The system is controllable if defined inputs, tractor and trailer steering angle for the TowPlow, are able to move the system to any state in its entire space. The system is uncontrollable if there exists some states that the system cannot reach with its inputs. To test such characteristic of the TowPlow, a controllability matrix needs to be created as

$$Co = [M^{-1}B \ \vdots \ M^{-1}AM^{-1}B \ \vdots \ (M^{-1}A)^2M^{-1}B \ \vdots \ (M^{-1}A)^3M^{-1}B] \quad (39)$$

When this matrix has full rank, meaning the rank of the matrix is equal to the number of states, $rank(Co) = 4$ for the linear TowPlow model, each of the states are reachable, thus the system is controllable.

As a result of the controllability evaluation with different longitudinal velocities (1 *km/h* ~ 130 *km/h*) and inertias of the TowPlow (minimum to maximum combination), the linear TowPlow model is controllable.

Dynamics and Open-loop Control of the TowPlow

In this section, dynamic responses of the TowPlow to various types of inputs are demonstrated through simulation of the linear TowPlow model. The simulator is programmed with MATLAB®/Simulink®. First, dynamic simulation of the TowPlow with a constant trailer steering angle, i.e., the uncontrolled system, is performed for step, pulse, and sine wave form inputs of the tractor steering angle (δ). Then, for the same tractor steering inputs, simulation of the controlled system is performed, where control input is the corrective trailer steering angle, deviation from the initial trailer steering angle ($\Delta\delta_T$), which helps the total articulation angle of the TowPlow be constant at 30 degrees during the maneuvers.

Figure 32 depicts the simulation scheme of the uncontrolled system. The plant represents the state-space model of the TowPlow, where outputs of the model are defined same as states – tractor lateral velocity (v_y), tractor yaw (ω), trailer yaw (ω_T) and deviation of the total articulation angle ($\Delta\theta_t$) from its initial angle – of the model as

$$\bar{y} = C\bar{x} \quad (40)$$

where C is a 4-by-4 unit matrix since the number of states is 4. The corrective trailer steering angle is set to be zero because there is no control of the trailer steering angle.

Copyright 2018. the authors

Vermeer Manufacturing Company – Ex. 2045
Kubota v. Vermeer
IPR2025-00168
Page 81 of 182

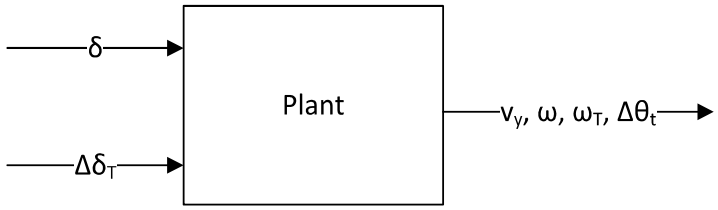


Figure 32. Scheme of the uncontrolled system simulation

Figure 33 presents the simulation scheme of the open-loop controlled system. For the look-up table, which decides the corrective trailer steering angle according to the tractor steering angle, the relationship between the two angles to maintain a constant total articulation angle of 30 degrees is shown in Figure 25.

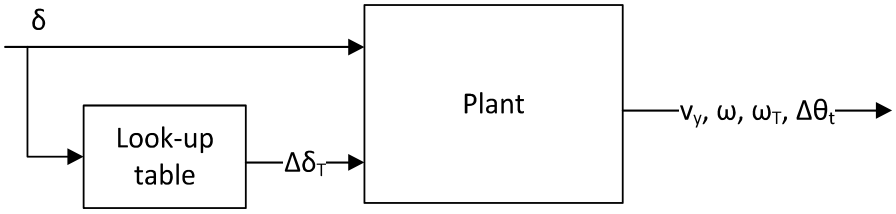


Figure 33. Scheme of the open-loop controlled system simulation using the lookup table show in in Error! Reference source not found.

Vehicle parameters in Table 6 are used for both uncontrolled system and controlled system simulations. Inertias of the TowPlow are considered with the maximum combination, and tractor's forward velocity of 40 *km/h* (25 *mph*), a moderate speed for the snow removal operation is applied to the model. The magnitude of the step and pulse input is 6 degrees, which allows the TowPlow to form turning radius of approximately 50 *m* (164 ft) when calculated geometrically. For these inputs, the tractor steering angle includes a transfer function to account for simple driver dynamics. The sine input has frequency of 0.2 Hz, and magnitude of 4 degrees.

Figure 34 shows simulation results of tractor yaw rate, trailer yaw rate, and total articulation angle for the step tractor steering input comparing the uncontrolled and controlled systems. A solid line represents results of the uncontrolled system, and a dashed line is for the controlled system. The same steering input for the towing unit is applied to both cases. The trailer steering angle for the uncontrolled case is fixed at its initial angle of 30 degrees, while the angle for the other case varies along with the tractor steering angle based on the look-up table. For the uncontrolled system, the total articulation changes up to 42.49 degrees according to the tractor unit steering, and the TowPlow intrudes into the adjacent lane. However, for the controlled system, yaw rates of the tractor and the trailer are almost synchronized, and the total articulation angle deviates only 0.13 degrees from its initial angle due to the trailer steering.

Figure 35 presents simulation results for the pulse tractor steering input. The corrective steering angle is input to the trailer steering angle. Thus, the total articulation angle of the controlled system deviates from its initial angle much less than the uncontrolled system.

Copyright 2018. the authors

Vermeer Manufacturing Company – Ex. 2045
Kubota v. Vermeer
IPR2025-00168
Page 82 of 182

However, one should note that, for the controlled system of the step and pulse input cases, the peak value of the tractor yaw rate is smaller than that of the uncontrolled system. Assuming that the tractor has a constant forward velocity during the maneuver, the tractor unit yields a slightly larger turning radius due to the corrective trailer steering, and understeers. Applying corrective steering to the tractor steering is required to compensate the yaw rate difference between the uncontrolled and controlled systems.

Simulation results of the sine input are shown in Figure 36. Corrective steering of the trailer helps the TowPlow maintain the total articulation angle of 30 degrees.

Summary

In this section, the linear dynamic model of the TowPlow is developed in lateral and yaw directions. Due to the characteristic of the TowPlow that it operates with a certain degree of total articulation angle, the model is linearized around the angles using Taylor's series. Stability and controllability of the TowPlow are investigated with the linear TowPlow model, for different values of the parameters – tractor forward velocity and inertias of the TowPlow. The TowPlow is stable and controllable with parameters in its operating range. Also, dynamic simulations of various maneuvers are performed, and open-loop control is implemented to investigate performance of the trailer's corrective steering defined in the section starting on page 45. The results with and without control are compared. Even though the control input is obtained from the kinematic analysis which does not take forces and inertia into account, the simulation results clearly show that the corrective steering helps the TowPlow reduce deviation of the total articulation angle from its initial angle during the maneuvers. However, for some cases, the corrective trailer steering causes understeer of the tractor unit, which requires additional control to the tractor steering.

Copyright 2018. the authors

Vermeer Manufacturing Company – Ex. 2045
Kubota v. Vermeer
IPR2025-00168
Page 83 of 182

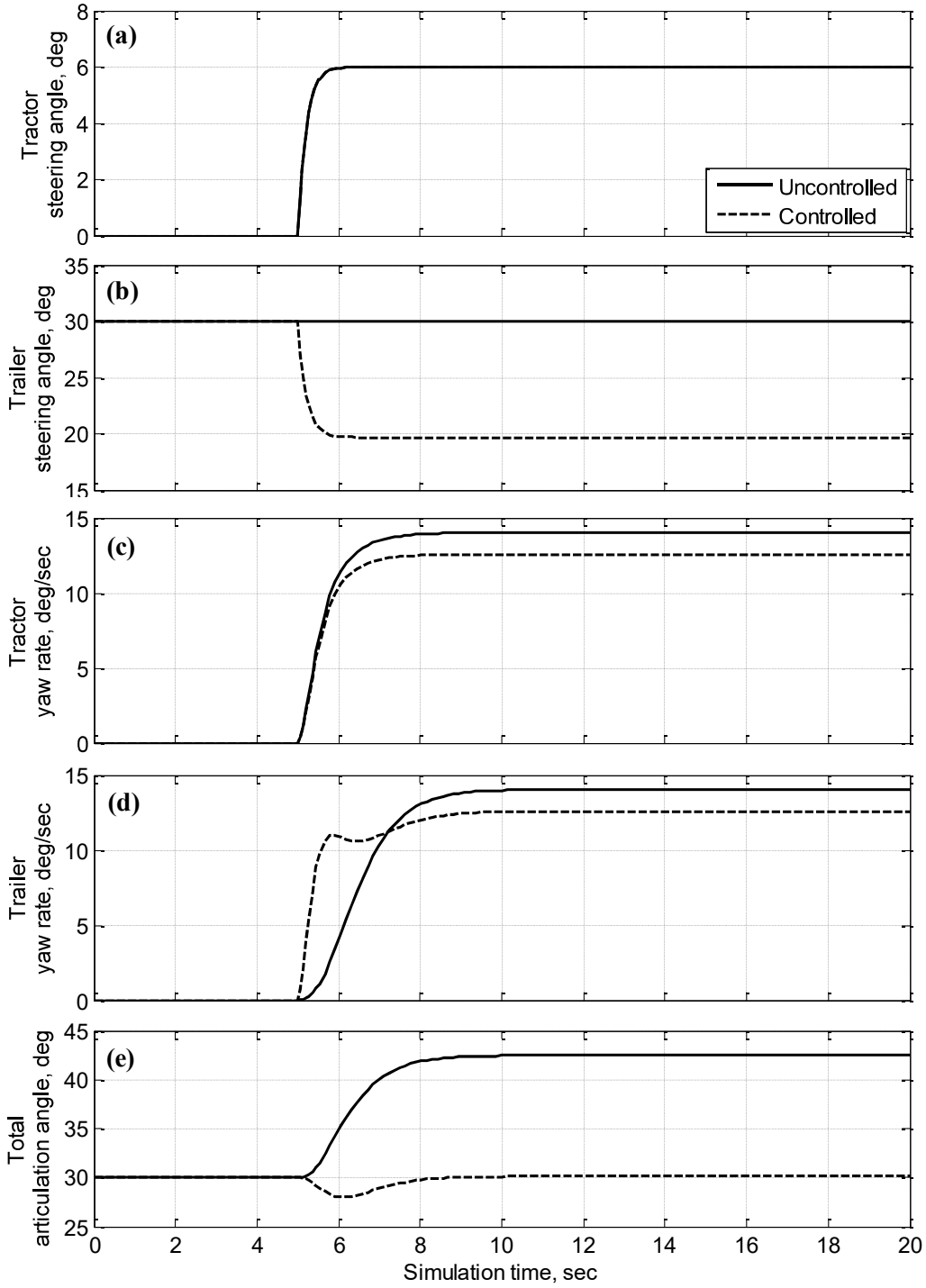


Figure 34. Simulation results of the TowPlow comparing uncontrolled and controlled system for the step input: (a) Tractor steering angle, (b) Trailer steering angle, (c) Tractor yaw rate, (d) Trailer yaw rate, (e) Total articulation angle

Copyright 2018. the authors

Vermeer Manufacturing Company – Ex. 2045
Kubota v. Vermeer
IPR2025-00168
Page 84 of 182

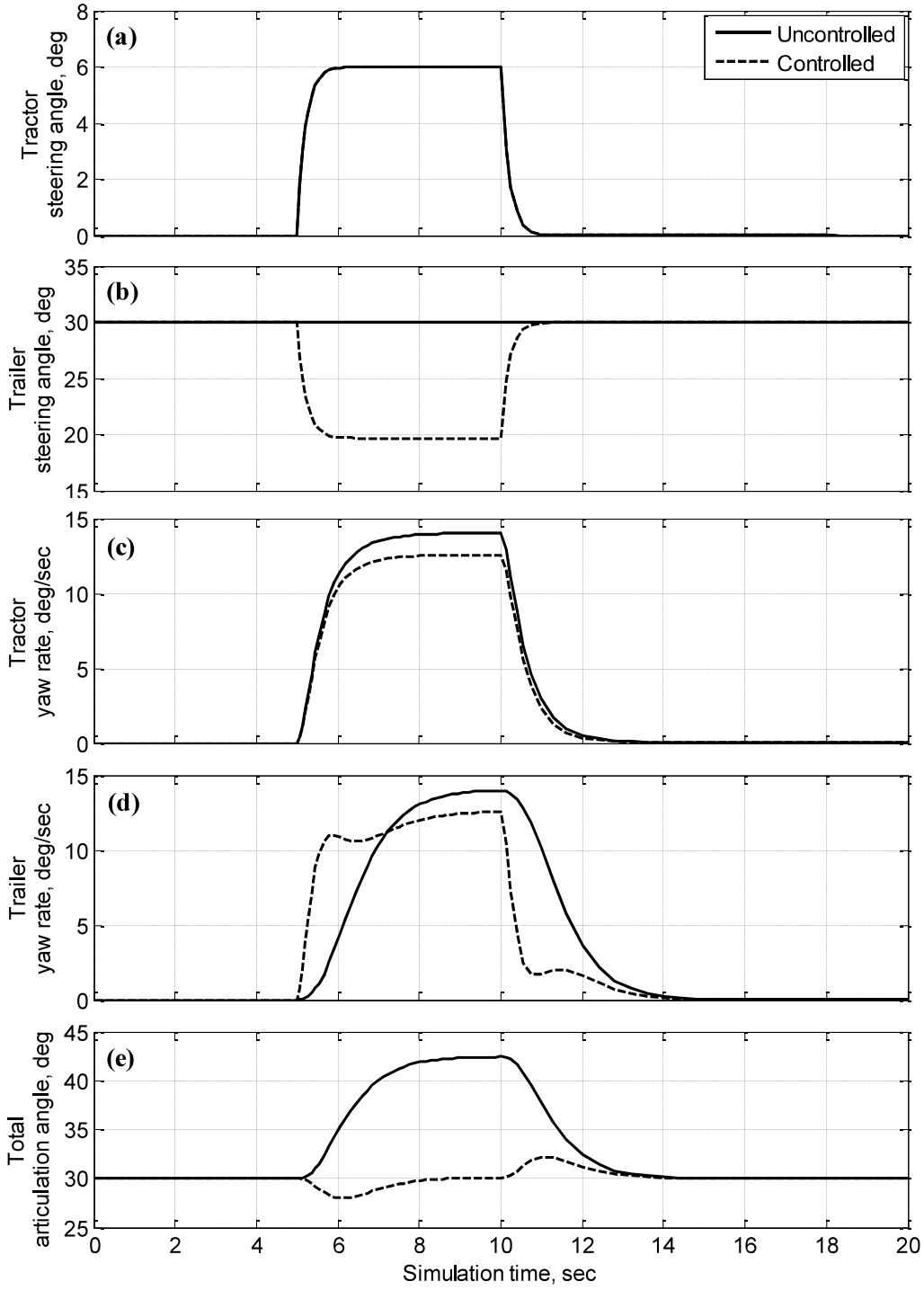


Figure 35. Simulation results of the TowPlow comparing uncontrolled and controlled system for the pulse input: (a) Tractor steering angle, (b) Trailer steering angle, (c) Tractor yaw rate, (d) Trailer yaw rate, (e) Total articulation angle

Copyright 2018. the authors

Vermeer Manufacturing Company – Ex. 2045
Kubota v. Vermeer
IPR2025-00168
Page 85 of 182

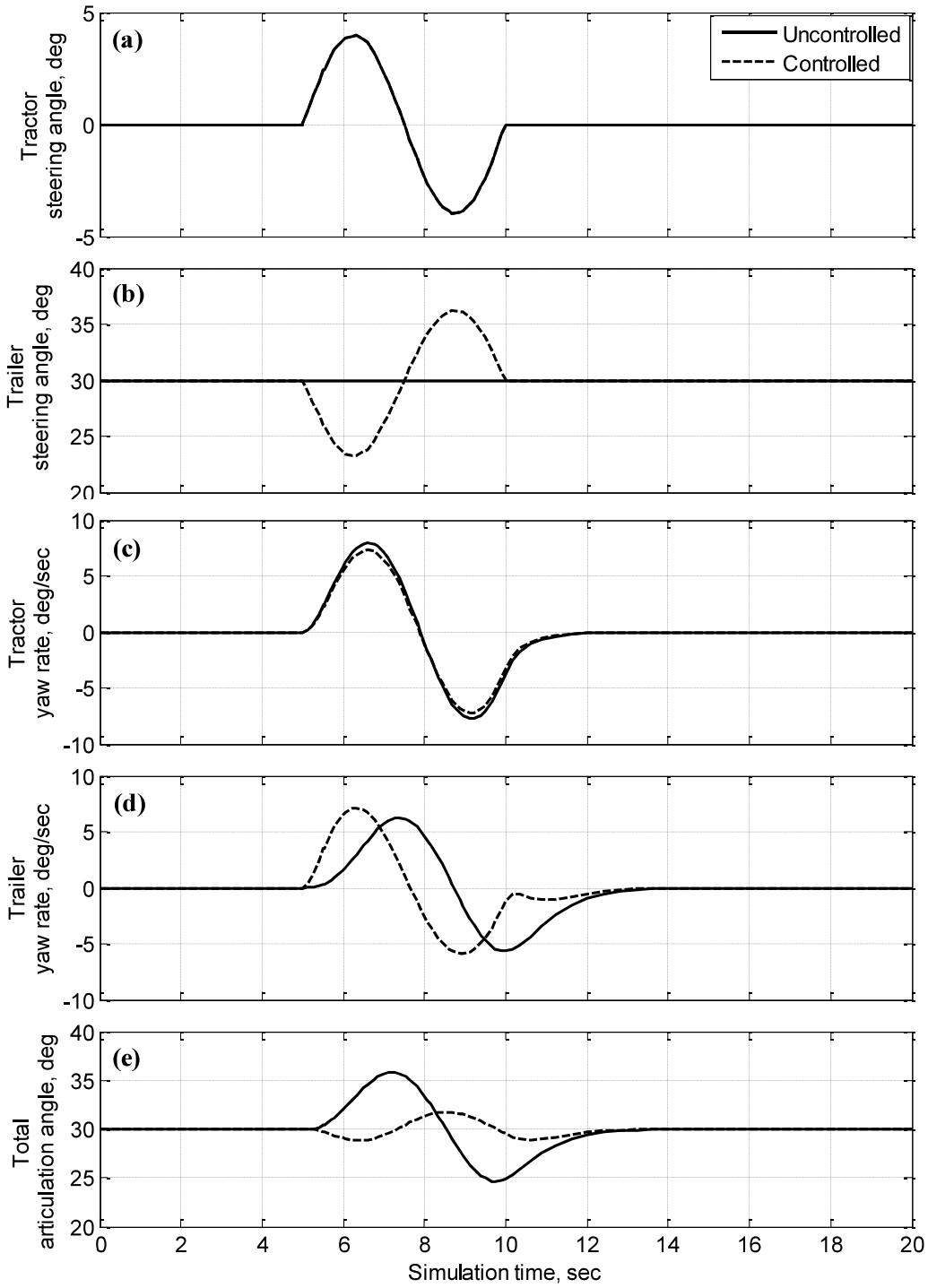


Figure 36. Simulation results of the TowPlow comparing uncontrolled and controlled system for the sine input: (a) Tractor steering angle, (b) Trailer steering angle, (c) Tractor yaw rate, (d) Trailer yaw rate, (e) Total articulation angle

Copyright 2018. the authors

Vermeer Manufacturing Company – Ex. 2045
Kubota v. Vermeer
IPR2025-00168
Page 86 of 182

Nonlinear Vehicle Dynamics of the TowPlow

Although the kinematic analysis and the linear dynamics provide basic understanding of how the TowPlow, as an articulated vehicle, operates according to the steering inputs, it is not sufficient to demonstrate the motion of the TowPlow in various operating conditions. It is necessary to consider nonlinearity of the tire forces and vehicle motion to understand the TowPlow in real world operation. A nonlinear dynamic model of the TowPlow for longitudinal, lateral, and yaw motions is developed with the state variables of longitudinal velocity, lateral velocity and yaw rate of the towing unit, yaw rate of the trailer unit, and the articulation angle between the two units. The model includes a modified Dugoff's tire friction model, tire rotation dynamics and the load transfer effect. The model is validated through full-scale experiments of the TowPlow under both steady-state and transient conditions.

Equations of Motion for the TowPlow

Figure 37 depicts the tractor unit of the TowPlow and the forces acting on the tires, front plow and hitch point, *P*. The tractor unit is a front wheel steering system with tandem rear axle, and is equipped with a front snowplow. Each tire force is composed of longitudinal and lateral components. Snow resistance against the plow is represented as the force acting at the center of the plow, where the support arm is located. At hitch point *P*, the force from the trailer unit is applied in an arbitrary direction.

Copyright 2018. the authors

Vermeer Manufacturing Company – Ex. 2045
Kubota v. Vermeer
IPR2025-00168
Page 87 of 182

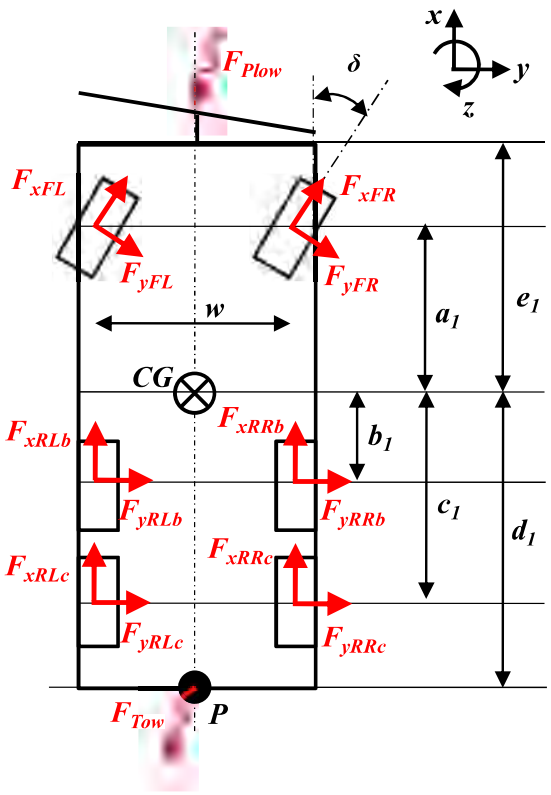


Figure 37. Scheme of the tractor unit and forces

Equations of longitudinal, lateral and yaw motions for the tractor unit are derived in the *xyz* body fixed coordinate system using Newton's second law of motion as

$$ma_x = m(\dot{v}_x - \omega v_y) = (F_{xFR} + F_{xFL})\cos\delta - (F_{yFR} + F_{yFL})\sin\delta + F_{xRRb} + F_{xRRc} + F_{xRLb} + F_{xRLc} - F_{xPlow} + F_{xTow}, \quad (41)$$

$$ma_y = m(\dot{v}_y + \omega v_x) = (F_{xFR} + F_{xFL})\sin\delta + (F_{yFR} + F_{yFL})\cos\delta + F_{yRRb} + F_{yRRc} + F_{yRLb} + F_{yRLc} - F_{yPlow} + F_{yTow}, \quad (42)$$

$$I_{zz}\alpha = I_{zz}\dot{\omega} = a_1\{(F_{xFR} + F_{xFL})\sin\delta + (F_{yFR} + F_{yFL})\cos\delta\} - b_1(F_{yRRb} + F_{yRLb}) - c_1(F_{yRRc} + F_{yRLc}) - d_1F_{yTow} + e_1F_{tPlow} + \frac{w}{2}\{(F_{xFL} - F_{xFR})\cos\delta + (F_{yFR} - F_{yFL})\sin\delta + F_{xRLb} + F_{xRLc} - F_{xRRb} - F_{xRRc}\}, \quad (43)$$

where a_x is longitudinal acceleration, F_x signifies longitudinal forces of each tire, subscripts *FR*, *FL*, *RR*, and *RL* indicate front-right, front-left, rear-right and rear-left wheel of the tractor unit, F_{xPlow} denotes the longitudinal component of the force on the plow, F_{yPlow} denotes the lateral component of the force on the plow, F_{xTow} and F_{yTow} denote the longitudinal and lateral components of the force at the hitch point, e_1 signifies the distance from the center of gravity (CG) to the plow support arm, and *w* is the axle track of the tractor unit.

Copyright 2018. the authors

Vermeer Manufacturing Company – Ex. 2045
Kubota v. Vermeer
IPR2025-00168
Page 88 of 182

The trailer unit of the TowPlow and the forces applied to the tires, snowplow, and hitch point, *Q* are illustrated in Figure 38. The trailer unit is equipped with a steerable tandem axle, and the articulation angle of the trailer unit with respect to the tongue assembly alters as the trailer axle is steered. The amount of articulation is the same as the trailer steering angle due to the hydraulic coupling feature. Snow forces on the trailer-plow are represented with a force vector in an arbitrary direction for now; this will be dealt comprehensively in the following section starting on page 89.

The equations of longitudinal, lateral and yaw motions for the trailer unit are derived in the x_T-y_T-z_T trailer body fixed coordinate system as

$$m_T a_{xT} = m_T(\dot{v}_{xT} - \omega_T v_{yT}) = (F_{xTRb} + F_{xTLb} + F_{xTRc} + F_{xTLc})\cos\delta_T - (F_{yTRb} + F_{yTLb} + F_{yTRc} + F_{yTLc})\sin\delta_T - F_{xTPlow} + F_{xTowed}, \quad (44)$$

$$m_T a_{yT} = m_T(\dot{v}_{yT} + \omega_T v_{xT}) = (F_{xTRb} + F_{xTRc} + F_{xTLb} + F_{xTLc})\sin\delta_T + (F_{yTRb} + F_{yTRc} + F_{yTLb} + F_{yTLc})\cos\delta_T - F_{yTPlow} + F_{tTowed}, \quad (45)$$

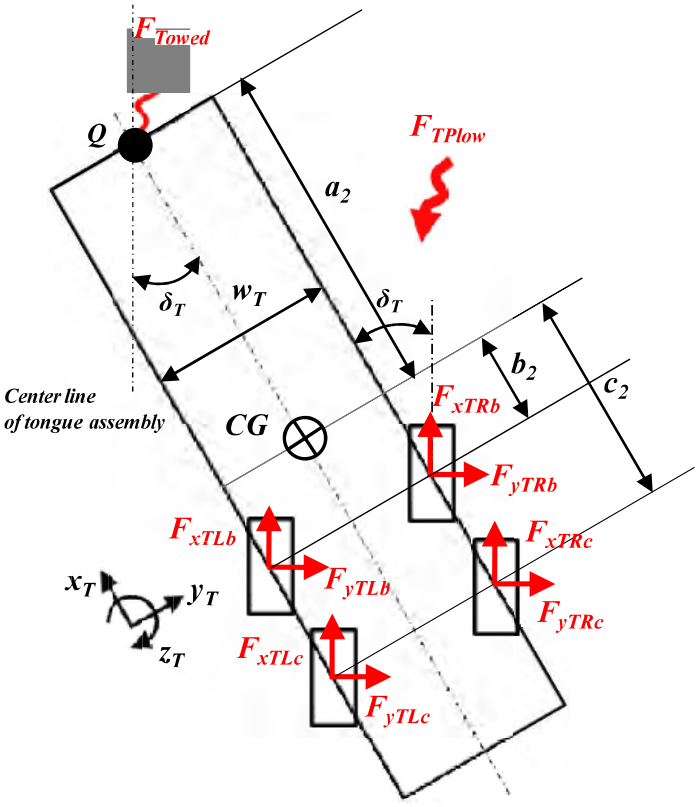


Figure 38. Scheme of the trailer unit and forces

Copyright 2018. the authors

Vermeer Manufacturing Company – Ex. 2045
Kubota v. Vermeer
IPR2025-00168
Page 89 of 182

$$I_{zzT}\alpha_T = I_{zzT}\dot{\omega}_T = a_2 F_{yTowed} - b_2\{(F_{xTLb} + F_{xTRb})\sin\delta_T + (F_{yTLb} + F_{yTRb})\cos\delta_T\}$$
$$- c_2\{(F_{xTLc} + F_{xTRc})\sin\delta_T + (F_{yTLc} + F_{yTRc})\cos\delta_T\} + M_{TPlow}$$
$$+ \frac{w_t}{2}\{(F_{xTLb} + F_{xTLc} - F_{xTRb} - F_{xTRc})\cos\delta_T + (F_{yTRb} + F_{yTRc} - F_{yTLb} - F_{yTLc})\sin\delta_T\} \quad (46)$$

where subscripts of the tire forces, *TR* and *TL*, signify trailer-right wheel and trailer-left wheel respectively, F_{xTPlow} and F_{yTPlow} are the longitudinal and lateral components of the force on the trailer-plow, and M_{TPlow} denotes the moment caused by F_{xTPlow} and F_{yTPlow}.

Figure 39 focuses on the tongue assembly and defines the kinematic and force relationship between the tractor unit and trailer unit. It is assumed that inertia properties of the tongue assembly are negligible since they are small compared to the two units.

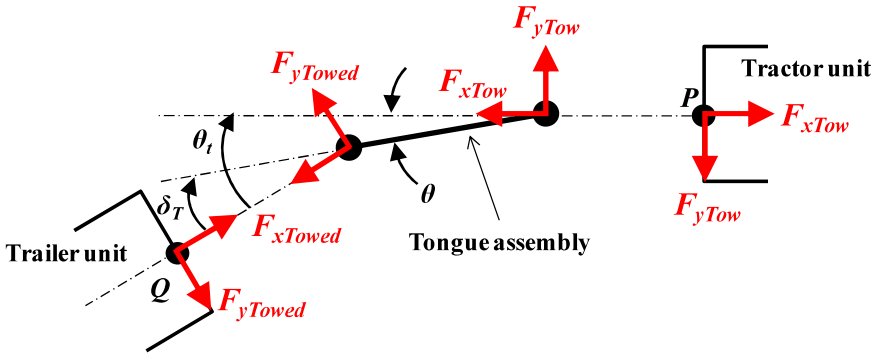


Figure 39. Scheme of the tongue assembly and forces

The kinematic relationship is described in the preceding section (starting on page 52) as Eq. (26) ~ (30). The force relationship is redefined considering the articulation angle and the fact that the sum of the forces on the tongue assembly should be equal to zero as

$$F_{xTow} = -F_{xTowed}\cos(\theta_t) - F_{yTowed}\sin(\theta_t), \quad (47)$$

$$F_{yTow} = F_{xTowed}\sin(\theta_t) - F_{yTowed}\cos(\theta_t). \quad (48)$$

In addition to Eq. (41) ~ Eq. (48), forces on each tire and each plow need to be defined to demonstrate the motions of the TowPlow.

Modified Dugoff's Tire Friction Model

The tire friction model is an essential part of vehicle dynamics, and determines the effect of the tire on performance of the vehicle such as driving, braking and cornering. Among the representative tire models (LuGre's mode [57], Magic Formula model [3], Dugoff's model [18], etc.) reported in the past, in this study, Dugoff's model with friction circle concept [26] is applied for the longitudinal and lateral forces of each tire with a modification that considers the effect of the normal load change on the coefficient of friction and the cornering stiffness.

Copyright 2018. the authors

Vermeer Manufacturing Company – Ex. 2045
Kubota v. Vermeer
IPR2025-00168
Page 90 of 182

Dugoff [18] described longitudinal and lateral forces (F_x and F_y respectively) of a tire in terms of slip ratio, s, and friction coefficient, μ. Generally, slip ratio of a tire is defined as

$$s = \frac{v_{wx} - r_t \omega_w}{v_{wx}}, \tag{49}$$

where v_{wx} is the longitudinal component of the tire velocity, r_t denotes the wheel radius, and ω_w is rotational speed of the tire. In Dugoff's model, the friction coefficient is defined as

$$\mu = \mu_0 (1 - \varepsilon V_s), \tag{50}$$

where μ_0 is nominal friction coefficient when V_s is zero, ε is a parameter dependent on road-tire interface, and V_s is the vehicle sliding velocity calculated as

$$V_s = v_{wx} (s^2 + \tan^2 \alpha)^{1/2}. \tag{51}$$

In the above equation, α is the slip angle of the wheel, the angle formed with the longitudinal axis and velocity direction of the wheel. The slip angle is obtained as

$$\alpha = \delta - \tan^{-1}(\frac{v_{wy}}{v_{wx}}), \tag{52}$$

where δ is the steering angle, and v_{wy} is the lateral component of the tire velocity.

When the wheel is locked, and the slip ratio is 1, the forces of a wheel are calculated as

$$F_x = \frac{C_x \mu F_n}{(C_x^2 + C_y^2 \tan^2 \alpha)^{1/2}}, \tag{53}$$

$$F_y = \frac{C_y (\tan \alpha) \mu F_n}{(C_x^2 + C_y^2 \tan^2 \alpha)^{1/2}}, \tag{54}$$

where C_x and C_y represent longitudinal and lateral tire stiffness, and F_n is the normal load on a tire.

When the wheel is not locked ($s \neq 1$), desired tire forces (F_{xd} and F_{yd}) and friction coefficient (μ_d) are determined as

$$F_{xd} = \frac{C_x s}{(1-s)}; \qquad F_{yd} = \frac{C_y \tan \alpha}{(1-s)}, \tag{55}$$

$$\mu_{bd} = \frac{F_{xd}}{F_n}; \quad \mu_{sd} = \frac{F_{yd}}{F_n}; \quad \mu_d = (\mu_{bd}{}^2 + \mu_{sd}{}^2)^{1/2}, \tag{56}$$

where μ_{bd} is the desired brake coefficient, and μ_{sd} is the desired side force coefficient. Here the friction circle concept comes into play. In the case that the desired friction coefficient is less than or equal to half of the available friction ($\mu_d \leq \mu/2$), $F_x = F_{xd}$, $F_y = F_{yd}$, and the resultant friction coefficient $\mu_{res}=\mu_d$. That is, the longitudinal and lateral tire forces are linear to the slip ratio and

Copyright 2018. the authors

Vermeer Manufacturing Company – Ex. 2045
Kubota v. Vermeer
IPR2025-00168
Page 91 of 182

slip angle, respectively. In the other case ($\mu_d > \mu/2$), the tire forces and the resultant friction coefficient attenuate nonlinearly. They can be obtained as

$$\mu_{res} = \mu(1 - \frac{\mu}{4\mu_d}); \quad , \tag{57}$$

$$F_x = F_{xd}\frac{\mu_{res}}{\mu_d}; \qquad F_y = F_{yd}\frac{\mu_{res}}{\mu_d} \quad . \tag{58}$$

Figure 40**Error! Reference source not found.** presents a flow chart of tire force calculation suggested by Guntur and Sankar using Dugoff's model especially for the vehicle simulation [26]. Using the calculation process, longitudinal and lateral tire forces under the conditions in Table 7 are computed, and shown in Figure 41.

To illustrate the dependency of tire forces on the slip ratio, slip angle and normal load, 'carpet plots' are plotted in Figure 42 varying the normal load, F_n. For the longitudinal force (a), slip angle is assumed to be zero, and free rolling of the tire ($s = 0$) is assumed for the lateral force (b).

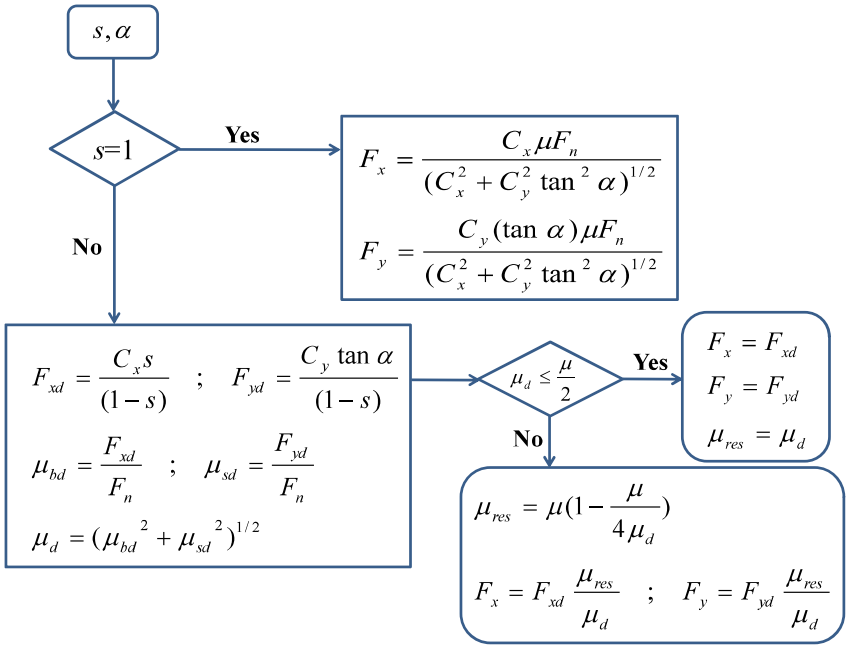


Figure 40. Flow chart of the tire force calculation [26]

Copyright 2018. the authors

Vermeer Manufacturing Company – Ex. 2045
Kubota v. Vermeer
IPR2025-00168
Page 92 of 182

Table 7. Parameters for tire friction calculation [26]

Symbol	Value	Unit	Description
C_x	230,000	*N*	Tire longitudinal stiffness
C_y	168,000	*N/rad*	Tire lateral stiffness
μ_0	0.53	-	Nominal friction coefficient
ε	0.0067	*s/m*	Road-tire interface coefficient
v_{wx}	40	*km/h*	Tire longitudinal velocity
F_n	43,254	*N*	Tire reference normal load

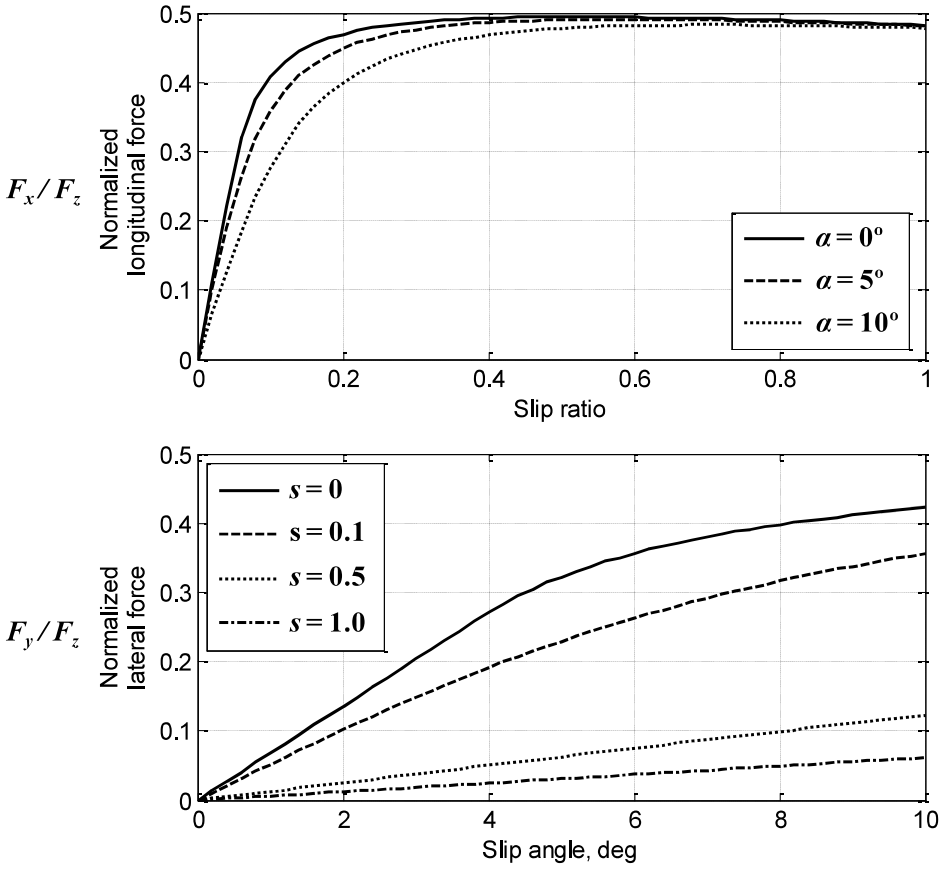


Figure 41. Computed longitudinal and lateral tire forces

Copyright 2018. the authors

Vermeer Manufacturing Company – Ex. 2045
Kubota v. Vermeer
IPR2025-00168
Page 93 of 182

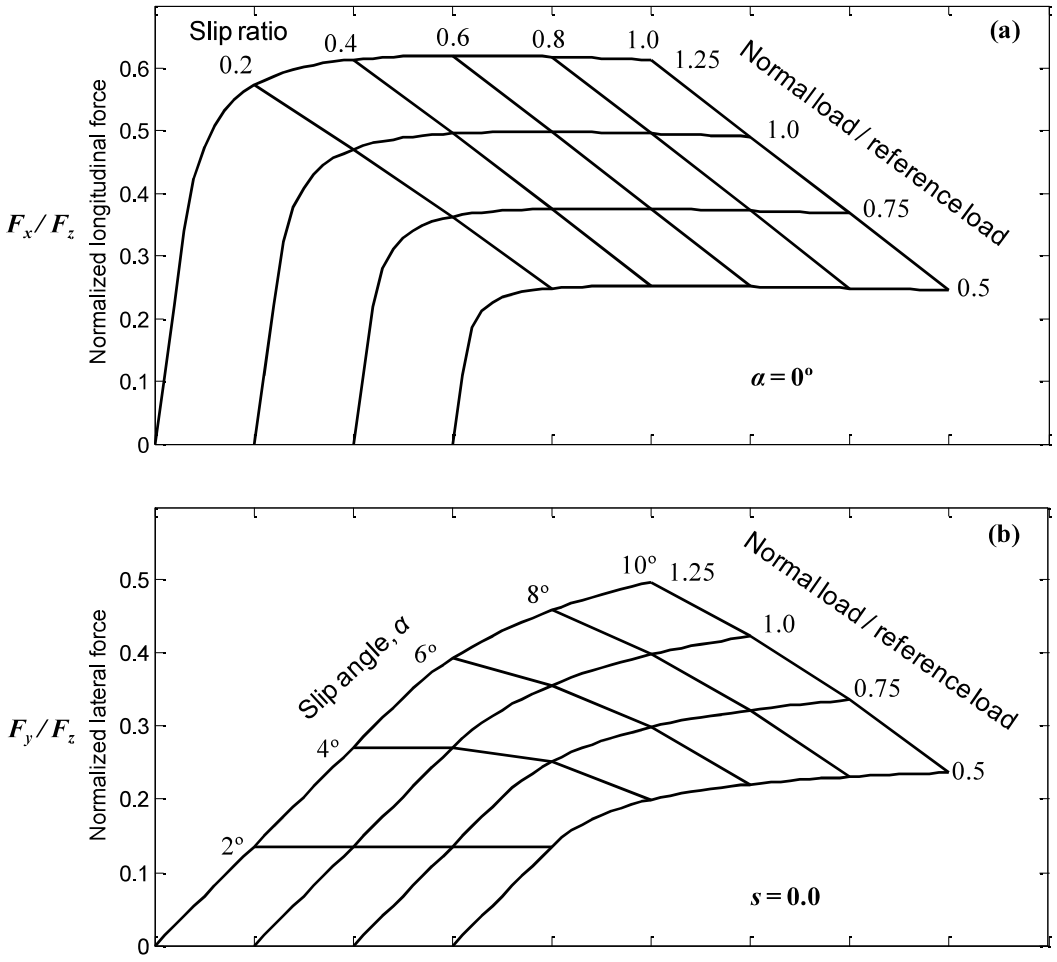


Figure 42. Carpet plots: (a) Longitudinal tire force and (b) lateral tire force varying normal load

In addition to the current Dugoff's model, modification of the tire friction model considering normal load change of each tire is implemented as per [58]. There exist parameters in the model affected by normal load change due to rolling and pitch motions of the vehicle. A simplified load effect model is suggested especially for friction coefficient and tire lateral stiffness in this study from the empirical results of [2].

For the original Dugoff model, the friction coefficient is defined as Eq. (50). A load factor, ξ, is incorporated to count for the load change effect as

$$\mu = \mu_0 (1 - \varepsilon V_s)(\xi), \tag{59}$$

where the load factor can be obtained from the empirical data assuming that it varies linearly with load change as

Copyright 2018. the authors

Vermeer Manufacturing Company – Ex. 2045
Kubota v. Vermeer
IPR2025-00168
Page 94 of 182

$$\xi = -0.2\left(\frac{normal\ load}{reference\ load}\right) + 1.2 \quad . \tag{60}$$

The empirical data suggests that the load factor decreases, thus the friction coefficient decreases as well, when the normal load increases compared to the reference load of the tire, which is the normal load when the vehicle is sitting on a level road and not moving.

Lateral stiffness of a tire is also affected by the load change, based on the empirical data. A load factor of the lateral stiffness, ζ, is also introduced to correct the lateral stiffness as

$$C_y = \zeta \cdot C_{y0}, \tag{61}$$

where C_{y0} denotes the lateral stiffness when the slip angle of the tire is equal to zero (α=0). The relationship between the load factor and normal load is estimated with a second order function as

$$\zeta = -0.9\left(\frac{normal\ load}{reference\ load}\right)^2 + 1.8\left(\frac{normal\ load}{reference\ load}\right) + 0.1 \quad , \tag{62}$$

Figure 43 presents the load factors of the friction coefficient (a) and lateral stiffness (b) according to the normal load change. The carpet plots for the longitudinal and lateral force of a tire with load change effect on the parameters are shown in Figure 44.

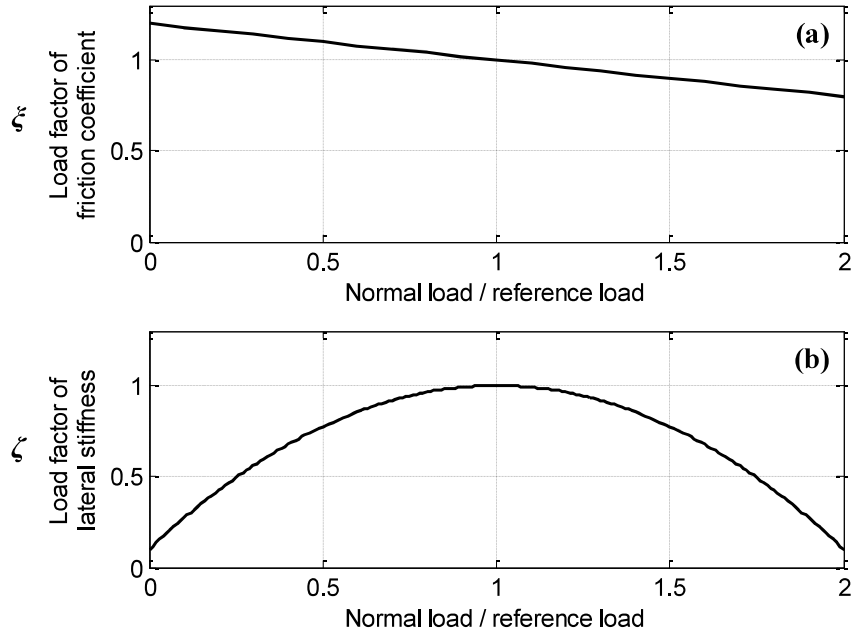


Figure 43. Load factors in relation with (a) friction coefficient and (b) lateral stiffness

Copyright 2018. the authors

Vermeer Manufacturing Company – Ex. 2045
Kubota v. Vermeer
IPR2025-00168
Page 95 of 182

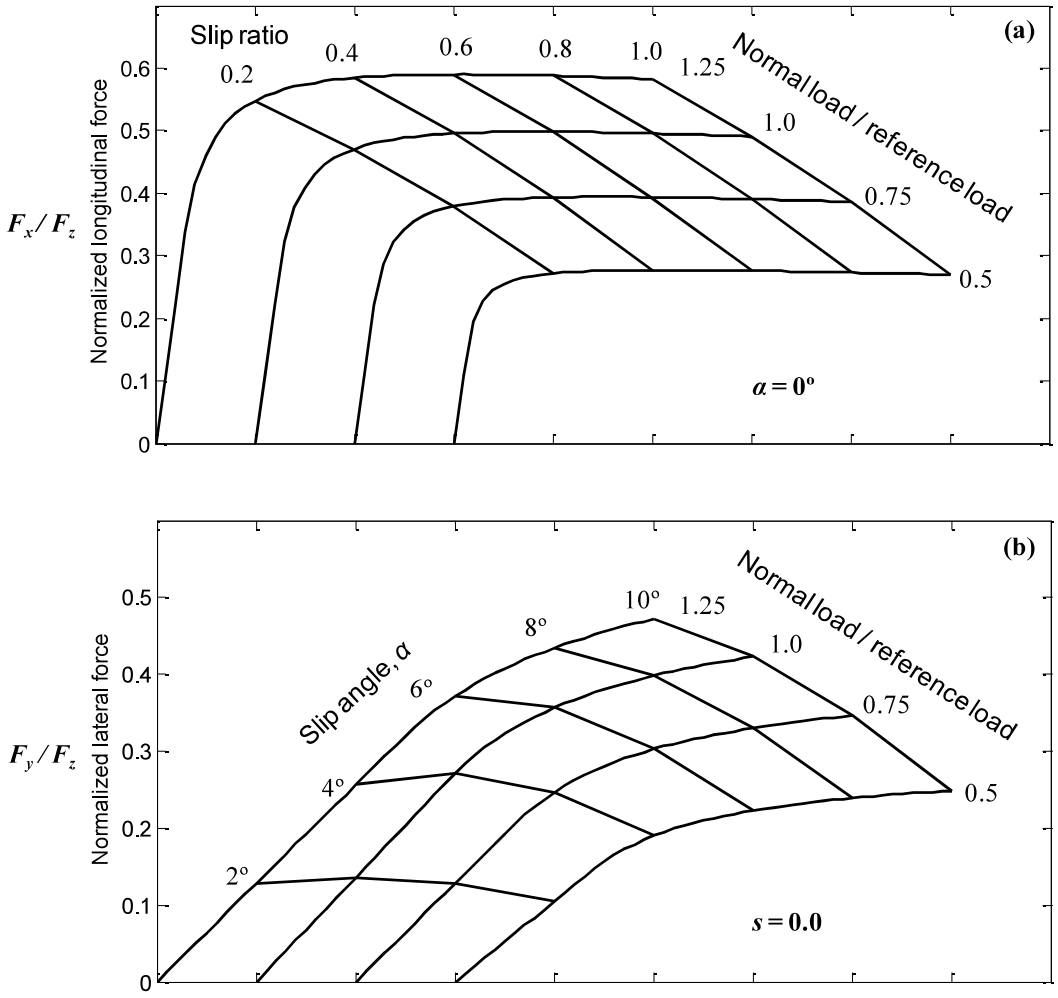


Figure 44. Carpet plots considering load change effect: (a) Longitudinal tire force and (b) lateral tire force

Tire Rotation Dynamics

Because the TowPlow will be simulated later under braking conditions, it will be necessary to account for tire slip accurately in the vehicle dynamics. In order to calculate the tire forces discussed in the preceding section, the rotational speed of each tire needs to be obtained from the tire rotation dynamics. Figure 45 depicts the free body diagram for a wheel of the driving axle of the tractor on the road.

Copyright 2018. the authors

Vermeer Manufacturing Company – Ex. 2045
Kubota v. Vermeer
IPR2025-00168
Page 96 of 182

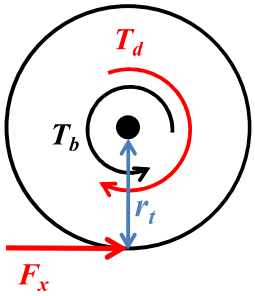


Figure 45. Free body diagram for a driving wheel

Based on the equilibrium of the moment around the wheel center, O, a differential equation for the tire rotation is derived as

$$\dot{\omega}_w = \frac{1}{J_w}(T_d - T_b - r_t F_x), \tag{63}$$

where ω_w is rotation speed of the wheel, J_w is rotational inertia of the wheel, T_d is driving torque, T_b is braking torque, r_t is tire radius, and F_x is longitudinal force of the wheel. The same equation applies to any driven wheel by setting the driving torque to zero.

Load Transfer Effect

The load transfer effect of the tractor unit is incorporated into the vehicle dynamic model to account for longitudinal and lateral acceleration coupling as well as road grade. Instead of including the complete roll and pitch dynamics that make the vehicle model very complex by increasing the number of degrees of freedom, a quasi-static approximation is employed [18]. Assuming that the coupling between roll and pitch motions is negligible, the influence of the longitudinal and lateral accelerations on the normal loads can be considered independently [36].

Figure 46 depicts side and rear views of the tractor unit of the TowPlow on an inclined road.

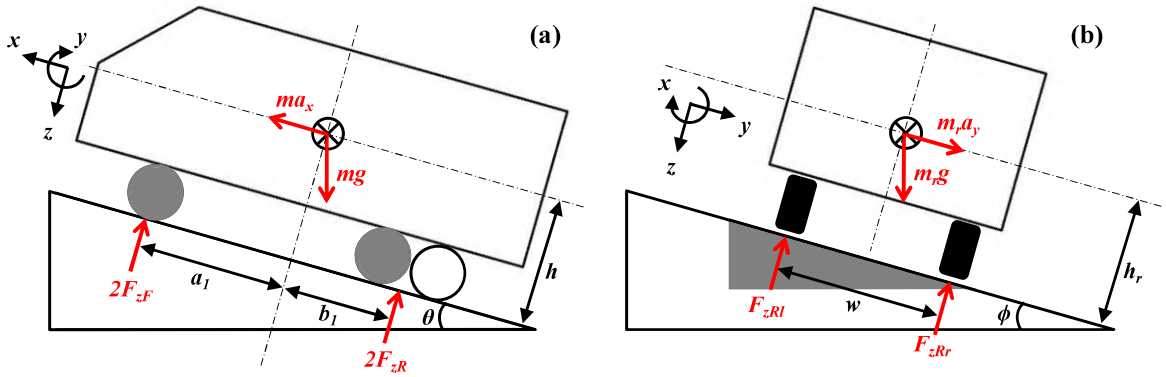


Figure 46. (a) Side and (b) rear views of the tractor unit and applied forces

Copyright 2018. the authors

Vermeer Manufacturing Company – Ex. 2045
Kubota v. Vermeer
IPR2025-00168
Page 97 of 182

For the load transfer effect in the longitudinal direction (Figure 46a), the chassis acceleration force ($m \cdot a_x$) and gravity force ($m \cdot g$) are applied at the center of gravity (CG) of the chassis, and normal loads on the front axle (F_{zF}) and the center of the rear axle (F_{zR}), a tandem axle, are applied. Longitudinal acceleration of the tractor unit generates a pitch moment that transfers the normal load of the front axle to the rear axle. Equilibrium of moments about each axle yields

$$F_{zF} = \frac{mg}{2(a_1 + b_1)}(b_1 \cos\theta - h \sin\theta) - \frac{ma_x h}{2(a_1 + b_1)}, \tag{64}$$

$$F_{zR} = \frac{mg}{2(a_1 + b_1)}(b_1 \cos\theta + h \sin\theta) + \frac{ma_x h}{2(a_1 + b_1)}, \tag{65}$$

where θ is road grade, and h is CG height of the chassis.

For the lateral direction in the rear view (Figure 46b), the acceleration force ($m_r \cdot a_y$), gravity force ($m_r \cdot g$), and normal loads on the left and right wheels (F_{zRl} and F_{zRr}, respectively) are applied. m_r is the virtual mass of the rear axle, defined as

$$m_r = \frac{F_{zR}}{g}. \tag{66}$$

Then, equilibrium of moments about each side of the wheels yields

$$F_{zRl} = \frac{m_r g \cos\phi}{2} - \frac{m_r h_r}{w}(a_y + g \sin\phi), \tag{67}$$

$$F_{zRr} = \frac{m_r g \cos\phi}{2} + \frac{m_r h_r}{w}(a_y + g \sin\phi), \tag{68}$$

where ϕ is the inclined angle of the road, and h_r is height of the center of mass of the rear virtual mass. The actual normal load applied to each wheel of the rear axle is half of F_{zRl} and F_{zRr} since the rear axle is a tandem axle. By analogy for the front axle, the normal load can be calculated as

$$F_{zFl} = \frac{m_f g \cos\phi}{2} - \frac{m_f h_f}{w}(a_y + g \sin\phi), \tag{69}$$

$$F_{zFr} = \frac{m_f g \cos\phi}{2} + \frac{m_f h_f}{w}(a_y + g \sin\phi), \tag{70}$$

where m_f is the virtual mass of the front axle, and h_f is height of the center mass of the virtual mass.

For the trailer unit, the load transfer effect is not considered, and the normal load of each tire is assumed to be constant because the CG height of the trailer unit is very low and the load transfer effect is assumed negligible.

Experimental Validation

The nonlinear vehicle model of the TowPlow including Dugoff's tire friction model and load transfer effect is developed above. To have confidence in the simulated dynamic characteristic of the TowPlow, the model needs to be validated. For the validation, a series of actual vehicle experiments for both steady-state and transient conditions are conducted, and data gathered from

Copyright 2018. the authors

Vermeer Manufacturing Company – Ex. 2045
Kubota v. Vermeer
IPR2025-00168
Page 98 of 182

the experiments are compared with the simulation results. Due to the restriction of the project that, at this point, the actual TowPlow is only available for experiment during non-snowy seasons, the TowPlow model is verified without snow resistant forces.

Experimental Configuration

For the experiments on a dry road, the TowPlow is prepared without plows (the minimum combination of the TowPlow shown in the section starting on page 52). The tractor unit has three axles, a front axle and rear tandem axle, and it weighs 13,925 *kgf*. The axle track is 2.01 *m*. The front axle is equipped with 315/80R22.5 tires, and the rear axles with 11R24.5 tires. Reference normal loads of the front axle and the tandem axle are 51,154 *N* and 85,406 *N* each when the trailer is connected. The trailer unit weighs 4,654 *kgf* with the following size tires: 385/65R22.5 at its first axle and 315/80R22.5 at its second axle. At each axle, the reference normal load of 22,820 *N* is applied. The TowPlow is in deployed position maintaining its trailer steering angle to be constant at 30 degrees for the experiment.

For both units, yaw rate, lateral acceleration, longitudinal velocity and steering angle are measured using commercially available sensors, and the data are collected using Arduino single-board microcontrollers [46]. Figure 47 presents the entire layout of the sensors and the Arduino set up. The inertia measurement unit (IMU), installed at the CGs of the tractor and trailer, is composed of a gyroscope, Analog Devices ADXRS453, and an accelerometer, Analog Devices ADIS16003, and it measures yaw rate and lateral acceleration with a sampling rate at 40 *Hz*. Sensor noise levels are 0.1 *deg/sec* for gyroscopes and 0.01 m/s^2 for the accelerometers. The longitudinal velocities are measured with Adafruit ultimate Global Positioning System (GPS) loggers built into the Arduino at 1.0 *Hz*. The steering angles are measured at 40 *Hz* with linear travel potentiometers installed at the steering pitman arm for the tractor unit, and at the steering cylinder for the trailer unit. An additional Arduino is placed in the driver's cab to provide the driver a display that indicates both the desired steering input and the actual steering input so that driver can follow the desired input during the experiment.

Copyright 2018. the authors

Vermeer Manufacturing Company – Ex. 2045
Kubota v. Vermeer
IPR2025-00168
Page 99 of 182

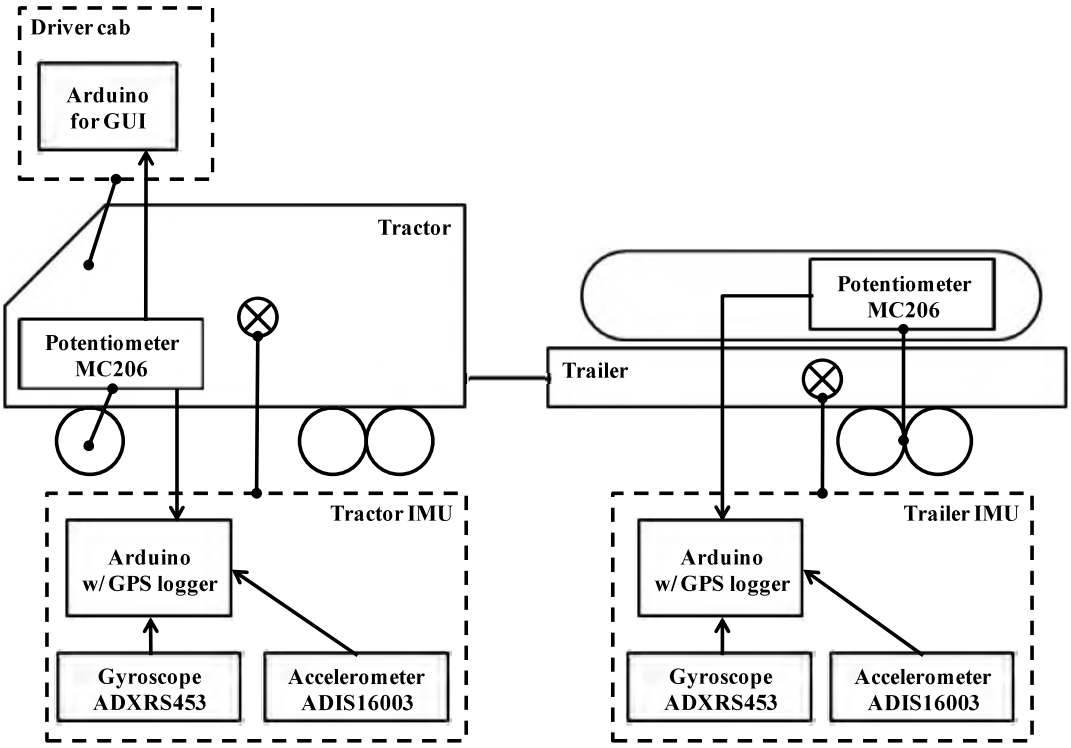


Figure 47. Layout of sensors and microcontrollers

For the experiment location, NASA Crows Landing, CA, an abandoned airfield for emergency landing is selected. The airfield is one of the most suitable candidates for both the steady-state and transient tests, providing a runway with approximate length of 2.5 *km* and width of 55 *m*.

Steady-State Circular Test – Constant Speed

The International Organization for Standardization (ISO) provides several established test methods for examining vehicle's circular driving characteristic at steady-state conditions. These methods are the constant radius test, constant steer angle test, constant speed with variable steer angle test, and constant speed with variable radius test [28]. Among the tests, in this study, the constant speed with variable steer angle test is conducted considering the TowPlow geometry and the given space.

The test procedure and test conditions follow the international standard. During the test, the required driver's inputs are a constant speed and constant steer angle. Figure 48 shows a flow chart of the test procedure for a test speed and direction. The test driver starts with a fixed steer angle, and accelerates the TowPlow until it reaches the desired speed. Then, the driver maintains the steering wheel position and speed as constant as possible until the TowPlow is in steady-state, and at the steady-state, waits at least 3 seconds for the acquisition of the data. The procedure is repeated at successively larger steer angles at three different speeds. The entire procedure is repeated for both clockwise and counter clockwise turns.

Copyright 2018. the authors

Vermeer Manufacturing Company – Ex. 2045
Kubota v. Vermeer
IPR2025-00168
Page 100 of 182

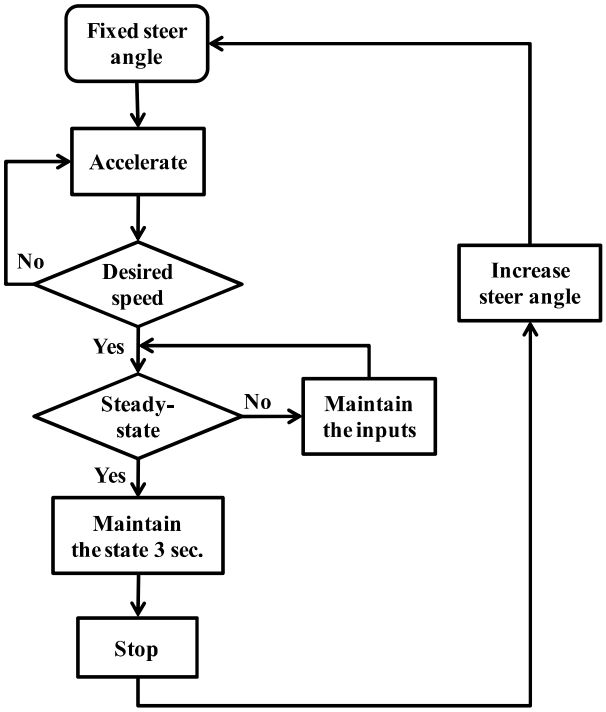


Figure 48. Test procedure of the steady-state test for a speed and direction

Test speeds of 8*km/h* (5*mph*), 24*km/h* (15*mph*) and 48*km/h* (30*mph*) are selected. For each test speed, several levels of constant steer angle are applied. For the slowest speed, only 10 degrees and 23 degrees are applied since a smaller increment does not show significant change in lateral acceleration level. For 24 *km/h* (15 *mph*) speed, test data are collected for every 3 degrees of steer angle from 1 to 19 degrees. At the highest speed, due to the constraint of the tractor performance, space and safety issues, constant steer angles of only 1 and 2 degrees are applied.

The collected test data are presented with steering-wheel angle characteristic curve, which describes the relationship between the tractor steering angle and the lateral acceleration of the tractor and trailer at each speed. Figure 49 shows the test results compared with results from simulation based on the nonlinear TowPlow dynamic model developed earlier in this section. Table 8 presents vehicle parameters used in the simulation for model validation.

Copyright 2018. the authors

Vermeer Manufacturing Company – Ex. 2045
Kubota v. Vermeer
IPR2025-00168
Page 101 of 182

Table 8. Vehicle parameters for model validation

Symbol	Value	Unit	Description
m	13,925	kg	Mass of tractor unit
m_T	4,654	kg	Mass of trailer unit
I_{zz}	40,018	$kg{\cdot}m^2$	Moment of inertia for tractor unit
I_{zzT}	13,374	$kg{\cdot}m^2$	Moment of inertia for trailer unit
C_x	230,000	N	Tire longitudinal stiffness
C_y	168,000	N/rad	Tire lateral stiffness
ε	0.0067	s/m	Road-tire interface coefficient
a_1	3.30	m	Distance from CG to front axle (tractor)
b_1	1.27	m	Distance from CG to first rear axle (tractor)
c_1	2.69	m	Distance from CG to second rear axle (tractor)
d_1	3.65	m	Distance from CG to articulation point (tractor)
l_s	2.19	m	Length of tongue assembly
a_2	4.34	m	Distance from CG to articulation point (trailer)
b_2	0.44	m	Distance from CG to first trailer axle
c_2	1.86	m	Distance from CG to second trailer axle
h	1.65	m	Tractor CG height
w	2.01	m	Tractor axle track
w_t	2.13	m	Trailer axle track
J_w	9.78 ~ 17.67	$kg{\cdot}m^2$	Moment of inertia for tires
r_t	0.52 ~ 0.54	m	Radius of tires

Copyright 2018. the authors

Vermeer Manufacturing Company – Ex. 2045
Kubota v. Vermeer
IPR2025-00168
Page 102 of 182

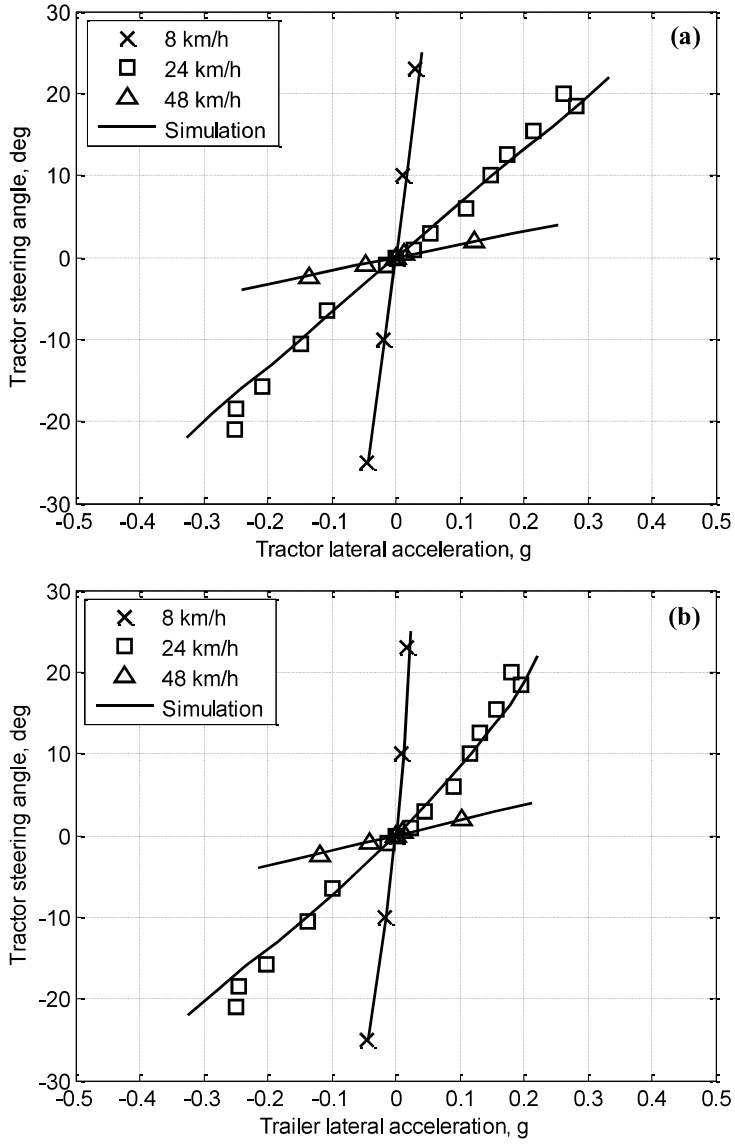


Figure 49. Steady-state test results compared with simulation results

The simulation results compare favorably to the experiment results for both the tractor and trailer. For the tractor (Figure 49a), the steering angle shows a linear relationship with the lateral acceleration throughout the tested region. However, for the trailer (Figure 49b), nonlinearity is observed when the tractor steering angle is greater than about 10 degrees in cases of the cornering speed of 8 *km/h* and 24 *km/h*.

Transient Maneuver Test

The nonlinear dynamic model of the TowPlow is also validated through a transient maneuver test [29]. For the transient maneuver, the test driver operates the TowPlow with sine-like

Copyright 2018. the authors

Vermeer Manufacturing Company – Ex. 2045
Kubota v. Vermeer
IPR2025-00168
Page 103 of 182

arbitrary steering angle at constant tractor speed of 48 *km/h*. The test procedure of the test is presented with a flow chart in Figure 50.

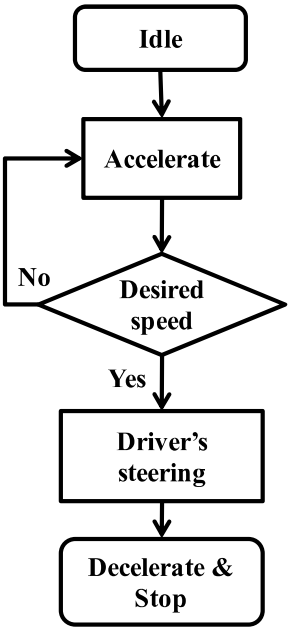


Figure 50. Test procedure of the transient maneuver test

As the test begins, the TowPlow stays idling about 20 seconds with data being collected. The data collected in this stage are used for the calibration of the yaw rate data in post-processing. Then, the driver accelerates the TowPlow until it reaches the desired speed of 48 *km/h*. While maintaining the desired speed, the driver applies the steering maneuver. Only the portion of experiment data collected in this stage is of interest for validation of the simulation. The steering input data are collected and used for the simulation input to compare the results of the experiment and simulation. For the simulation, the tractor velocity is maintained at a constant speed of 48 *km/h* (25 *mph*). Figure 51 presents inputs for both experiment and simulation.

Copyright 2018. the authors

Vermeer Manufacturing Company – Ex. 2045
Kubota v. Vermeer
IPR2025-00168
Page 104 of 182

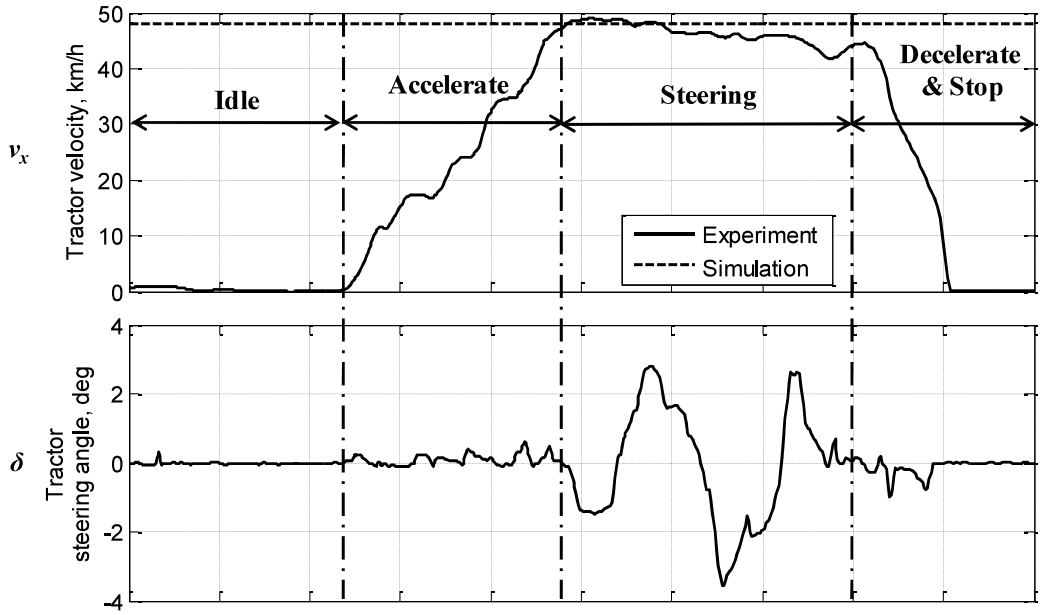


Figure 51. Transient test inputs for the experiment and simulation

The comparison of the results is shown in Figure 52. Especially the section of interest is blown up. The results between the experiment and simulation data for the yaw rates of both units compare favorably and this verify the model.

Summary

In this section, the nonlinear vehicle dynamic model of the TowPlow is developed including Dugoff's tire friction model with modification accounting for the normal load change of each tire, tire rotational dynamics and quasi-static load transfer effect of the tractor unit. The developed model is validated through full-scale vehicle experiments in steady-state and transient conditions. For the steady-state experiment, constant velocity cornering is conducted with different tractor steering angles. Arbitrary steering input by the test driver is applied for the transient maneuver experiment. From the comparison between the experiment and simulation results, it is demonstrated that the developed nonlinear model accurately predicts the dynamic characteristic of the TowPlow.

Copyright 2018. the authors

Vermeer Manufacturing Company – Ex. 2045
Kubota v. Vermeer
IPR2025-00168
Page 105 of 182

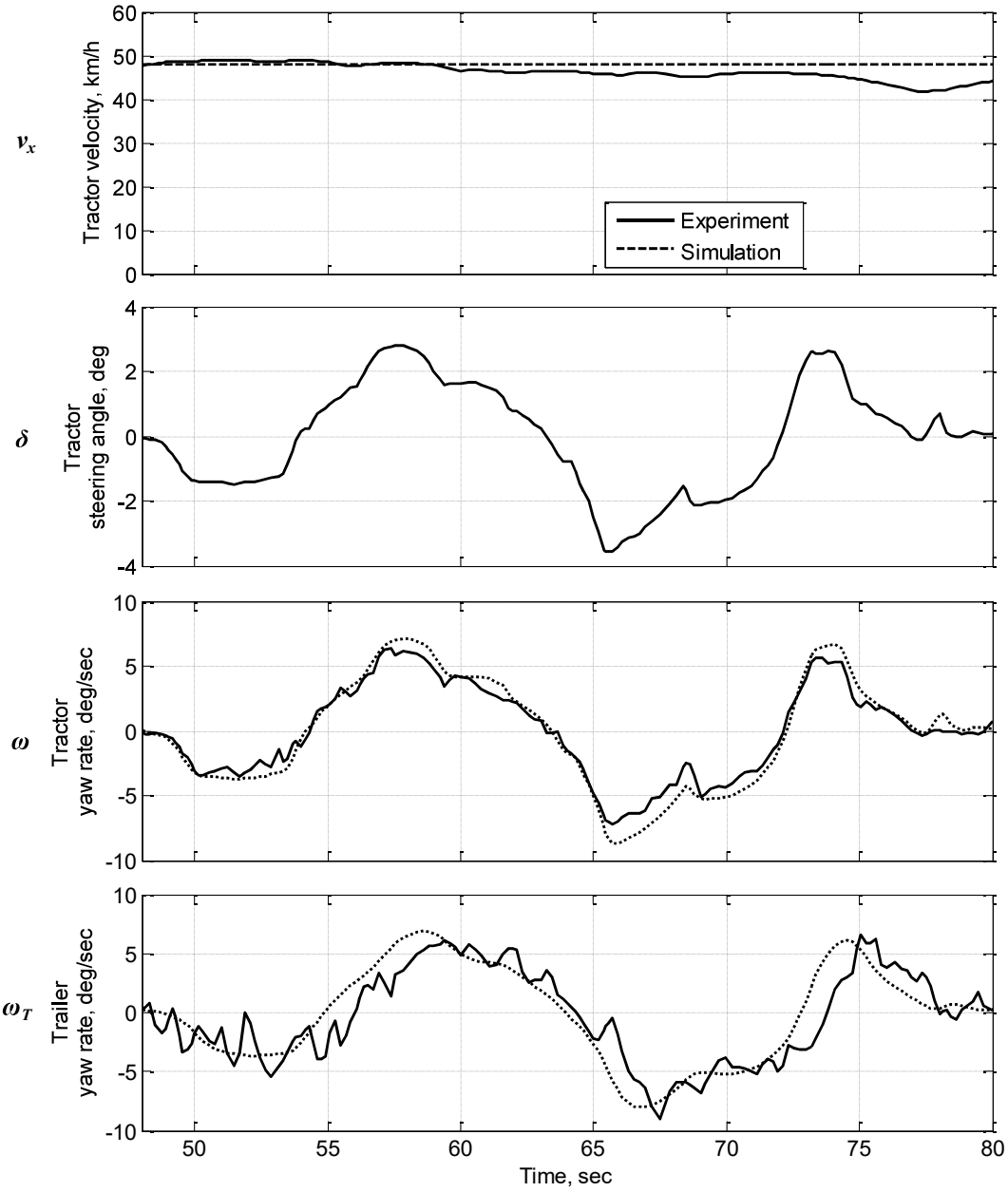


Figure 52. Transient test results compared with simulation results

Copyright 2018. the authors

Vermeer Manufacturing Company – Ex. 2045
Kubota v. Vermeer
IPR2025-00168
Page 106 of 182

Snow Resistance Model and Dynamic Simulation of the TowPlow

The snow resistant efforts of the snowplows of the TowPlow, F_{xPlow}, F_{yPlow}, F_{xTPlow}, F_{yTPlow}, M_{TPlow} are introduced for the nonlinear vehicle dynamic model in the preceding section. They make the dynamic characteristics of the TowPlow different from ordinary multi-articulated vehicles. Also, these forces make it difficult to intuitively predict the motion of the TowPlow. In this section, existing snowplowing resistance models are adopted to estimate the snow resistant forces. Dynamic simulations of the nonlinear TowPlow model including the snow resistance are performed without any controller. The effect of the snow resistance on the dynamics and stability of the TowPlow is discussed for various maneuvers such as cornering, slalom, up and down hill, and split friction coefficient braking.

Snow Resistance Model

In this section, the snow resistance model is proposed for a snowplow by combining main ideas of the existing models – control volume of the incoming snow, from Ravani's work [49], and speed change of the snow due to its compressibility, from Kaku's work [34]. Later, the model is expanded for the application to each snowplow of the TowPlow. For the model, plow sliding resistance (F_{psr}), plow air resistance (F_{par}), snow impact force on the plow (F_{si}), and friction force between the snow and plow (F_{spfr}) are considered at constant vehicle velocity, as defined by Ravani and shown in Figure 53. Figure 54 depicts the control volume of the snow being plowed and the parameters used to define each component of the snow resistance. The dashed region indicates the control volume, and the gray region indicates the instantaneous volume of the incoming snow into the control volume.

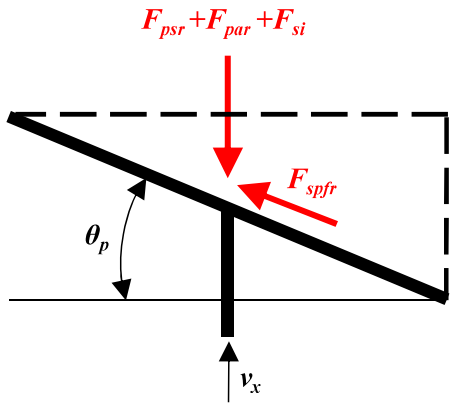


Figure 53. Components of the snow resistance

Copyright 2018. the authors

Vermeer Manufacturing Company – Ex. 2045
Kubota v. Vermeer
IPR2025-00168
Page 107 of 182

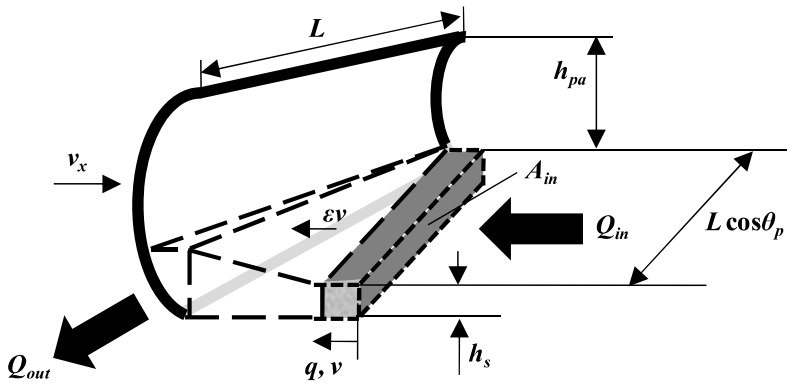


Figure 54. Scheme of the snow resistance

The following assumptions are made to simplify the modeling:

- The height of incoming snow into the control volume (h_s) is constant across the width of the plow;
- The snow at the boundary of the plow face is nudged parallel to the plow face with a constant velocity;
- Curvature of the plow is ignored.

The plow sliding resistance in the direction of travel, F_{psr}, represents the friction force between the plow blade and road surface, which is obtained as

$$F_{psr} = \mu_{pr} W_p , \tag{71}$$

where μ_{pr} is the friction coefficient between the blade of the plow and the road, and W_p is weight of the plow.

The plow air resistance in the direction of travel, F_{par}, is calculated as

$$F_{lar} = 0.5 C_d \rho_a (h_{pa} L \cos\theta_p) v^2 , \tag{72}$$

where C_d is the drag coefficient, ρ_a is the density of air, h_{pa} is the height of the plow above the snow level, L is the width of the plow, θ_p is the plowing angle, and v is the plowing velocity in the direction of travel. Note that the plowing velocity is equal to the vehicle's forward velocity and represents the relative speed of the incoming snow.

The snow impact force includes the impact force from the incoming snow into the control volume as well as from the snow in the control volume. The former is calculated from the derivative of the momentum of the incoming snow as

$$F_{si_inc} = \frac{dp_{in}}{dt} = \frac{d(m_{in} v)}{dt} = v Q_{in} , \tag{73}$$

where *inc* denotes incoming, p_{in} is the momentum of the incoming snow, m_{in} is the mass of the incoming snow into the control volume through the cross-sectional area (A_{in}), and Q_{in} is the input flow of the snow into the control volume, which is described as

Copyright 2018. the authors

Vermeer Manufacturing Company – Ex. 2045
Kubota v. Vermeer
IPR2025-00168
Page 108 of 182

$$Q_{in} = \frac{dm_{in}}{dt} = \frac{d(\rho_{sn} V_{in})}{dt} = \rho_{sn} \frac{d(A_{in} q)}{dt} = \rho_{sn} A_{in} v = \rho_{sn} h_s L \cos\theta_p v \quad . \tag{74}$$

In Eq. (74), ρ_{sn} is the snow density, V_{in} is the volume of the snow coming through A_{in}, h_s is the height of the incoming snow, and q is the displacement of the snow into the control volume in the opposite direction of the travel. The latter, suggested by Kaku, considers decrease of the snow flow speed and change of the snow flow angle in the control volume due to its compressibility. A coefficient that accounts for the effect of these changes is introduced as

$$F_{si_in} = Q_{in} \{\varepsilon v \cos(\alpha - \theta_p)\}, \tag{75}$$

where *in* denotes inside, ε denotes the coefficient for the decreasing snow speed, and α denotes the changing angle of the snow. Then, the total snow impact force, F_{si}, is expressed as

$$F_{si} = F_{si_inc} + F_{si_in} = Q_{in} \{v + \varepsilon v \cos(\alpha - \theta_p)\} = \rho_{sn} A_{in} v \{v + \varepsilon v \cos(\alpha - \theta_p)\} \quad , \tag{76}$$

The friction force between the snow and the plow, F_{spfr} is equated as

$$F_{spfr} = \mu_{sp} N_p = \mu_{sp} F_{si} \cos\theta_p \quad , \tag{77}$$

where μ_{sp} is the friction coefficient between the plow surface and snow at the boundary layer, and N_p is the normal force on the plow due to the incoming snow, which is a component, perpendicular to the plow surface, of the snow impact force.

From the defined snow resistant forces, the total snow resistance against the plow in the longitudinal direction is calculated as

$$F_{long} = F_{psr} + F_{par} + F_{si} - F_{spfr} \sin\theta_p \tag{78}$$

and that in the lateral direction as

$$F_{lat} = F_{spfr} \cos\theta_p \quad . \tag{79}$$

The proposed model is validated through comparison between the calculated snow resistant forces and Kaku's experimental data. The calculation of the snow resistant forces in the longitudinal and lateral directions is conducted for the same snowplowing environment given in Kaku's work, with the parameters in Table 9.

Copyright 2018. the authors

Vermeer Manufacturing Company – Ex. 2045
Kubota v. Vermeer
IPR2025-00168
Page 109 of 182

Table 9. Plow parameters for the snow resistance calculation [34,49]

Symbol	Value	Unit	Description
θ_p	45	°	Plowing angle
W_p	5884	N	Weight of snow plow
μ_{pr}	0.27	-	Friction coefficient between plow blade and road surface
C_d	1.98	-	Drag coefficient of snow plow
ρ_a	1.28	kg/m^3	Air density
h_{pa}	0.63	m	Height of plow above the snow level
h_s	0.2	m	Depth of snow (height of the incoming snow)
L	2.1	m	Plow blade length
ρ_{sn}	100	kg/m^3	Snow density
ε	0.6	-	Coefficient of the decreasing snow speed
α	90	°	Angle change of the snow
μ_{sp}	0.53	-	Friction coefficient between the plow surface and snow

Figure 55 and Figure 56, respectively, compare longitudinal and lateral forces calculated from Eq. (78) and Eq. (79) to the Kaku's model and Kaku's experimental data. For the comparison, the results are presented with "resistance ratio, N_r" introduced by Kaku as,

$$N_{rlong} = F_{long} \Big/ \rho_{sn} A_{in} g \quad , \tag{80}$$

$$N_{rlat} = F_{lat} \Big/ \rho_{sn} A_{in} g \, , \tag{81}$$

where g denotes gravitational acceleration, *long* denotes longitudinal and *lat* denotes lateral.

The comparative results clearly demonstrate that the proposed model gives closer results to the experimental data than Kaku's model at all speeds for both longitudinal and lateral directions.

Copyright 2018. the authors

Vermeer Manufacturing Company – Ex. 2045
Kubota v. Vermeer
IPR2025-00168
Page 110 of 182

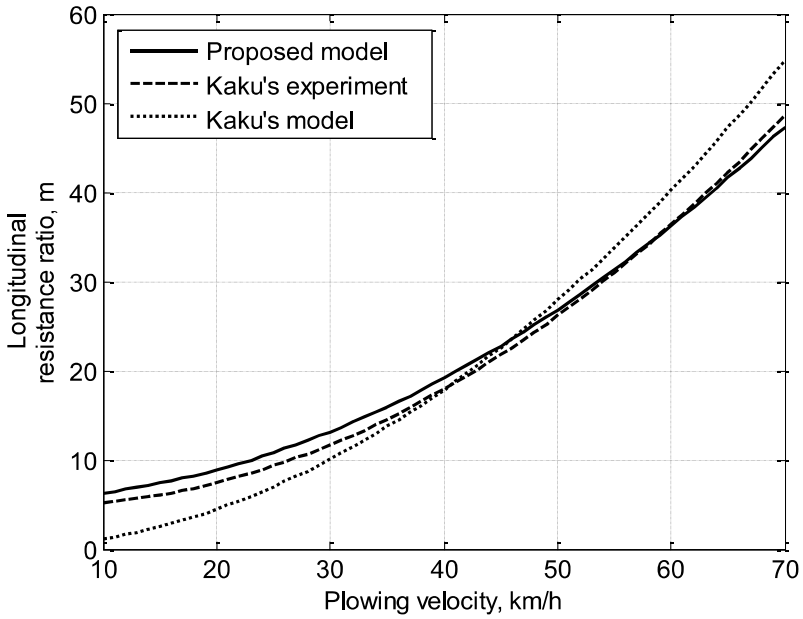


Figure 55. Comparison of resistance ratios for longitudinal snow resistance

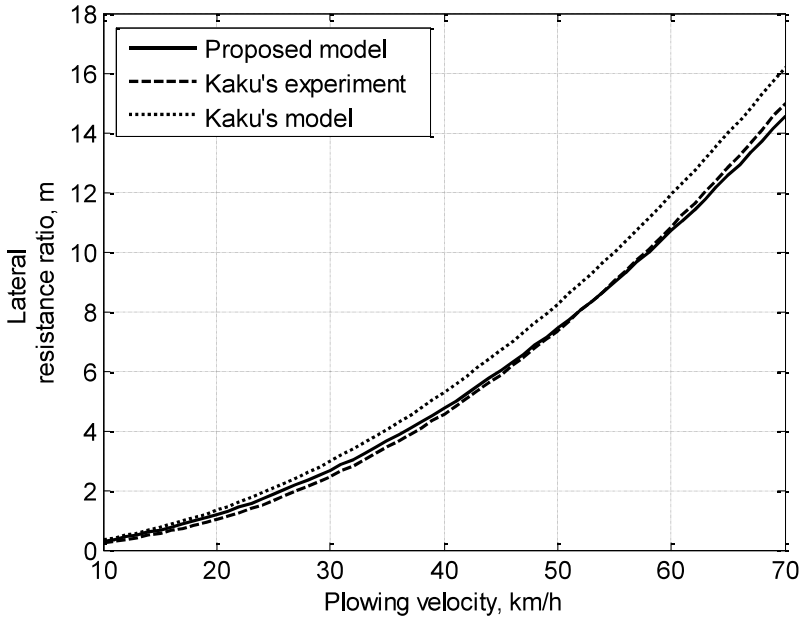


Figure 56. Comparison of resistance ratios for lateral snow resistance

Application of the Snow Resistance Model

Based on the proposed and validated model, forces acting on the front plow and the trailer plow of the TowPlow are applied. Figure 57 depicts the layout, control volumes, and forces at

Copyright 2018. the authors

Vermeer Manufacturing Company – Ex. 2045
Kubota v. Vermeer
IPR2025-00168
Page 111 of 182

the mounting arms of the snowplows. As shown in the figure, the TowPlow is equipped with three moldboard plows – a 3.66-meter (12-foot) front plow, denoted 1, and two trailer plows combining a 3.66-meter (12-foot) moldboard and a 4.27-meter (14-foot) one, denoted 2 and 3 respectively. The front plow, *Plow 1*, forms a plowing angle of θ_p with the frame of the tractor. *Plow 2* and *Plow 3* have the same plowing angle of θ_{tp}, which depends on the total articulation angle between the tractor and trailer. Each plow induces forces to the TowPlow through plow mounting arms in the longitudinal and lateral directions. Q_{in} denotes the flow rate of the incoming snow into each control volume, and Q_{out} denotes that of the outgoing snow from each control volume.

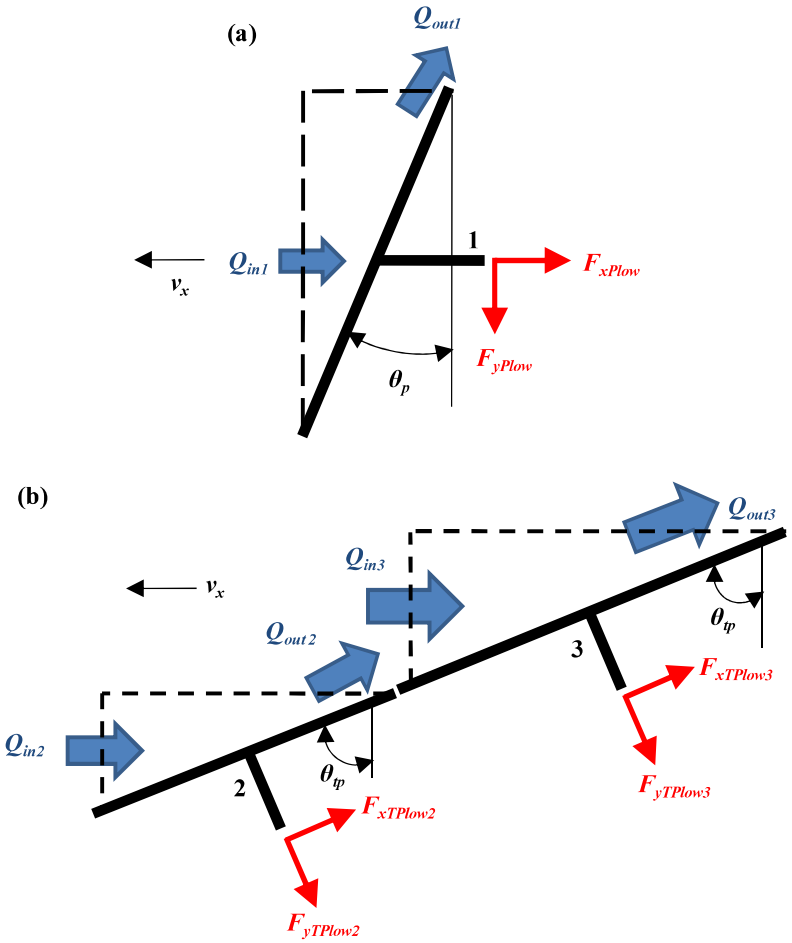


Figure 57. Schemes of the snowplows: (a) front plow and (b) trailer plows

When the snow resistance model proposed in the previous section is applied to each plow of the TowPlow, the plow sliding resistance, F_{psr}, and plow air resistance, F_{par}, are independent of each other among the snowplows. However, the snow impact force, F_{si}, and friction force between the snow and the plow, F_{spfr}, are mutually dependent because these forces are

Copyright 2018. the authors

Vermeer Manufacturing Company – Ex. 2045
Kubota v. Vermeer
IPR2025-00168
Page 112 of 182

determined by the flow rate of the incoming snow. Assuming that there is negligible gap between any two consecutive snowplows, the total flow rate of the incoming snow into *Plow2*, includes the flow rate of the incoming snow through the cross sectional area of the control volume, Q_{in2}, as well as the outgoing snow of *Plow 1*, Q_{out1}. This is also the case for *Plow 3*, which means that these flow rates have the following relation:

$$Q_{out1} = Q_{in1}, \tag{82}$$

$$Q_{out2} = Q_{out1} + Q_{in2} = Q_{in1} + Q_{in2}, \tag{83}$$

$$Q_{out3} = Q_{out2} + Q_{in3} = Q_{in1} + Q_{in2} + Q_{in3}. \tag{84}$$

The snow resistant forces of the three plows in the longitudinal and lateral directions are presented in Figure 58 and Figure 59, respectively. The plowing angle of the trailer plows, θ_{tp}, is 60 degrees assuming that the total articulation angle between the tractor and trailer is 30 degrees. The longitudinal force of *Plow 3* is greatest followed by *Plow 2* and *Plow 1* at all speeds since its incoming snow includes the snow from *Plow 1* and *Plow 2*. However, in the case of the lateral force, even though *Plow 1* has less flow rate of incoming snow than *Plow 2*, it is subjected to greater force than *Plow 2* because it has a larger plowing angle than the trailer plows.

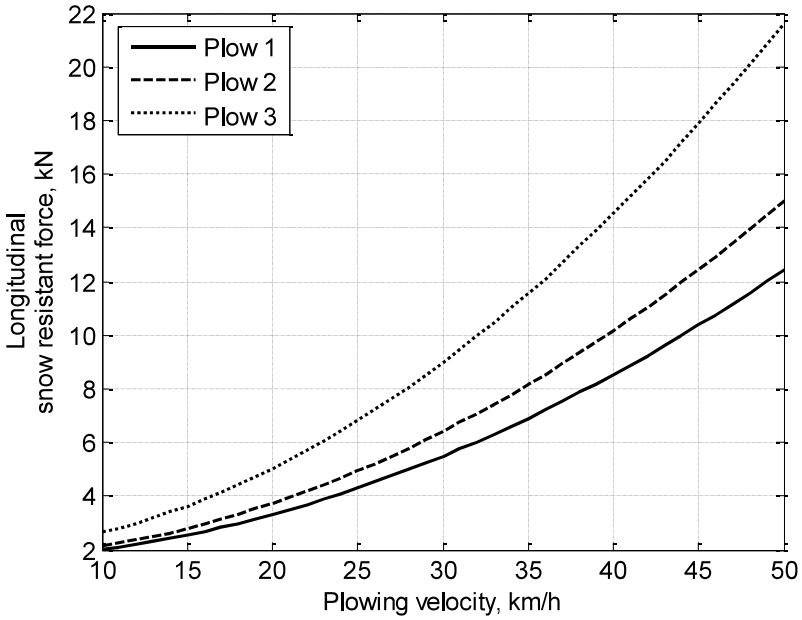


Figure 58. Longitudinal snow resistant forces of the plows

Copyright 2018. the authors

Vermeer Manufacturing Company – Ex. 2045
Kubota v. Vermeer
IPR2025-00168
Page 113 of 182

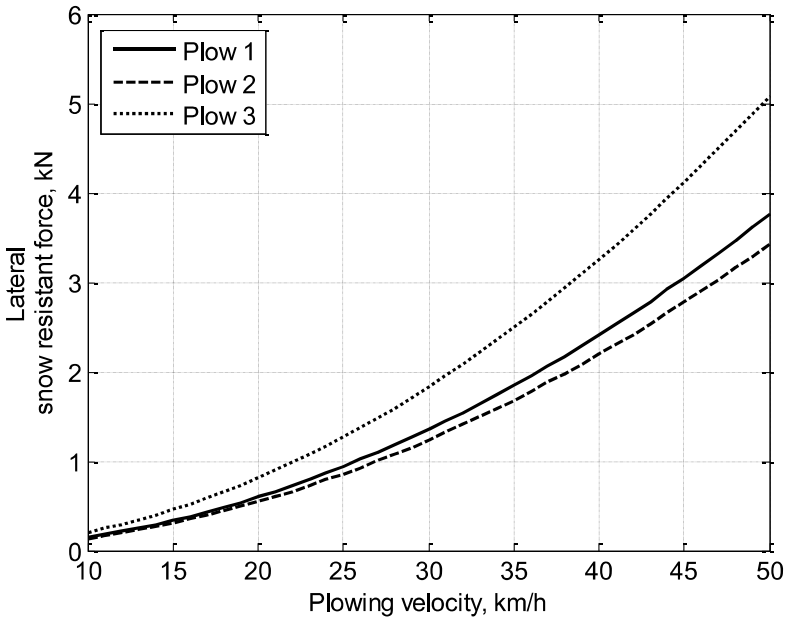


Figure 59. Lateral snow resistant forces of the plows

Dynamic Simulation of the TowPlow Without Control of the Trailer Axle

In this section, dynamic simulations of the nonlinear TowPlow model implementing the snow resistance model to each plow are performed for various maneuvers, which the TowPlow is expected to experience during its snow removal operation. Based on the nonlinear TowPlow model the simulation program is built with MATLAB/Simulink. Table 10 presents parameters of the TowPlow for the dynamic simulation.

Copyright 2018. the authors

Vermeer Manufacturing Company – Ex. 2045
Kubota v. Vermeer
IPR2025-00168
Page 114 of 182

Table 10. Vehicle parameters for dynamic simulation

Symbol	Value	Unit	Description
m	29,031	kg	Mass of tractor unit
m_T	17,040	kg	Mass of trailer unit
I_{zz}	196,120	$kg{\cdot}m^2$	Moment of inertia for tractor unit
I_{zzT}	104,150	$kg{\cdot}m^2$	Moment of inertia for trailer unit
C_x	230,000	N	Tire longitudinal stiffness
C_y	168,000	N/rad	Tire lateral stiffness
ε	0.0067	s/m	Road-tire interface coefficient
a_1	3.30	m	Distance from CG to front axle (tractor)
b_1	1.27	m	Distance from CG to first rear axle (tractor)
c_1	2.69	m	Distance from CG to second rear axle (tractor)
d_1	3.65	m	Distance from CG to articulation point (tractor)
l_s	2.19	m	Length of tongue assembly
a_2	4.34	m	Distance from CG to articulation point (trailer)
b_2	0.44	m	Distance from CG to first trailer axle
c_2	1.86	m	Distance from CG to second trailer axle
p_1	6.09	m	Distance from tractor CG to *Plow 1* support
p_2	2.55	m	Distance from trailer CG to *Plow 2* support
p_3	1.54	m	Distance from trailer CG to *Plow 3* support
h	1.65	m	Tractor CG height
w	2.01	m	Tractor axle track
w_t	2.13	m	Trailer axle track
J_w	9.78 ~ 17.67	$kg{\cdot}m^2$	Moment of inertia for tires
r_t	0.52 ~ 0.54	m	Radius of tires

Driver Model

A simple driver model, which decides driving/braking torque and steering angle for the tractor's driving axle, is introduced for the simulation of various maneuvers. The former is to let the TowPlow follow the desired speed, and the latter is to keep the TowPlow tracking the desired path. Figure 60 depicts the control scheme of the driving/braking torque. The tractor speed, v_x, is compared to the desired value, v_{x_d}, and the error is fed to the bang-bang controller. The driving/braking torque is decided by adding the torque, a feed forward signal, to overcome the longitudinal resistant force, which includes the snow resistance, air drag and road grade, to the control torque from the controller.

Copyright 2018. the authors

Vermeer Manufacturing Company – Ex. 2045
Kubota v. Vermeer
IPR2025-00168
Page 115 of 182

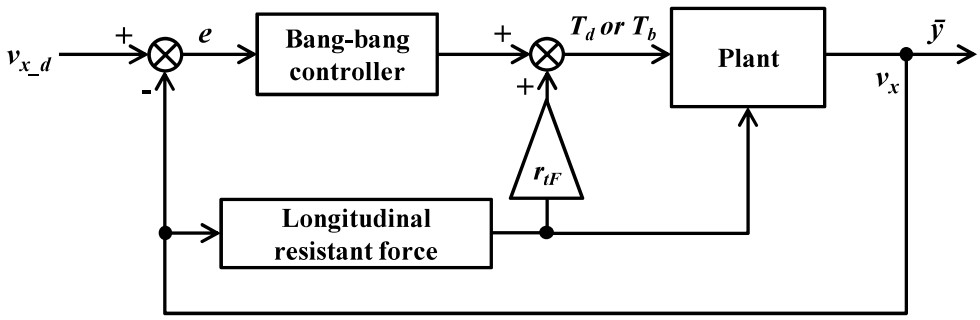


Figure 60. Driver model – control scheme of the driving/braking torque

Figure 61 depicts the control scheme of the tractor steering angle. According to the TowPlow's desired path curvature and velocity, the reference plant based on the linear TowPlow model derived in the section starting on page 52 decides the reference value of the tractor yaw rate. From the error between the reference and actual value, the tractor steering angle is determined by applying proportional and integral gains to the error value.

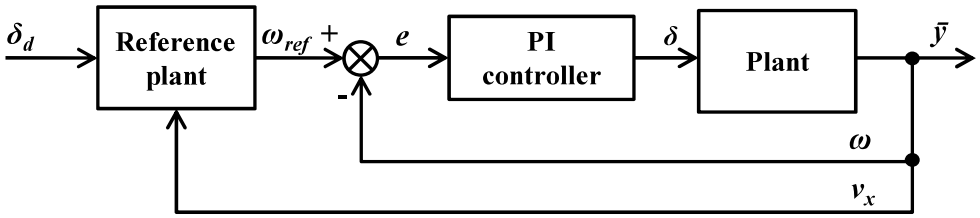


Figure 61. Driver model – control scheme of the tractor steering angle

Figure 62shows comparison of the simulation results of the TowPlow running straight with and without the driver model. The initial state of the TowPlow is that the forward velocity of the tractor is 40 *km/h* (25 *mph*), the trailer steering angle is 30 degrees, and the total articulation angle is also 30 degrees. After 5 seconds, the TowPlow hits and plows 50 *mm* depth of snow. The results without a driver model show a drastic decrease of the forward velocity and counterclockwise yawing of the tractor and trailer. However, with the driver model, the velocity and yaw rate of the tractor are maintained around their initial values. Thus, the driver model well demonstrates a driver's effort to maintain the desired velocity and path.

Deploying trailer plow and cornering

For the first dynamic simulation of the TowPlow, the scenario that includes deploying the trailer plow from the transporting position and constant radius cornering is simulated. The TowPlow starts with the transporting position at its initial velocity of 40 *km/h* (25 *mph*). Shortly after, the TowPlow deploys its trailer plow up to 30 degrees through steering of the trailer axle. Then, it experiences constant radius cornering clockwise and counterclockwise consecutively. The TowPlow is assumed to be operating on a snow packed road ($\mu_0 = 0.4$) plowing 50 *mm* depth

Copyright 2018. the authors

Vermeer Manufacturing Company – Ex. 2045
Kubota v. Vermeer
IPR2025-00168
Page 116 of 182

of snow. Figure 63 shows the simulation results, velocities, steering angles, yaw rates of the tractor and trailer, and total articulation angle between the tractor and trailer.

Throughout the simulation, the velocity of the tractor is maintained around 40 *km/h* (25 *mph*) by the driver model (a). The TowPlow starts with no trailer steering angle and no articulation angle. After 2 seconds, the trailer steering angle increases up to 30 degrees causing the trailer to rotate counterclockwise, and the total articulation angle also increases (b, c). Even though the TowPlow reaches steady-state after deploying the trailer plow, the total articulation angle is less than 30 degrees due to the snow resistance causing the tongue assembly to form a negative articulation angle (d). The TowPlow runs straight down the road during the first 15 seconds. During the time, however, there exists the tractor steering angle exerted by the driver model preventing yaw motion of the TowPlow against the snow resistance (b). After 15 seconds, the TowPlow turns a 100-meter radius corner clockwise. During the cornering, the total articulation angle increases up to 35 degrees, which means the trailer plow intrudes into the adjacent lane about 0.6 *m* based on Eq. (12) and Eq. (13). After the TowPlow comes back to the steady-state from the clockwise cornering, it turns another corner counterclockwise with 65-meter radius. In the case of counterclockwise cornering, the total articulation angle decreases to 20 degrees, which implies the trailer plow misses about 1.39 *m* of the lane (d).

Slalom, Up, and Down Hill

In this simulation, the TowPlow starts with the deployed position with 30-degree trailer steering angle at the initial speed of 40 *km/h* (25 *mph*). It first maneuvers slalom, then goes up and down a 6% grade hill. The snowplowing condition is the same as of the previous simulation. Figure 64 shows the simulation results.

During the first 20 seconds, the TowPlow maneuvers slalom with about 10 degrees of tractor steering angle peak-to-peak variation. The steering input allows the tractor to change one lane to the right and change back to the original lane, which simulates the TowPlow passing a stationary obstacle. Similar to cornering, the total articulation angle varies according to the tractor steering angle (b, d). After the slalom maneuver, the TowPlow goes up and down the hill. The effect of 6% grade hill on the TowPlow is less noticeable than any other maneuvers. Nevertheless, entering and exiting the hill do cause a little rotation of the trailer either clockwise or counterclockwise (c), thus the total articulation angle changes as well (d).

Copyright 2018. the authors

Vermeer Manufacturing Company – Ex. 2045
Kubota v. Vermeer
IPR2025-00168
Page 117 of 182

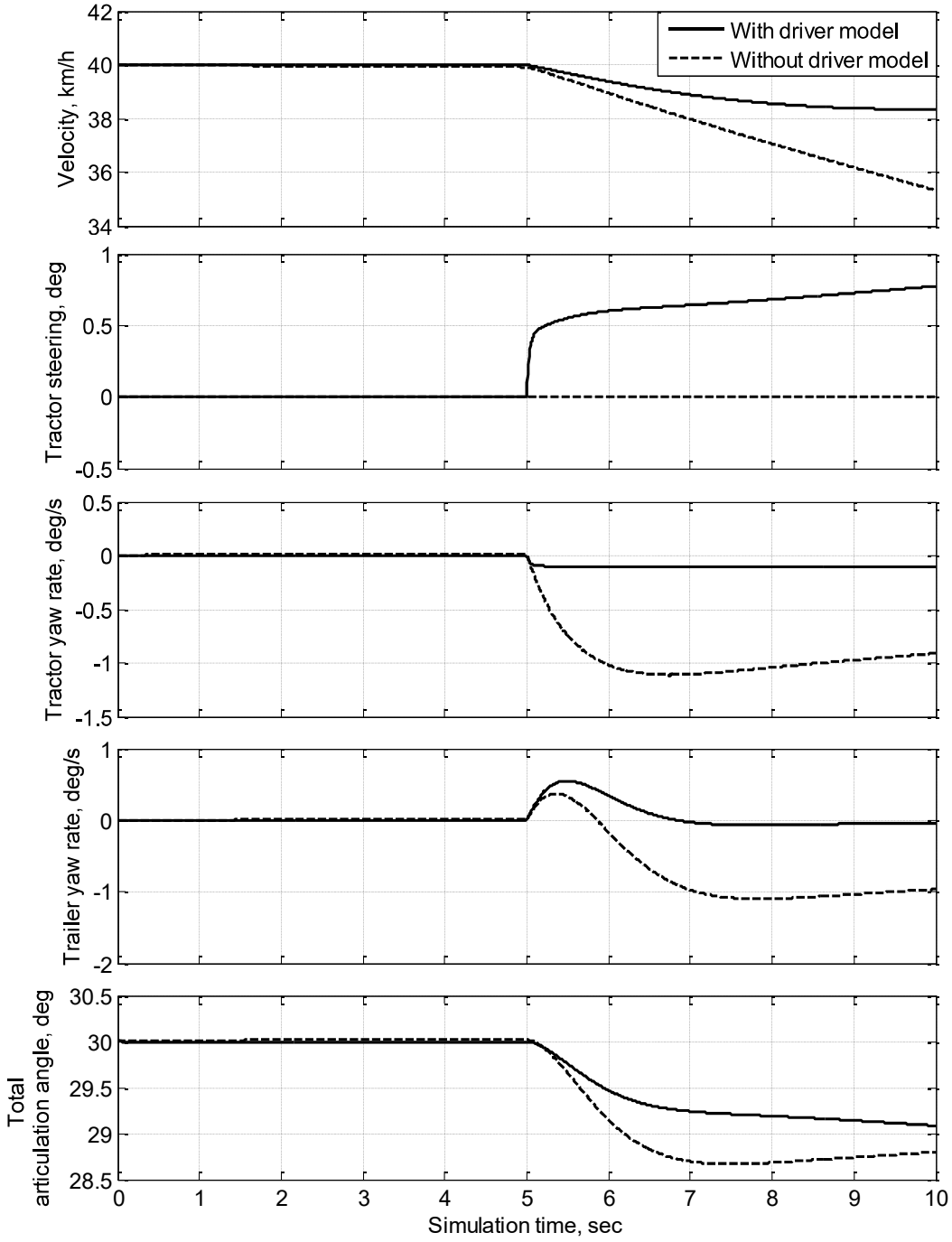


Figure 62. Simulation results of the TowPlow running straight with and without driver model

Copyright 2018. the authors

Vermeer Manufacturing Company – Ex. 2045
Kubota v. Vermeer
IPR2025-00168

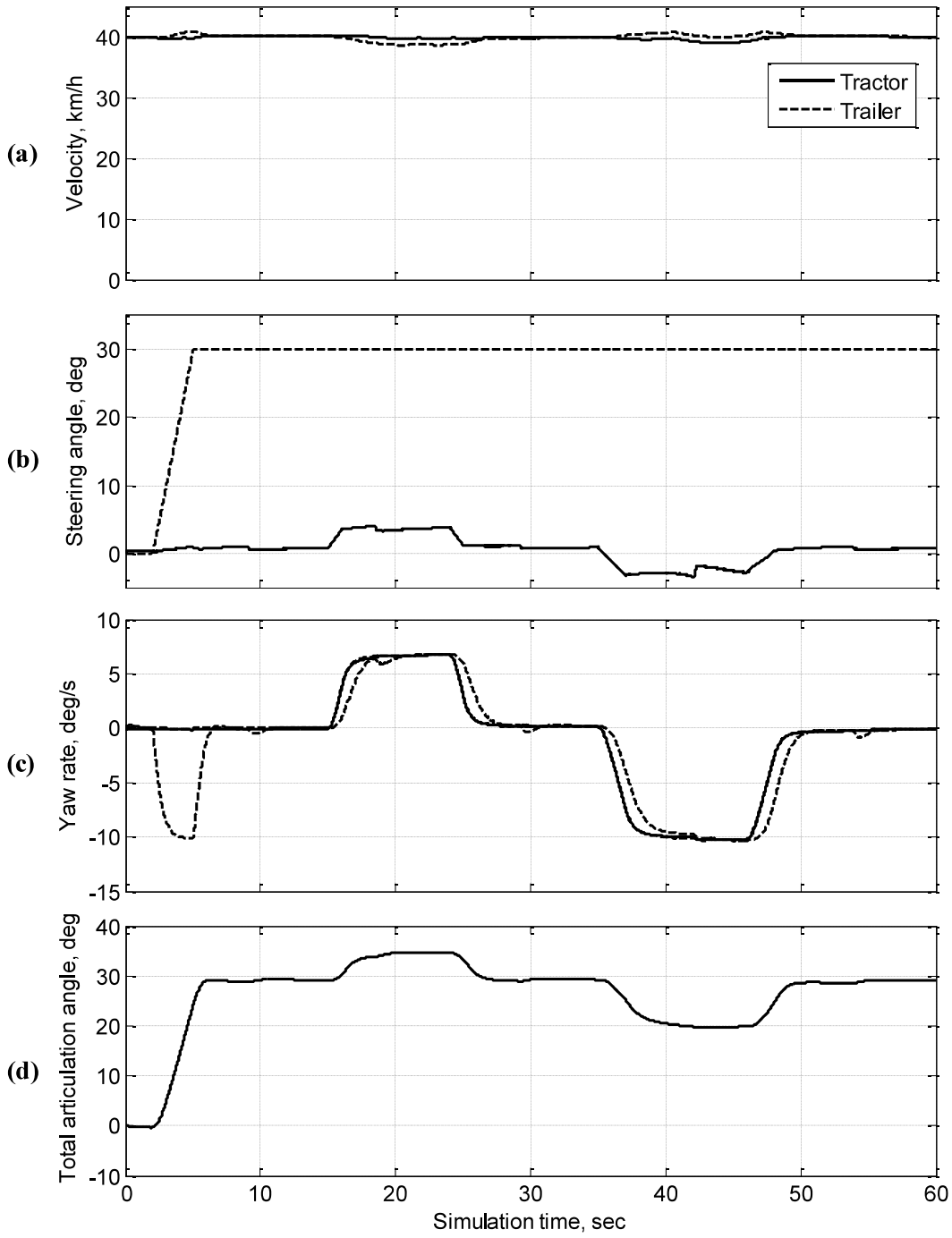


Figure 63. Simulation results of deploying trailer plow and cornering

Copyright 2018. the authors

Vermeer Manufacturing Company – Ex. 2045
Kubota v. Vermeer
IPR2025-00168
Page 119 of 182

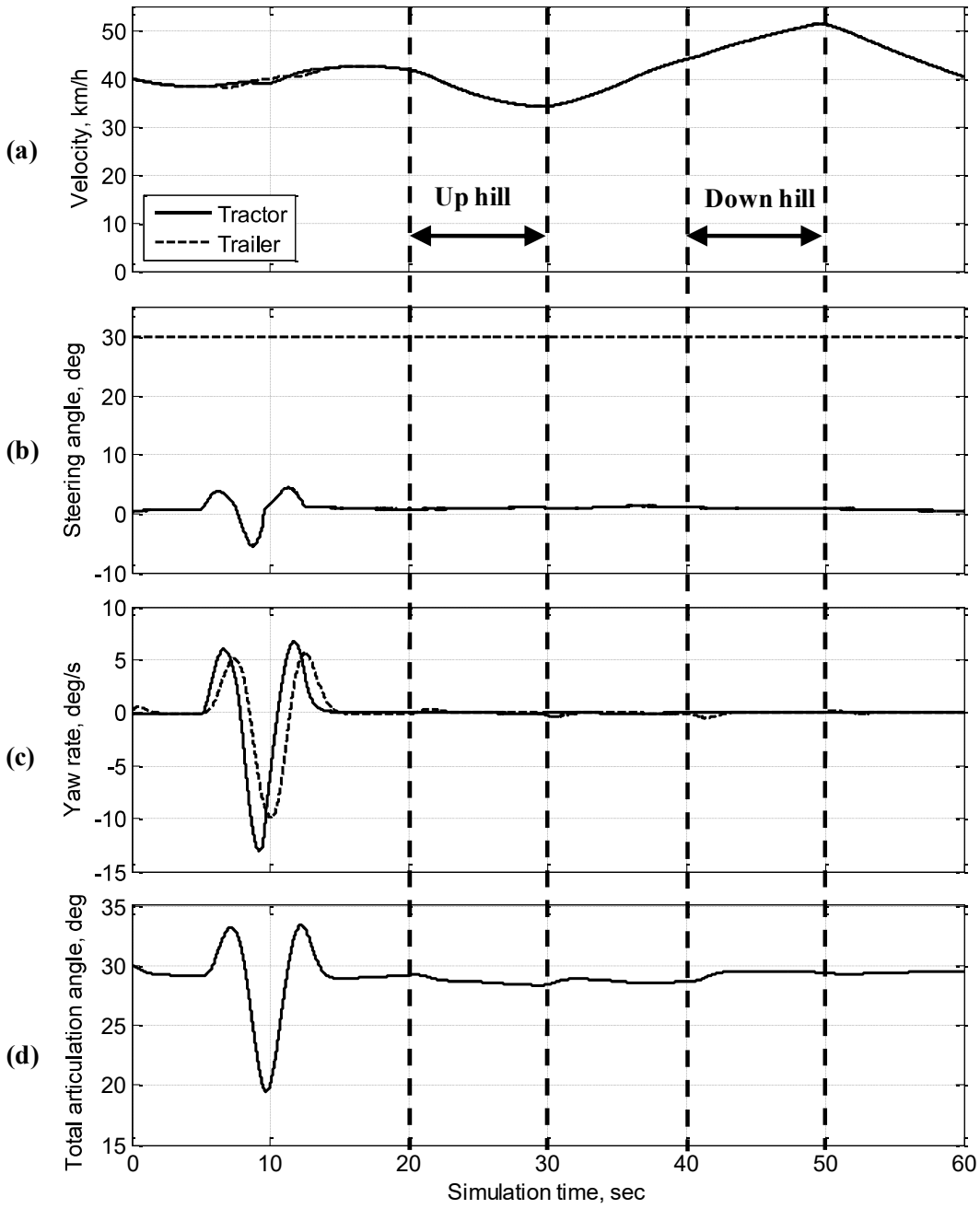


Figure 64. Simulation results of slalom, up and down hill

Split Friction Coefficient Braking

In this simulation, the TowPlow brakes hard through the road with split friction coefficient. It is highly possible for the TowPlow that the tractor and trailer are in different road conditions when the trailer plow is deployed. Only braking with split friction coefficient is simulated because, typically, split friction coefficient accelerating and cruising are less hazardous and have

Copyright 2018. the authors

Vermeer Manufacturing Company – Ex. 2045
Kubota v. Vermeer
IPR2025-00168
Page 120 of 182

less effect on the vehicle dynamics than braking. For the simulation, the TowPlow starts with the trailer in the deployed position, and brakes from 40 *km/h* (25 *mph*) to 0 *km/h* (0 *mph*). Three simulations with different road conditions, one with both the tractor and trailer on a snow packed road(μ_0 = 0.4), another with the tractor on a wet road (μ_0 = 0.6) and the trailer on a snow packed road, and the other with the tractor on a snow packed road and the trailer on a wet road, are conducted.

Figure 65 shows the simulation results of the first case that the tractor and trailer are on a snow packed road having the same friction coefficient for reference to the other two cases. The TowPlow completely stops at 3.9 seconds (a). Braking torque is distributed to each wheel so that the wheel is not locked, and that the total articulation angle changes similarly as when the TowPlow is plowing snow at a constant speed (d). Figure 66 presents the simulation results of the second case that the tractor is on a wet road, the higher friction coefficient, and the trailer is on a snow packed road. In this case, the TowPlow stops at 3 seconds, shorter than the previous case, with the same braking torque distribution since one of the TowPlow units, especially the tractor, is on the road that has higher friction coefficient (a). However, the lower friction of the trailer provides lower grip of the road than the tractor resulting in smaller deceleration and counterclockwise rotation of the trailer with respect to the hitch point, which increases the total articulation angle meaning that the trailer intrudes into the adjacent lane (d). At the same time, the trailer pushes the tractor at the hitch point to the left causing clockwise rotation of the tractor (c). Figure 67 presents the exact opposite case. Due to the trailer's higher grip of the road than the tractor, the trailer decelerates more and rotates clockwise and the total articulation angle decreases (d). The trailer also drags the tractor through the hitch point causing the tractor to rotate counterclockwise (c).

Copyright 2018. the authors

Vermeer Manufacturing Company – Ex. 2045
Kubota v. Vermeer
IPR2025-00168
Page 121 of 182

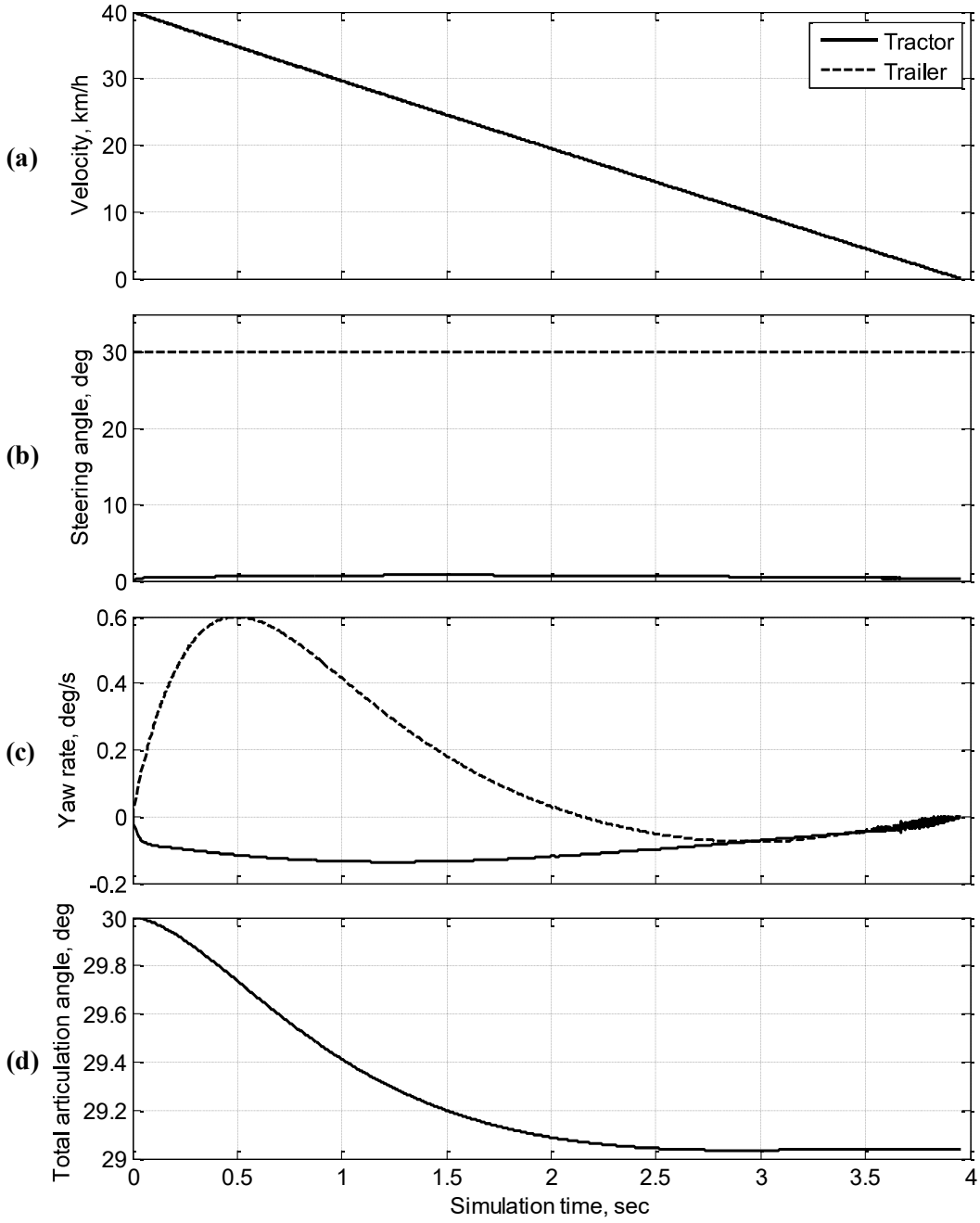


Figure 65. Simulation results of braking on a snow packed road ($\mu_0 = 0.4$)

Copyright 2018. the authors

Vermeer Manufacturing Company – Ex. 2045
Kubota v. Vermeer
IPR2025-00168

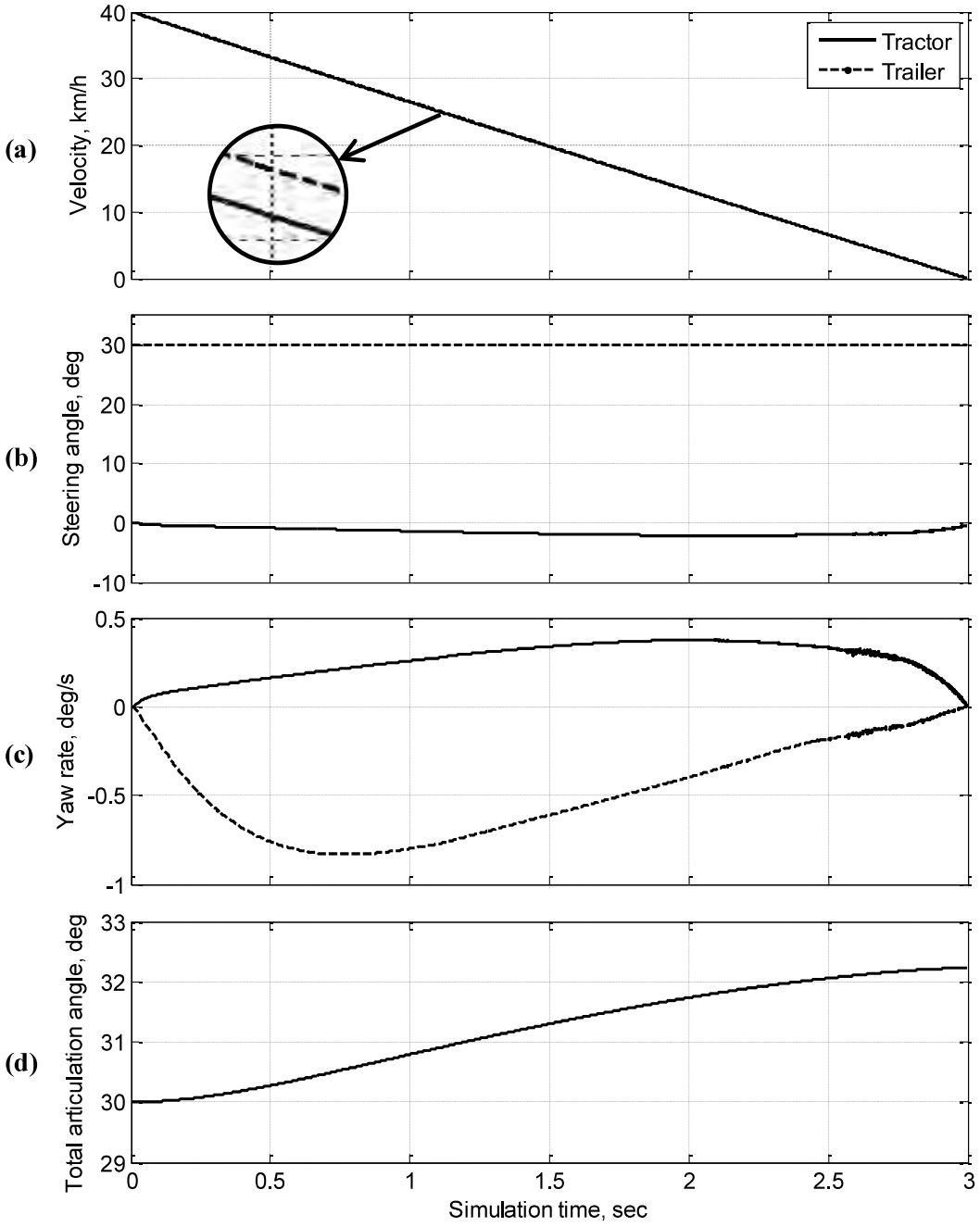


Figure 66. Simulation results of split friction coefficient braking – tractor on a wet road ($\mu_0 = 0.6$) and trailer on a snow packed road ($\mu_0 = 0.4$)

Copyright 2018. the authors

Vermeer Manufacturing Company – Ex. 2045
Kubota v. Vermeer
IPR2025-00168
Page 123 of 182

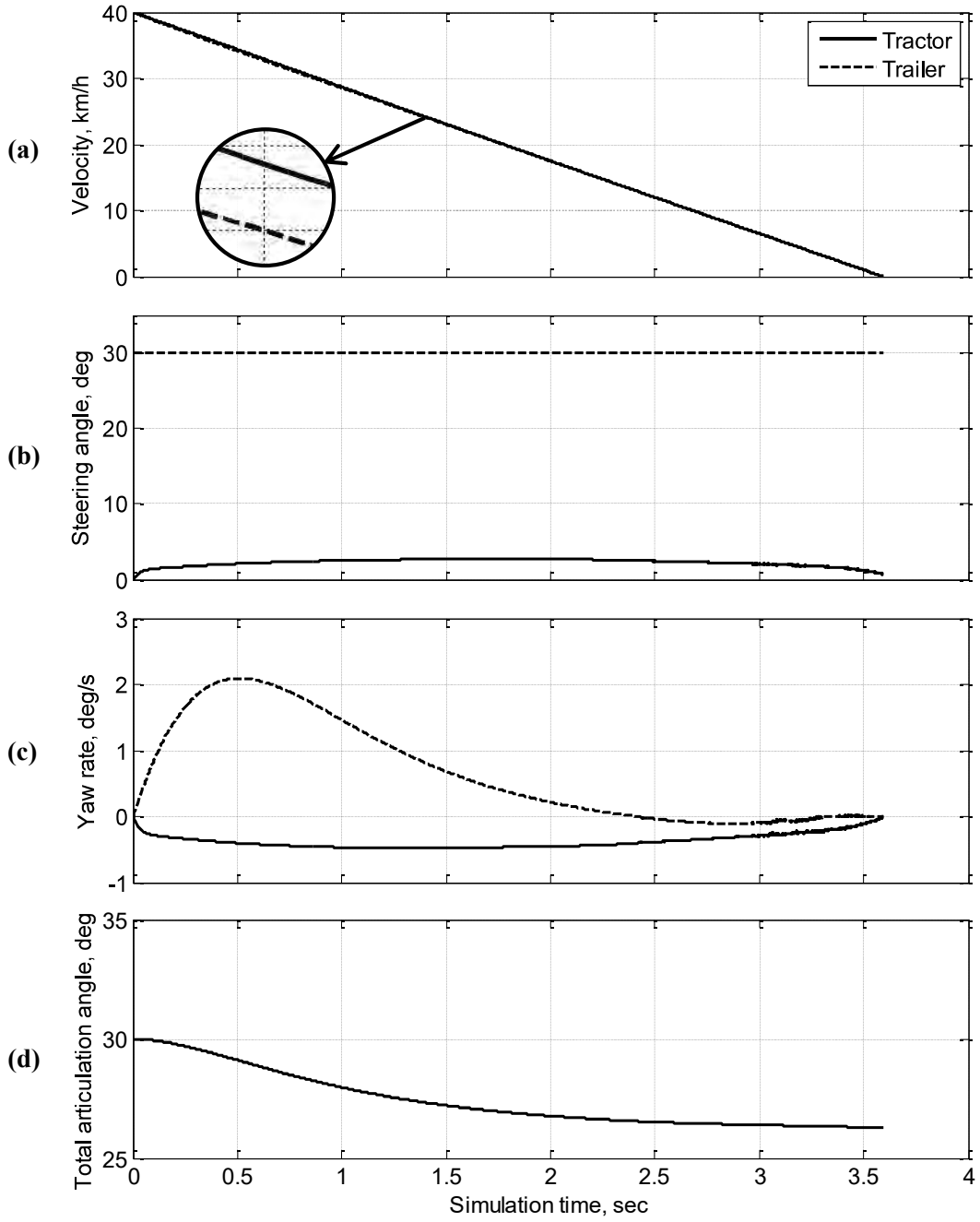


Figure 67. Simulation results of split friction coefficient braking – tractor on a snow packed road ($\mu_0 = 0.4$) and trailer on a yet road ($\mu_0 = 0.6$)

Summary

In this section, the snow resistance model is developed and added to the nonlinear dynamic model of the TowPlow. The model combines the control volume method and the snow compressibility effect from two different existing models, and compares more favorably to

Copyright 2018. the authors

Vermeer Manufacturing Company – Ex. 2045
Kubota v. Vermeer
IPR2025-00168
Page 124 of 182

experiment data than the previously existing models. Dynamic simulations of the nonlinear TowPlow model with the snow resistance model applied to each plow are performed for various maneuvers such as cornering, slalom, up and down hill, and split friction coefficient braking. The simulation results demonstrates that the TowPlow experiencing those maneuvers during its snow removal operation, except up and down hill maneuvers, may cause problems like the trailer intruding into the adjacent lane or missing large portions of the road. As such, the next section will investigate whether these problems can be resolved with active control of the trailer steering system.

Control of the TowPlow for the Snow Removal Operation

In this section, active steering control of the trailer axle is introduced to prevent the TowPlow from intruding into the adjacent lane and also from missing certain portions of the lane during its snow removal operation. The linear quadratic regulator (LQR) based closed-loop controller is developed utilizing the linear TowPlow model (developed starting on page 89). Performance of the Linear-quadratic regulator (LQR) controller is compared to that of a simple Proportional Integrator (PI) controller. Dynamic simulations of the TowPlow with the trailer active steering control are performed for the maneuvers simulated with the uncontrolled system in the previous section (starting on page 89).

Optimal Controller Design - LQR

In order to prevent the TowPlow from trailer-swing, and to maintain the total articulation angle, the trailer needs to be actively steered. The LQR can be used to design a closed-loop controller because the desired state of the system is to regulate one of the state variables in the linear model, which is the deviation of the total articulation angle, $\Delta\theta_t$, from its initial angle. The quadratic cost function [32] is expressed as

$$J(u) = \int_0^\infty (\bar{x}^T Q \bar{x} + \bar{u}^T R \bar{u}) dt \quad , \tag{85}$$

where $\bar{x}$ and $\bar{u}$ denote state variable vector and input vector, respectively, for the linear TowPlow system defined starting on page 52, Q is a diagonal weighting matrix that penalizes components of the state variables, and the R matrix penalizes the input elements. Typically, a diagonal matrix is used for Q and R as

$$Q = \begin{bmatrix} Q_1 & 0 & 0 & 0 \\ 0 & Q_2 & 0 & 0 \\ 0 & 0 & Q_3 & 0 \\ 0 & 0 & 0 & Q_4 \end{bmatrix}; \quad R = \begin{bmatrix} R_1 & 0 \\ 0 & R_2 \end{bmatrix} \quad . \tag{86}$$

To keep $\Delta\theta$ minimum, Q_4 should be larger than other elements in the Q matrix. By adjusting the R matrix, a controlled system that satisfies the design objective can be found. Once these matrices are specified ($Q_1 = Q_2 = Q_3 = R_1 = 1$, $Q_4 = 4000$, $R_2 = 0.05$), the LQR gain matrix, K,

Copyright 2018. the authors

Vermeer Manufacturing Company – Ex. 2045
Kubota v. Vermeer
IPR2025-00168
Page 125 of 182

and the input vector can be obtained through solving the Steady-State Riccati Equation (SSRE) for the system as

$$(M^{-1}A)^T S + S(M^{-1}A) - S(M^{-1}B)R^{-1}(M^{-1}B)^T S + Q = 0 , \tag{87}$$

$$K = R^{-1}(M^{-1}B)^T S , \tag{88}$$

$$\bar{u} = -K\bar{x} , \tag{89}$$

where A, B and M are matrices that define the linear TowPlow system defined in the section starting on page 52. S is the Riccati matrix, which is an unknown variable in the equation. Then, the state-space representation of the controlled system becomes

$$\dot{\bar{x}} = (M^{-1}A - M^{-1}BK)\bar{x} . \tag{90}$$

The stability of the controlled closed-loop system is examined, and Figure 68 shows the locus of the eigenvalues of the controlled system with the maximum combination of the TowPlow varying longitudinal velocity (1 *km/h* ~ 130 *km/h*, 0.6 *mph* ~ 80 *mph*). As noticeable in the figure, the eigenvalues of the system stay in the left-hand plane, thus the system is stable.

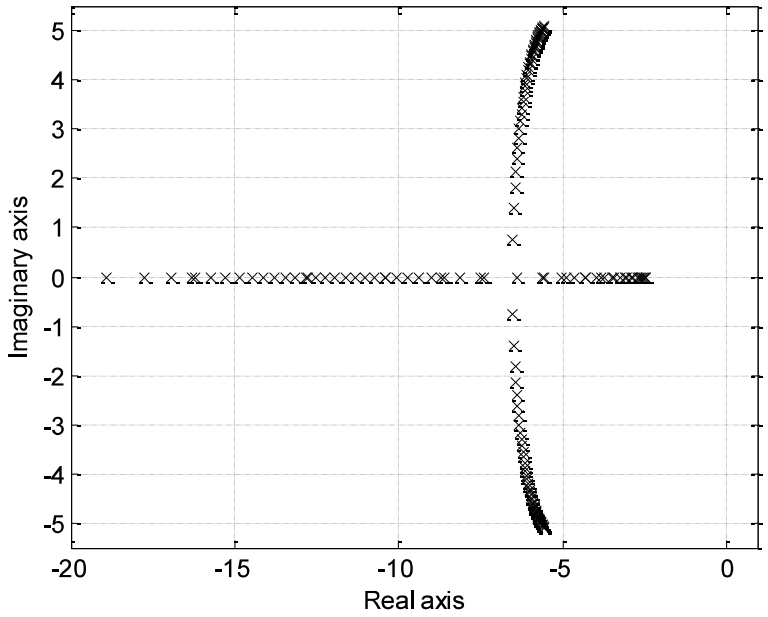


Figure 68. Locus of the eigenvalues of the controlled system with varying longitudinal velocity

To evaluate the performance of the LQR controller, dynamic simulation of the controlled system is performed for the cornering maneuver used in the previous section (starting on page 89). Figure 69 depicts the LQR control scheme of the active steering control for the trailer axle. The LQR controller requires feedback of the entire state variables of the linear system, which are the tractor's lateral velocity, the tractor's yaw rate, the trailer's yaw rate and the deviation of the total articulation angle. Since the linear system matrices for the controller design are subject to

Copyright 2018. the authors

Vermeer Manufacturing Company – Ex. 2045
Kubota v. Vermeer
IPR2025-00168
Page 126 of 182

the longitudinal velocity of the tractor, the gain matrix K is pre-calculated for possible longitudinal velocity ranges and formed into the look-up table. The gain matrix K is selected according to the longitudinal velocity and multiplied by the state variable vector, resulting in the input vector of the controlled system. Among the two inputs from the controller, the tractor steering angle and the trailer steering angle, the latter is used for the active trailer steering because the former is determined by the driver model according to the path curvature.

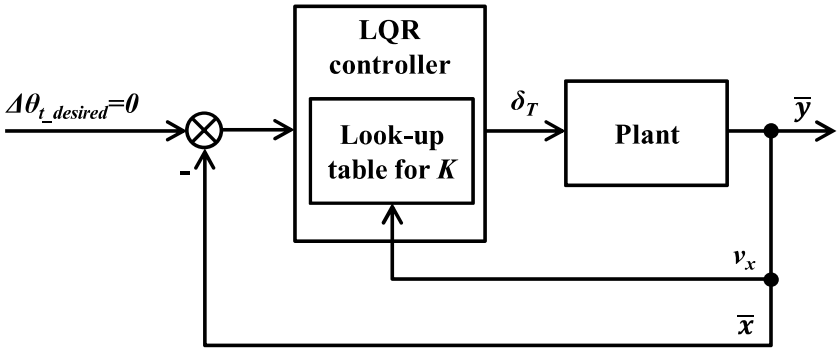


Figure 69. LQR control scheme for the active steering of the trailer axle

For the simulation, the TowPlow starts with the deployed position with 30-degree trailer steering angle at the initial speed of 40km/h, and maneuvers clockwise and counterclockwise cornering while maintaining its speed. Figure 70 compares simulation results of the controlled and uncontrolled systems. As a result of the trailer steering control (b), the total articulation angle of the controlled system is maintained at 30 degrees throughout the simulation while that of the uncontrolled system varies due to the snow resistance and cornering maneuver (e). At the beginning of the simulation and between the cornering maneuvers, even though the TowPlow is going straight, the trailer requires corrective steering to overcome the decrease of the total articulation angle due to the snow resistance (b). The trailer's corrective steering causes the yaw rate of the trailer to synchronize with that of the tractor (c, d) so that the total articulation angle is constant at its desired angle (d).

Copyright 2018. the authors

Vermeer Manufacturing Company – Ex. 2045
Kubota v. Vermeer
IPR2025-00168
Page 127 of 182

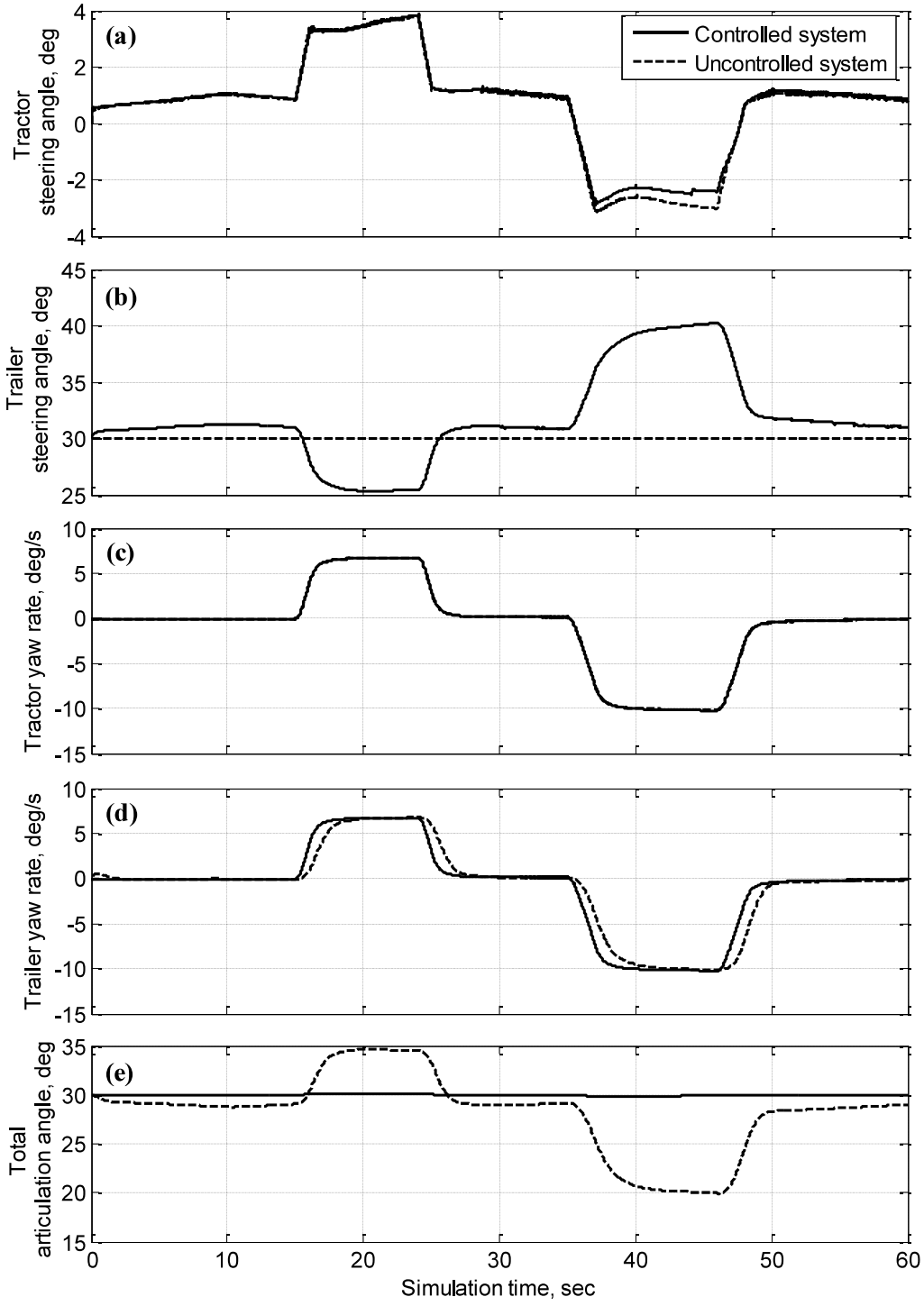


Figure 70. Cornering simulation results of the active trailer steering control

Copyright 2018. the authors

Vermeer Manufacturing Company – Ex. 2045
Kubota v. Vermeer
IPR2025-00168
Page 128 of 182

PI Controller Design

In this section, with a simple PI controller, the active steering control of the trailer axle is proposed. The PI controller requires feedback of the total articulation angle only while the LQR controller, designed in the previous section, requires feedback of every state variable. Figure 71 depicts the active trailer steering control scheme with the PI controller. The total articulation angle from outputs of the system is compared to the desired angle. Using the error between the two values, with appropriate proportional and integral gains, trailer steering angle is determined.

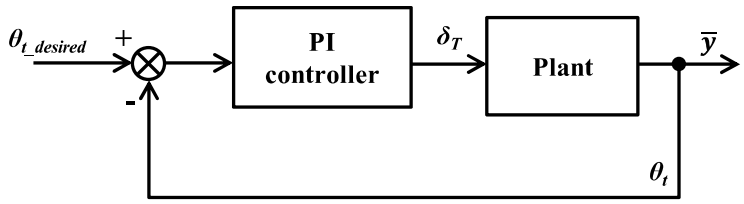


Figure 71. PI control scheme for the active steering of the trailer axle

Performance of the PI controller is simulated with the same cornering maneuver used in the previous section. Figure 72 shows that trailer's corrective steering angles from the two controllers are identical; meaning that responses of the system to the trailer steering inputs are also identical. Even though the LQR control and PI control produce the same results, the PI control is less expensive than the LQR control for implementation to the control system of the TowPlow since it is accomplished with the feedback of just one variable.

Dynamic Simulation of the TowPlow With PI Control of the Trailer Axle

In this section, dynamic simulation of the nonlinear TowPlow model with the active steering control of the trailer axle is conducted for the same maneuvers applied to the uncontrolled system in the preceding section (starting on page 89). PI control, which is simpler than the LQR control, is employed for the control system.

Copyright 2018. the authors

Vermeer Manufacturing Company – Ex. 2045
Kubota v. Vermeer
IPR2025-00168
Page 129 of 182

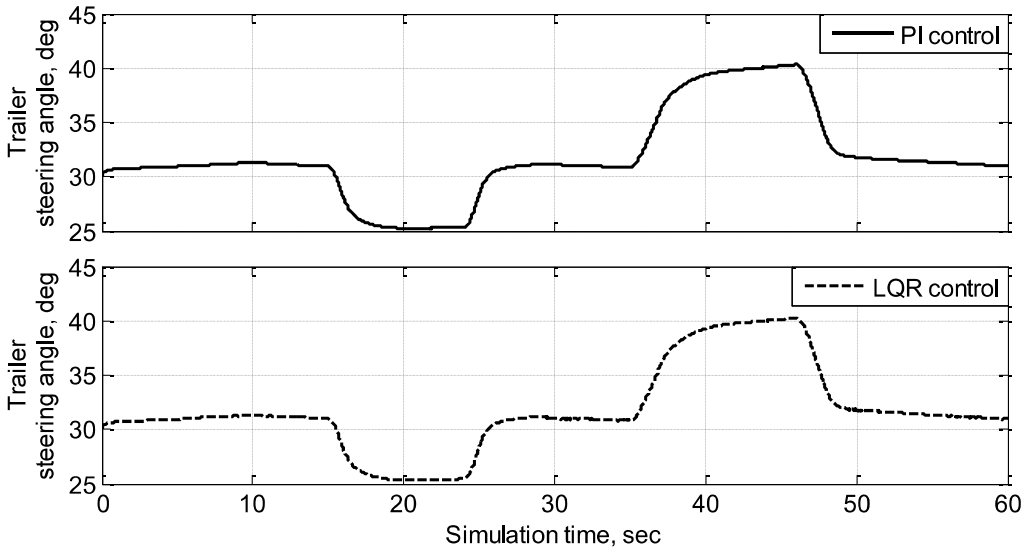


Figure 72. PI control scheme for the active steering of the trailer axle

Slalom, Up, and Down Hill

Figure 73 shows comparison of the simulation results between the controlled and uncontrolled system for the slalom, up and down hill maneuvers. The total articulation of the controlled system is maintained at 30 degrees with the active steering of the trailer axle during the maneuvers, while that of the uncontrolled system varies according to the tractor steering and road grade (b, e).

Split Friction Coefficient Braking

As shown in Figure 74 and Figure 75, the trailer's corrective steering helps the TowPlow maintain its total articulation angle through the split friction coefficient braking maneuvers simulated in the previous section (starting on page 89).

Copyright 2018. the authors

Vermeer Manufacturing Company – Ex. 2045
Kubota v. Vermeer
IPR2025-00168
Page 130 of 182

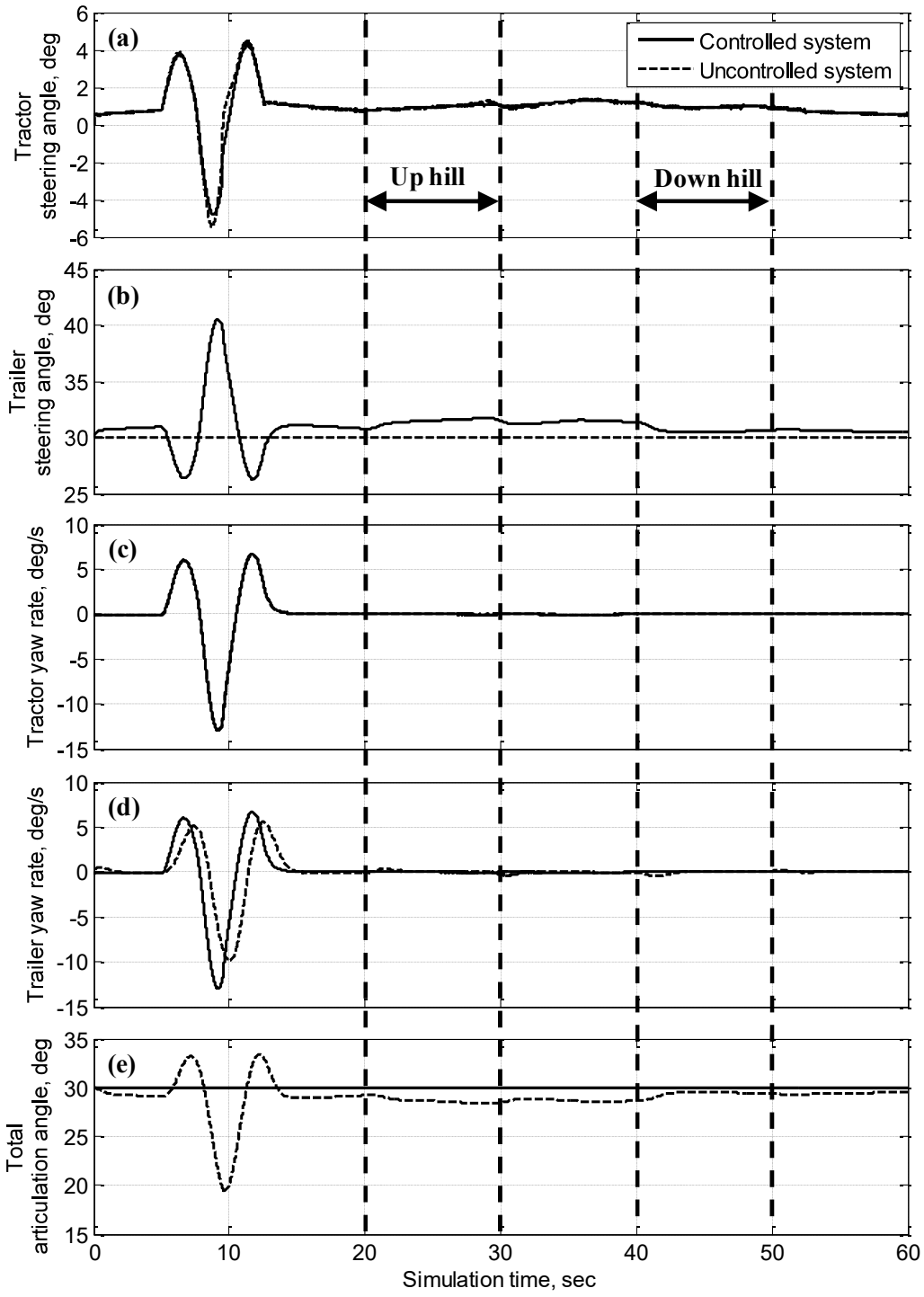


Figure 73. Slalom, up and down hill simulation results of the active trailer steering control

Copyright 2018. the authors

Vermeer Manufacturing Company – Ex. 2045
Kubota v. Vermeer
IPR2025-00168

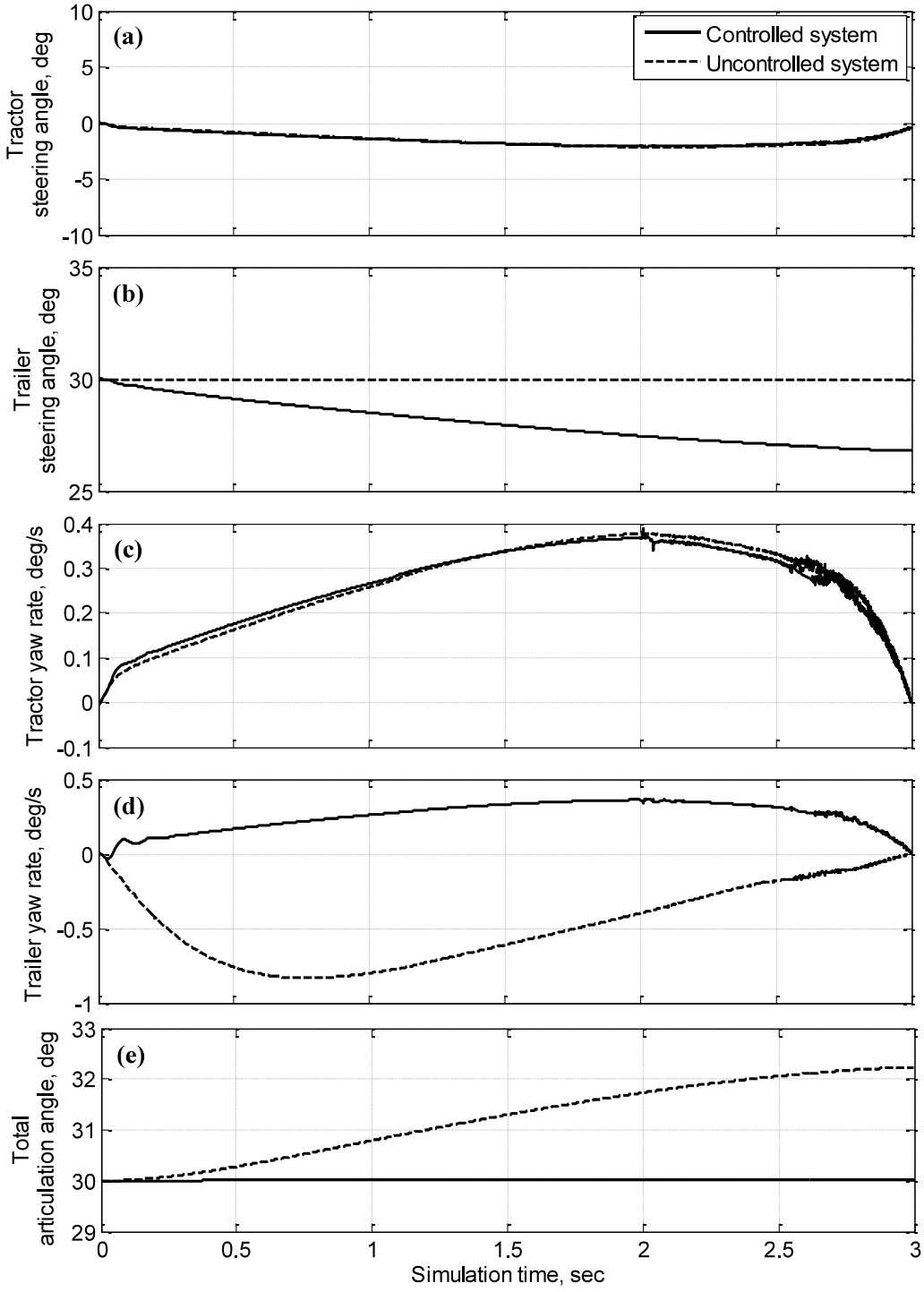


Figure 74. Split friction coefficient simulation results of the active trailer steering control - tractor on a wet road ($\mu_0 = 0.6$) and trailer on a snow packed road ($\mu_0 = 0.4$)

Copyright 2018. the authors

Vermeer Manufacturing Company – Ex. 2045
Kubota v. Vermeer
IPR2025-00168
Page 132 of 182

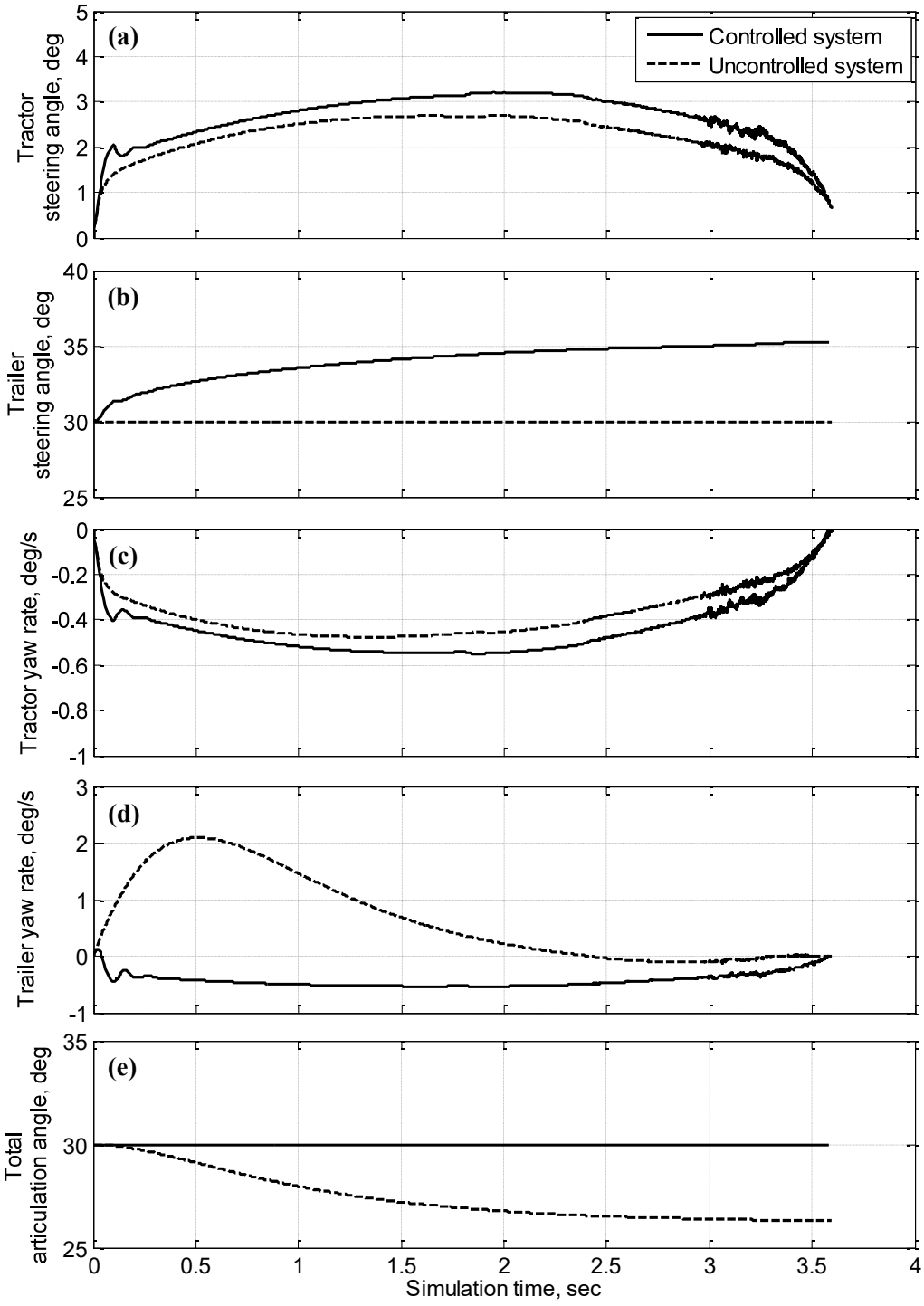


Figure 75. Split friction coefficient simulation results of the active trailer steering control - tractor on a snow packed road ($\mu_0 = 0.4$) and trailer on a wet road ($\mu_0 = 0.6$)

Copyright 2018. the authors

Vermeer Manufacturing Company – Ex. 2045
Kubota v. Vermeer
IPR2025-00168
Page 133 of 182

Summary

To improve safety and efficiency of the TowPlow, active steering control of the trailer axle is proposed. As a control algorithm, first, LQR control, which requires feedback of the full states, is designed since the objective of the control is to regulate the deviation of the total initial angle, one of the state variables of the linear system. Then, a simpler control algorithm, PI control, which requires feedback of only a state variable, is also designed. It is confirmed that the both control algorithms produce the same output to the trailer steering axle of the TowPlow. Performance of the control system is demonstrated through dynamic simulations of the TowPlow for various maneuvers such as cornering, slalom, up and down hill, and split friction coefficient braking, and the simulation results are compared to the uncontrolled system. It is clearly shown that the active steering control of the trailer axle helps the TowPlow maintain its total articulation angle during the maneuvers. Thus, it prevents the TowPlow from either intruding into the adjacent lane or missing certain portions of the lane.

Copyright 2018. the authors

Vermeer Manufacturing Company – Ex. 2045
Kubota v. Vermeer
IPR2025-00168
Page 134 of 182

APPENDIX B: TOWPLOW OPERATOR SURVEY - QUESTIONNAIRE WITH RESULTS

Copyright 2018. the authors

Vermeer Manufacturing Company – Ex. 2045
Kubota v. Vermeer
IPR2025-00168
Page 135 of 182

AHMCT 4/8/14

Tow Plow Configuration Questionnaire

Caltrans Maintenance Kingvale and Truckee questionnaire responses on 4/8/14

5 filled out forms were returned on 4/8/14 from people who all had firsthand Tow Plow plowing experience on I80. The number in "( )" indicates the number of people who made the corresponding response.

1. What kind of material application capability should be on the Tow Plow?
   - Brine*(1)*
   - Sander*(5)*
   - Both*(1) – This was indicated by someone filling in both circles*
   - None
   - *COMMENT(GB) should "ON" in the question be changed to behind*
2. What kind of material application capability should be on the truck?
   - Brine*(1)*
   - Sander*(5)*
   - None *(1)*
   - *COMMENT(GB) should "ON" in the question be changed to behind*
3. Should the system be log any material application rates and location?
   - Important*(4)*
   - No opinion
   - Do not want
   - No Answer*(1)*
4. Should supplemental hazard lighting be added to the Tow Plow
   - Important*(5)*
   - No opinion
   - Do not want
5. Should a rear camera system be installed?
   - Yes*(1)*
     i. *Comment: Only ti if will work in a snow removal situation*
   - No*(4)*
6. Should the truck have a rear facing work light to illuminate the Tow Plow moldboard?
   - Yes(5)
     i. *Comment: but more concerned about just lighting up the lane that the tow plow is in.*
   - No
7. What kind of traction control aid should be used on the Tow Plow
   - Cable chains*(5)*
     i. *Comment: Studded tires?*
   - Automatic traction control device (Ex. Onspots)

Copyright 2018. the authors

Vermeer Manufacturing Company – Ex. 2045
Kubota v. Vermeer
IPR2025-00168
Page 136 of 182

AHMCT 4/8/14

i. *Discussion Comment – Onspots do not work well in situations where the truck is stopped, such as on-grade or on superelevations*

8. Should the Tow Plow have a forward projected laser pointer in order to forward project the maximum location that the Tow Plow can be (see image)?



   - Important*(5)*
   - Non opinion
   - Do not want

9. Should the truck have a "benching" front moldboard?
   - *Comment: change "benching" to "standard", may want to make a comment about a "C" plow*
   - *BM Comment:* Discussion was to keep the existing type of moldboard on plow truck. (This question is still confusing).
   - Yes *(3-this was replaced to mean standard)*
   - No *(1)*
   - *1 - Unclear*

10. Do you think the Tow Plow has potential to reduce the pack operational costs during a snow event?
    - Yes *(4)*
    - No *(1)*
      i. *Comment: Maybe if it could also sand*

11. Do you think incorporating a Tow Plow in the fleet has potential to improve the level of service in snow fighting operations?
    - Yes *(5)*
    - No

12. Do you think training was adequate to operate the Tow Plow
    - Yes *(3)*
    - No *(1)*
    - *No Answer (1)*

13. Do you think the controls were easy to understand?
    - Yes *(3)*
    - No *(1)*
    - *No Answer (1)*

14. Is the Auto Return function a critical feature of the control system?
    - Yes *(4)*
    - No
    - *No Answer(1)*

Copyright 2018. the authors

Vermeer Manufacturing Company – Ex. 2045
Kubota v. Vermeer
IPR2025-00168
Page 137 of 182

AHMCT 4/8/14

15. The following table is intended to give a sense on the general snow fighting operation. The goal is to get a sense of what happens when and at what rate.
    - *The chart was filled out intermittingly by 4 people. No comments on rates were stated and not comments on plowing were made.*

Event Time	Location	Activity				
		Consumables				
		Class (CHECK ONE)			Application Rate (lb/ln-mi or gal/ln-mi)	Plowing
		Liquid	Abrasives	None		
Pre	Ramps	4				NA
	Mainline	4				NA
	Shoulders					NA
During	Ramps		4			
	Mainline	1	4			
	Shoulders					
Post	Ramps	3	3	1		
	Mainline	3	3	1		
	Shoulder			1		

16. Are there any other comments and or concerns you would like to make about the tow plow? Any suggestion on how to efficiently implement a Tow Plow in the winter maintenance fleet would also be appreciated.
    - Comments
        i. Air or ? to lock trailer in transport mode (Safety!)
        ii. Better Tongue Jack
        iii. More room for chains/ Tow Plow fenders
    - Comments
        i. Different lift on Trailer, no more hand crank
    - Comments
        i. Add air lockers that can be controlled from the cab of the truck to keep the tow plow from steering on its own
    - Discussion Notes:
        i. Tow Plow frees truck to cover lanes and ramps so that everything is done in a single pass
            1. Reduction in Public Impact (i.e. Level of service improovment)

Notes From Bob Meline

A. Bryan would like to keep the existing TowPlow in Kingvale
B. Bryan prefers paper logs instead of automated electronic logging
C. Truck had plenty of power but want / need to try plowing heavier snow

Copyright 2018. the authors

Vermeer Manufacturing Company – Ex. 2045
Kubota v. Vermeer
IPR2025-00168
Page 138 of 182

AHMCT 4/8/14

D. Brine: Spray is fine, would like to cover 2 lanes (24 ft wide)
    a. De-ice spray should work
    b. Brine doesn't need to be dribbled
E. Bryan thinks they can get a plow truck reduction by using the TowPlow
F. Camera would work in wet but not dry snow. Some comments that a camera would not work well in the conditions.
G. Discussion on adding a light similar to a wing plow light to the side of the plow truck to illuminate the lane next to the plow truck (ahead of the TowPlow).
H. With TowPlow, fewer drivers are trying to get around the plow train and it is slowing traffic.
I. Could use the TowPlow as a safety barrier, in some circumstances.
J. Related to question 10 and partially mentioned in the comments section:
    a. The TowPlow will allow clearing of the mainline and on/off ramps at one time
    b. Noted that they could switch or rotate the spinner of the right plow truck travelling behind the TowPlow to cover behind the TowPlow
    c. Also noted that the Epoke could cover both lanes behind the TowPlow
K. Brine application rate mentioned was 80 gal / lane mile, existing brining by:
    a. 1,200 gallon brine vehicle
    b. 3,000 gallon brine tanker
    c. 2 Epoke units
L. Chain / cable items:
    a. Add clearance for chains. One closest to mold board is already a close fit.
    b. They run without fenders during some storms
    c. Make it easy to remove fenders
    d. Discussion that in a maintenance workzone, fenders not required per Vehicle Code

Copyright 2018. the authors

Vermeer Manufacturing Company – Ex. 2045
Kubota v. Vermeer
IPR2025-00168
Page 139 of 182

APPENDIX C: POWER VS. PERFORMANCE ANALYSIS

The prime mover truck's power output is a critical concern. As such, a very basic analysis will be performed. The power required for TowPlow operation consists of 4 primary parts consisting of: grade requirements (P_{grade}), rolling resistance (P_{rr}), aerodynamic drag (P_{ad}), and plowing forces (P_{pf}). The total power demand of the system during operation is the sum of all four components and is expressed as

$$P_{total} = P_{grade} + P_{rr} + P_{ad} + P_{PF}. \tag{91}$$

Estimating the power needed to plow snow involves a fairly complex model. Since this discussion is intended to be a simple analysis, the plowing forces will be ignored from the numerical analysis. However, the reader should keep in mind that plowing snow will place additional power demands. However, since the power requirements are speed dependent, it is also important to recognize that plowing occurs at speeds of 40.2 k/hr (25 mph) or less.

The power to overcome the grade is very easy to compute. The general formula for power is

$$P = \vec{F} \cdot \vec{v}. \tag{92}$$

For the case of the demand caused by the grade, the force vector is simply the gravitation force, which is simply the weight of the system. The velocity vector is simply the forward speed of the vehicle. Figure 76 presents a basic free body diagram for the analysis.

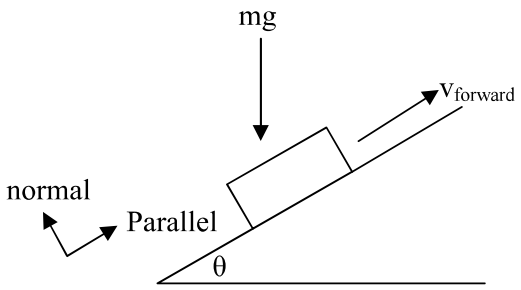


Figure 76. Basic diagram for power analysis

In order to compute the power to travel up the grade, the force gravity force vector needs to be resolved into two components, which are parallel and normal to the road surface. This can be expressed as

$$\vec{F} = \begin{bmatrix} F_{normal} \\ F_{parallel} \end{bmatrix} = mg \begin{bmatrix} -\cos(\emptyset) \\ -\sin(\emptyset) \end{bmatrix}. \tag{93}$$

Copyright 2018. the authors

Vermeer Manufacturing Company – Ex. 2045
Kubota v. Vermeer
IPR2025-00168
Page 140 of 182

In order to overcome the grade, the velocity vector only consists of a parallel component which is equal to the forward vehicle velocity. Therefore, the power required to climb the hill can be expressed as.

$$P_{grade} = mg * \sin(\emptyset) * v_{forward} \quad (94)$$

Rolling resistance, F_{RR}, can be expressed as

$$F_{RR} = \mu_{RR} F_{normal}, \quad (95)$$

where μ_{RR} is the coefficient of rolling resistance (which is a tire property). According to [39], "for heavy vehicles, industry has claimed that rolling resistance varies linearly with heavy vehicle load and varies only slightly with speed." This means that the coefficient of rolling resistance can be assumed constant with respect to speed. The force to overcome rolling resistance lies parallel to the surface. Therefore the power used to overcome rolling resistance can be expressed as

$$P_{RR} = F_{RR} v_{forward} \quad (96)$$

Equation (96) can be expressed as

$$P_{RR} = \mu_{RR} mg * \cos(\theta)\, v_{forward}. \quad (97)$$

The coefficient of rolling resistance is a tire property. According to [39], the coefficient of rolling resistance for a super single trailer axle is 0.00345. The prime mover truck uses 315/80R22.5 front tires, which have a coefficient of 0.00626 (high rolling resistance). The drive tires on the prime mover truck are 11R24.5. Based on the same reference, the coefficient used is equal to 0.00744. To simplify computing P_{RR}, a value for the equivalent rolling resistance will be determined. The value for $\mu_{RR\text{-}eq}$ can be determined using the relationship

$$\mu_{RR-eq} = \frac{\mu_{RR-front} F_{front} + \mu_{RR-rear} Ft_{tan} + \mu_{RR-trailer} Ftp_{tan}}{F_{total}}. \quad (98)$$

Table 11 presents the parameters used in the analysis herein. The unloaded weights are the measure certified weights, while the loaded weight distribution numbers are based on the analysis of TowPlow2.3, with the prime mover truck's payload distributed for maximum handling.

Table 11. Summary of estimated axle loads for determining rolling resistance

Axle Location	Unloaded	Loaded
F_{front}	68,860 N (15,480 lb)	80,070 N (18,000 lb)
$\mu_{RR\text{-}front}$	0.00626	
F_{tan}	83,630 N (18,800 lb)	128,130 N (28,810 lb).
$\mu_{RR\text{-}tan}$	0.0074	
Ft_{tan}	63,970 N (14,380 lb)	147,660 N (33,200 lb).
$\mu_{RR\text{-}trailer}$	0.00345	
F_{total}	216,450 N (48,660 lb)	355,860 N 80,000 lb
$\mu_{RR\text{-}eq}$	0.00587	0.00550

Copyright 2018. the authors

Vermeer Manufacturing Company – Ex. 2045
Kubota v. Vermeer
IPR2025-00168
Page 141 of 182

Aerodynamic drag is expressed as

$$F_{drag} = \frac{1}{2}\rho_{air} C_d A_{front} \left(v_{forward}\right)^2, \quad (99)$$

where ρ_{air} is the density of air, C_d is the drag coefficient, A_{front} is the projected area of the prime mover truck that is perpendicular to the forward velocity. The power to overcome the drag force can be expressed as

$$P_{ad} = F_{drag} v_{forward} = \frac{1}{2}\rho_{air} C_d A_{front} \left(v_{forward}\right)^3 \quad (100)$$

Going back to the original power equation and ignoring the power required to plow yields the following equation:

$$P_{total} = mg * sin(\emptyset) * v_{forward} + \mu_{RR} mg * cos(\theta)\, v_{forward} + \frac{1}{2}\rho_{air} C_d A_{front} \left(v_{forward}\right)^3 \quad (101)$$

This expression gives an estimate of the power demands on the system. Next, the various parameter values are estimated. According to [19], the coefficient of drag for a large tractor trailer ranges from 0.7 to 0.9. The moldboard on the prime mover truck will greatly increase the drag on the system, and therefore the worst-case value of 0.9 will be used. The density of air is roughly 1.29 kg/m^3 when the air temperature is 0^0C. Generally speaking, the prime mover truck is at the maximum legal width which is 2.59 m (102 in.), and the height of the prime mover truck is ~3 m (118 in.). This yields a frontal area of 7.77 m^2 (12,043 in^2). From previous measurements, the empty TowPlow2.3 weighs 216,360 N (48,640 lb). For the purpose of this analysis, a value of 222,410 N (50,000 lb) will be used for the empty weight, while a value of 355,860 N (80,000lb) will be used for the loaded weight.

Concerning grade, the maximum grade on Donner Pass is 6%. This equates to an angle of 3.4^0. For completeness, a 3% grade will also be used which equates to an angle of 1.7^0.

Now that all the parameters have been defined, the power demands can be plotted vs. the speed of the system as shown in Figure 77. As one would expect, as the grade increases, the power demand also increases. Additionally, due to the added weight, there is large increase in the power demand.

Copyright 2018. the authors

Vermeer Manufacturing Company – Ex. 2045
Kubota v. Vermeer
IPR2025-00168
Page 142 of 182

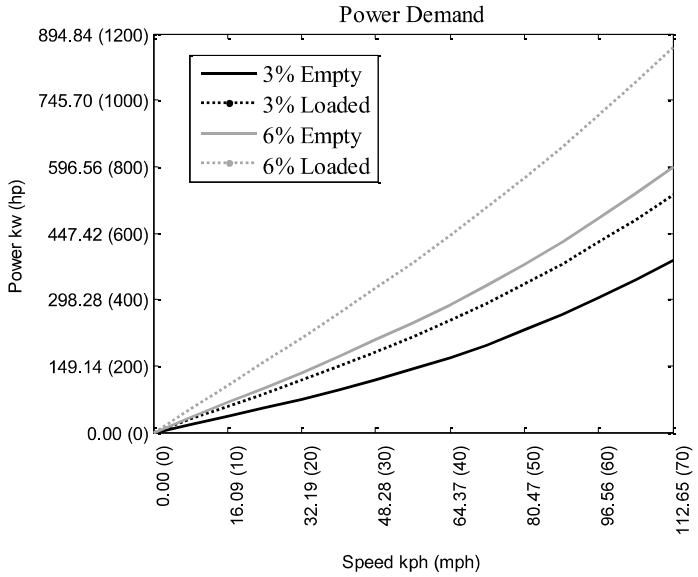


Figure 77. Power demand curves for the TowPlow

Similar analyses were investigated to help validate these results. Based on work by Caterpillar [8], the power demand due to drag, rolling resistance, and grade is given for a Flat-bed (weighing 355,860 N (80,000 pounds)) on a 3% grade at various speeds. Table 12 compares the results from the above analysis and the published Caterpillar data. Results are generally consistent despite the differences in the vehcles considered.

Table 12 Comparison on UC-Davis analysis and published Caterpillar data

Speed	P_{AR}	P_{RR}	P_{grade}
	Caterpillar *UC Davis*	Caterpillar *UC Davis*	Caterpillar *UC Davis*
48.28 km/h (30 mph)	9.71 kW (13 hp) *10.87 kW (14.55 hp)*	32.35 kW (43 hp) *26.25kW (35.14 hp)*	143.42 kW (192 hp) *143.36 kW (191.92 hp)*
56.33 km/h (35 mph)	15.31 kW (20.5 hp) *17.26 kW (23.11 hp)*	39.59 kW (53 hp) *30.62 kW (40.99 hp)*	167.33 kW (224 hp) *167.25 kW (223.90 hp)*
64.37 km/h (40 mph)	22.78 kW (30.5 hp) *25.77 kW(34.49 hp)*	46.31 kW (62 hp) *35.00 kW (46.85 hp)*	191.23 kW (256 hp) *191.15 kW(255.89 hp)*
72.42 km/h (45 mph)	32.49 kW (43.5 hp) *36.69 kW (49.11 hp)*	54.53 kW (73 hp) *39.37 kW(52.71 hp)*	215.14 kW (288 hp) *215.04 kW(287.87 hp)*
80.47 km/h (50 mph)	44.45 kW (59.5 hp) *50.32 kW (67.37 hp)*	62.75 kW (84 hp) *43.75 kW (58.56 hp)*	239.04 kW (320 hp) *238.94 kW(319.86 hp)*
88.51 km/h (55 mph)	59.39 kW (79.5 hp) *66.90kW (89.67 hp)*	94.87 kW (127 hp) *48.12 kW (64.41 hp)*	262.94 kW(352 hp) *262.83 kW (351.85 hp)*

Copyright 2018. the authors

Vermeer Manufacturing Company – Ex. 2045
Kubota v. Vermeer
IPR2025-00168
Page 143 of 182

The above analysis considered power demands at the rear wheels. However, the vehicle's power rating is generally given in terms of engine rating. Based on testing of the TowPlow1 prime mover truck, the drivetrain is approximately 80% efficient. Therefore, superimposed on the plots, three lines will be drawn at 329 kW (440 hp), 284 kW (380 hp), and 254 kW (340 hp). These numbers correspond to systems with an engine rating of 311 kW (550 hp), 355 kW (475 hp), and 317 kW (425 hp), respectively. Figure 78 through Figure 81 present the power demands on the system in several scenarios. The legend for these plots is presented in Figure 82. An additional line was added to the plots as a crude attempt to show the effect of deploying the TowPlow trailer. For the point of illustration, when the TowPlow trailer is deployed, the frontal area increases. The rolling resistance and grade power demands remain the same. This is calculated by multiplying the value P_{ar} by 2 in the analysis.

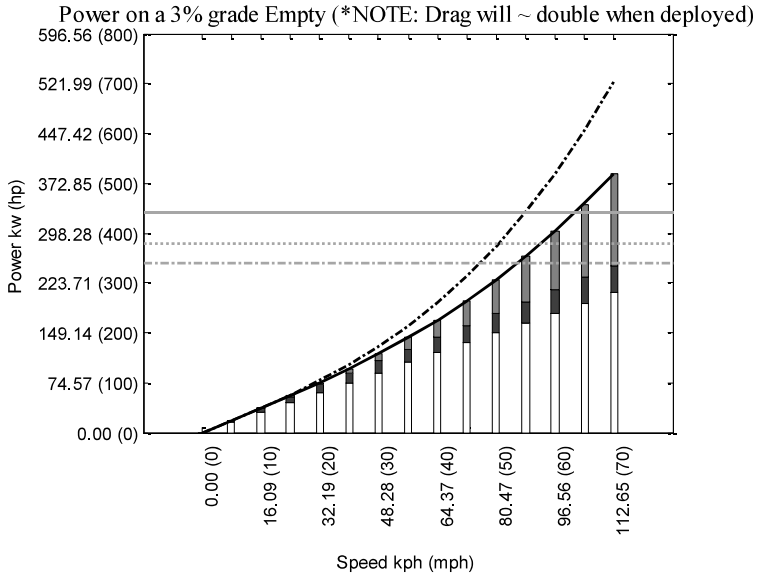


Figure 78. Power demand on for an empty TowPlow on 3% grade

Copyright 2018. the authors

Vermeer Manufacturing Company – Ex. 2045
Kubota v. Vermeer
IPR2025-00168
Page 144 of 182

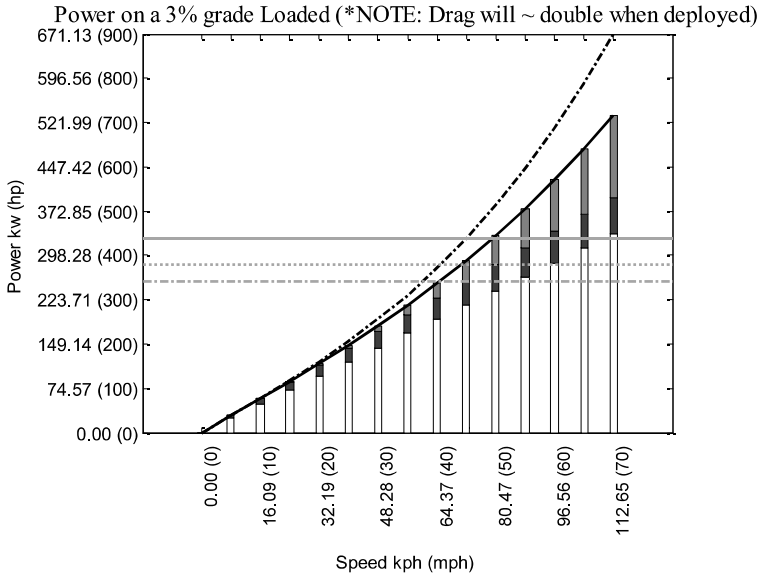


Figure 79. Power demand on for a loaded TowPlow on 3% grade

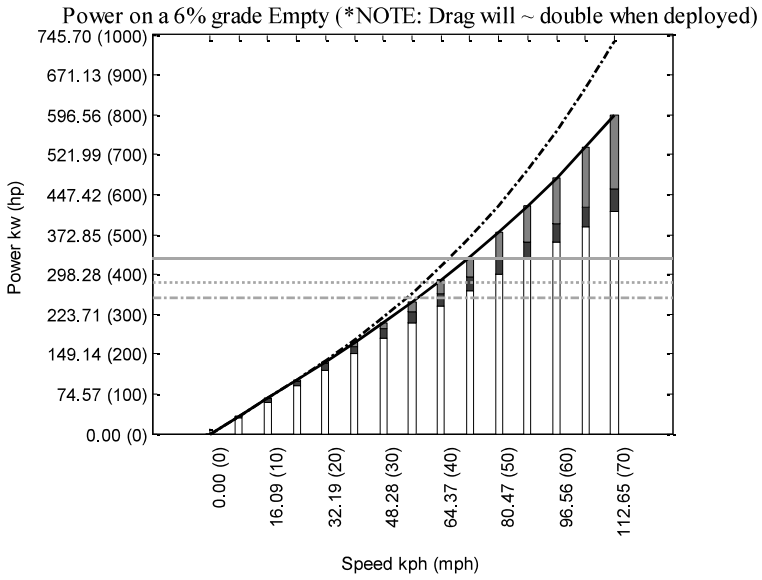


Figure 80. Power demand on for an empty TowPlow on 6% grade

Copyright 2018. the authors

Vermeer Manufacturing Company – Ex. 2045
Kubota v. Vermeer
IPR2025-00168
Page 145 of 182

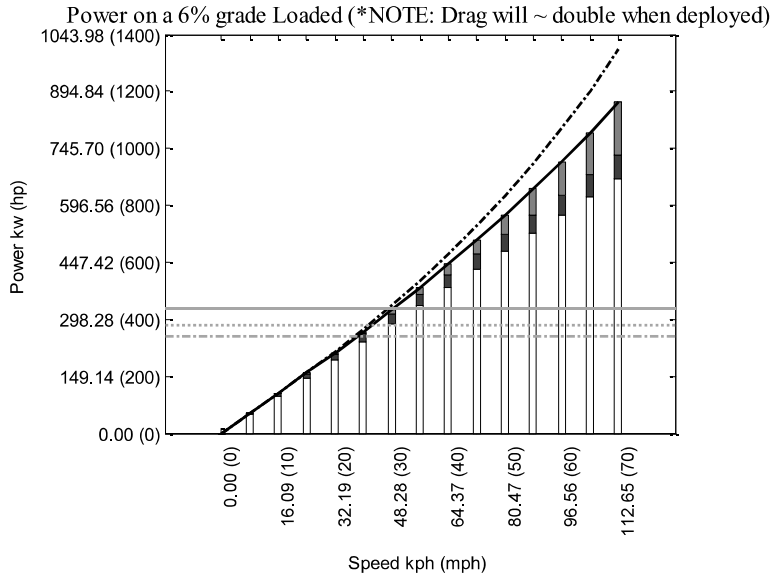


Figure 81. Power demand on for a loaded TowPlow on 6% grade



Figure 82. Legend for power demand curves

The plots above show the general trend in regards to the power demanded. From this analysis, rough predictions of the maxium system speeds can be made and these are presented in Table 13. Note that these speeds are based on a steady state condition. Typical chain control plowing operations are done at about 40.23 km/h (25 mph). Clearly this table shows that the 355 kW (475 hp) system will not be able to maintain that speed while trying to plow snow with a fully loaded system travelling up a 6% grade. Also, the addition of 60 hp to the rear wheels between the 411 kW (550 hp) system and the 355 kW (475hp) engine would result in a top speed increase of about 6-8 km/h (4-5 mph).

Copyright 2018. the authors

Vermeer Manufacturing Company – Ex. 2045
Kubota v. Vermeer
IPR2025-00168
Page 146 of 182

Table 13. Prediced top speeds for the TowPlow in various conditions

	Max Speed km/h (mph): stowed/*deployed*		
Case	411 kW (550 hp) engine 329 kW (440 hp) rear wheel	329 kW (475 hp) engine 284 kW (380 hp) rear wheel	317 kW (425 hp) engine 254 kW (340 hp) rear wheel
3% Empty	101.86 (63.29) *88.22(54.82)*	92.84(57.69) *81.19(50.45)*	86.29(53.62) *75.96(47.20)*
3% Loaded	79.61(49.47) *72.53(45.07)*	70.91 (44.06) *65.36(40.61)*	64.78(40.25) *60.14(37.37)*
6% Empty	71.91(44.68) *66.61(41.39)*	63.60(39.52) *59.56(37.01)*	57.79(35.91) *54.59(33.92)*
6% Loaded	48.99(30.44) *47.52(29.53)*	42.66(26.51) *41.65(25.88)*	38.37(23.84) *37.59(23.36)*

One can also consider the additional power that is available when plowing snow at the typical speed of 40 km/h (25 mph) by looking at Figure 78 through Figure 81.

Table 14. Excess power available to plow snow at 25mph

		Power available kW (hp)		
Case	Power demand(hp)	411 kW (550 hp) engine 329 kW (440 hp) rear wheel	355 kW (475 hp) engine 284 kw (380 hp) rear wheel	317 kW (425 hp) engine 254 kW (340 hp) rear wheel
3% Empty	101.9 (136.4)	226.8 (303.6)	182.0 (243.6)	152.1 (203.6)
3% Loaded	154.0 (206.1)	174.7 (233.9)	129.8 (173.8)	100.0 (133.9)
6% Empty	176.3 (236.0)	152.4 (204.0)	107.6 (144)	77.7 (104.0)
6% Loaded	266.8 (357.1)	66.4 (88.9)	17.1 (22.9)	-12.8 (-17.1)

In summary, this analysis provides a basic understanding of the power requirements for the TowPlow system. The grade power demand in the Donner Pass area is quite significant. Both 355 kW (475 hp) and 411 kW (550 hp) power systems will likely be unable to maintain speed while climbing long steep grades. However, when plowing snow, the 411 kW (550 hp) prime mover truck should have significantly more power available.

Copyright 2018. the authors

Vermeer Manufacturing Company – Ex. 2045
Kubota v. Vermeer
IPR2025-00168
Page 147 of 182

APPENDIX D: PRELIMINARY AXLE LOAD ANALYSIS

Establishing a Baseline from the TowPlow2 Static Weights

The empty TowPlow2 was driven to a certified scale for weight measurements. Prior to weighing the system, the fuel tanks were filled to capacity. The scale consisted of three load plates. The first plate only supported the front axle of the prime mover truck. The second plate supported the prime mover truck's tandem axles. The third plate supported the TowPlow2 trailer tandem axles. Two sets of measurements were taken. The first measurement was done with the TowPlow2 trailer connected to the prime mover truck and the second was done with the TowPlow2 trailer disconnected. When the Towplow2 trailer was disconnected, its landing gear fell on the third load plate. This would mean that the scale measurement on the third plate is the total weight of the TowPlow2 trailer. The results of these measurements are presented in Table 15. For the analysis to follow, a convention was developed to refer to these measurements. For example the variable F_{front_a}, will be used to refer to the front axle weight of the prime mover truck in the disconnected state. Ft_{tan_b} refers to the weight of prime mover truck's tandem axle set in the connected state.

Table 15. TowPlow2 static weights

TowPlow2 trailer configuration	Prime mover truck front axle (F_{front})	Prime mover truck tandem axle set (Ft_{tan})	TowPlow2 trailer tandem axle set (Ftp_{tan})	Total
Connected (_b)	56,670 N (12,740 lb)	100,710 N (22,640 lb)	66,280 N (14,900lb)	223,660 N (50,280 lb)
Disconnected (_a)	60,050 N (13,500 lb)	79,890 N (17,960lb)	83,720 N (18,820 lb)	223,660 N (50,280 lb)

When a TowPlow trailer is connected, weight will be added to the rear axles. Since the hitch point lies behind the rear axles, one would expect weight to come off of the front axle as shown in the measurements. Also, the sum of the three load plate measurements for both cases are equal as expected.

Since the axles are weighed as a group, they will be treated as a single support located at the midpoint of the tandem axle set, which is the standard approach for providing permits to trucks. The TowPlow2 free body diagram is presented in Figure 83**.** Table 16 presents the key physical dimensions required for the analysis, which were measured by AHMCT.

Copyright 2018. the authors

Vermeer Manufacturing Company – Ex. 2045
Kubota v. Vermeer
IPR2025-00168
Page 148 of 182

Table 16. Physical system measurements

Parameter	Value
Dt_{hitch}	7.288 m (23.91 ft)
Dt_{axle}	5.816 m (19.08ft)
Dtp_{axle}	7.62 m (25 ft)

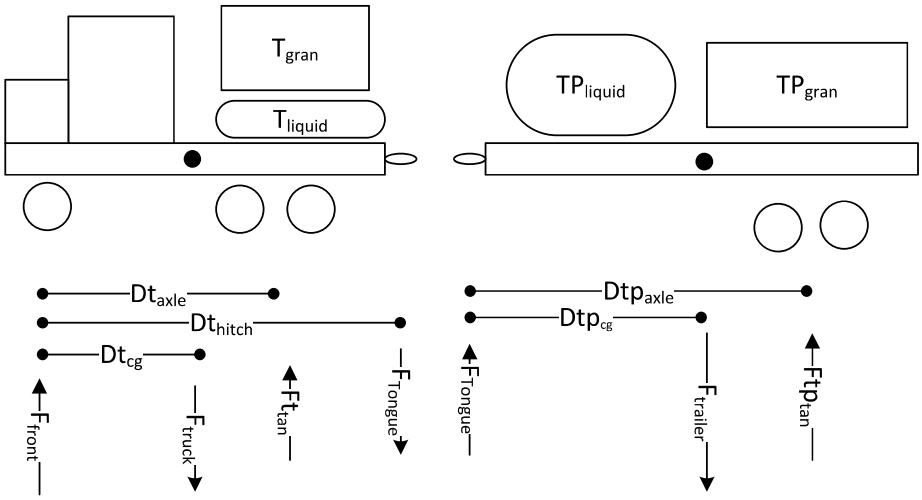


Figure 83. Free body diagram of TowPlow2

The weight of the TowPlow2 trailer, $F_{trailer}$, is very simple to determine. During the weighing process, when the TowPlow2 trailer was disconnected, the landing gear and axle where on a common plate and therefore this measurement is equivalent to the total weight of the TowPlow2 trailer. Using the convention described above, the TowPlow2 trailer weight, $F_{trailer}$, can be expressed in terms of the measured values as

$$F_{trailer} = Ftp_{\tan_a} = 83{,}720 \text{ N } (18{,}820 \text{ lb}). \quad (102)$$

The value Ftp_{tan} is the weight on the TowPlow2 trailer tandem axle set when connected. Mathematically this is presented as

$$Ftp_{tan} = Ftp_{\tan_b} = 66{,}280 \text{ N } (14{,}900 \text{ lb}) \quad (103)$$

Sstatics can used to determine the tongue weight, F_{tongue}, by summing forces in the vertical direction as

$$\sum F_x = 0 = F_{tongue} - F_{trailer} + Ftp_{tan}. \quad (104)$$

This equation can be rearranged to solve for F_{tongue} as

$$F_{tongue} = F_{trailer} - Ftp_{tan} = 83{,}720 \text{ N } - 66{,}280 \text{ N} = 17{,}440 \text{ N } (3{,}920\ lbs.) \quad (105)$$

The TowPlow2 trailer's center of gravity location, Dtp_{cg} can be computed by summing the moments about the hitch as

Copyright 2018. the authors

Vermeer Manufacturing Company – Ex. 2045
Kubota v. Vermeer
IPR2025-00168
Page 149 of 182

$$\sum M_{hitch} = 0 = Ftp_{tan} * Dtp_{axle} - F_{trailer} * Dtp_{cg}. \quad (106)$$

This equation can be used to solve for Dtp_{cg} as

$$Dtp_{cg} = \frac{Ftp_{tan} * Dtp_{axle}}{F_{trailer}} = \frac{66{,}280\ N * 7.62\ m}{83{,}720\ N} = 6.03\ m\ (19.79\ ft). \quad (107)$$

The weight of the prime mover truck is the sum of the weights on the front axle (F_{front}) and the tandem axle set (Ft_{tan}) from the case when the system was weighed with the TowPlow2 trailer disconnected ($_a$). This is also equivalent to summing the forces in the "*y*" direction given as

$$F_{truck} = F_{front_a} + Ft_{\tan_a} = 60{,}050\ \text{N} + 79{,}890\ \text{N} = 139{,}940\ \text{N}\ (31{,}460\ lbs). \quad (108)$$

The prime mover truck's center of gravity, Dt_{cg} can be computed by summing the moments about the front axle as

$$\sum M_{front} = Ft_{\tan_a} * Dt_{axle} - F_{truck} * Dt_{cg}. \quad (109)$$

Equation (109) can be rearranged to solve for Dt_{cg} given as

$$Dt_{cg} = \frac{Ft_{tan} * Dt_{axle}}{F_{truck}} = \frac{79{,}890\ \text{N} * 5.816\ m}{139{,}940\ N} = 3.320\ \text{m}\ (10.89 ft). \quad (110)$$

The difference between the sums of the prime mover truck's axles in the both cases should be equal to the tongue weight. This can be mathematically represented as

$$\left(F_{front_b} + Ft_{\tan_b}\right) - \left(F_{front_a} + Ft_{\tan_a}\right) = F_{hitch}. \quad (111)$$

Substituting numbers into equation (111) yields the hitch force

$$(56{,}670\ \text{N} + 100{,}710\ \text{N}) - (60{,}050\ \text{N} + 79{,}890\ \text{N}) = 17{,}440\ \text{N}\ (3{,}920 lbs). \quad (112)$$

The result is consistent with equation (105) as expected.

Fully Loaded Weight of the TowPlow2

Now that the key values for the empty TowPlow2 have been determined, the next step is to predict the weights when every part of the system is loaded to capacity. The turn-key system has 4 areas where material can be stored. Both the prime mover truck and the TowPlow2 trailer have the ability to store granular and liquid materials. The Caltrans specification for the weight of sand, ρ_{sand}, is 17.45 kN/m^3 (3000 lb/yd^3) is used. The weight of brine liquid is 11.75 N/liter (10 lb/gal). The manufacturer provided the capacities of the various systems on TowPlow2, which are summarized in Table 17.

Table 17. Summary of hopper/tank capacities and corresponding weights for the TowPlow2

	Granular		Liquid	
	Volume	Weight	Volume	Weight
Prime mover truck	7.26 m^3 (9.5 yd^3)	126,690 N (28,500 lb)	1,022 liters (270 gal.)	12,010 N (2,700 lb)
TowPlow2 trailer	5.96 m^3 (7.8 yd^3)	104,000 N (23,400 lb)	2,840 liters (750 gal.)	33,370 N (7,500 lb)

Copyright 2018. the authors

Vermeer Manufacturing Company – Ex. 2045
Kubota v. Vermeer
IPR2025-00168
Page 150 of 182

A calculation can be performed to look at the gross combined weight. This can be determined by summing all the weights given in Table 17 with the total system weight given in Table 15. This yields a total weight of 499,890 N (112,380 lb). This is over the legal maximum for the gross combined weight rating. Note that the front plow is not included. According to the vendor, the weight of the plow, F_{plow}, is 8,450 N (1,900 lb). Caltrans Division of Equipment independently performed a similar analysis that also determined that TowPlow2 will exceed legal weight limitations when loaded fully.loaded.

Group Axle Weights

For completeness, calculations will be performed to estimate the static weights of the individual axle groups. The free body diagram for this is presented in Figure 84. Some additional distance parameters are required for the computations and these are presented in Table 18.

Table 18. Additional distance parameters need to compute the overloaded axle load which were measured by AHMCT

Parameter	Description	Value
Dt_{hop}	Distance from the prime mover truck's front axle to the CG of its granular load	6.187 m (20.30 ft)
Dt_{tank}	Distance from the prime mover truck's front axle to the CG of its liquid load	6.494 m (21.30 ft)
D_{plow}	Distance from the prime mover truck's front axle to the CG of the front plow	2.530 m (8.30 ft)
Dtp_{tank}	Distance from the TowPlow2 trailer's hitch to the CG of the its liquid load	3.840 m (12.60 ft)
Dtp_{hop}	Distance from the TowPlow2 trailer's hitch to the CG ofits granular load	6.370 m (20.90 ft)

Copyright 2018. the authors

Vermeer Manufacturing Company – Ex. 2045
Kubota v. Vermeer
IPR2025-00168
Page 151 of 182

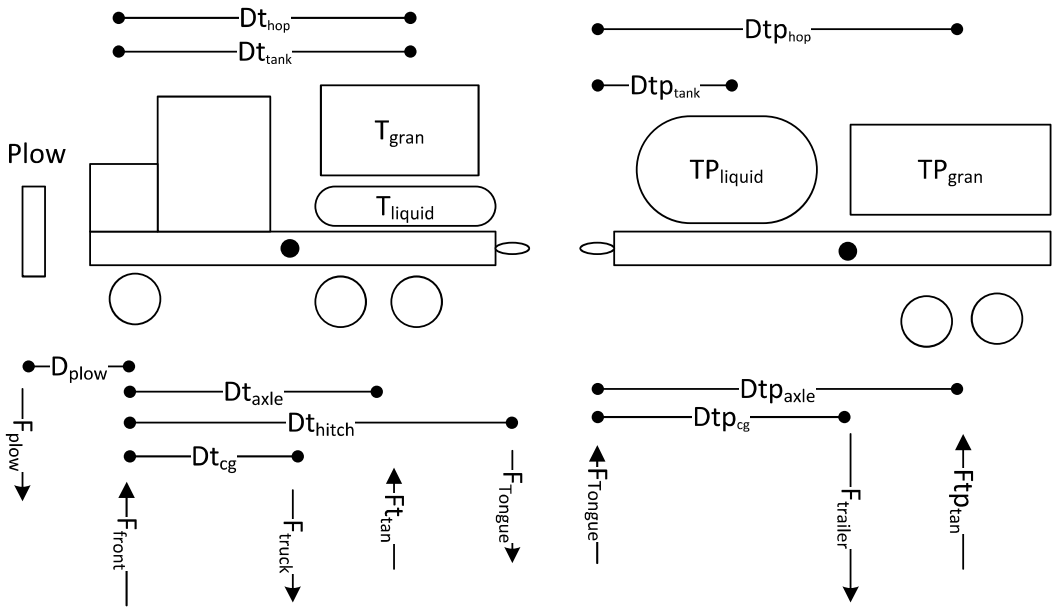


Figure 84. Free body diagram of TowPlow2

Considering the TowPlow2 trailer and use of the value for Dtp_{cg} from equation (110), summing moments about the hitch yields

$$\sum M_{tongue} = 0 = Ftp_{tan} * Dtp_{axle} - F_{trailer} * Dtp_{CG} - TP_{gran} * Dtp_{hop} - TP_{liquid} * Dtp_{tank} \quad (113)$$

where TP_{liquid} is the weight in the brine tank, and TP_{gran} is the weight of the sand in the hopper. Equation (113) can be used to solve for the weight on TowPlow2's tandem axles Ftp_{tan} as

$$Ftp_{tan} = \frac{F_{trailer} * Dtp_{CG} + Dtp_{hop} * TP_{gran} + Dtp_{tank} * TP_{liquid}}{Dtp_{axle}}. \quad (114)$$

Substitution into equation (114) yields

$$Ftp_{tan} = \frac{83{,}720\ \text{N} * 6.032\ \text{m} + 6.37\ \text{m} * 104{,}000\ \text{N} + 3.840\ \text{m} * 33{,}370\ \text{N}}{7.62\ \text{m}} = 170{,}030\ \text{N}\ (38{,}220\ \text{lb}) \quad (115)$$

This is over the legal limit.

The tongue weight is determined by summing the vertical forces given as

$$\sum F = 0 = Ftp_{Tan} + F_{tongue} - F_{trailer} - TP_{gran} - TP_{liquid}. \quad (116)$$

Equation (116) can be rearranged to determine the tongue force as

$$F_{tongue} = F_{trailer} + TP_{gran} + TP_{liquid} - Ftp_{tan}. \quad (117)$$

Substitution into equation (117) yields

$$F_{tongue} = 83{,}720\ \text{N} + 104{,}090\ \text{N} + 33{,}360\ \text{N} - 170{,}030\ \text{N}, \quad (118)$$

Copyright 2018. the authors

Vermeer Manufacturing Company – Ex. 2045
Kubota v. Vermeer
IPR2025-00168
Page 152 of 182

and results in tongue load, F_{tongue}, of 51,140 N (11,500 lb).

The load on the prime mover truck's tandem axle set is then determined by summing moments about the front axle as

$$\sum M = 0 = F_{plow} * D_{plow} - F_{truck} * Dt_{cg} - T_{gran} * Dt_{hop} - T_{liquid} * Dt_{tank} + Ft_{tan} * Dt_{axle} - F_{tongue} * Dt_{hitch}. \quad (119)$$

Equation (119) can be used to solve for the prime mover truck's tandem axle set weight given by

$$Ft_{tan} = \frac{F_{truck} * Dt_{cg} - F_{plow} * D_{plow} + T_{gran} * Dt_{hop}}{Dt_{axle}} + \frac{T_{liquid} * Dt_{tank} + F_{tongue} * Dt_{hitch}}{Dt_{axle}}. \quad (120)$$

Substitution into equation (120) yields

$$Ft_{tan} = \frac{139{,}940\ \text{N} * 3.320\ \text{m} - 8{,}450\ \text{N} * 2.53\ \text{m} + 126{,}690\ \text{N} * 6.187\ \text{m}}{5.816\ \text{m}} + \frac{12{,}010\ \text{N} * 6.494\ \text{m} + 51{,}140\ \text{N} * 7.288\ \text{m}}{5.816\ \text{m}} \quad (121)$$

and a prime mover truck tandem axle set weight of 288,470 N (64,850 lb) which is over the manufacturer's rating. The front axle weight is determined by summing the forces as

$$\sum F = 0 = -F_{plow} - F_{truck} - T_{gran} - T_{liquid} + Ft_{tan} - F_{tongue} + F_{Front}. \quad (122)$$

Equation (122) can be rearranged to solve for the front axle force as

$$F_{Front} = F_{plow} + F_{truck} + T_{gran} + T_{liquid} - Ft_{tan} + F_{tongue}. \quad (123)$$

Substitution into equation (123) results in

$$F_{Front} = 8{,}450\ \text{N} + 139{,}940\ \text{N} + 126{,}690\ \text{N} + 12{,}010\ \text{N} - 288{,}470\ \text{N} + 51{,}140\ \text{N}, \quad (124)$$

which yields a front axle weight, F_{front}, of 49,760 N (11,190 lb).

In summary, the above analysis shows that the TowPlow2 is overweight. This was also the conclusion that DOE arrived at independently.

Copyright 2018. the authors

Vermeer Manufacturing Company – Ex. 2045
Kubota v. Vermeer
IPR2025-00168
Page 153 of 182

APPENDIX E: PREDICTIVE LOAD ANALYSIS FOR MOVING THE TOWPLOW2 TRAILER'S SANDER

The physical measurments used in this analysis are based on the TowPlow2 system. The goal is to use analysis to guide any descisions for moving the sander. In order to analyze moving the sander, it is first necessary to analytically decouple the sander from the rest of the TowPlow2 trailer. Figure 85 shows two equivalent free body diagrams of the TowPlow2 trailer. According to the vendor, the weight of the empty sander, Ftp_{hop}, is 15,570 N (3,500 lb). The center of mass of the sander, Dtp_{hop}, is located 7.498 m (24.60ft) from the hitch based on the manufacturer's drawing, which is more accurate then the measured value presented in Table 18. On the same datasheet, the original CG of the granular material, Dtp_{gran} is located at 7.77 m (25.5 ft) from the hitch. It should be noted that in this analysis, the weight of the tank is ignored. This is deemed acceptable as the weight of the tank is relatively small compared to the rest of the system.

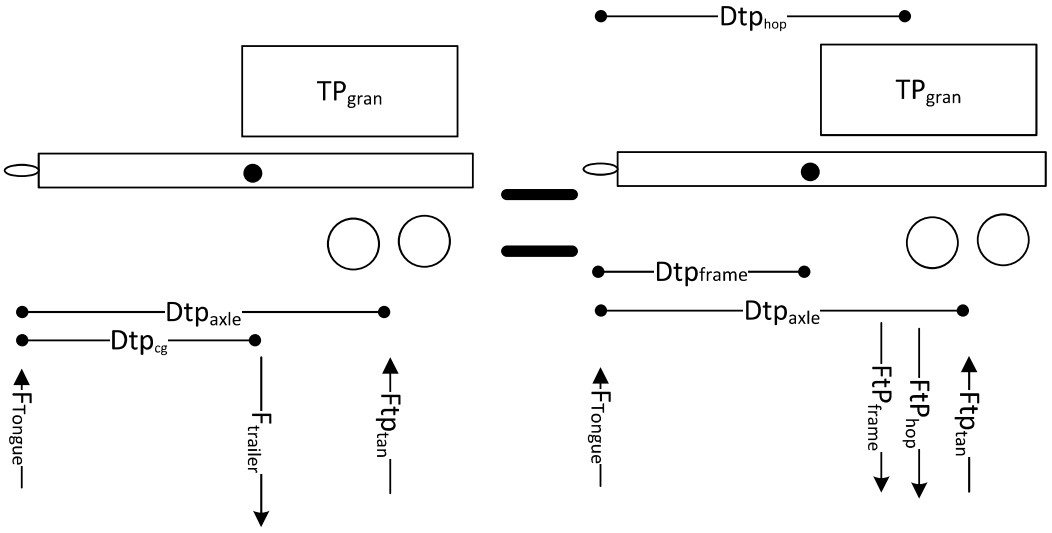


Figure 85. TowPlow2 trailer free body diagrams

There are two values which are not determined in the system above; Ftp_{frame} and Dtp_{frame}. Ftp_{frame} is the weight of the TowPlow2 trailer minus the weight of the sander and is mathematically represented by

$$Ftp_{frame} = F_{trailer} - Ftp_{hop} = 83{,}720\text{ N} - 15{,}570\text{ N} = 68{,}150\text{ N (15,320 lb)}. \quad (125)$$

Dtp_{frame} is the distance from the hitch to the TowPlow2 frame's CG. Summing moments about the hitch of the right free body diagram shown in Figure 85 yields the mathematical relationship

Copyright 2018. the authors

Vermeer Manufacturing Company – Ex. 2045
Kubota v. Vermeer
IPR2025-00168
Page 154 of 182

$$\sum M_{hitch} = 0 = Ftp_{tan} * Dtp_{axle} - Ftp_{hop} * Dtp_{hop} - Ftp_{frame} * Dtp_{frame}. \quad (126)$$

Equation (126) can be rearranged to solve for Dtp_{frame} as shown in

$$Dtp_{frame} = \frac{Ftp_{tan} * Dtp_{axle} - Ftp_{hop} * Dtp_{hop}}{Ftp_{frame}}$$

$$= \frac{66{,}280\ \text{N} * 7.62\ m - 15{,}570\ \text{N} * 7.498\ \text{m}}{68{,}150\ \text{N}} = 5.698\ \text{m}\ (18.69\ ft). \quad (127)$$

After presenting the Option 3 modification to the vendor, it was determined that there was a maximum distance that the sander could be moved. The limiting factor was interference between a structural member of the TowPlow2 trailer's frame and the spinner for the spreader system. The maximum distance it can be moved, D_{move}, is 1.153 m (45.375 in.). This would be the best option for reducing weight on the rear axles. The value D_{move} affects the sander location and the mass center of the granular material.

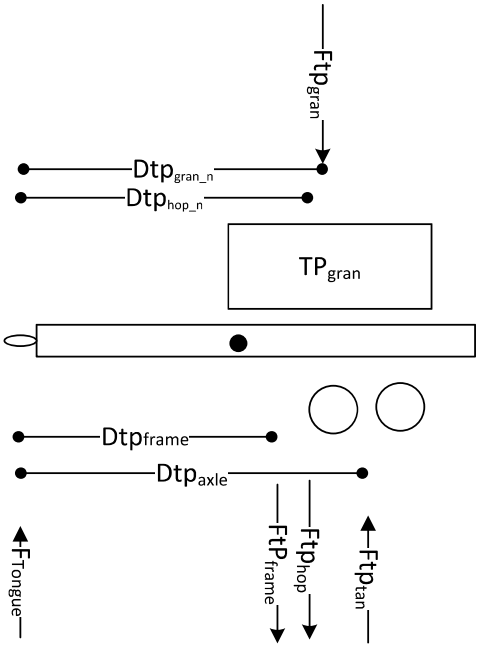


Figure 86. Free body diagram for computing new weights after moving the sander.

The goal of this analysis is to predict the weight on the TowPlow2 trailer's tandem axle set once the sander has been relocated. Therefore the first part of the analysis will focus on those axles. Step one will be to determine the values of Dtp_{gran_n} and Dtp_{hop_n}, shown in Figure 86, which are defined as

$$Dtp_{hop_n} = Dtp_{hop} - D_{move} = 7.498\ \text{m} - 1.153\ \text{m} = 6.345\ \text{m}\ (20.82 ft). \quad (128)$$

Copyright 2018. the authors

Vermeer Manufacturing Company – Ex. 2045
Kubota v. Vermeer
IPR2025-00168
Page 155 of 182

and

$$Dtp_{gran_n} = Dtp_{gran} - D_{move} = 7.772 \text{ m} - 1.153 \text{ m} = 6.619 \text{ m } (21.72ft). \quad (129)$$

The next step is to sum moments about the Towplow2 trailer's hitch which is represented mathematically by

$$\sum M_{hitch} = 0 = Ftp_{tan} * Dtp_{axle} - Ftp_{hop_n} * Dtp_{hop} - Ftp_{frame} * Dtp_{frame} - Ftp_{gran} * Dtp_{gran_n}. \quad (130)$$

Equation (130) is re-arranged in order to determine the new TowPlow2 trailer's tandem axle set weight as

$$Ftp_{tan} = \frac{Ftp_{hop_n} * Dtp_{hop_n} + Ftp_{frame} * Dtp_{frame} + Ftp_{gran} * Dtp_{gran_n}}{Dtp_{axle}}. \quad (131)$$

Plugging in numbers into equation (131) yields equation (132) below,

$$Ftp_{tan} = \frac{15{,}570 \text{ N} * 6.345 \text{ m} + 68{,}150 \text{ N} * 5.698 \text{ m} + 104{,}000 \text{ N} * 6.619 \text{ m}}{7.62 \text{ m}} = 154{,}260 \text{ N } (34{,}680 \ lbs). \quad (132)$$

This means that the TowPlow2 trailer tandem axle set is still overloaded using the Caltrans specified value of sand density.

During this process, Viking-Cives also performed a similar computation and arrived at a predicted load of 155,430 N (34,941 lb) on the TowPlow2's tandem axle set, which is close to the results of equation (132). Viking-Cives repeated the analysis using a lower sand weight of 16,290 N/m^3 (2,800 lb/yd^3) which yielded a rear tandem load of 149,400 N (33,586 lb). Changing the weight of sand to match this number in the UC-Davis calculation yields a tandem weight of 148,770 N (33,344 lb). As these two cases show, the correlation between the two independent analyses is reasonably good. The fundamental differences between these two approaches are that the Viking-Cives approach is based purely on a theoretical model, while the UC-Davis approach is based on the weight of physical TowPlow2 systems. Ultimately the UC-Davis analysis was used to determine the weight of sand that could be used with a resultant legal weight on the TowPlow trailer's rear tandem axle set. Thus a sand density of 16,850 N/m^3 (2,897 lb/yd^3) would allow for maximum legal load. The Towplow2 trailer tandem axle set load (Ftp_{tan}) using this weight of sand was 151,240 N (34,000 lb).

The TowPlow2 trailer's tongue force is next calculated. This is computed by summing the forces in the vertical direction, resulting in

$$\sum F = 0 = Ftp_{tan} + F_{tongue} - Ftp_{gran} - Ftp_{hop} - Ftp_{frame}. \quad (133)$$

The value for Ftp_{gran} is simply the density of sand (16,850 N/m^3 or 2,897 lb/yd^3) times the hopper size (5.96 m^3 or 7.8 yd^3) which yields a value of 100,430 N (22,580 lb). Rearranging Equation (133) to solve for the tongue force yields

$$F_{tongue} = Ftp_{gran} - Ftp_{tan} + Ftp_{hop} + Ftp_{frame}. = 100{,}430 \text{ N} - 151{,}240 \text{ N} + 15{,}570 \text{ N} + 68{,}150 \text{ N} = 32{,}910 \text{ N } (7{,}400 \ lbs) . \quad (134)$$

Copyright 2018. the authors

Vermeer Manufacturing Company – Ex. 2045
Kubota v. Vermeer
IPR2025-00168
Page 156 of 182

The % of weight on the tongue is of interest. Typically, trailer designers try to keep this value between 10-15%. This is simply the percentage of the trailer weight that is carried by the truck. This is mathematically expressed as

$$\%_{Tonque} = \frac{F_{tongue}}{Ftp_{gran}+Ftp_{hop}+Ftp_{frame}} * 100\%$$
$$= \frac{32{,}910\ \text{N}}{100{,}430\ \text{N}+15{,}570\ \text{N}+68{,}150\ \text{N}} * 100\% = 17.9\% \quad (135)$$

This value is slightly higher than typical values. However, this is lower than 20% value that was given in DOE Option 3.

The next part in the load calculations is to look at the resulting effect on the prime mover truck. For DOE Option 3, the recommendation was to remove the sander from the prime mover truck. This means that a new CG location needs to be determined. A similar process to the TowPlow2 trailer (equation (125)) is used to update the prime mover truck's CG value. The free body diagram for this process is shown in Figure 87. According to the vendor, the weight of the slip-in sander for the prime mover truck, $Ft_{hop,}$ is equal to 13,880 N (3,120lb).

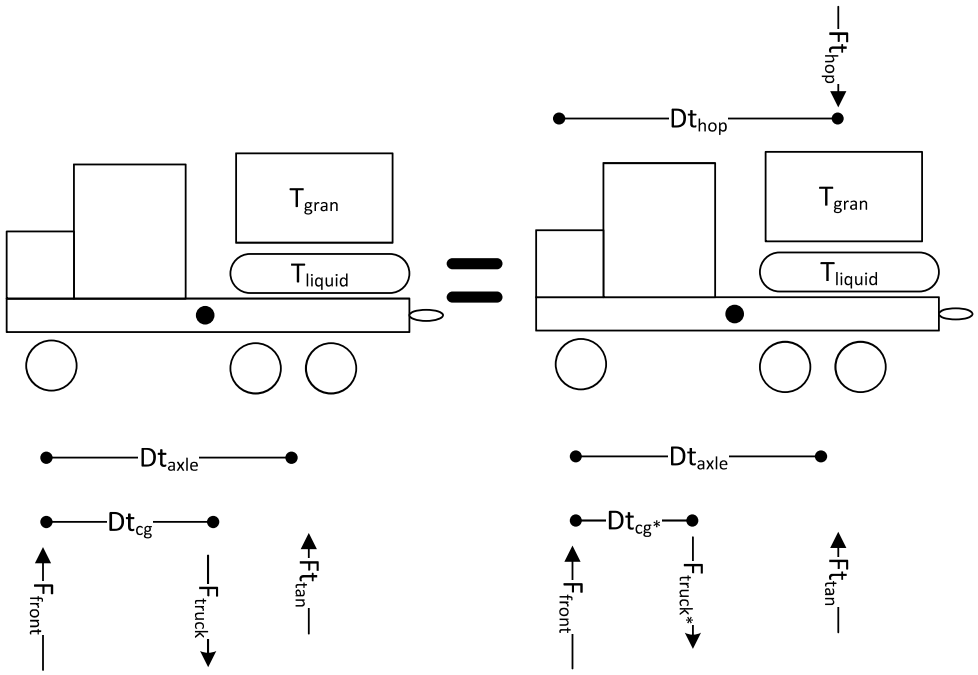


Figure 87. Free body diagram for the prime mover truck

The value used for the axle forces, Ft_{tan} and F_{front}, are simply the measured scale values for the prime mover truck when the TowPlow2 trailer is disconnected. The required relationship to determine the new prime mover truck weight, F_{truck*} is

Copyright 2018. the authors

Vermeer Manufacturing Company – Ex. 2045
Kubota v. Vermeer
IPR2025-00168
Page 157 of 182

$$F_{truck*} = F_{truck} - Ft_{hop} = 139{,}940 \text{ N} - 13{,}880 \text{ N} = 126{,}060 \text{ N } (28{,}340\ lbs). \quad (136)$$

Applying the moment equilibrium equation to the right free body diagram (FBD) from Figure 87 results in

$$\sum M = 0 = Ft_{tan} * Dt_{axle} - F_{truck*} * Dt_{cg*} - Ft_{hop} * Dt_{hop}. \quad (137)$$

Equation (137) can be used to solve for the new center of gravity location , Dt_{cg*}, given by

$$Dt_{cg*} = \frac{Ft_{tan} * Dt_{axle} - Ft_{hop} * Dt_{hop}}{F_{truck*}}$$

$$= \frac{79{,}890 \text{ N} * 5.816 \text{ m} - 13{,}880 \text{ N} * 6.187 \text{ m}}{126{,}060 \text{ N}} = 3.005 \text{ m } (9.86ft) \quad (138)$$

where the values for Dt_{axle} came from the prime mover truck's build sheet, and Dt_{hop} was measured from the physical system.

Now that the new center of gravity location, Dt_{cg*}, and the prime mover truck weight, F_{truck*}, is determined, the predicted axle forces can be determined using the maximum TowPlow2 tongue weight (from equation (134)). The free body diagram of this analysis is shown below in Figure 88.

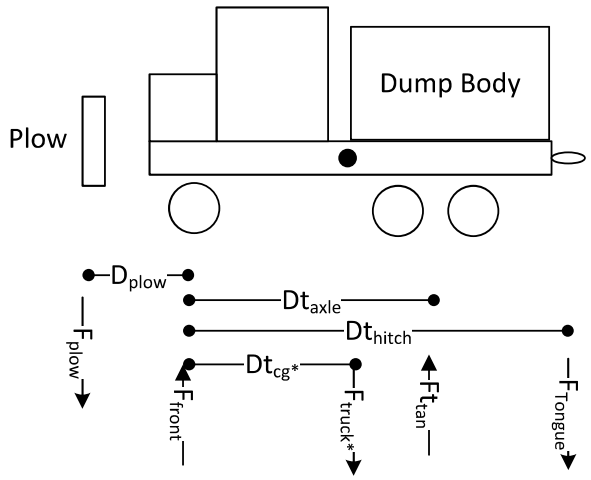


Figure 88. Prime mover truck free body diagram

As previously mentioned, the weight of the plow, F_{plow}, is equal to 8,450 N (1,900 lb). The distance from the front axle to the hitch, Dt_{hitch}, is 7.288 m (23.91 ft) according to the prime mover truck build sheet. According to the same source, the distance from the plow to the front axle, D_{plow}, is equal to 2.53 m (8.3 ft). The first thing to compute is the force on the prime mover truck tandem, Ft_{tan}, which can be done by summing moments about the front axle. This is expressed as

$$\sum M = 0 = F_{plow} * D_{plow} + Ft_{tan} * Dt_{axle} - F_{truck} * Dt_{cg*} - F_{tonque} * Dt_{hitch}. \quad (139)$$

Equation (139) can be rearranged to solve for the load on the tandem axle set, given by

Copyright 2018. the authors

Vermeer Manufacturing Company – Ex. 2045
Kubota v. Vermeer
IPR2025-00168
Page 158 of 182

$$Ft_{tan} = \frac{F_{truck*} * Dt_{cg*} - F_{plow} * D_{plow} + F_{tonque} * Dt_{hitch}}{Dt_{axle}}$$
$$= \frac{126{,}060 \text{ N} * 3.005 \text{ m} - 8{,}450 \text{ N} * 2.530 \text{ m} + 32{,}910 \text{ N} * 7.288 \text{ m}}{5.816 \text{ m}} = 102{,}700 \text{ N } (23{,}090\ lbs). \quad (140)$$

One thing to note is that 48,540 N (10,910 lb) is below the legal maximum for the tandem axle set. Now, the weight of the front axle can be determined by summing the forces. Starting with

$$\sum F = 0 = F_{front} - F_{plow} - F_{truck*} - F_{tonque} + Ft_{tan}. \quad (141)$$

which can be re-arranged to solve for the front axle force, F_{front}, as

$$F_{front} = F_{plow} + F_{truck*} + F_{tonque} - Ft_{tan}$$
$$= 8{,}450 \text{ N} + 126{,}060 \text{ N} + 32{,}910 \text{ N} - 102{,}700 \text{ N} = 64{,}720 \text{ N } (14{,}550\ lbs). \quad (142)$$

This is below the legal limit of 88,960 N (20,000 lb) by 24,240 N (5,450 lb).

The next step is to look at the GCWR. As previously stated, the maximum legal value is 80,000 lb The maximum allowable prime mover truck payload is determined by

$$Payload = GCWR_{max} - F_{front} - Ft_{tan} - Ftp_{tan}$$
$$= 355{,}860 \text{ N} - 64{,}720 \text{ N} - 102{,}700 \text{ N} - 151{,}240 \text{ N} = 37{,}200 \text{ N } (8{,}360\ lbs) \quad (143)$$

The reader should appreciate the fact that if the entire payload from equation (143) is carried by the prime mover truck's tandem axle set, the value for Ft_{tan} will still be below the maximum value of 151,240 N (34,000 lb). The bigger question is whether the maximum payload in the bed will cause the load on the front axle to be overloaded.

Based on the prime mover truck's build schematic, the center of the dump bed, Dt_{bed_cg} is located 5.176 m (16.98 ft) from the front axle. The portion of the payload carried by the front axle can be expressed by be equation (144) below.

$$Payload_{front} = Payload\left(1 - \frac{Dt_{bed_cg}}{Dt_{axle}}\right) \quad (144)$$
$$= 37{,}200 \text{ N}\left(1 - \frac{5.176 \text{ m}}{5.816 \text{ m}}\right) = 4{,}090 \text{ N } (920\ lbs).$$

This value is significantly lower than the 24,240 N (5,460 lb) stated above, and therefore will not be any issue. Generally speaking, operators may wish to move the payload forward in the bed to increase the amount of the payload carried by the front axle in order to improve handling.

The whole purpose of putting weight in the bed of the prime mover truck is to increase traction on the rear tandem. The vehicle's traction is proportional to the normal force on the tires. The reader should realize that tongue weight also adds additional weight on the prime mover truck's rear tandem axle set. Theoretically, this should help to reduce the amount of ballast that is required in the back of the prime mover truck in order to maintain sufficient traction for operation.

In summary, in an effort to implement DOE Option 3, efforts were made between UC-Davis and the vendor to move the sander as far forward as possible. Given the physical design constraints of the TowPlow2 trailer, moving the sander forward a distance of 1.153 m (45.375 in.) is the best that can be done without a complete structural redesign of the TowPlow2 trailer. This will allow for a maximum sander payload of 100,510 N (22,600 lb). This means that if the

Copyright 2018. the authors

Vermeer Manufacturing Company – Ex. 2045
Kubota v. Vermeer
IPR2025-00168
Page 159 of 182

sand density is less than 16,854 N/m^3 (2,897 lb/yd^3), the TowPlow2 trailer's hopper can be loaded to capacity. The tongue percentage of the system in the proposed case is 17.9%, which is lower than the DOE value that was presented in meetings. Also, it is estimated that in this configuration, the maximum prime mover truck payload will be 37,200 N (8,360 lb). Ultimately, all the numbers above are theoretical and the system will need to be weighed to determine final operating load capacities. These results were presented to the team, including DOE. These results seemed acceptable to the team once an acceptable contingency plan was presented. The contingency plan was to re-weigh the system and place fill lines on the hopper in the event that a sander loaded to capacity overloads the rear tandem. However, DOE requested an additional analysis of the load distribution between the TowPlow2 trailer's axles.

Analyzing the Axles on the TowPlow2 Trailer

UC-Davis was requested to analyze the individual axle loads on the rear axles of the TowPlow2 trailer once the sander is relocated. The concern is that the 80,070 N(18,000 lb) static load rating of the TowPlow2 trailer axles cannot be exceeded. Viking-Cives stated to UC-Davis that they have not seen any significant axle issues on their TowPlows with standard sanding systems. They noted that such a system will have a higher load on the axles than the DOE Option 3 system. In general, leveling the TowPlow trailer when the system is fully loaded is critical to equally sharing the load on tandem axles. Also, the axle load ratings are based on static weights and have safety factors built into the specifications, which deal with system dynamics. Two different analytical approaches were used. An energy method based on the principle of stationary potential energy was used. The other method utilized a Newton-Euler approach. Ultimately, these two methods should have identical solutions, thus verifying the analysis.

Principle of stationary potential energy approach

This analysis assumes that this is a rigid indeterminate structure supported on 3 springs as presented in Figure 89. The first step of this process is to define the energy stored in each spring which is given by

$$U_i = \frac{1}{2} f_i F_i^2, \tag{145}$$

where f_i is the flexibility associated with each spring, and F_i is the associated load [4]. The variable n represents the number of springs in the system. The variable m represents the degree of indeterminacy. This allows relationships for all the system forces $F_{i(n)}$ to be expressed in terms of the redundant forces $F_{i(m)}$. Once these relationships are determined, the total system energy can be determined by

$$`U_s = \sum_{i=1}^{n} U_i(F_1, F_2, \ldots F_m), \tag{146}$$

The principle of stationary potential energy can then be applied which is mathematically expressed as

$$\frac{\partial U_s}{\partial R_j} = 0, \tag{147}$$

Copyright 2018. the authors

Vermeer Manufacturing Company – Ex. 2045
Kubota v. Vermeer
IPR2025-00168
Page 160 of 182

where *j* ranges from 1 to the number of redundant forces, *m*. This will result in a system of *m* equations which have *m* unknowns and can be solved.

Figure 89 shows a free body diagram of the system. There are a total of three unknown forces (*n*=3), which means that there is only a single degree of indeterminacy, *m*=1.

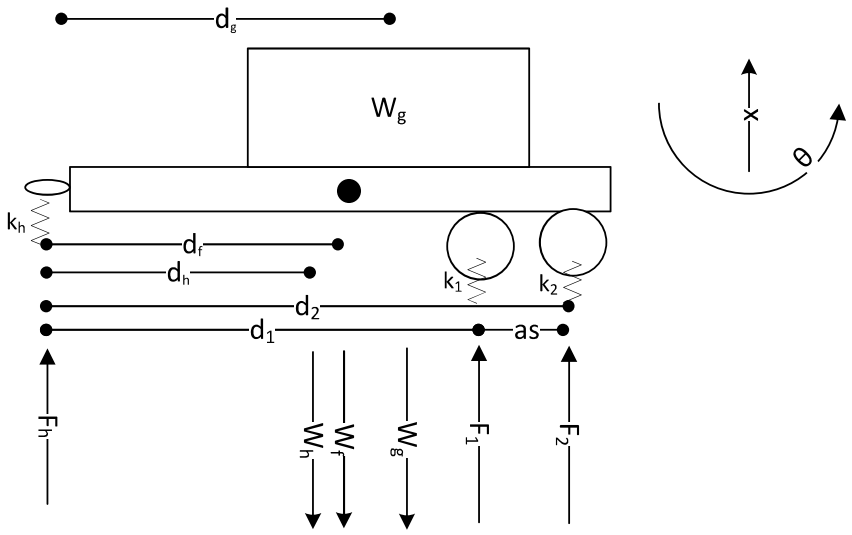


Figure 89. Free body diagram for the indeterminate analysis of the TowPlow trailer

The first step is to write the forces in terms of the indeterminate force. In this analysis, let F_h be the indeterminate force. Using the sum of the moments about the tongue yields

$$0 = -W_h d_h - W_f d_f - W_g d_g + F_1 d_1 + F_2 d_2. \quad (148)$$

In order to simplify the derivation, the relationship

$$M_{mass} = W_g d_g + W_f d_f + W_h d_h \quad (149)$$

will be defined. Equation (149) will be substituted into equation (148), yielding

$$0 = -M_{mass} + F_1 d_1 + F_2 d_2. \quad (150)$$

Next, summing the forces in the vertical direction yields

$$F_h - W_h - W_f - W_g + F_1 + F_2 = 0. \quad (151)$$

In order to simplify the derivation, the relationship

$$W_{mass} = W_h + W_f + W_g \quad (152)$$

will be defined. Equation (152) will now be substituted into equation (151) yielding

$$F_h + F_1 + F_2 - W_{mass} = 0. \quad (153)$$

Next, equation (153) can be solved for F_1, defined as

Copyright 2018. the authors

Vermeer Manufacturing Company – Ex. 2045
Kubota v. Vermeer
IPR2025-00168
Page 161 of 182

$$F_1 = W_{mass} - F_2 - F_h. \tag{154}$$

Substituting the relationship from equation (154) into equation (150) yields

$$0 = -M_{mass} + (W_{mass} - F_2 - F_h)d_1 + F_2 d_2. \tag{155}$$

The next step will be to solve equation (155) for F_2 in terms of the indeterminate force F_h. First, expanding all the terms, results in

$$0 = -M_{mass} + W_{mass}d_1 - F_2 d_1 - F_h d_1 + F_2 d_2. \tag{156}$$

Next, combine the coefficients for F_2 and move them to the left hand side of the equation, which results in

$$(d_2 - d_1)F_2 = M_{mass} - W_{mass}d_1 + F_h d_1. \tag{157}$$

Next, divide both sides of the equation by $(d_2\text{-}d_1)$. This yields the solution for F_2 in terms of the force, F_h as

$$F_2 = \frac{M_{mass} - W_{mass}d_1 + F_h d_1}{(d_2 - d_1)}. \tag{158}$$

Plugging in the relationship for F_2 defined in equation (158) into equation (154) gives F_1 as a function of F_h expressed as

$$F_1 = W_{mass} - \frac{M_{mass} - W_{mass}d_1 + F_h d_1}{(d_2 - d_1)} - F_h. \tag{159}$$

Applying equation (145) to all of the storage elements in the system yields equation (160) which expresses the potential energy of the system as

$$U_s = \frac{1}{2}f_h F_h^2 + \frac{1}{2}f_1 F_1^2 + \frac{1}{2}f_2 F_2^2. \tag{160}$$

It is next assumed that each axle will have the same flexibility constant since each axle is using the same tires. This is defined mathematically as

$$f_1 = f_2 = f_a, \tag{161}$$

where f_a is the flexibility of the axle. This simplifies equation (160) to

$$U_s = \frac{1}{2}f_h F_h^2 + \frac{1}{2}f_a F_1^2 + \frac{1}{2}f_a F_2^2. \tag{162}$$

Next, the principle of stationary potential energy given in equation (147) is rewritten in terms of the single redundant force resulting in

$$\frac{\partial U_s}{\partial F_h} = 0. \tag{163}$$

Applying equation (163) to equation (160) yields

$$\frac{\partial U_s}{\partial F_h} = f_h F_h \frac{\partial F_{Tc}}{\partial F_h} + f_a F_1 \frac{\partial F_1}{\partial F_h} + f_a F_2 \frac{\partial F_2}{\partial F_h} = 0. \tag{164}$$

The relationship $\partial F_h / \partial F_h = 1$, which simplifies equation (164) to

$$f_h F_h + f_a F_1 \frac{\partial F_1}{\partial F_h} + f_a F_2 \frac{\partial F_2}{\partial F_h} = 0. \tag{165}$$

To simplify the derivation, the equation (165) will be divided by f_a, resulting in

$$\frac{f_h}{f_a} F_h + F_1 \frac{\partial F_1}{\partial F_h} + F_2 \frac{\partial F_2}{\partial F_h} = 0. \tag{166}$$

Copyright 2018. the authors

Vermeer Manufacturing Company – Ex. 2045
Kubota v. Vermeer
IPR2025-00168
Page 162 of 182

Next, in order to simplify the notation, a brief explanation of the flexibility for each spring will be made. The reference problem given above defines the potential energy in each spring as a function of the force and the flexibility constant. The flexibility is the inverse of the stiffness which is mathematical represented as

$$f_l = \frac{1}{k_l}. \tag{167}$$

The stiffness ratio S will be defined as

$$S = \frac{f_h}{f_a} = \frac{k_a}{k_h}. \tag{168}$$

This represents the ratio of the of the hitch flexibility (f_h) to the axle flexibility (f_a). This can also be written in terms of stiffness (k_a and k_h).

Now, substituting S into equation (166), yields

$$0 = SF_h + F_1 \frac{\partial F_1}{\partial F_h} + F_2 \frac{\partial F_2}{\partial F_h}. \tag{169}$$

Next, the partial derivative F_1, defined in equation (159), with respect to F_h, results in

$$\frac{\partial F_1}{\partial F_h} = -\frac{d_1}{d_2 - d_1} - 1 \tag{170}$$

Taking the same partial derivation for F_2 as given in equation (158), results in

$$\frac{\partial F_2}{\partial F_h} = \frac{d_1}{d_2 - d_1}. \tag{171}$$

Next, the relationships given in equations (158), (159), (170), and (171) can be substituted into equation (169) resulting in

$$\begin{aligned} 0 = SF_h + \left(W_{mass} - \frac{M_{mass} - W_{mass}d_1 + F_h d_1}{(d_2 - d_1)} - F_h\right)\left(-\frac{d_1}{d_2 - d_1} - 1\right) \\ + \left(\frac{M_{mass} - W_{mass}d_1 + F_h d_1}{(d_2 - d_1)}\right)\left(\frac{d_1}{d_2 - d_1}\right). \end{aligned} \tag{172}$$

The next step is to solve equation (172) for the indeterminate force F_h. The first step is to expand out the second term resulting in

$$\begin{aligned} 0 = SF_h + W_{mass}\left(-\frac{d_1}{d_2 - d_1} - 1\right) - \left(\frac{M_{mass} - W_{mass}d_1 + F_h d_1}{(d_2 - d_1)}\right)\left(-\frac{d_1}{d_2 - d_1} - 1\right) \\ -F_h\left(-\frac{d_1}{d_2 - d_1} - 1\right) + \left(\frac{M_{mass} - W_{mass}d_1 + F_h d_1}{(d_2 - d_1)}\right)\left(\frac{d_1}{d_2 - d_1}\right). \end{aligned} \tag{173}$$

The terms in equation (173) are rearranged in order to work on isolating the redundant force F_h shown below as

$$\begin{aligned} 0 = SF_h - F_h\left(-\frac{d_1}{d_2 - d_1} - 1\right) + W_{mass}\left(-\frac{d_1}{d_2 - d_1} - 1\right) \\ + \left(\frac{M_{mass} - W_{mass}d_1 + F_h d_1}{(d_2 - d_1)}\right)\left(\frac{d_1}{d_2 - d_1} + 1\right) + \left(\frac{M_{mass} - W_{mass}d_1 + F_h d_1}{(d_2 - d_1)}\right)\left(\frac{d_1}{d_2 - d_1}\right) \end{aligned} \tag{174}$$

The coefficients for F_h can be combined. Additionally, the coefficients for the fourth and fifth terms in equation (174) are the same and can be combined, resulting in

$$0 = F_h\left(\frac{d_1}{d_2 - d_1} + 1 + S\right) - W_{mass}\left(\frac{d_1}{d_2 - d_1} + 1\right) + \left(\frac{M_{mass} - W_{mass}d_1 + F_h d_1}{(d_2 - d_1)}\right)\left(\frac{2d_1}{d_2 - d_1} + 1\right). \tag{175}$$

Copyright 2018. the authors

Vermeer Manufacturing Company – Ex. 2045
Kubota v. Vermeer
IPR2025-00168
Page 163 of 182

The third term in equation (175) can be expanded, yielding

$$0 = F_h\left(\frac{d_1}{d_2-d_1}+1+S\right) - W_{mass}\left(\frac{d_1}{d_2-d_1}+1\right) + \frac{M_{mass}-W_{mass}d_1+F_hd_1}{(d_2-d_1)} + \left(\frac{M_{mass}-W_{mass}d_1+F_hd_1}{(d_2-d_1)}\right)\left(\frac{2d_1}{d_2-d_1}\right). \quad (176)$$

Next, the third term in equation (176) is expanded, yielding

$$0 = F_h\left(\frac{d_1}{d_2-d_1}+1+S\right) - W_{mass}\left(\frac{d_1}{d_2-d_1}+1\right) + \frac{M_{mass}-W_{mass}d_1}{(d_2-d_1)} + \frac{F_hd_1}{(d_2-d_1)} + (M_{mass}-W_{mass}d_1+F_hd_1)\left(\frac{2d_1}{(d_2-d_1)^2}\right). \quad (177)$$

The terms in equation (177) are reordered slightly to yield

$$0 = F_h\left(\frac{d_1}{d_2-d_1}+1+S\right) + \frac{F_hd_1}{(d_2-d_1)} - W_{mass}\left(\frac{d_1}{d_2-d_1}+1\right) + \frac{M_{mass}-W_{mass}d_1}{(d_2-d_1)} + (M_{mass}-W_{mass}d_1+F_hd_1)\left(\frac{2d_1}{(d_2-d_1)^2}\right). \quad (178)$$

The next step is to combine terms in equation (178) in order to fully isolate F_h given below as

$$0 = F_h\left(\frac{2d_1}{d_2-d_1}+1+S+\frac{2d_1^2}{(d_2-d_1)^2}\right) - W_{mass}\left(\frac{d_1}{d_2-d_1}+1\right) + \frac{M_{mass}-W_{mass}d_1}{(d_2-d_1)} + (M_{mass}-W_{mass}d_1)\left(\frac{2d_1}{(d_2-d_1)^2}\right). \quad (179)$$

For simplicity of numerically implementing the equation and for further analysis, equation (179) will be rewritten in the form:

$$0 = A_EF_h - B_EW_{mass} + C_EM_{mass}. \quad (180)$$

The subscript "*E*" refers to the fact that this is associated with the energy approach. The coefficient A_E can defined from equation (179), yielding

$$A_E = \frac{2d_1}{d_2-d_1}+1+S+\frac{2d_1^2}{(d_2-d_1)^2}. \quad (181)$$

Substituting (181) into equation ((179) yields

$$0 = A_EF_h - W_{mass}\left(\frac{d_1}{d_2-d_1}+1\right) + \frac{M_{mass}-W_{mass}d_1}{(d_2-d_1)} + (M_{mass}-W_{mass}d_1)\left(\frac{2d_1}{(d_2-d_1)^2}\right). \quad (182)$$

The terms in equation (182) are expanded in order to help solve for the coefficients B_E and C_E, given below as

$$0 = A_EF_h - W_{mass}\left(\frac{d_1}{d_2-d_1}+1\right) + \frac{M_{mass}}{(d_2-d_1)} - \frac{W_{mass}d_1}{(d_2-d_1)} + \left(\frac{2d_1}{(d_2-d_1)^2}\right)M_{mass} - W_{mass}d_1\left(\frac{2d_1}{(d_2-d_1)^2}\right) \quad (183)$$

Next, the coefficients for W_{mass} and M_{mass} will be combined as shown in equation (184) below:

$$0 = A_EF_h - W_{mass}\left(\frac{d_1}{d_2-d_1}+1+\frac{d_1}{d_2-d_1}+\frac{2d_1^2}{(d_2-d_1)^2}\right) + M_{mass}\left(\frac{1}{(d_2-d_1)}+\frac{2d_1}{(d_2-d_1)^2}\right). \quad (184)$$

Copyright 2018. the authors

Vermeer Manufacturing Company – Ex. 2045
Kubota v. Vermeer
IPR2025-00168
Page 164 of 182

The relationship for B_E can be defined from equation (184) as shown below:

$$B_E = \frac{d_1}{d_2-d_1} + 1 + \frac{d_1}{d_2-d_1} + \frac{2d_1^2}{(d_2-d_1)^2}. \quad (185)$$

Terms in equation (185) are regrouped yielding

$$B_E = \frac{d_1}{d_2-d_1} * \frac{d_2-d_1}{d_2-d_1} + 1 * \left(\frac{d_2-d_1}{d_2-d_1}\right)^2 + \frac{d_1}{d_2-d_1} * \frac{d_2-d_1}{d_2-d_1} + \frac{2d_1^2}{(d_2-d_1)^2}. \quad (186)$$

Equation (186) now simplifies to

$$B_E = \frac{d_1(d_2-d_1)+(d_2-d_1)^2+d_1(d_2-d_1)+2d_1^2}{(d_2-d_1)^2}. \quad (187)$$

Next, the numerator can be expanded to

$$B_E = \frac{d_1d_2-d_1^2+d_2^2-2d_2d_1+d_1^2+d_1d_2-d_1^2+2d_1^2}{(d_2-d_1)^2}. \quad (188)$$

Finally, various terms in equation (188) can be canceled, B_e becomes

$$B_E = \frac{d_2^2+d_1^2}{(d_2-d_1)^2}. \quad (189)$$

The term C_E can also be simplified. Starting from equation (184), C_E can be defined as

$$C_E = \frac{1}{(d_2-d_1)} + \frac{2d_1}{(d_2-d_1)^2}. \quad (190)$$

Using similar steps as above, C_E can be represented as

$$C_E = \frac{d_2-d_1+2d_1}{(d_2-d_1)^2} = \frac{d_2+d_1}{(d_2-d_1)^2}. \quad (191)$$

Now that all the coefficients A_E, B_E, and C_E are defined, a solution for the indeterminate force, F_h can be expressed as

$$F_h = \frac{B_EW_{mass}-C_EM_{mass}}{A_E}. \quad (192)$$

Once equation (192) is defined, F_1 and F_2 can then be determined using equations (159) and (158). The only unknown parameters for this are the flexibility constants f_h and f_a, or their inverses k_h and k_a. However, before looking at the numerical implementation of the above derivation, an alternative analytical approach will be made. The major point to performing an alternate approach for the analysis is that the two analytical models should result in the same closed form solution.

Newton-Euler approach

The Newton-Euler approach provides an alternative means of performing the same analysis. In this model, the forces in the springs can be written in terms of a vertical displacement and rotation of the rigid beam. Since all the forces can be determined using these two variables, there are only 2 unknown values and therefore simple statics can be applied. The free body diagram used for this analysis is shown in Figure 89. The value for x is defined as the vertical displacement of the hitch. $\emptyset$ is defined as a rotation about the hitch.

All the forces can be defined in terms of x and $\emptyset$ as shown in equations (193), (194), and (195). The value for the hitch force is defined as

Copyright 2018. the authors

Vermeer Manufacturing Company – Ex. 2045
Kubota v. Vermeer
IPR2025-00168
Page 165 of 182

$$F_h = -k_h x. \tag{193}$$

F_1 is defined as

$$F_1 = -k_1(x + d_1 \sin \emptyset). \tag{194}$$

F_2 is defined as

$$F_2 = -k_2(x + d_2 \sin \emptyset). \tag{195}$$

Summing the forces in the vertical direction yields

$$F_h - W_h - W_f - W_g + F_1 + F_2 = 0. \tag{196}$$

Equation (196) can be simplified by substituting the relationship defined by equation (152), yielding

$$F_h + F_1 + F_2 - W_{mass} = 0. \tag{197}$$

Summing the moments about the hitch results in

$$0 = -W_h d_h - W_f d_f \cos \emptyset - W_g d_g \cos \emptyset + F_1 d_1 \cos \emptyset + F_2 d_2 \cos \emptyset. \tag{198}$$

Next, the values for F_h, F_1 and F_2 from equations (193), (194), and (195) are substituted into equations (197) and (198), yielding

$$-k_h x - k_1(x + d_1 \sin \emptyset) - k_2(x + d_2 \sin \emptyset) - W_{mass} = 0 \tag{199}$$

and

$$0 = -W_h d_h \cos \emptyset - W_f d_f \cos \emptyset - W_g d_g \cos \emptyset - k_1(x + d_1 \sin \emptyset) d_1 \cos \emptyset$$
$$-k_2(x + d_2 \sin \emptyset) d_2 \cos \emptyset. \tag{200}$$

Since the TowPlow trailer will be sitting relatively level in the loaded condition, the small angle approximations can be used. Mathematically, these are expressed as

$$\sin \emptyset = \emptyset \tag{201}$$

and

$$\cos \emptyset = 1. \tag{202}$$

Substituting the small angle approximations shown in equations (201) and (202) into equations (199) and (200) yields

$$-k_h x - k_1(x + d_1 \emptyset) - k_2(x + d_2 \emptyset) - W_{mass} = 0 \tag{203}$$

and

$$0 = -W_h d_h - W_f d_f - W_g d_g - k_1(x + d_1 \emptyset) d_1 - k_2(x + d_2 \emptyset) d_2. \tag{204}$$

After applying the small angle approximation, the relationship for M_{mass}, equation (149), can be substituted into equation (204), yielding

$$0 = -k_1(x + d_1 \emptyset) d_1 - k_2(x + d_2 \emptyset) d_2 - M_{mass} \tag{205}$$

Similar to the analysis above, the axles will have a common stiffness. This is equivalent to the relationship given in equation (161) as shown below:

$$k_1 = k_2 = k_a. \tag{206}$$

Substituting in equation (206) into equations (203) and (205) yields

Copyright 2018. the authors

Vermeer Manufacturing Company – Ex. 2045
Kubota v. Vermeer
IPR2025-00168
Page 166 of 182

$$0 = -k_a(x + d_1\emptyset)d_1 - k_a(x + d_2\emptyset)d_2 - M_{mass} \quad (207)$$

and

$$-k_h x - k_a(x + d_1\emptyset) - k_a(x + d_2\emptyset) - W_{mass} = 0. \quad (208)$$

Equation (207) is expanded in order to facilitate combining like terms as shown below:

$$0 = -k_a(d_1 + d_2)x - k_a(d_1^2 + d_2^2)\emptyset - M_{mass}. \quad (209)$$

Equation (209) can now be solved for ∅ in terms of x as shown below:

$$\emptyset = \frac{-k_a(d_1+d_2)x - M_{mass}}{k_a(d_1^2+d_2^2)}. \quad (210)$$

Equation (208) will be rearranged, showing a linear relationship of ∅ and *x*, shown below as

$$-(k_h + 2k_a)x - k_a(d_1 + d_2)\emptyset - W_{mass} = 0. \quad (211)$$

Now equation (211) can be expressed in terms of *x* only by substituting equation (210), resulting in

$$-(k_h + 2k_a)x - k_a(d_1 + d_2)\frac{-k_a(d_1+d_2)x - M_{mass}}{k_a(d_1^2+d_2^2)} - W_{mass} = 0. \quad (212)$$

Equation (212) can be simplified in order to write the equation as a linear expression of *x* given as

$$-\left(k_h + 2k_a - k_a\frac{(d_1+d_2)^2}{(d_1^2+d_2^2)}\right)x + \frac{(d_1+d_2)}{(d_1^2+d_2^2)}M_{mass} - W_{mass} = 0. \quad (213)$$

Equation (213) can be rewritten to come up with a closed form solution for *x* as shown in

$$x = \frac{\frac{(d_1+d_2)}{(d_1^2+d_2^2)}M_{mass} - W_{mass}}{\left(k_h + 2k_a - k_a\frac{(d_1+d_2)^2}{(d_1^2+d_2^2)}\right)}. \quad (214)$$

Once values for the stiffness or flexibility are determined, a solution for *x* can then be determined from equation (214). Once *x* is known, ∅ can be determined (equation (210)) as well as the forces from equations (193), (194), and (195).

Comparing the two approaches

The two approaches above gave analytical solutions for the indeterminate forces. However in order to validate the analytical solution, these two solutions should be identical. The section below compares the two results.

First, equation (193) is solved for *x* which can then be substituted in equation **Error! Reference source not found.**(214) This process will lead to an expression for the hitch force, F_h, as

$$F_h = -k_h\frac{\frac{(d_1+d_2)}{(d_1^2+d_2^2)}M_{mass} - W_{mass}}{\left(k_h + 2k_a - k_a\frac{(d_1+d_2)^2}{(d_1^2+d_2^2)}\right)}. \quad (215)$$

Equation (215) is now expanded to write the expression as a linear expression of M_{mass} and W_{mass} as

Copyright 2018. the authors

Vermeer Manufacturing Company – Ex. 2045
Kubota v. Vermeer
IPR2025-00168
Page 167 of 182

$$F_h = \frac{-k_h\frac{(d_1+d_2)}{(d_1^2+d_2^2)}}{\left(k_h+2k_a-k_a\frac{(d_1+d_2)^2}{(d_1^2+d_2^2)}\right)}M_{mass} + \frac{k_h}{\left(k_h+2k_a-k_a\frac{(d_1+d_2)^2}{(d_1^2+d_2^2)}\right)}W_{mass} \tag{216}$$

In order to simplify the process, equation (216) is rewritten as

$$F_h = D_{NE}M_{mass} + E_{NE}W_{mass}, \tag{217}$$

where

$$D_{NE} = \frac{-k_h\frac{(d_1+d_2)}{(d_1^2+d_2^2)}}{\left(k_h+2k_a-k_a\frac{(d_1+d_2)^2}{(d_1^2+d_2^2)}\right)} \tag{218}$$

and

$$E_{NE} = \frac{k_h}{\left(k_h+2k_a-k_a\frac{(d_1+d_2)^2}{(d_1^2+d_2^2)}\right)} \tag{219}$$

The subscript "*NE*" refers to the Newton-Euler approach. Comparing equation (194) to equation (180), relationships

$$D_{NE} = -\frac{C_E}{A_E} \tag{220}$$

and

$$E_{NE} = \frac{B_E}{A_E} \tag{221}$$

must be true if the analytical expressions are correct. Ultimately, this means that all terms must cancel out.

Starting with equation (220), and replacing D_{NE}, C_E, and A_E with the analytical expressions gives

$$\frac{-k_h\frac{(d_1+d_2)}{(d_1^2+d_2^2)}}{\left(k_h+2k_a-k_a\frac{(d_1+d_2)^2}{(d_1^2+d_2^2)}\right)} = -\frac{\frac{1}{(d_2-d_1)}+\frac{2d_1}{(d_2-d_1)^2}}{\frac{2d_1}{d_2-d_1}+1+S+\frac{2d_1^2}{(d_2-d_1)^2}}. \tag{222}$$

Equation (168) can be used to remove *S* from the equation as

$$\frac{-k_h\frac{(d_1+d_2)}{(d_1^2+d_2^2)}}{\left(k_h+2k_a-k_a\frac{(d_1+d_2)^2}{(d_1^2+d_2^2)}\right)} = -\frac{\frac{1}{(d_2-d_1)}+\frac{2d_1}{(d_2-d_1)^2}}{\frac{2d_1}{d_2-d_1}+1+\frac{k_a}{k_h}+\frac{2d_1^2}{(d_2-d_1)^2}}. \tag{223}$$

Cross-multiplying equation (223) yields.

$$k_h\frac{(d_1+d_2)}{(d_1^2+d_2^2)}\left(\frac{2d_1}{d_2-d_1}+1+\frac{k_a}{k_h}+\frac{2d_1^2}{(d_2-d_1)^2}\right)$$
$$= \left(\frac{1}{(d_2-d_1)}+\frac{2d_1}{(d_2-d_1)^2}\right)\left(k_h+2k_a-k_a\frac{(d_1+d_2)^2}{(d_1^2+d_2^2)}\right). \tag{224}$$

Next, the value k_h will be distributed on the left hand side yielding

$$\frac{(d_1+d_2)}{(d_1^2+d_2^2)}\left(\frac{2d_1k_h}{d_2-d_1}+k_h+\frac{k_ak_h}{k_h}+\frac{2d_1^2k_h}{(d_2-d_1)^2}\right)$$

Copyright 2018. the authors

Vermeer Manufacturing Company – Ex. 2045
Kubota v. Vermeer
IPR2025-00168
Page 168 of 182

$$= \left(\frac{1}{(d_2-d_1)} + \frac{2d_1}{(d_2-d_1)^2}\right)\left(k_h + 2k_a - k_a\frac{(d_1+d_2)^2}{(d_1^2+d_2^2)}\right). \quad (225)$$

Equation (225) is now multiplied by the term (d_2-d_1) resulting in

$$\frac{(d_1+d_2)}{(d_1^2+d_2^2)}\left(2d_1k_h + k_h(d_2-d_1) + k_a(d_2-d_1) + \frac{2d_1^2k_h}{(d_2-d_1)}\right)$$
$$= \left(1 + \frac{2d_1}{(d_2-d_1)}\right)\left(k_h + 2k_a - k_a\frac{(d_1+d_2)^2}{(d_1^2+d_2^2)}\right). \quad (226)$$

Multiplying both sides by $d_1^2 + d_2^2$, yields

$$(d_1+d_2)\left(2d_1k_h + k_h(d_2-d_1) + k_a(d_2-d_1) + \frac{2d_1^2k_h}{(d_2-d_1)}\right)$$
$$= \left(1 + \frac{2d_1}{(d_2-d_1)}\right)\left(k_h + 2k_a - k_a\frac{(d_1+d_2)^2}{(d_1^2+d_2^2)}\right)(d_1^2+d_2^2). \quad (227)$$

Distributing $d_1^2 + d_2^2$, on the right hand side yields

$$(d_1+d_2)\left(2d_1k_h + k_h(d_2-d_1) + k_a(d_2-d_1) + \frac{2d_1^2k_h}{(d_2-d_1)}\right)$$
$$= \left(1 + \frac{2d_1}{(d_2-d_1)}\right)\left((k_h + 2k_a)(d_1^2+d_2^2) - k_a(d_1+d_2)^2\right). \quad (228)$$

Re-arranging and simplifying equation (228) results in

$$(d_1+d_2)\left(2d_1k_h + k_h(d_2-d_1) + k_a(d_2-d_1) + \frac{2d_1^2k_h}{(d_2-d_1)}\right)$$
$$= \left(\frac{(d_2-d_1)}{(d_2-d_1)} + \frac{2d_1}{(d_2-d_1)}\right)\left((k_h + 2k_a)(d_1^2+d_2^2) - k_a(d_1+d_2)^2\right). \quad (229)$$

Equation (229) can be further reduced to

$$(d_1+d_2)\left(2d_1k_h + k_h(d_2-d_1) + k_a(d_2-d_1) + \frac{2d_1^2k_h}{(d_2-d_1)}\right)$$
$$= \left(\frac{(d_2+d_1)}{(d_2-d_1)}\right)\left((k_h + 2k_a)(d_1^2+d_2^2) - k_a(d_1+d_2)^2\right). \quad (230)$$

Both sides are now divided by d_1+d_2, yielding

$$\left(2d_1k_h + k_h(d_2-d_1) + k_a(d_2-d_1) + \frac{2d_1^2k_h}{(d_2-d_1)}\right).$$
$$= \left(\frac{1}{(d_2-d_1)}\right)\left((k_h + 2k_a)(d_1^2+d_2^2) - k_a(d_1+d_2)^2\right) \quad (231)$$

Multiplying both sides by *(d_2-d_1)* yields

$$(d_2-d_1)\left(2d_1k_h + k_h(d_2-d_1) + k_a(d_2-d_1) + \frac{2d_1^2k_h}{(d_2-d_1)}\right)$$
$$= \left((k_h + 2k_a)(d_1^2+d_2^2) - k_a(d_1+d_2)^2\right). \quad (232)$$

The terms in the parenthesis on the left hand side are expanded and combined which yields

$$(d_2-d_1)\left(k_hd_1 + k_hd_2 + k_ad_2 - k_ad_1 + \frac{2d_1^2k_h}{(d_2-d_1)}\right)$$
$$= \left((k_h + 2k_a)(d_1^2+d_2^2) - k_a(d_1+d_2)^2\right). \quad (233)$$

The right hand side is fully expanded, yielding

Copyright 2018. the authors

Vermeer Manufacturing Company – Ex. 2045
Kubota v. Vermeer
IPR2025-00168
Page 169 of 182

$$(d_2 - d_1)\left(k_h d_1 + k_h d_2 + k_a d_2 - k_a d_1 + \frac{2d_1^2 k_h}{(d_2 - d_1)}\right)$$
$$= k_h d_1^2 + 2k_a d_1^2 + k_h d_2^2 + 2k_a d_2^2 - k_a d_1^2 - 2k_a d_1 d_2 - k_a d_2^2. \quad (234)$$

Combining right hand side terms gives

$$(d_2 - d_1)\left(k_h d_1 + k_h d_2 + k_a d_2 - k_a d_1 + \frac{2d_1^2 k_h}{(d_2 - d_1)}\right)$$
$$= k_h d_1^2 + k_a d_1^2 + k_h d_2^2 + k_a d_2^2 - 2k_a d_1 d_2. \quad (235)$$

Simplifying the left hand sides gives

$$(d_2 - d_1)(k_h d_1 + k_h d_2 + k_a d_2 - k_a d_1) + 2d_1^2 k_h$$
$$= k_h d_1^2 + k_a d_1^2 + k_h d_2^2 + k_a d_2^2 - 2k_a d_1 d_2. \quad (236)$$

Rearranging terms yields

$$(d_2 - d_1)(k_h d_1 + k_h d_2 + k_a d_2 - k_a d_1)$$
$$= k_a d_1^2 + k_h d_2^2 + k_a d_2^2 - 2k_a d_1 d_2 - d_1^2 k_h. \quad (237)$$

Expanding the left hand side yields

$$k_h d_1 d_2 + k_h d_2^2 + k_a d_2^2 - k_a d_1 d_2 - k_h d_1^2 - k_h d_1 d_2 - k_a d_1 d_2 + k_a d_1^2$$
$$= k_a d_1^2 + k_h d_2^2 + k_a d_2^2 - 2k_a d_1 d_2 - 2d_1^2 k_h. \quad (238)$$

Combining terms yields

$$k_h d_2^2 + k_a d_2^2 - 2k_a d_1 d_2 - k_h d_1^2 + k_a d_1^2$$
$$= k_a d_1^2 + k_h d_2^2 + k_a d_2^2 - 2k_a d_1 d_2 - d_1^2 k_h. \quad (239)$$

As can be seen in equation (239), all terms cancel out meaning that the relationship described in equation (220) is true. Next the relationship described in equation (221) is considered. First, the terms in the equation are replaced with their detailed representations yielding

$$\frac{k_h}{\left(k_h + 2k_a - k_a \frac{(d_1 + d_2)^2}{(d_1^2 + d_2^2)}\right)} = \frac{\frac{d_2^2 + d_1^2}{(d_2 - d_1)^2}}{\frac{2d_1}{d_2 - d_1} + 1 + S + \frac{2d_1^2}{(d_2 - d_1)^2}} \quad (240)$$

Now substituting for *S* from equation (168) yields

$$\frac{k_h}{\left(k_h + 2k_a - k_a \frac{(d_1 + d_2)^2}{(d_1^2 + d_2^2)}\right)} = \frac{\frac{d_2^2 + d_1^2}{(d_2 - d_1)^2}}{\frac{2d_1}{d_2 - d_1} + 1 + \frac{k_a}{k_h} + \frac{2d_1^2}{(d_2 - d_1)^2}}. \quad (241)$$

The right hand side is rewritten as

$$\frac{k_h}{\left(k_h + 2k_a - k_a \frac{(d_1 + d_2)^2}{(d_1^2 + d_2^2)}\right)} = \frac{d_2^2 + d_1^2}{(d_2 - d_1)^2\left(\frac{2d_1}{d_2 - d_1} + 1 + \frac{k_a}{k_h} + \frac{2d_1^2}{(d_2 - d_1)^2}\right)}. \quad (242)$$

This simplifies to

$$\frac{k_h}{\left(k_h + 2k_a - k_a \frac{(d_1 + d_2)^2}{(d_1^2 + d_2^2)}\right)} = \frac{d_2^2 + d_1^2}{\left(2d_1(d_2 - d_1) + \left(1 + \frac{k_a}{k_h}\right)(d_2 - d_1)^2 + 2d_1^2\right)}. \quad (243)$$

The right hand side denominator is simplified to

Copyright 2018. the authors

Vermeer Manufacturing Company – Ex. 2045
Kubota v. Vermeer
IPR2025-00168
Page 170 of 182

$$\frac{k_h}{\left(k_h+2k_a-k_a\frac{(d_1+d_2)^2}{(d_1^2+d_2^2)}\right)}=\frac{d_2^2+d_1^2}{\left(2d_1d_2+\left(1+\frac{k_a}{k_h}\right)(d_2-d_1)^2\right)}. \quad (244)$$

The fractions are cross-multiplied, yielding

$$k_h\left(2d_1d_2+\left(1+\frac{k_a}{k_h}\right)(d_2-d_1)^2\right) = (d_2^2+d_1^2)\left(k_h+2k_a-k_a\frac{(d_1+d_2)^2}{(d_1^2+d_2^2)}\right). \quad (245)$$

The left side expands to

$$2k_hd_1d_2+(k_h+k_a)(d_2^2-2d_2d_1+d_1^2)=(d_2^2+d_1^2)\left(k_h+2k_a-k_a\frac{(d_1+d_2)^2}{(d_1^2+d_2^2)}\right). \quad (246)$$

Rearranging the left hand side yields

$$2k_hd_1d_2+k_h(d_2^2+d_1^2)-2\,k_h2d_2d_1+k_a(d_2^2-2d_2d_1+d_1^2) = (d_2^2+d_1^2)\left(k_h+2k_a-k_a\frac{(d_1+d_2)^2}{(d_1^2+d_2^2)}\right). \quad (247)$$

The left hand side simplifies to

$$k_h(d_2^2+d_1^2)+k_a(d_2^2-2d_2d_1+d_1^2)=(d_2^2+d_1^2)\left(k_h+2k_a-k_a\frac{(d_1+d_2)^2}{(d_1^2+d_2^2)}\right). \quad (248)$$

Subtracting the first term on the left hand side from both sides of the equation yields

$$k_a(d_2^2-2d_2d_1+d_1^2)=(d_2^2+d_1^2)\left(2k_a-k_a\frac{(d_1+d_2)^2}{(d_1^2+d_2^2)}\right). \quad (249)$$

The right hand side expands to

$$k_a(d_2^2-2d_2d_1+d_1^2)=\left(2k_a(d_2^2+d_1^2)-k_a\frac{(d_1+d_2)^2(d_2^2+d_1^2)}{(d_1^2+d_2^2)}\right). \quad (250)$$

This reduces to

$$k_a(d_2^2-2d_2d_1+d_1^2)=2k_a(d_2^2+d_1^2)-k_a(d_1+d_2)^2. \quad (251)$$

Both sides can be divided by the stiffness value k_a, yielding

$$d_2^2-2d_2d_1+d_1^2=2(d_2^2+d_1^2)-(d_1+d_2)^2. \quad (252)$$

Completing the right hand side expansion gives

$$(d_2^2-2d_2d_1+d_1^2)=2d_2^2+2d_1^2-d_1^2-2d_1d_2-d_2^2. \quad (253)$$

As can be seen, all the terms cancel out as expected.

The above section shows that both the energy-based approach and the Newton-Euler approach arrive at the same analytical solution. Now that the analytical derivation is completed, an estimate for the tire stiffness properties needs to be determined.

Evaluation of spring constants

The above derivation required an estimation of two spring constants, the spring constant at the hitch and the spring constant at the axles. The hitch spring constant is a combination of the

Copyright 2018. the authors

Vermeer Manufacturing Company – Ex. 2045
Kubota v. Vermeer
IPR2025-00168
Page 171 of 182

prime mover truck's tires and suspension. The axle spring stiffness is a physical product of the tires only as the axles are rigidly connected to the TowPlow trailer.

Prime Mover Truck's Spring Stiffness

The prime mover truck's spring stiffness is easy to estimate. Previous analysis showed that the as delivered tongue weight of the TowPlow2 trailer was 17,440 N (3,920 lb). Measurements were taken in order to estimate the change in hitch height due to the load that resulted in a displacement of 7.938 mm (0.3125 in.). The formula for k_h is given by

$$k_h = \frac{\Delta F}{\Delta x} = \frac{17{,}440 \text{ N}}{7.938 \text{ mm}} = 2{,}192 \frac{\text{kN}}{\text{mm}} \left(12{,}546 \frac{lbs}{in}\right). \quad (254)$$

Tire Spring Stiffness

The tire spring stiffness is more difficult to evaluate. From equation (102), it was determined that the total TowPlow2 trailer weight ($F_{Trailer}$) is 83,720 N (18,820 lb), and that the tandem axle set weight (F_{tan}) is 66,280 N (14,900 lb) from equation (103). In order to compute the tire stiffness, the empty load CG needs to be used. Equation (107) presents the calculation of the center of gravity for the turn-key TowPlow2 trailer which is 6.03 m (19.79 ft).

The assumption will be made that the weight in the empty condition will be equally shared between the two axles. This means that in the unloaded condition, the values can be estimated as

$$F_1 = F_2 = \frac{F_{tan}}{2} = \frac{66{,}280 \text{ N}}{2} = 33{,}140 \text{ N } (7{,}450\ lbs). \quad (255)$$

The axle height was measured using three cases. First, the front axle center height was measured for the case where the tires were barely off the ground and not carrying any load, yielding an average height of 0.540 m (21.25 in.). Next, the axle height was measured at its ride height when it is supporting the empty weight of the TowPlow2 trailer, yielding an average height of 0.522 m (20.56 in.). Lastly, both tires on the rear TowPlow2 trailer tandem axle were removed and the average front axle height was 0.502 m (19.75 in.). This gives a displacement difference of 38 mm (1.5 in.) from the unloaded case.

In order to compute the new load on the front axle only, simple statics can be applied to compute the new force on the tires as

$$F_1 = \frac{F_{trailer} d_{cg}}{d_1} = \frac{83{,}720 \text{ N} * 6.03 \text{ m}}{6.858 \text{ m}} = 73{,}610 \text{ N } (16{,}550\ lbs). \quad (256)$$

This is the theoretical load on the front axle when the rear tires are removed.

Figure 90 shows a plot of the tire stiffness as a function of force. It is important to note that as the load on the tire increases, the stiffness of the tire increases in a non-linear fashion. The plot demonstrates that as the force on the tires increase, the stiffness increases. This means that using a linear approximation between the empty case resting on 4 tires verses only resting on the front tandem will under-estimate the tire stiffness in the loaded case.

Copyright 2018. the authors

Vermeer Manufacturing Company – Ex. 2045
Kubota v. Vermeer
IPR2025-00168
Page 172 of 182

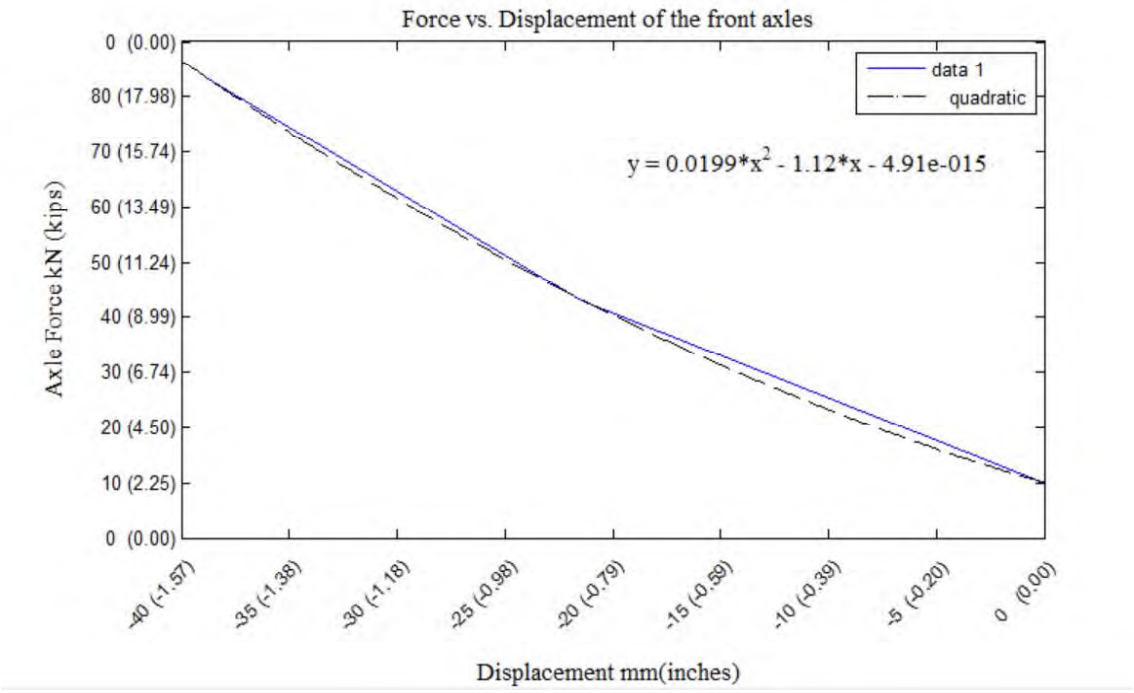


Figure 90. Force vs. displacement of the trailer tires

A quadratic data fitting algorithm in MATLAB gives a relationship between the axle load and the vertical displacement presented as

$$F = 0.0199x^2 - 1.12x + 4.91E - 15. \tag{257}$$

Generally speaking, the value for k is equal to the slope of the force displacement curve, which is the derivative of equation (257) with respect to x given as

$$\frac{dF}{dx} = 2 * 0.0199x - 1.12 = k_{a@x}. \tag{258}$$

Next, the value of k_a will be evaluated at a displacement of 38 mm (1.5 in.) which is closer to the operating range and yields a value for k_{tire_fit} defined as

$$k_{a_fit} = 2 * 0.0199(-38\text{ mm}) - 1.12 = 2.63\frac{\text{kN}}{\text{mm}}\left(15{,}030\frac{lbs}{in}\right). \tag{259}$$

A linear stiffness can also be approximated using a linear approximation between the two loaded cases. This can be represented as

$$k_{a_lin} = \frac{\Delta F}{\Delta x} = \frac{73{,}610\text{ N} - 33{,}140\text{ N}}{0.502\text{ m} - .522\text{ m}} = 2.02\frac{\text{kN}}{\text{mm}}\left(11{,}560\ \frac{lbs}{in}\right). \tag{260}$$

Analytical Results

The parameters required for the analysis are summarized in Table 19.

Copyright 2018. the authors

Vermeer Manufacturing Company – Ex. 2045
Kubota v. Vermeer
IPR2025-00168
Page 173 of 182

Table 19. Parameter summary for analysis

Para.	Description	Value	Source
W_g	Weight of the granular material	100,510 N (22,600 lb)	Sand density of 16,850 N/m^3 (2,897 lb/yd^3)
d_g	CG location of granular load	6.619 m (21.72 ft)	Estimated location after moving the sander (Eq. (129))
W_h	Weight of the sander	15,570 N (3,500 lb)	From manufacturer
d_h	CG location of the sander	6.345 m (20.82 ft)	Estimated sander location based on manufacturer diagram after move (Eq. (128))
W_f	Weight of the frame	68,150 N (15,320 lb)	Eq. (125)
d_f	CG location of the frame	5.698 m (18.69 ft)	Eq. (127)
d_1	Distance from hitch to first TowPlow axle	6.858 m (22.50 ft)	Measured/Viking-Cives schematic
d_2	Distance from the hitch to the second TowPlow axle	8.382 m (27.50 ft)	Measured/Viking-Cives schematic
k_h	Hitch Stiffness	$2{,}192\frac{\text{kN}}{\text{mm}}\left(12{,}546\frac{lbs}{in}\right)$	Experimental – Eq. (254)
k_a	Axle Stiffness	$2.63\frac{\text{kN}}{\text{mm}}\left(15{,}030\frac{lbs}{in}\right)$	Experimental – Eq. (259)

Evaluating the Indeterminate Forces

First, M_{mass} (Eq. (149)) and W_{mass} (Eq. (152)) are calculated as 1,152,390 Nm (850,000 ft-lb) and 184,230 N (41,420 lb), respectively. From equation (189) B_e has a value of 50.50, which is a dimensionless constant. Use of equation (191) gives C_e equal to 6.562/m (2.00/ft). The term A_e is evaluated in two parts. First, A_e is given as

$$A_E = 50.5 + S. \tag{261}$$

Use of equation (193) gives

$$F_h = \frac{50.50*184{,}230\text{ N} - \frac{6.562}{m}*1{,}152{,}390\text{ Nm}}{50.5+S} = \frac{1{,}741{,}630\text{ N}}{50.5+S}\left(\frac{391{,}550lbs}{50.5+S}\right). \tag{262}$$

A numerical representation of equation (169) can be determined using equation (239) and gives

$$F_2 = \frac{1{,}152{,}390\,Nm - 184{,}230\text{ N}*6.858\text{ m} + \frac{1{,}741{,}630}{50.5+S}6.858\text{ m}}{8.382\text{ m} - 6.858\text{ m}} = \frac{-111{,}059\text{ Nm} + \frac{11{,}944{,}100}{50.5+S}Nm}{1.524\text{ m.}}. \tag{263}$$

Next, a numerical equation for F_1 will be determined starting from equation (154) which yields

Copyright 2018. the authors

Vermeer Manufacturing Company – Ex. 2045
Kubota v. Vermeer
IPR2025-00168
Page 174 of 182

$$F_1 = 184{,}230\ \text{N} - \frac{-111{,}059\ \text{Nm} + \frac{11{,}944{,}100}{50.5+S}\,Nm}{1.524\ \text{m}} - \frac{1{,}741{,}630}{50.5+S}. \quad (264)$$

S is defined in (168) and becomes equal to 0.833. Using this value in equations (262), (263), and (264) yields a tongue force of 33,930 N (7,628 lb), a front tandem axle force (F_1) of 70,500 N (15,850 lb) and a rear tandem axle force (F_2), of 79,800 N (17,941 lb).
These results show that the rear axle is more heavily loaded than the front axle.

These results seem reasonable. The hitch force defined in equation (134) from the static analysis yielded a value of 32,910 N (7,400 lb) which is very close to that derived through the indeterminate analysis result of 33,930 N (7,628 lb). The total weight on the tandem axle set for the indeterminate analysis yields 150,300 N (33,790lb) which is close to the design value of 151,230 N (34,000 lb).

First, the TowPlow trailer needs to be properly leveled when the system is under load. From the Newton-Euler analysis, the equations for the axle forces are given by equations (194) and (195). If the TowPlow trailer is level, the value for ∅ is equal to 0. The above analysis can be also used to determine the deviation from level. Using equations (194) and (195) a relationship for the TowPlow trailer rotation angle can be determined. First, equation (194) can be used to define *x*as

$$-\frac{F_1}{k_1} - d_1 \sin \emptyset = x. \quad (265)$$

Equation (265) can then be substituted into equation (195), yielding

$$F_2 = -k_2 \left(-\frac{F_1}{k_1} - d_1 \sin \emptyset + d_2 \sin \emptyset\right). \quad (266)$$

Using the fact that the axle stiffness values are equal as defined by (206), an explicit relationship for the trailer angle can be defined as

$$\emptyset = sin^{-1}\left(\frac{F_1 - F_2}{k_a(d_2 - d_1)}\right) = sin^{-1}\left(\frac{70{,}500\ N - 79{,}800\ N}{2.63\frac{kN}{mm} * 10^6 (8.382 - 6.858)}\right). \quad (267)$$

Equation (267) results in a value for ∅ of -.133 degrees. This shows that the TowPlow2 trailer is not perfectly level. It is noted that this angle is highly sensitive to the stiffness in the system which was approximated. Furthermore, the negative rotation angle implies that the hitch is higher than either TowPLow2 trailer axle, which in turn means that the rear axle should be more highly loaded as the results show.

Copyright 2018. the authors

Vermeer Manufacturing Company – Ex. 2045
Kubota v. Vermeer
IPR2025-00168
Page 175 of 182

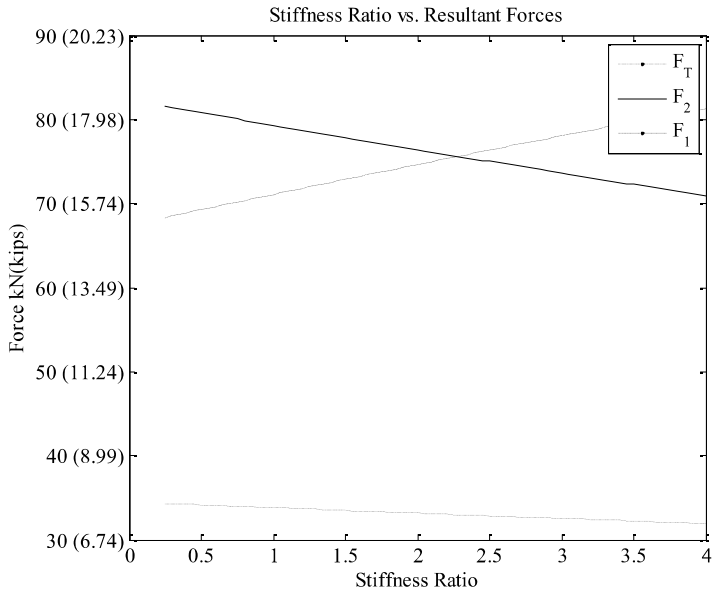


Figure 91. Resultant forces vs. stiffness ratio

Figure 91 shows plots of load versus parameter *S*. This figure shows that as the stiffness ratio increases, there is a value for which the two axle forces are exactly equal. Looking back at equation (267), this is the point, for which value for ∅ is zero and the TowPlow2 trailer is level. The value for *S* at this point can be solved for analytically, using equations (263) and (264) as

$$S = \frac{\left(\frac{2*11{,}944{,}100\ \text{Nm}}{1.524\ m}+1{,}741{,}630\ \text{N}\right)}{\left(184{,}230\ \text{N}+2*\frac{111{,}059\ \text{Nm}}{1.524\ m}\right)} - 50.5 = 2.28. \quad (268)$$

Using a value of 2.28 for S in equations (263) and (264) yield forces of 75,620 N (17,000 lb) and 75,610 N (17,000 lb) respectively for the axles. The tongue force in this analysis is 33,000 N (7,420 lb). The reader should appreciate that this tongue force is very close to the result from the static analysis given in equation (134), 32,910 N (7,400 lb). The sum of the two axle forces is 151,230 N (34,000 lb) matching the design weight.

Ultimately, leveling TowPlow2 is important to ensure that the axles are not overloaded. Moreover, it is recommended that the physical system be weighed to verify the analytical results presented herein.

Copyright 2018. the authors

Vermeer Manufacturing Company – Ex. 2045
Kubota v. Vermeer
IPR2025-00168
Page 176 of 182

APPENDIX F: ANALYTICAL ESTIMATE OF LOADED AXLE WEIGHTS OF THE OPTION 3 MODIFIED TOWPLOW2 (TOWPLOW2.3)

This Appendix contains the detailed analysis for the TowPlow2.3 system. Specifically, we are concerned with estimating the static weights of the TowPlow2.3 trailer when fully loaded. The analysis follows.

The center of gravity for the TowPlow2.3 trailer's granular load was estimated to act at 6.614 m (21.7 ft) from the hitch and is denoted as Dtp_{gran}.

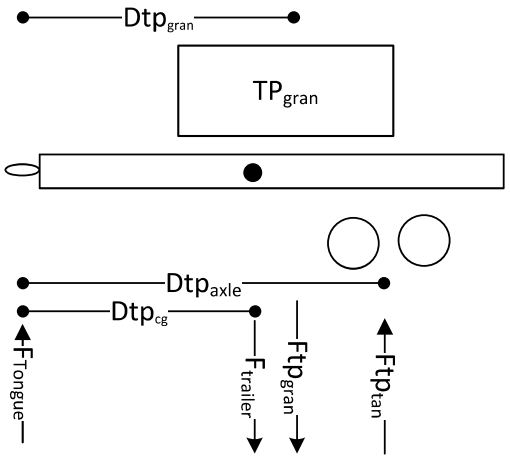


Figure 92. FBD of DOE Option 3 system

Equation (102) is used to determine the weight of the TowPlow2.3 trailer, which is 82,020 N (18,440 lb). Using equation (107) with the new measurements yields a TowPlow2.3 trailer CG location of 5.943 m (19.5 ft). This makes sense as the original TowPlow2 trailer value was 6.031 m (19.79 ft). Since the sander was moved forward, one would think that the CG would also come forward. However, it should be noted that removing some of the brine equipment, which is close to the tongue, pushes the CG towards the axles, and hence counteracts the effect of moving the sander forward.

For this analysis, a value of 16,850 N/m^3 (2,897 lb/yd^3) will be used to estimate the total payload weight of the 5.96 m^3 (7.8 yd^3) hopper. This yields a total granular weight, Ftp_{gran}, of 100,510 N (22,600 lb). Summing moments about the hitch yields

$$\sum M_{hitch} = Dtp_{axle} * Ftp_{tan} - Dtp_{cg} * F_{trailer} - Dtp_{gran} * Ftp_{gran} = 0. \qquad (269)$$

Equation (269) can be rearranged to solve for the load on TowPlow2.3's tandem axle set as shown in

Copyright 2018. the authors

Vermeer Manufacturing Company – Ex. 2045
Kubota v. Vermeer
IPR2025-00168
Page 177 of 182

$$Ftp_{tan} = \frac{Dtp_{cg} * F_{trailer} + Dtp_{gran} * Ftp_{gran}}{Dtp_{axle}}. \quad (270)$$

Plugging in numbers into equation (270) as shown in

$$Ftp_{tan} = \frac{5.943 \text{ m} * 82{,}020 \text{ N} + 6.345 \text{ m} * 100{,}510 \text{ N}}{7.62 \text{ m}}, \quad (271)$$

yields a weight of 147,660 N (33,200 lb) on the tandem axles. This number based on physical system weights is very close to the design value of 151,240, N (34,000 lb) which was used in the analysis presented in Appendix E. Next, summing the forces will help to determine the tongue load. The force relationship is

$$\sum F = 0 = Ftp_{tan} + F_{Tongue} - Ftp_{gran} - F_{trailer}. \quad (272)$$

This relationship can be rearranged to determine the tongue load as

$$F_{Tongue} = Ftp_{gran} - Ftp_{tan} + F_{trailer}. \quad (273)$$

Plugging numbers into equation (277) yields a tongue force, F_{tongue}, of 34,870 N (7,840 lb). Equation (134) yielded a theoretical tongue weight of 32,910 N (7,400 lb).

The next thing to analyze is the prime mover truck, which is shown in Figure 93**Error! Reference source not found.**. The weight of the prime mover truck, F_{truck}, can be determined using equation (108), which yields a weight of 134,340 N (30,200 lb).

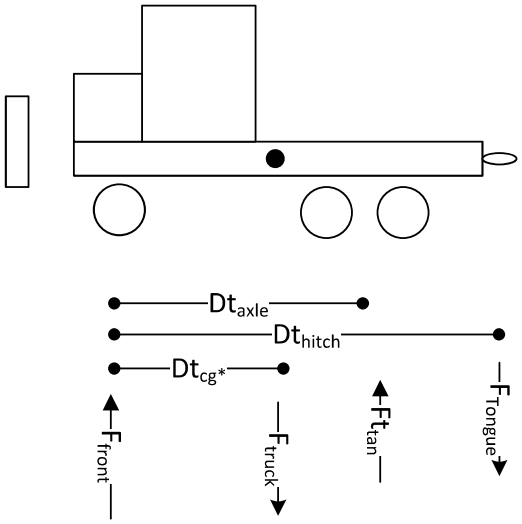


Figure 93. DOE Option 3 prime mover truck FBD

The prime mover truck's center of gravity location is defined as Dt_{cg*}. This can be determined using equation (110), which yields a value of 2.676 m (8.78 ft) from the front axle. This is shifted further forward than the previously determined value of 3.005 m (9.86 ft) from equation (138). This analysis includes the front plow while the previous analysis did not.

In order to determine the weight on the rear tandem axles on the prime mover truck, the moment equation will be applied about the front axle, given by

Copyright 2018. the authors

Vermeer Manufacturing Company – Ex. 2045
Kubota v. Vermeer
IPR2025-00168
Page 178 of 182

$$\sum M_{front} = Dt_{axle} * Ft_{tan} - Dt_{cg*} * F_{truck} - Dt_{hitch} * F_{Tongue} = 0. \quad (274)$$

Equation (274) can be rearranged to solve for the force on the tandem axle set as

$$Ft_{tan} = \frac{Dt_{cg*} * F_{truck} + Dt_{hitch} * F_{Tongue}}{Dt_{axle}}. \quad (275)$$

Plugging numbers into equation (275) yields a load of 105,510 N (23,720 lb) on the prime mover truck's tandem axle set. The value determined from equation (140) is 102,700 N (23,090 lb). This value is very close to the predicted value.

Next, the loaded front axle weight can be determined. This is done by summing the forces in the vertical direction. Performing this analysis yields a loaded front axle weight of 63,790 N (14,340 lb). Previously, equation (152) yielded a value of 64,720 N (14,550 lb) which is extremely close to this result.

The maximum available payload in the bed of the prime mover truck is calculated next. The maximum combined weight of the system is 355,860 N (80,000 lb). In the "as planned" analysis, a prime mover truck payload of 37,200 N (8,360 lb) from equation (143) was calculated. In the TowPlow2.3 analysis presented above, the maximum prime mover truck payload is 38,900 N (8,750 lb).

Clearly the analytical estimates based on the TowPlow2.3 as built measured weights presented in this appendix show good correlation to the values that were predicted based on the TowPlow2 measured weights. Although the analytical results are very reasonable, the next phase will be to load the system to get actual measurements.

Copyright 2018. the authors

Vermeer Manufacturing Company – Ex. 2045
Kubota v. Vermeer
IPR2025-00168
Page 179 of 182

REFERENCES

1. J.C. Alexander and J.H. Maddocks, "On the Maneuvering of Vehicles," *SIAM Journal on Applied Mathematics*, **48**(1): pp. 38-51, 1988.
2. R.W. Allen, T.J. Rosenthal, and H.T. Szostak, "Analytical Modeling of Driver Response in Crash Avoidance Maneuvering Volume I: Technical Background," Systems Technology, Inc, Hawthorne, 1988.
3. E. Bakker, L. Nyborg, and H.B. Pacejka, "Tyre Modelling for Use in Vehicle Dynamics Studies," *SAE Technical Paper 870421*, 1987.
4. I. Bombay, "Lecture 3 : Analysis of Statically Indeterminate Structures by Energy Method " http://nptel.ac.in/courses/105101085/downloads/lec-31.pdf.
5. R.T. Bundorf, "Directional Control Dynamics of Automobile-Travel Trailer Combinations," *SAE Technical Paper 670099*, 1967.
6. D. Burton, A. Delaney, S. Newstead, D. Logan, and B. Fildes, "Evaluation of Anti-Lock Braking Systems Effectiveness," Monash University, Australia, 2004.
7. C. Canudas de Wit, H. Olsson, K.J. Astrom, and P. Lischinsky, "A New Model for Control of Systems with Friction," *IEEE Transactions on Automatic Control*, **40**(3): pp. 419-425, 1995.
8. Caterpillar, http://pdf.cat.com/cda/files/2222280/7/legt6380.pdf, 2006.
9. H. Chen and S. Velinsky, "Designing Articulated Vehicles for Low-Speed Maneuverability," *Journal of Transportation Engineering*, **118**(5): pp. 711-728, 1992.
10. C. Chieh and M. Tomizuka, "Dynamic Modeling of Articulated Vehicles for Automated Highway Systems," *1995 American Control Conference*, **1**: pp. 653-657, 1995.
11. T. Chojnacki, J. Carney, G. Duncan, B. Hoffman, S. Lund, S. McCarthy, and W. Murray, "Towplow Closeout Report," 2012.
12. T.C. Christensen and W. Blythe, "Offtracking History, Analysis, and Simulation," *SAE Technical Paper 2000-01-0465*, 2000.
13. S. Colson, "Evaluation of the Viking-Cives Towplow," Rept. # 09-4, 2009.
14. S. Colson, "Second Year Evaluation of the Viking-Cives Tow Plow," Rept. # 10-4, 2010.
15. M. Corbett and R. POITRAS, "Two Plows-One Operator: The Use of Tow Plows on an Arterial Highway in Northern New Brunswick," 2009.
16. V. Deligiannis, G. Davrazos, S. Manesis, and T. Arampatzis, "Flatness Conservation in the N-Trailer System Equipped with a Sliding Kingpin Mechanism," *Journal of Intelligent and Robotic Systems*, **46**(2): pp. 151-162, 2006.
17. W. Deng, Y.H. Lee, and M. Tian, "An Integrated Chassis Control for Vehicle-Trailer Stability Handling Performance," *SAE Technical Paper 2004-01-2046*, 2004.
18. H. Dugoff, P.S. Fancher, and L. Segel, "Tire Performance Characteristics Affecting Vehicle Response to Steering and Braking Control Inputs : Final Report," University of Michigan, Ann Arbor, 1969.
19. G. Elert, "The Physics Hypertextbook," http://physics.info/drag/.
20. J.R. Ellis, *Vehicle Dynamics*, Business Books, London, 1969.
21. T.W. Erkert, J. Sessions, and R.D. Layton, "A Method for Determining Offtracking of Multiple Unit Vehicle Combinations," *Journal of Forest Engineering*, **1**(1): pp. 9-16, 1989.
22. M.A.A. Fernandez and S.R. S., "Caravan Active Braking System-Effective Stabilisation of Snaking of Combination Vehicles," *SAE Technical Paper 2001-01-3188*, 2001.
23. E. Fiala, "Lateral Forces at the Rolling Pneumatic Tire," *Verein Deutscher Ingenieure Zeitschrift*, (29): pp. 973-979, 1954.
24. D. Frame, "Caltrans Annual Budget," 2015.

Copyright 2018. the authors

Vermeer Manufacturing Company – Ex. 2045
Kubota v. Vermeer
IPR2025-00168
Page 180 of 182

25. A. Goodarzi, M. Behmadi, and E. Esmailzadeh, "Optimized Braking Force Distribution During a Braking-in-Turn Maneuver for Articulated Vehicles," *Mechanical and Electrical Technology (ICMET), 2010*: pp. 555-559, 2010.
26. R. Guntur and S. Sankar, "A Friction Circle Concept for Dugoff's Tyre Friction Model," *International Journal of Vehicle Design*, **1**(4): pp. 373-377, 1980.
27. A. Hac, D. Fulk, and H. Chen, "Stability and Control Consideration of Vehicle-Trailer Combination," *SAE Technical Paper 2008-01-1228*, 2008.
28. ISO/TC, "Road Vehicle - Heavy Commercial Vehicles and Buses - Steady-State Circular Tests," *ISO 14792*, pp, 2011.
29. ISO/TC, "Road Vehicles - Heavy Commercial Vehicles and Busses - Lateral Transient Response Test Method," *ISO 14793*, pp, 2011.
30. F. Jindra, "Off-Tracking of Tractor-Trailer Combinations," *Automobile Engineer*: pp. 96-101, 1963.
31. F. Jindra, "Handling Characteristics of Tractor-Trailer Combinations," *SAE Technical Paper 650720*, 1965.
32. S.S. Joshi, Class Note from Mae272 (Theory and Design of Modern Control Systems).
33. I. Kageyama, "A Stability Control Method for Articulated Vehicle at Braking," *International Symposium on Advanced Vehicle Control (AVEC'92)*: pp. 334-338, 1992.
34. T. KaKu, "A Study on the Resistance of Snowplowing and the Running Stability of a Snow Removal Truck," *Transportation Research Board Special Report, Snow Removal and Ice Control Research*, (185): pp. 232-239, 1979.
35. A. Kempainen, D. Milacic, M.D. Osborne, and W.V. Olson, "Modelling and Testing Snow Ploughing Forces on Trucks," *International Journal of Vehicle Design*, **19**(4): pp. 472-491, 1998.
36. U. Kiencke and L. Nielsen, *Automotive Control Systems for Engine, Driveline, and Vehicle*, Springer, New York, 2005.
37. S. Kimbrough and C. Chiu, "Automatic Steering System for Utility Trailers to Enhance Stability and Maneuverability," *1990 American Control Conference*: pp. 2924-2929, 1990.
38. A.I. Krauter, "Determination of Tire Characteristics from Vehicle Behavior," *SAE Technical Paper 750211*, 1975.
39. N.R.E. Laboratory, April 3, 2002.
40. R.G. Lannert, "Towed Snowplow and Method of Plowing," Cives Corporation Patent 2008.
41. P. Lugner, M. Plochl, and A. Riepl, "Investigation of Passenger Car-Trailer Dynamics Controlled by Additional Braking of Trailer," *International Symposium on Advanced Vehicle Control (AVEC'96)*: pp. 763-778, 1996.
42. S.A. Manesis, "Off-Tracking Elimination in Road Trains of Heavy Duty Trucks with Multiple Semitrailers," *8th IFAC International Symposium on Large Scale Systems: Theory and Applications*, **1**: pp. 355-360, 1998.
43. S.A. Manesis, N.T. Koussoulas, and G.N. Davrazos, "On the Suppression of Off-Tracking in Multi-Articulated Vehicles through a Movable Junction Technique," *Journal of Intelligent & Robotic Systems*, **37**(4): pp. 399-414, 2003.
44. M. Mellor, "Snow Removal and Ice Control," Cold Regions Research and Engineering Laboratory, Hanover, 1965.
45. A.M.C. Odhams, R.L. Roebuck, B.A. Jujnovich, and D. Cebon, "Active Steering of a Tractor-Semi-Trailer," *Proceedings of the Institution of Mechanical Engineers, Part D: Journal of Automobile Engineering*, **225**(7): pp. 847-869, 2011.
46. OpenSource, "Arduino - Products," *Arduino - HomePage*, 2013.
47. R.L. Pretty, "On the Off-Tracking of Semi-Trailers," *Australian Road Research Board Conference*: pp. 394-402, 1964.
48. K. Rangavajhula and H.S.J. Tsao, "Active Trailer Steering Control of an Articulated System with a Tractor and Three Full Trailers for Tractor-Track Following," *International Journal of Heavy Vehicle Systems*, **14**(3): pp. 271-293, 2007.

Copyright 2018. the authors

Vermeer Manufacturing Company – Ex. 2045
Kubota v. Vermeer
IPR2025-00168
Page 181 of 182

49. B. Ravani, M. Gabibulayev, and T.A. Lasky, "A Snowplowing Resistance Model for Use in Vehicle Dynamic Modeling," *Mechanics Based Design of Structures and Machines*, **33**(3-4): pp. 359-372, 2005.
50. Y. Saito, "On the Stability and Followability of the Semi-Trailer Vehicle with an Automatic Steering System," *Vehicle System Dynamics*, **8**(2-3): pp. 206-211, 1979.
51. K.R. Santiago-Chaparro, M. Chitturi, T. Szymkowski, and D.A. Noyce, "Evaluation of Performance of Automatic Vehicle Location and Towplow for Winter Maintenance Operations in Wisconsin," *Transportation Research Record: Journal of the Transportation Research Board*, **2272**(1): pp. 136-143, 2012.
52. I. Schneider, H. William, C. Miller, M. Crow, and W.A. Holik, "Evaluation of the Viking-Cives Towplow for Winter Maintenance," 2014.
53. L. Segel and R.D. Ervin, "The Influence of Tire Factors on the Stability of Trucks and Tractor Trailers," *Vehicle System Dynamics*, **10**(1): pp. 39-59, 1981.
54. S.H. Tamaddoni and S. Taheri, "Yaw Stability Control of Tractor Semi-Trailers," *SAE Technical Paper 2008-01-2595*, 2008.
55. X. Tong, N. Mrad, and M. El-Gindy, "Sensitivity of Rearward Amplication Control of a Truck/Full Trailer to Tyre Cornering Stiffness Variations," *Proceedings of the Institution of Mechanical Engineers, Part D: Journal of Automobile Engineering*, **215**(5): pp. 579-588, 2001.
56. J.J. Uicker, G.R. Pennock, and J.E. Shigley, *Theory of Machines and Mechanisms*, Oxford University Press, New York, 2003.
57. E. Velenis, P. Tsiotras, and C. Canudas-de-Wit, "Extension of the Lugre Dynamic Tire Friction Model to 2d Motion," *IEEE Mediterranean Conference on Control and Automation*, 2002.
58. S.A. Velinsky, Class Notes from Mae 234 (Design and Dynamics of Road Vehicles).
59. F. Vlk, "Handling Performance of Truck-Trailer Vehicles: A State-of-the-Art Survey," *International Journal of Vehicle Design*, **6**(3): pp. p. 323-361, 1985.
60. Y.J. Wang and M.P. Cartmell, "Trajectory Generation for a Four Wheel Steering Tractor-Trailer System: A Two-Step Method," *Robotica*, **16**: pp. 381-386, 1998.
61. Western Highway Institute. Sizes and Weights-Equipment Committee., "Offtracking Characteristics of Trucks and Truck Combinations," Western Highway Institute, San Francisco, 1970.
62. K. Zhou, W.-B. Zhang, and M. Tomizuka, "Dynamic Modeling and Simulation of Snowplow: Normal Operation and Icepack Impacts," Partners for Advanced Transit and Highways, Berkeley, 2000.
63. S.W. Zhou, S.Q. Zhang, and G.Y. Zhao, "Stability Control on Tractor Semi-Trailer During Split-Mu Braking," *Advanced Materials Research*, **230-232**: pp. 549-553, 2011.

Copyright 2018. the authors

Vermeer Manufacturing Company – Ex. 2045
Kubota v. Vermeer
IPR2025-00168
Page 182 of 182